Full-Depth Reclamation with Hydraulic Road Binders

by

Eskedil Abebaw Melese

A thesis
presented to the University of Waterloo
in fulfillment of the
thesis requirement for the degree of
Doctor of Philosophy
in
Civil Engineering

Waterloo, Ontario, Canada, 2019

Examining Committee Membership

The following served on the Examining Committee for this thesis. The decision of the Examining Committee is by majority vote.

External Examiner	**Dr. Michel Vaillancourt** École de Technologie Supérieure, Quebec, Canada
Supervisor	**Dr. Hassan Baaj** Civil and Environmental Engineering, University of Waterloo
Supervisor	**Dr. Susan Tighe** Civil and Environmental Engineering, University of Waterloo
Internal Member	**Dr. Adil Al-Mayah** Civil and Environmental Engineering, University of Waterloo
Internal Member	**Dr. Liping Fu** Civil and Environmental Engineering, University of Waterloo
Internal-external Member	**Dr. Goretty Dias** School of Environment, Enterprise and Development, University of Waterloo

Author's Declaration

This thesis consists of material all of which I authored or co-authored: see Statement of Contributions included in the thesis. This is a true copy of the thesis, including any required final revisions, as accepted by my examiners.

I understand that my thesis may be made electronically available to the public.

Statement of Contributions

This thesis is partially the product of co-authored publication as follows: Chapter 4, entitled " Characterisation of full-depth reclaimed pavement materials treated with hydraulic road binders" is authored by myself and reviewed by my supervisors. Our industry partners, Tim Smith and Steve Zupko, participated in reviewing the manuscript. Chapter 5 " Fatigue behaviour of reclaimed pavement materials treated with hydraulic road binders" is authored by myself and reviewed by supervisors. Chapter 6 "Effects of hydraulic road binders on life-cycle impacts of full-depth reclamation" is authored by myself and reviewed by Professor Goretty Dias and my supervisors. The analysis and discussions in all of the papers were done by myself under the supervision and guidance of my supervisors. The experimental plans were prepared together with my supervisors.

Chapter 4

- Melese E, Baaj H, Tighe S, Zupko S, Smith T. Characterisation of full-depth reclaimed pavement materials treated with hydraulic road binders. Construction and Building Materials. 2019 May; doi.org/10.1016/j.conbuildmat.2019.07.317

Chapter 5

- Melese E, Baaj H, Tighe S. Fatigue Behaviour of Reclaimed Pavement Materials Treated with Cementitious Binders. Submitted to Construction and Building Materials (conditionally accepted for publication)

Chapter 6

- Melese E, Baaj H, Dias G, Tighe S. Effects of Cementitious binders on the Life-Cycle Impacts of Full-depth Reclamation. Submitted to Road Materials and Pavement Design (under revision)

ABSTRACT

According to a recent report, 16.4% of Canadian roads are in a poor or very poor condition. This means 146,255 km of the Canadian roads are either unfit for service or are approaching the end of their service life. The roads in these conditions require immediate action to restore their serviceability. One of the plausible techniques that could be applied to restore the serviceability of roads in poor or very poor conditions is full-depth reclamation (FDR). Full depth reclamation is a type of pavement cold in-place recycling in which the existing old and deteriorated pavement is pulverised, treated with appropriate stabilizer and compacted to form a strong base layer. In Canada, the stabilizers commonly used in the FDR process are asphalt emulsions, foamed asphalt, and Portland cement. Hydraulic road binders (HRB), however, are alternative cementitious stabilizers that can be used in full-depth reclamation process with some better attributes than Portland cement. The main objectives of this research are characterisation and impact assessment of fully reclaimed pavement materials treated with HRB. The study was conducted in the form of comparative assessment by using reclaimed materials treated with General Use (GU) cement as control mixes. Four types of reclaimed materials and four types of cementitious binders, including GU cement, were used to make sixteen different mixes. Characterisation and performance tests were conducted to understand the behaviour of the mixtures under static and dynamic loadings. Besides, life-cycle assessment was conducted to investigate the environmental impacts of the different cementitious binders. The findings of the study indicate that HRB, of the type used in the study, can be used in full-depth reclamation process without compromising the strength and durability of the mixtures. However, not all HRB substantially reduce the environmental

impacts and energy requirements. Among the binders used in the study, the HRB with the lowest C/S ratio can significantly reduce the global warming potential.

ACKNOWLEDGEMENTS

I would like to express my sincere gratitude to my supervisors Professor Hassan Baaj and Professor Susan Tighe for their unflagging support, superb guidance and encouragement throughout my PhD study. I would also like to thank Professor Goretty Dias for her assistance in the life-cycle assessment part of the study. I wish to express my sincere appreciation to my PhD committee members Professor Adil Al-Mayah, Professor Liping Fu, Professor Goretty Dias from University of Waterloo and my external examiner Professor Michel Vaillancourt from École de Technologie Supérieure.

This study was funded by the Natural Science and Engineering Research Council of Canada (NSERC) and Lafarge Canada Inc. I would like to thank Tim Smith and Steve Zupko for their useful feedbacks and support. I would also like to thank Chris Thompson, Roto Mill Inc., Niagara-on-the-Lake Town Hall and Stabilization Canada for their contribution in the field work.

My heartfelt gratitude goes to the Civil and Environmental Engineering Department staffs, particularly Richard Morrison, Peter Volcic, Douglas Hirst, Anne Allen, Mark Sobon and Victor Lewis for their professional advise and support in the laboratory. I would also like to thank Chris Peace, Rick Forgett, Mark Kuntz and Fred Bakker for their technical assistance and advice.

I am very grateful to my best friends Engineer Kedamawit Giramy and Dr. Shimelies Ahmed for their constant encouragement and emotional support.

I would like to acknowledge CORE Consulting Engineers Plc, Engineer Amdemichael Menkir and Engineer Teshome Worku and other staffs for their support during my study.

I would like to thank my CPATT colleagues for their help with field and laboratory works and also for their emotional support.

Last but not the least, I would like to express my sincere respect and love for my wife Shewit and my son Fikir for their patience and understanding throughout the research period. My warm appreciation and gratitude also extend to all those who supported and encouraged me, but are not mentioned above by name, for their concern and kindness.

To

the late Engineer Efrem Gebre-egziabher

TABLE OF CONTENTS

List of Figures

List of Tables

List of Abbreviations

AADTT	Average Annual Daily Truck Traffic
ASTM	American Society for Testing and Materials
BS	British Standard
CDE	Cumulative Dissipated Energy
CPATT	Centre for Pavement and Transportation Technology
C/S	Calcium to Silica ratio
DMI	Distress Manifestation Index
US EPA	United States Environmental Protection Agency
FDR	Full-Depth Reclamation
FDRm	Full-Depth Reclaimed Materials
FRPMC	Fully Reclaimed Pavement Materials Treated with Cementitious Binders
GU	General Use
HRB	Hydraulic Road Binders
IDT	Indirect Tensile Strength
IRI	International Roughness Index
LCA	Life Cycle Assessment
MDD	Maximum Dry Density
ME	Mechanistic-Empirical
MOE	Modulus of Elasticity
MTO	Ontario Ministry of Transportation
NCHRP	National Cooperative Highway Research Program
OBC	Optimum Binder Content
OMC	Optimum Moisture Content
PCA	Portland Cement Association
PCI	Pavement Condition Index
RAP	Reclaimed Asphalt Pavement
RDEC	Rate of Dissipated Energy Change
SCM	Supplementary Cementitious Materials
UCS	Unconfined Compressive Strength

1. INTRODUCTION

1.1. Preface

The thesis is composed of the contents of one published and two yet unpublished journal articles along with introductory and concluding chapters. The first article, which was published in the Journal of Construction and Building Materials presents the characteristics of full-depth reclaimed pavement materials treated with hydraulic road binders. In this article, the mechanical properties of fully reclaimed pavement materials treated with hydraulic road binders were investigated and compared with the corresponding properties of the same materials treated with General Use (GU) cement. The findings on the journal can be used to understand how hydraulic road binders affect the mechanical properties of stabilized full-depth reclaimed pavement materials. In the second paper, which was submitted to the Journal of Construction and Building Materials, the fatigue behaviour of fully reclaimed pavement materials treated with cementitious binders (FRPMC) was presented. In this paper, the behaviour of FRPMC under repeated loading was studied using phenomenological and energy-based approaches. The study was conducted based on the results of four-point bending test. The findings of the study can be used to assess how hydraulic road binders affect the fatigue performance of FRPMC. The fatigue performance models in this article can be used to design semi-rigid pavement with FRPMC layer. The third paper was submitted to the Journal of Road Materials and Pavement Design. It presents how the use of hydraulic road binders affects the life cycle impacts of full-depth reclamation. The second and third articles are still under the review process.

The study presented in this thesis was conducted under the supervision of Prof. Hassan Baaj and Prof. Susan Tighe. The research was funded by the Natural Science and Engineering Research Council of Canada (NSERC) and Lafarge Canada Inc. Tim Smith and Steve Zupko have participated in the first paper by reviewing the contents and indentifying areas for improvement. Professor Goretty Dias has participated in the third paper by reviewing and providing feedbacks. All the materials in the composition of the original articles provided in the thesis are the sole production of the primary investigator listed as the first author in the journal publications.

1.2. Motivation

According to a recent report (1), 16.4% of Canadian roads are in a poor or very poor condition. This means 146,255 km of the Canadian roads are either unfit for service or are approaching the end of their service life. The roads in these conditions require immediate action to restore their serviceability.

One of the plausible techniques that could be applied to restore the roads in poor or very poor conditions is full-depth reclamation. Full-depth reclamation (FDR) is a sustainable rehabilitation technique which has become popular over the last three decades. It is a type of pavement cold in-place recycling in which the existing old and deteriorated pavement is pulverised, treated with appropriate binding agent, and compacted to form a strong base layer.

The binding agent that is used in FDR could be asphalt emulsions, foamed asphalt, or Portland cement. The FDR materials that are treated with bituminous stabilizers (asphalt emulsion and foamed asphalt) are flexible and have a good fatigue resistance. However, they

are more vulnerable to moisture induced damage compared to the Portland cement treated FDR materials. The materials treated with Portland cement often characterized by a good moisture resistance, high early strength and better resistance to traffic induced deformation (2,3). However, the manufacturing of Portland cement generates huge amount of anthropogenic emissions with adverse environmental impacts. Studies indicate that approximately 5% of the global anthropogenic carbon dioxide (CO_2) emissions are generated from cement manufacturing (4–6). Besides, during the full-depth reclamation process, the allowable time gap between the mixing and compaction operations is very short. After the cement is mixed with water and the pulverised pavement material, the mixing and compaction activities should be completed within two hours (7) .

The potential alternative stabilizers that could mitigate the problems associated with Portland cement are hydraulic road binders. Hydraulic road binders (HRB) are factory made blends that are specifically designed for application in road and rail bases, sub-bases, capping layers, soil stabilization and soil improvement. Hydraulic road binders contain substantial amount of supplementary cementitious materials (SCM) such as granulated blast furnace slag, fly ash, natural pozzolanas, calcined natural pozzolanas, burnt shale, and limestone (8,9).

The presence of such silica-rich SCM in hydraulic road binders changes the composition of the calcium silicate hydrate (C-S-H) by reducing the Calcium/Silicate (C/S) ratio. Most SCM are characterized by lower C/S ratio compared to Portland cement as SCM contain less calcium. As a result, hydrates of SCM are different from that of Portland cement. This difference in the composition of hydration products affects the strength and durability of HRB mixtures (10). Blending SCM into Portland cement also influences water demand, setting time, heat evolution and pore structure (11) of the binders. Consequently, the

properties of HRB mixtures could be different from the properties of Portland cement mixtures.

Currently, the use of hydraulic road binders in full-depth reclamation processes is not common in Canada. The properties of mixtures treated with hydraulic road binders were not well documented. There are no pavement design and performance prediction models specifically established for HRB mixtures. The environmental influence of HRB mixtures was also not studied under the Canadian conditions. This study was initiated with the motivation of addressing these gaps and evaluating the viability of HRB for application in FDR process in Canada.

1.3. Research Hypotheses and Objectives

Partial replacement of Portland cement clinker with SCM is one of the proposed innovative approaches to reduce the CO_2 emissions due to cement manufacturing (4,6,12). Production of Portland cement clinker is a resource and energy intensive process and the major source of greenhouse gas emissions (13). SCM, on the other hand, are materials that are often obtained in the form of industrial by-products or as natural material that do not require intensive industrial processing (10,11).

Studies indicate that the CO_2 emissions can be reduced by 5% - 20% by applying the partial replacement approach (6,14). Based on this premise, the amount of CO_2 emissions due to the manufacturing of HRB could be lower than that of Portland cement as HRB contain substantial amount of SCM. This leads to the assumption that the environmental impact of HRB mixtures is less than the impact of Portland cement mixtures.

The hydration of cementitious binders with multiple components is influenced by the hydration of the main components (11). Accordingly, the rate of hydration of HRB mixtures could be normal or slow depending on its prominent constituent. However, regardless of the binders composition, mixtures with the desired strength can be attained with proper mix design (11). Also, binders containing SCM have better chemical resistance to aggressive solutions (11). Therefore, the use of HRB might not have negative influence on the strength and durability of mixtures.

The main hypotheses of the research can be summarized as:

i. HRB can substitute Portland cement as stabilizer in full depth reclamation without compromising mixture performance.
ii. Using hydraulic road binders in the FDR process can reduce environmental impacts.

To test the research hypotheses, the optimum compositions of HRB mixtures should be identified, the mechanical properties of HRB mixtures should be characterised and the behaviour of the compacted mixtures should be studied under static and dynamic loading conditions. Furthermore, comparative life-cycle assessment should be conducted to assess the environmental impacts and compare with the base-case scenario. Therefore, the main objectives of the research are:

i. To characterize the properties of FDR mixtures treated with HRB.
ii. To study the response of HRB treated FDR mixtures to repeated loading.
iii. To develop empirical models and calibrate performance prediction models that can be used for pavement design
iv. To identify the influence of HRB on the environmental impacts of FDR mixtures.

2. BACKGROUND

2.1. Hydraulic Road Binders

According to the British Standard, BS 6100 (15), hydraulic binder is defined as a binder that sets and hardens by chemical interaction with water and is capable of doing so under water. The same definition is given to hydraulic cement in ASTM C 219 (16). Thus, hydraulic binder and hydraulic cement are the same terms that can be used interchangeably. Hydraulic **road** binders are a type of hydraulic binder that are specifically designed for road construction (17). They are factory produced materials that are made for direct use in roadbases, sub-bases, capping layers, and for soil stabilization or soil improvement (8,9).

Hydraulic road binders have different composition and properties than the standard classic cements. The main ingredients of hydraulic road binders can be chosen among Portland cement clinker, granulated blastfurnace slag, natural pozzolanas, thermally activated clays and shales, fly ash, burnt shale, and limestone. Inorganic natural materials and inorganic mineral materials derived from the clinker production process can also be added in a proportion not exceeding 5% by mass of the total mixture. Further, calcium sulfate (in the form of gypsum, hemihydrate or anhydrite) and other additives can be incorporated to improve the properties of the hydraulic road binders. The amount of additives shall not exceed 1% by mass of the binder (18). There is no fixed composition formula that is suggested for combining these materials except that the amount of Portland cement clinker should at least be 20% for higher strength class HRB (HRB with 28 days strength of 22.5 MPa and 32.5 MPa) (18). Because HRB contain significant proportion of the supplementary cementitious

materials other than clinker, the cost of hydraulic road binders is generally lower than the cost of Portland cement.

According to the European Standards (8,9), hydraulic road binders are classified into fast-hardening and normal-hardening based on their setting times. Each of these classes is further divided into four depending on their compressive strength. The fast-hardening hydraulic road binders are designated as E2, E3, E4, and E4 RS; whereas the normal-hardening hydraulic road binders are designated as N1, N2, N3, and N4. The minimum initial setting time of E2, E3, and E4 class HRB is 90 minutes; however, the initial setting time of E4 RS shall be less than 90 minutes. On the other hand, for each of the four classes of the normal-hardening HRB, the minimum initial setting time is 150 minutes (8,9,17). The strength requirements of the fast-hardening and normal-hardening hydraulic road binders are shown in Table 2.1 and Table 2.2, respectively. In North America, there is no standard equivalent to the European standard that had been developed for hydraulic road binders. This could be because of the limited use of hydraulic road binders in the North American road industry.

Table 2.1 Strength Requirements for Fast-Hardening HRB

Mechanical Classes	Compressive Strength (MPa)		
	7 days	28 days	
	Minimum	Minimum	Maximum
E2	5.0	12.5	32.5
E3	10.0	22.5	42.5
E4	16.0	32.5	52.5
E4 RS	16.0	32.5	–

Table 2.2 Strength Requirements for Normal-Hardening HRB

Mechanical Classes	Compressive Strength at 56 days (MPa)	
	Minimum	Maximum
N1	5.0	22.5
N2	12.5	32.5
N3	22.5	42.5
N4	32.5	52.5

2.1.1 Manufacture of Hydraulic Road Binders

The hydraulic road binders used in this study are proprietary products manufactured by blending General Use (GU) cement or Portland-Limestone (GUL) cement with SCM. The SCM need to be ground to a powder form (unless it is naturally in powder form) before blending with the GU/GUL cement. Then the GU/GUL and the selected SCM are blended at the predetermined proportions in a blender. The manufacturing steps of HRB are shown in Figure 2.1.

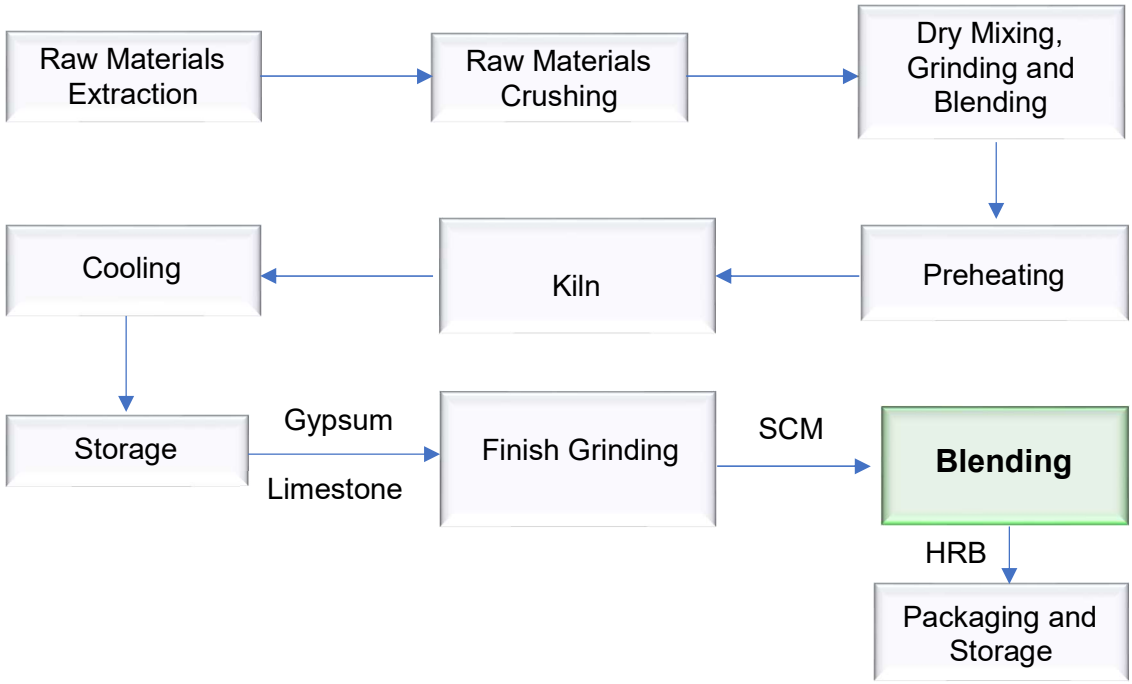

Figure 2.1 Manufacturing steps of Hydraulic Road Binders

2.1.2 Chemical Reactions

The supplementary cementitious materials, which are ingredients of HRB, are composed of pozzolans. Pozzolans are siliceous or siliceous and aluminous materials that have little or no cementing property naturally, but react with calcium hydroxide to form compounds possessing cementing property (19). Thus, when a hydraulic road binder interacts with water two types of reactions take place. First, the components of the Portland cement undergo hydration reaction and form hydrated calcium silicate (C-S-H) and calcium hydroxide (lime). Then, the lime from the first reaction activates the pozzolans in the HRB and pozzolanic reaction takes place to form C-S-H. C-S-H is the important compound of the chemical reaction that contributes to the strength of the cementitious products. The hydration reaction of the Portland cement components and the pozzolanic reactions, which take place when HRB interacts with water are shown in Eq. (2.1) – Eq. (2.3) and Eq. (2.4) – Eq. (2.7), respectively (20) .

Hydration reaction

$$(CaO)_3\, SiO_2 + H_2O \rightarrow (CaO)_x\, (SiO_2)_y\, (H_2O)_z + Ca(OH)_2 \quad (2.1)$$

$$(CaO)_2\, SiO_2 + H_2O \rightarrow (CaO)_x\, (SiO_2)_y\, (H_2O)_z + Ca(OH)_2 \quad (2.2)$$

$$(CaO)_3\, Al_2O_3 + H_2O \rightarrow (CaO)_x\, (Al_2O_3)_y\, (H_2O)_z \quad (2.3)$$

$$(CaO)_4\, Al_2O_3\, Fe_2O_3 + H_2O \rightarrow (CaO)_x\, (Al_2O_3)_y\, (Fe_2O_3)_z\, (H_2O)_w \quad (2.4)$$

Pozzolanic reaction

$$Ca(OH)_2 + SiO_2 \rightarrow (CaO)_x\, (SiO_2)_y\, (H_2O)_z \quad (2.5)$$

$$Ca(OH)_2 + Al_2O_3 + H_2O \rightarrow (CaO)_x\, (Al_2O_3)_y\, (H_2O)_z \quad (2.6)$$

$$Ca(OH)_2 + Al_2O_3 + Fe_2O_3 + H_2O \rightarrow (CaO)_x\, (Al_2O_3)_y\, (Fe_2O_3)_z (H_2O)_w \quad (2.7)$$

2.2. Full-Depth Reclamation

The process of recovering and re-using of materials from the existing pavement without heating the materials to produce a rehabilitated pavement is termed as cold recycling. Cold recycling can be performed either in-plant or in-place (21,22). Full depth reclamation is a type of pavement cold in-place recycling in which the existing old pavement is pulverised, blended with a stabilizer, and compacted to form a strong base layer. In the FDR process, the surfacing layer is pulverised along with partial or full depth of the underlying pavement layers. The pulverisation could extend beyond the pavement structural layers to include certain portion of the subgrade material. The reclaimed materials are often treated with stabilizers for improved performance. The Asphalt Recycling and Reclaiming Association (2) defined full-depth reclamation as:

> "*a pavement rehabilitation technique in which the full flexible pavement section and a predetermined portion of the underlying materials are uniformly crushed, pulverised or blended, resulting in a stabilised base course; further stabilization may be obtained through the use of available additives*."

Full-Depth Reclamation is particularly a preferred method of rehabilitation when the existing pavement is highly deteriorated and requires 15%-20% patching; when the pavement problems are associated with the underlying layers; and when the pavement is found to be structurally inadequate to sustain the existing and future traffic volume (7). After the FDR process, the existing deteriorated pavement will be converted into new structurally sound base layer. As a result, provision of only thin bituminous wearing course or surface treatment over the FDR base would be adequate (2).

Over the past three decades, full depth reclamation has gained popularity and implemented in various provinces and states of Canada and USA. Some of these include Ontario, Quebec, Saskatchewan, Georgia, Kansas, Louisiana, Maine, Nevada, Texas, Utah, and Wisconsin. (23–25).

2.1.3 Common Stabilizers in FDR Process

In the FDR process, the reclaimed materials are often treated with various types of stabilizers to improve their strength and durability. The most commonly used stabilizers in FDR projects are Portland cement, asphalt emulsions and foamed asphalt (also known as expanded asphalt). The way these stabilizers interact with the reclaimed materials to impart their stabilizing function is different. Each of these stabilizers has their own merits and demerits over each other as discussed in the following subsections. The choice of appropriate stabilizer for FDR project depends on the cost, availability, and previous performance of the stabilizer; and the type of the reclaimed material (2,26).

- *Asphalt emulsions*

The type of asphalt emulsions that are commonly used for full-depth reclamation are medium setting and slow setting asphalt emulsions. Emulsions are usually composed of 60% bitumen and 40% water. When blended with the reclaimed materials, the asphalt emulsion coats the coarser fractions, which eventually bind to the finer fractions to form a stable layer. The typical application rate of emulsified asphalt by weight of the FDR material is 5%. The application rate may need to be lowered to 3%-4% if the reclaimed material contains thick asphalt layer (27–29).

The emulsion treated FDR base is flexible with improved resistance to fatigue cracking. However, the emulsion treated materials require long time to cure and acquire full strength. Besides, when applied to moist materials, the moisture content of the mixture may go beyond the optimum and become difficult to compact. Further, asphalt emulsions may cost more than foamed asphalt due to their additional manufacturing cost. These are the major limitations of using emulsified asphalts in full depth reclamation process (2,26,30).

- *Foamed asphalt*

The use of foamed asphalt has increased following the invention of improved and safe foaming equipment. The asphalt is made to foam by introducing a small amount of water, typically 2% by mass, to a hot asphalt. The foaming of the asphalt facilitates the mixing of the normal grade bitumen with the cold reclaimed materials. When applied to the reclaimed material, the minute asphalt on the foam stick to the finer fractions to form a mastic that binds the coarser fractions together. The typical range of the application rate of the expanded asphalt in full-depth reclamation is between 3% and 5%. Reduced application rates of 2%-3% could be feasible when the reclaimed material contains thick asphalt layers (2,26).

Most of the limitations of the emulsified asphalt can be overcome by using foamed asphalt. As the foaming of the asphalt can be performed on the site, there is no manufacturing cost attached to the foamed asphalt. Thus, the cost of the expanded asphalt is lower than emulsified asphalt. Furthermore, the material, stabilized with the foamed asphalt gains its strength rapidly since the water added to create the foaming evaporates immediately after the foaming takes place. Similar to the emulsified asphalt base, the resulting base layer is flexible with good fatigue resistance. The major shortcoming of the foamed asphalt is its demand for finer fractions. To be treated with expanded asphalt, the reclaimed materials must contain 5%-

15% of the fractions passing 75μm (No. 200) sieve. Besides, it is required to heat the asphalt to a temperature of about 180^{o}C during the foaming operation, which is not required in the case of emulsified asphalt (2,30).

- *Portland cement*

Portland cement undergoes hydration reaction by reacting with the moisture in the reclaimed material to form silica gel. The silica gel cements the grains of the reclaimed materials together to create a strong and stable base. The typical application rate of Portland cement ranges 2% - 4%. It is recommended to limit the application rate to the maximum of 6% to minimize the risk of shrinkage cracking. In the full-depth reclamation projects, Portland cement can be applied either in dry form or in the form of a slurry with the later being the preferred option to avoid dust nuisance, especially, in residential areas.

The cement treated reclaimed materials have good early strength and better resistance to moisture damage. Additionally, the Portland cement bases are less susceptible to traffic induced deformation if properly designed and constructed. The major problem that is associated with Portland cement treatment is the shrinkage cracking of the stabilized base. The shrinkage cracks in the stabilized base can create tensile stress build-up at the bottom of the surfacing layer, which can cause bottom-up cracking or reflective cracking at the surface layer (2,26,30,31). The other limitation of the cement treated FDR materials is the short time interval between the mixing and compaction steps. The maximum allowable time gap between the mixing and the compaction operation is 2-hours (7). Thus, unlike bituminous mixtures, extended stockpiling and delayed compaction are not possible when using Portland cement as a stabilizer.

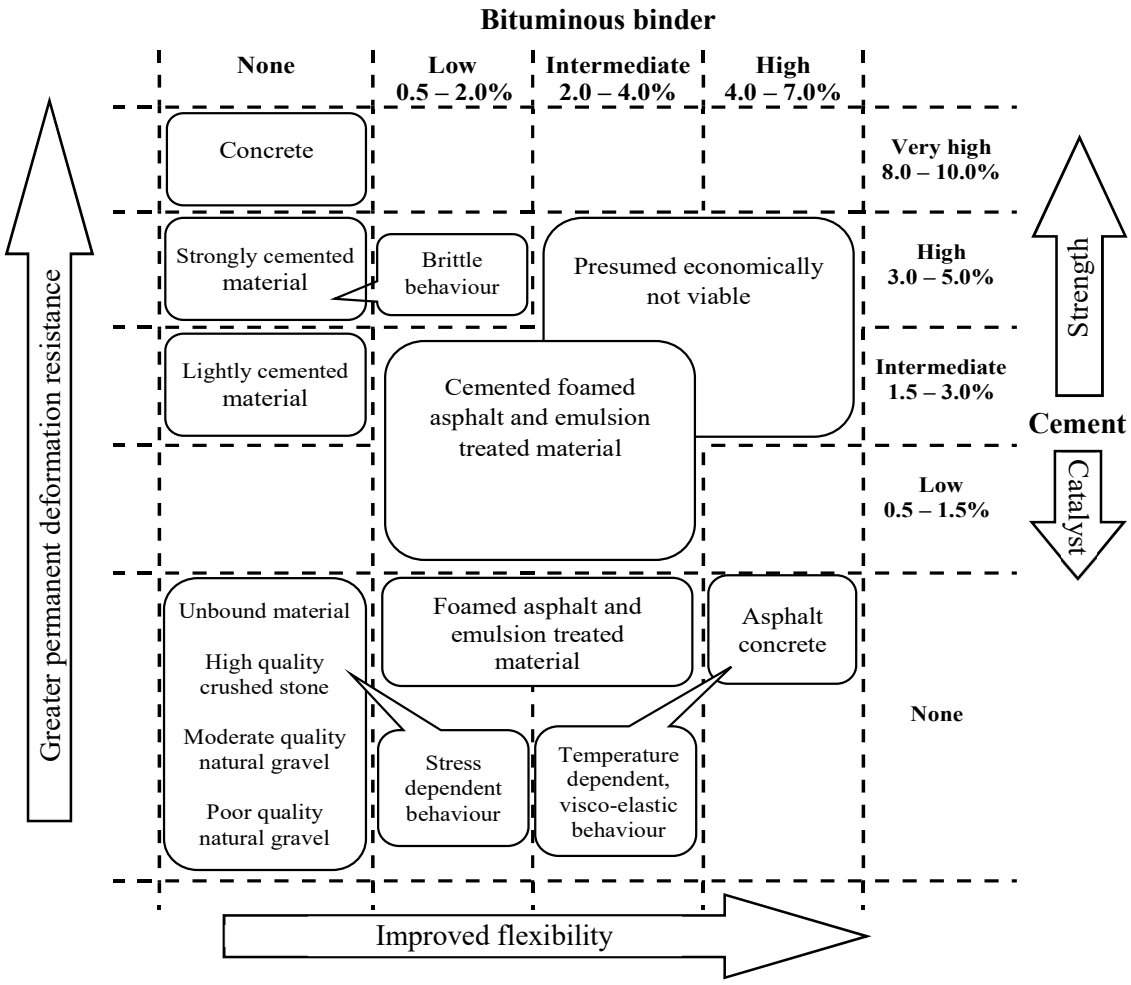

Figure 2.2 Matrix of the basic characteristics of road-building materials (32)

Portland cement can be used along with both asphalt emulsions and foamed asphalt. The addition of 1% - 3% of Portland cement in the bituminous mixtures helps to reduce the stripping problem by enhancing the adhesion of bitumen to the aggregate; facilitating the development of early strength by minimizing the curing time; and increasing the ultimate strength of the treated materials. However, the combined use of the bituminous stabilizers with Portland cement is expensive and the design needs to be done with extreme care to balance the effects of the different stabilizers (2,30). The basic characteristics of the pavement materials when treated with the bituminous binders and Portland cement are well illustrated in the matrix shown in Figure 2.2.

From the foregoing discussion, it can be noted that neither the bituminous stabilizers nor Portland cement imparts the combined qualities of strength, flexibility, and durability. Although the current practice of using the bituminous stabilizers in combination with the Portland cement seems sound performance wise, it is an expensive treatment option.

2.1.4 Mix Design of Cement Treated Full-Depth Reclaimed Materials

The mix design procedures for FDR mixes vary depending on the type of stabilizing agent used. For the cement treated materials, the rational mix design method is the one recommended by the Portland Cement Association (PCA) in their Guide to Full Depth Reclamation with Cement (7,33). Many agencies and researchers have used this approach as it is or by making slight modification to design cement stabilized FDR mixes. The method was adapted from the Soil-Cement Laboratory Handbook of PCA (34).

According to the PCA method, the design steps of the FDR mixes begin with collection of sufficient representative samples of the existing pavement layers. The gradation of the reclaimed material is adjusted, if it fails to meet the project specification, by blending with aggregates from external sources. Then, the optimum moisture content of the soil-cement mixture is determined by moisture-density test, per ASTM D 558. The cement content that is predetermined for different soil group in the PCA Soil-Cement Laboratory Handbook can be used to prepare the initial soil-cement mixture for moisture-density test. Next, trial mixes are prepared with various cement contents and the optimum moisture content. The mixtures are then compacted, cured for 7 days, and subjected to unconfined compressive strength (UCS) test, according to ASTM D 1633. The cement content of the mixture that fulfill the UCS requirement is the candidate optimum cement content. The PCA guide specified that the UCS

within a range of 2.1 MPa (300psi) to 2.8 MPa (400psi) is acceptable for FDR mixes. The moisture susceptibility of the mixture with optimum cement content should be assessed using the tube suction test before the final approval of the mix (35). The wet-dry test, per ASTM D 559, and the freeze-thaw test, per ASTM D 560, are the other two common tests that are conducted to assess the resistance of the proposed mix to moisture and frost effects. The wet-dry and freeze-thaw requirements are said to be fulfilled when the soil-cement losses after 12-cycles of the tests are less than 14% for A-1, A-2-4, A-2-5, and A-3 soils; less than 10% for A-2-6, A-2-7, A-4, and A-5 soils; and less than 7% for A-6 and A-7 soils (34). It was specified that samples with a dielectric constant of less than 10 over a ten days period would fulfill the wet-dry or freeze-thaw requirements satisfactorily (36). Thus, according to the PCA method, the cement content that provides the mixture 7 day UCS within the range of 2.1 MPa (300psi) – 2.8 MPa (400psi) can be selected as an optimum binder content and the moisture susceptibility of the mixture is recommended to be assessed with the tube suction test.

2.1.5 Design of Cement Treated FDR Pavements

FDR pavements are designed in the same manner as the new pavement since the FDR pavements are reconstructed up from the subgrade level (35,37). Most of the current practices of FDR pavement design are based on empirical methods. There is no design parameter for cement treated FDR pavements in the current mechanistic-empirical pavement design procedures. For cement treated FDR base, Halsted et al. (38) and Luhr et al. (35) pointed out that the pavement can be designed by AASHTO 1993 method of pavement design considering the FDR base as cement treated base and assigning a structural coefficient within the range of 0.12 to 0.3. Structural catalogues or design charts are used to design cement treated recycled

base in European countries like Spain, Australia, and UK (37). In California, the FDR pavement is designed empirically by using the granular equivalency method. In this method, the gravel factor, G_f, for the cement treated FDR varies from 0.4 to 1.2 based on the depth of pulverized materials and the percentage of the reclaimed asphalt.

3. METHODOLOGY AND MATERIALS

This was experimental research conducted mainly based on laboratory testing. The first step of the research was sample collection and material quality assessment. The reclaimed material samples were collected from four full-depth reclamation projects located at different parts of Ontario, Canada. The four sampling locations were Bruce County, Niagara-on-the-Lake, Kossuth Road and Nafziger Road. The sample locations are shown in Figure 3.1 and Figure 3.2. For simplicity, the reclaimed materials were designated based on the sample locations as shown in Table 3.1. These designations were used for the discussions throughout the thesis.

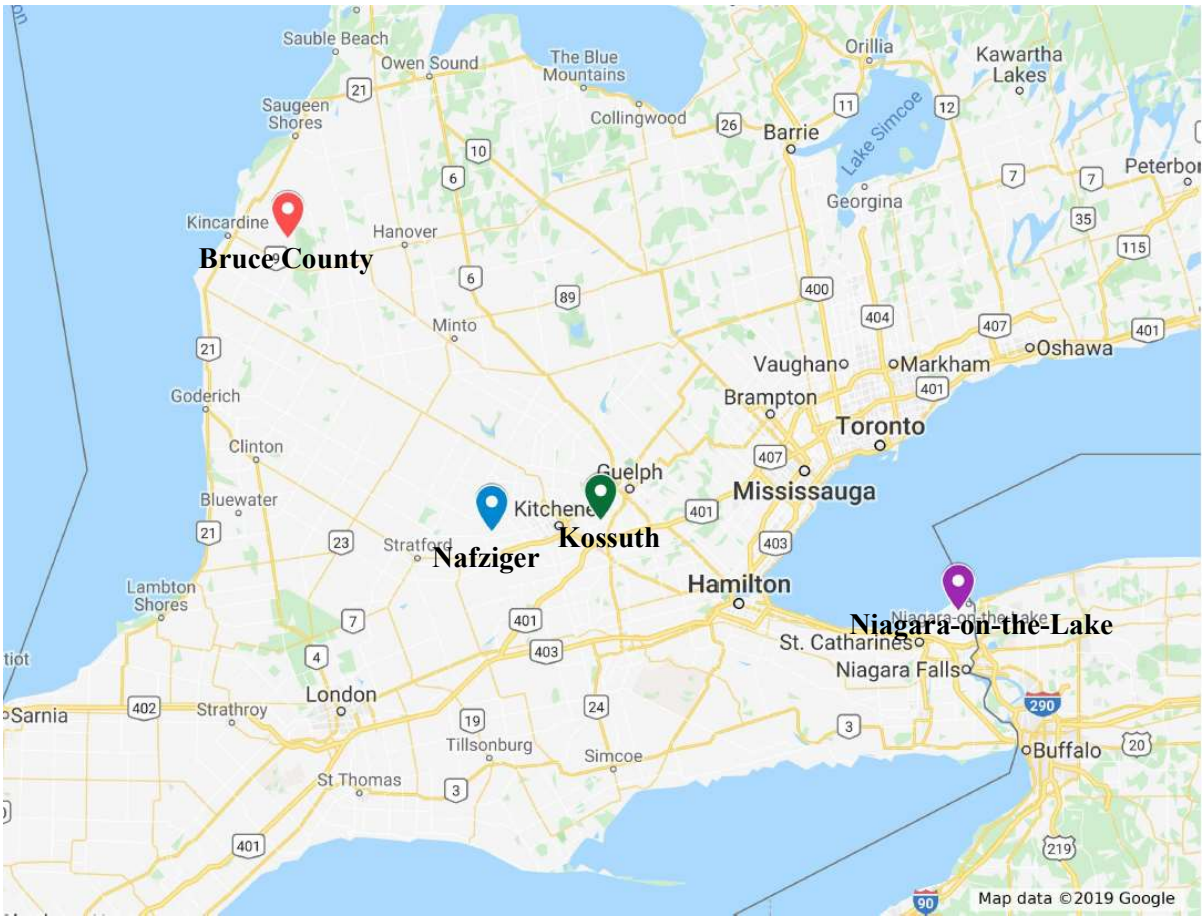

Figure 3.1 Reclaimed material sample locations

Figure 3.2 Full-depth reclamation projects A) Niagara-on-the- Lake, B) Bruce County, C) Kossuth, D) Nafziger

Table 3.1 Designation of Reclaimed Materials

Designation	Reclaimed Material Source
FDR-BC	Bruce County
FDR-NL	Niagara-on-the-Lake
FDR-Koss	Kossuth Road
FDR-NAF	Nafziger Road

Four types of cementious binders, three types of hydraulic road binders and General Use (GU) cement, were used in this study. All of the cementitious binders were supplied by Lafarge Canada Inc. The GU cement was mainly used to make control specimens. The three

hydraulic road binders were designated as HRB1, HRB2 and HRB3 for the discussions throughout the thesis.

The reclaimed materials were subjected to various tests to identify their quality and index properties. The second step was designing the mixture compositions to identify the optimum moisture content, maximum dry density and optimum binder contents of each mixture. Then various test specimens were prepared and cured for the designated period. The cured specimens were subjected to characterization and performance tests. The type and number of tests conducted for the study are shown in Table 3.2. Finally, the test results were analysed and interpreted in-line with the research hypothesis and objectives. The research methodology was outlined in Figure 3.3.

Table 3.2 List of Laboratory Tests Conducted for the Research

Test Description	Test Method	Number of Test/Specimens
Particle Size Analysis	ASTM D 6913	8
Liquid Limit	AASHTO T 89	8
Plastic Limit	AASHTO T 90	8
Micro-Deval Abrasion Loss	ASTM D 6928	8
Methylene Blue Value	AASHTO TP 57	8
pH	ASTM D 4972	8
Standard Proctor Test	ASTM D 558	16
Freeze-thaw	ASTM D 560	36
Unconfined Compressive Strength	ASTM D 1633	96
Modulus of Elasticity	ASTM C 469	30
Indirect Tensile Strength	AP-T101/08	99
Fatigue Test	AASHTO T 321	48
	Total Number of Tests	**373**

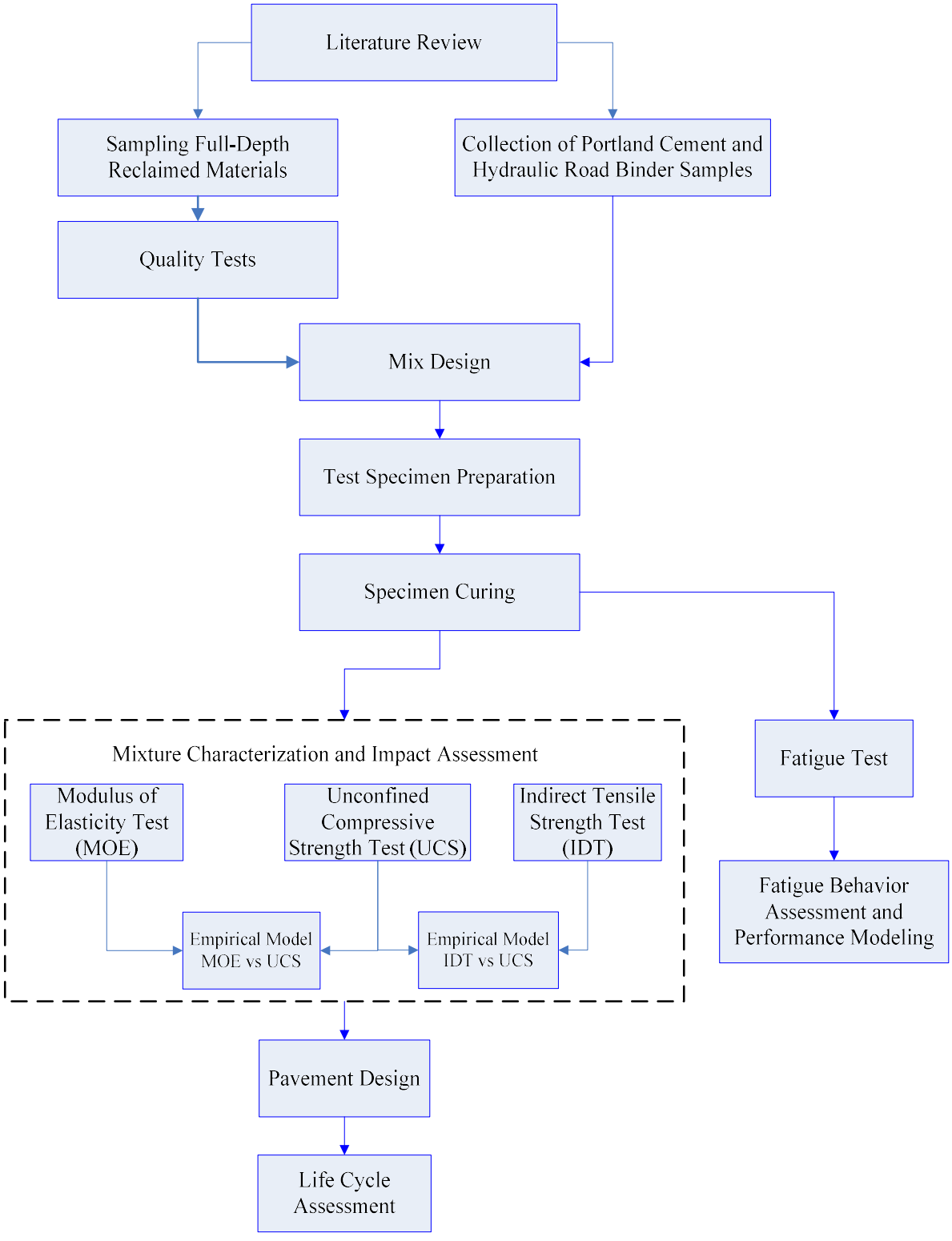

Figure 3.3 Outline of Research Methodology

4. CHARACTERIZATION OF FULL-DEPTH RECLAIMED PAVEMENT MATERIALS TREATED WITH HYDRAULIC ROAD BINDERS

Summary

Hydraulic road binders (HRB) are factory made blends which are composed of a substantial amount of supplementary cementitious materials and Portland cement. Previous studies indicated that the use of chemical stabilizers containing supplementary cementious materials is a sustainable approach that can reduce carbon dioxide (CO_2) emission by 5% - 25%. Thus, the use of HRB in full-depth reclamation process could make the practice more sustainable if strength, stiffness, and durability of treated materials are not compromised. The primary objective of this study is to evaluate the mechanical properties of full-depth reclaimed pavement materials treated with hydraulic road binders. The study was conducted in the form of comparative assessment by using full-depth reclaimed pavement materials treated with General Use (GU) cement as a control mix. For this study, three types of full-depth reclaimed pavement materials and four types of cementitious binders, including GU cement, were used to make eleven different types of mixes. Unconfined compressive strength, modulus of elasticity, and indirect tensile strength tests were used to assess the mechanical properties of the eleven mixes. The test results indicated that hydraulic road binders could provide equivalent strength and stiffness as GU cement. The study also revealed that the HRB content, required to attain equivalent strength and stiffness as GU mixes, is the same or less than GU cement content. Based on the study findings, hydraulic road binders can be sustainable alternative binders that can replace GU cement in full-depth reclamation process without compromising the structural function of the treated layer.

4.1. Introduction

In an effort to meet sustainability requirements and comply with environmental regulations, the cement industries are looking for a variety of options that lead towards sustainable cement production. Among these options is partial replacement of the clinker in Portland cement with supplementary cementitious materials (SCM) (39,40). Previous studies show that, approximately, 5% of the global CO_2 emission comes from cement industries (4,5) and this can be reduced by 5% - 25% if the clinker in the Portland cement is partially replaced by SCM (6,14). For example, replacing 40% of the clinker in Portland cement by SCM would eliminate up to 400 million tonnes of CO_2 emissions per annum (41). According to the assessment of Portland Cement Association (PCA), production of cement containing supplementary cementitious materials with U.S industry average composition emits 10%-15% fewer greenhouse gases, requires 12% less energy and consumes 6% fewer material resources than production of Portland cement (42,43). It follows that cements containing significant amount of SCM could be the preferred alternatives with less adverse environmental impacts as compared to the ordinary Portland cement.

The use of cements with substantial amount of SCM, however, becomes plausible provided that the engineering performance of the mixes they make is not compromised. When the clinker in cement is partly substituted with SCM, the properties of the original cement would be changed. The change could be significant to the extent that affects the strength and durability of the mixes (40) or it could be inconsequential depending on the type and amount of SCM replacing the clinker. One way to identify the effects of the cement with the modified composition is laboratory characterisation tests.

In this study, material characterisation tests were performed to evaluate the strength, stiffness and durability of full-depth reclaimed pavement materials (FDRm) treated with hydraulic road binders. Hydraulic road binders (HRB) are types of chemical stabilizers which are made by blending substantial amount of supplementary cementitious materials (SCM) with Portland cement clinker. The SCM used in HRB can be granulated blast furnace slag, pozzolans, fly ash, burned shale, and limestone (44). Typical composition of the main constituents of Portland cement and SCM is shown in Fig. 4.1.

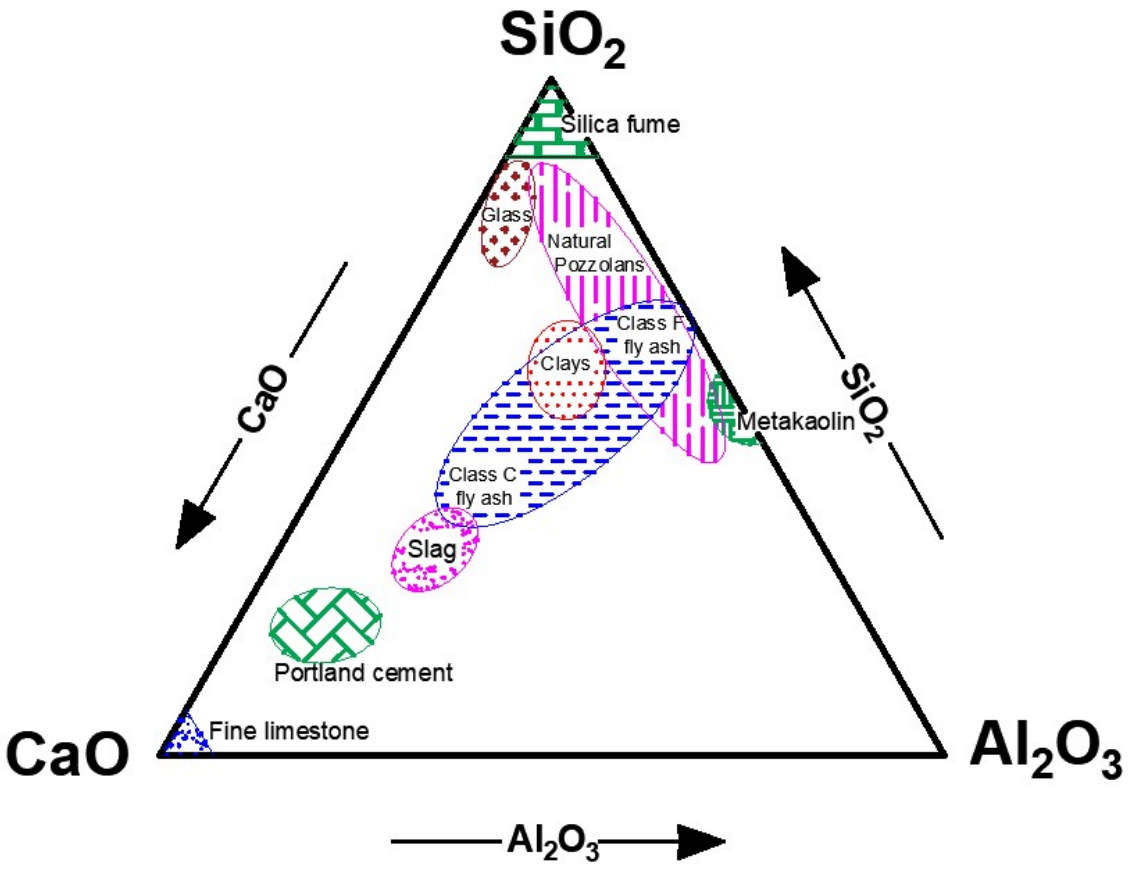

Figure 4.1 Typical Compositions of Cementitious Materials [adapted from (10,11,45)]

Hydraulic road binders are not standardized in North America. Based on their composition, however, HRB can be fairly described with the ASTM C 219 (16) definition for blended cement, which is read as:

'*hydraulic cement consisting of two or more inorganic constituents (at least one of which is not Portland cement or Portland cement clinker) which separately or in combination contribute to the strength gaining properties of the cement, (made with or without other constituents, processing additions and functional additions, by intergrinding or other blending).*'

The standard definition of HRB is given in the European standard EN 13282 (44) as:

'a factory produced hydraulic binder, supplied ready for use, having properties specifically suitable for treatment of materials for bases, sub-bases and capping layers as well as earthworks, in roads, railways, airports and other types of infrastructures.'

The presence of silica-rich SCM in hydraulic road binders changes the composition of the calcium silicate hydrate (C-S-H) by reducing the C/S ratio. Most SCM are characterized by low calcium/silica ratio (C/S) as they contain less calcium compared to Portland cement. As a result, hydrates of SCM are different from that of Portland cement. This difference in the composition of hydration products affects their strength and durability (10). Blending SCM into Portland cement also influences water demand, setting time, heat evolution and pore structure (11) of the binders.

Although HRB are formulated to treat road materials, their use in full-depth reclamation processes is not common. There is hardly any published work (to the authors best

knowledge) that presents the properties of full-depth recycled pavement materials treated with hydraulic road binders. Most of the previous studies have been done on reclaimed pavement materials treated with ordinary Portland cement. The primary objective of the study is, thus, to investigate the mechanical properties HRB treated FDRm and assess the effects of various hydraulic road binders on the strength, stiffness and durability of the treated FDRm.

For the purpose of this study, three types of FDRm and three types of hydraulic road binders were used. Additionally, GU cement was used to make control mixes. Overall, eleven FDRm-binder mixes were prepared for the study. The three FDRm, used in this study, represent materials with low, medium, high RAP percentages. Unlike most of the previous studies, the blends of RAP and the virgin aggregates were not produced in the laboratory, rather the blends were directly collected from the full-depth reclamation project sites. The study, however, was performed purely based on laboratory experiments. The tests involved in this study are unconfined compressive strength, modulus of elasticity, indirect tensile strength and freeze-thaw.

4.1.1. Review of Previous Studies

Several studies have been conducted over the last half century on reclaimed pavement materials treated with ordinary Portland cement (also known as General Use (GU) cement) (8–17). Some of these are reviewed and presented in this section.

Kolias (47) investigated the effects of reclaimed asphalt pavement (RAP) on the mechanical properties of cement-treated mixtures by blending milled bituminous concrete with crushed limestone aggregate with different blending ratio. In this study, the influence of RAP on the compressive strength, tensile strength, and modulus of elasticity of 7 days, 28

days and 1 year cured specimens were examined using five different types of mixtures. The RAP/limestone aggregate proportions, in percent, of the five mixes were 100/0, 75/25, 50/50, 25/75 and 0/100. All the five mixes were stabilized with 5% cement. The compressive strength tests were done on 100 mm X 100 mm X 100 mm cube specimens while the modulus of elasticity tests were conducted on 100 mm X 100 mm X 200 mm specimens. The tensile strength was determined using the diametrical split tensile test. The split tensile strength tests were performed on 100 mm diameter and 200 mm high cylindrical specimens. Some of the test results are shown in Table 4.1. The study findings indicated that increasing the RAP percentage would decrease the strength and modulus of elasticity of the mix. This was attributed to the poor adhesion properties of the cement paste with the asphalt coated aggregates and the weak asphalt bound lumps of fine fractions in the RAP. The study also pointed out, with increasing RAP percentage, the static modulus of elasticity values decreased at a higher rate than the corresponding complex modulus values. Similar study (48) indicated, as the RAP percentage increased, the flexural strength decreased at a lower rate than the corresponding compressive strength.

Likewise, Guthrie et al. (50) evaluated the effects of RAP on the strength and durability of cement-treated materials using unconfined compressive strength (UCS) and tube suction tests (TST). The UCS test was performed according to ASTM D 1633 in which the loading rate is 0.05 inch/ minute. Texas Department of Transportation Test Method, Tex-144-E, was used to conduct the tube suction test. The study was performed on mixtures containing 20% to 100% RAP and cement contents varying from 0.5 to 2%. The UCS of the mixes with 0% RAP ranges from 50 psi (0.34 MPa) to 820 psi (5.65 MPa) while the UCS of the mixes with 100% RAP is in the range of 50 psi (0.34 MPa) to 340 psi (2.34 MPa). The study findings

indicated that as the RAP content increases, the UCS and dielectric values of the mixes decrease. This implied that increasing the RAP content negatively affected the strength but improved the durability of the mixtures.

Table 4.1 Summary of Laboratory Test Results from Previous Studies

Source	RAP Content (%)	Cement Content (%)	Compressive Strength (MPa)		Tensile Strength (MPa)		Modulus of Elasticity (MPa)
			7 days	28 days	7 days	28 days	28 days
(47)	0	5	15.96	19.56	0.75	1.32	32,170
	25	5	-	-	-	-	19,000
	50	5	8.40	10.74	0.56	0.87	14,000
	75	5	-	-	-	-	-
	100	5	5.03	5.97	0.43	0.71	7,330
(51)	0	6	12.50	18.05	-	2.03	17,360
	25	6	10.55	14.70	-	1.55	15,430
	50	6	8.30	11.30	-	1.29	12,960
	75	6	6.75	8.95	-	1.12	9,620
	100	6	5.85	8.35	-	1.04	4,689
(49)	0	3	3.60	4.00	-	-	32.5
	20	3	3.45	3.95	-	-	29.5
	40	3	2.00	2.35	-	-	22.4
	60	3	1.25	2.10	-	-	9.0
	0	4	4.00	4.20	-	-	34.5
	20	4	3.80	4.10	-	-	32.0
	40	4	2.25	2.90	-	-	24.4
	60	4	2.05	2.40	-	-	11.0
	0	5	4.40	4.50	-	-	37.0
	20	5	4.15	4.30	-	-	36.2
	40	5	2.85	3.70	-	-	28.3
	60	5	2.25	2.95	-	-	13.0
	0	6	4.75	5.20	-	-	39.3
	20	6	4.50	4.90	-	-	38.4
	40	6	3.25	4.15	-	-	31.7
	60	6	2.80	3.40	-	-	14.0

Saloua El et al. (51) assessed the compressive strength, modulus of elasticity, flexural strength and indirect tensile strength of five mixtures RAP/aggregate mixtures

containing 6% cement (by weight of the total dry mix). The compressive strength was done according to French standard, NF P 18-455 on 16 cm diameter and 32 cm long cylindrical specimens. Similarly, the indirect tensile strength test was conducted per French standard NF P 12390-6 on cylindrical specimen having the same dimension as the compressive strength test. The elastic modulus test, in contrast, was performed using pulse velocity method according to ASTM C 597-02. Summary of the test results is shown in Table 4.1. The study results indicated all the compressive, tensile, and flexural strength, and stiffness of the mixes decreased as the RAP percentage increased.

Similarly, Ghanizadeh et al. (49) investigated the mechanical properties of cement treated reclaimed asphalt pavement materials. In this work, the authors assessed how the UCS, elastic modulus and CBR are affected as the RAP proportion and cement content of the mix vary. The test samples were prepared by blending RAP samples with GW-GC and SP-SC gravels. The UCS test was done per ASTM D 1633 while CBR test was done according to ASTM D 1883. The UCS and modulus of elasticity of GW-GC mixes are shown in Table 1. The elastic modulus values of the mixes in this study is substantially smaller than the values on the other literatures as shown in Table 4.1. The main reason for this discrepancy is not clear as not much information was given about elastic modulus test in Ghanizadeh et al (49).

In general, the studies on the mechanical properties of cement treated materials showed stiffness and strength decrease with increase in RAP proportion (47,48,50–54). Nevertheless, cement treated materials containing RAP was proven to make a suitable base layer provided that they are properly designed (46,51,55).

4.2. Materials and Methods

4.2.1. Full-depth reclaimed materials

Samples of the reclaimed materials were collected from three FDR projects in Northern and Southern Ontario, Canada. The project in the North was on County Road 1 in Bruce County. The existing pavement of the County Road 1 was composed of a granular base and sub-base layers with high float surface treatment and micro-surfacing surface layers. The County Road 1 FDRm contained 40% RAP (chip seal and micro-surfacing) and 60% granular material. The FDR projects in the South were on the Line 8 Road close to the town of Niagara-on-the-Lake and on Kossuth Road in the City of Cambridge, Ontario. The pavement of Line 8 Road was constituted of granular base and sub-base with chip seal surfacing. The Line 8 Road material was composed of 20% RAP (chip seal material) and 80% granular material. Similarly, Kossuth Road had pavement structure with granular base and sub-base layers but with asphalt concrete surfacing. The RAP proportion of the FDRm from Kossuth Road was 60%. Accordingly, depending on their composition, the materials from Line 8 Road (FDR-NL), County Road 1 (FDR-BC) and Kossuth Road (FDR-Koss) can be considered as reclaimed materials with low, medium and high RAP percentages, respectively.

Particle size analysis, Atterberg limits, Methylene Blue Value, Micro-Deval Abrasion Resistance and pH tests were conducted on the collected material samples. The results of the tests are presented in Table 4.2 and Figure 4.2.

Table 4.2 Properties and Compositions of Reclaimed Materials

Test Description	Test Method	Test Results		
		FDR-BC	FDR-NL	FDR-Koss
Composition, RAP : Granular		40:60	20:80	60:40
Liquid Limit (%)	AASHTO T 89	Non-plastic	22	Non-plastic
Plasticity Index	AASHTO T 90	Non-plastic	5	Non-plastic
AASHTO Soil Class	AAHTO M 145	A-1-b	A-1-a	A-1-a
Micro-Deval Abrasion Loss (%)	ASTM D 6928	10.8	45.6	12.7
Methylene Blue Value (mg/g)	AASHTO TP 57	1.3	8.7	2.7
pH	ASTM D 4972	8.5	7.5	9.0

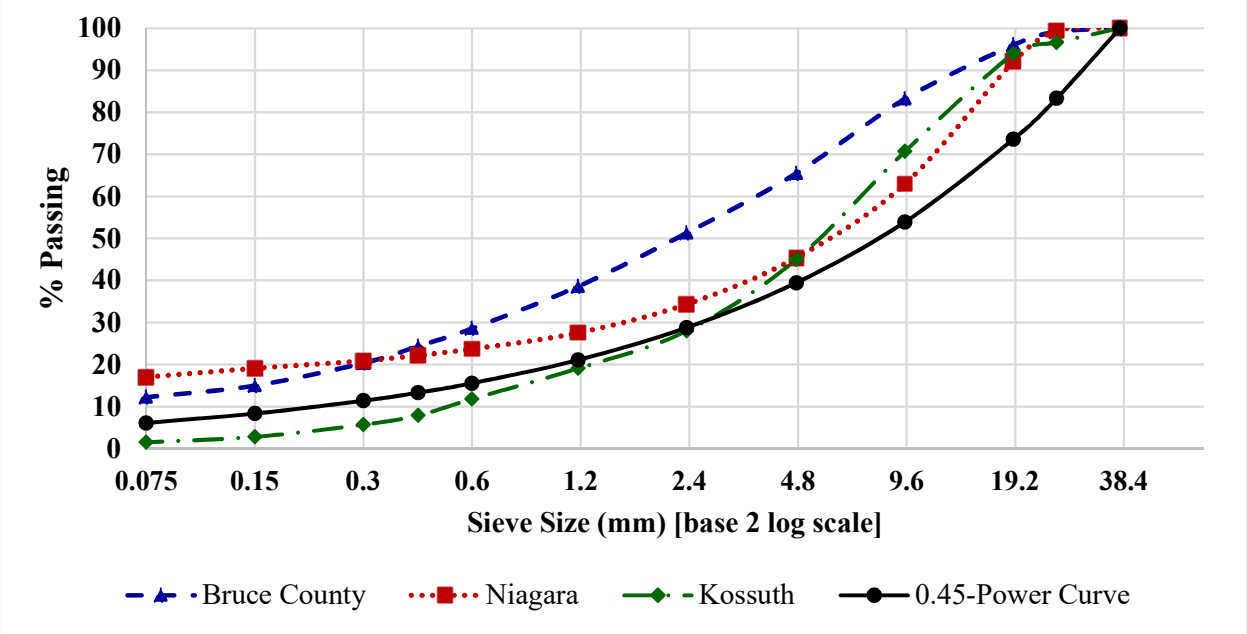

Figure 4.2 Particle size distribution of the reclaimed materials

4.2.2. Binders

The physical properties and chemical compositions of the three hydraulic road binders and GU cement used in this research are shown in Table 4.3 and Table 4.4, respectively. As shown in Table 3, the initial setting times of the three HRB are way higher than that of GU cement. It follows that when using HRB in the full-depth reclamation process, the allowable time gap between the mixing and compaction operations is higher than the time gap allowed when

using GU cement. Table 4.4 shows, the three hydraulic road binders contain higher silica and lower Calcium Oxide than the GU cement. This is due to the substantial amount of SCM present in the HRB. As a result, the calcium/silica ratio of the three HRB are lower than the GU cement.

Table 4.3 Physical Properties of HRB and GU Cement

Physical Properties	GU	HRB-1	HRB-2	HRB-3
Fineness 45μm sieve, % retained	4	5.0	1.9	4.1
Blaine Fineness, m^2/kg	383	465	497	389
Autoclave, % Expansion	0.05	0.0	0.0	0.0
Initial time of set, minutes	90	161	173	153
Compressive Strength at 28 days, MPa	40.5	34.8	41.5	35.0
Sulphate Resistance, % expansion at 6 months	0.014	-	0.005	0.040

Table 4.4 Chemical Compositions of HRB and GU Cement

Chemical Components	GU	HRB-1	HRB-2	HRB-3
SiO_2 (%)	19.6	28.4	22.3	26.2
Al_2O_3 (%)	5.0	7.6	5.7	7.0
Fe_2O_3 (%)	3.3	2.1	2.3	2.3
CaO (%)	62.2	49.4	55.4	53.4
MgO (%)	2.5	7.2	4.7	5.9
SO_3 (%)	3.9	3.3	3.7	3.6
Loss on ignition @ 950 (%)	2.3	1.5	4.3	1.7
Equivalent alkalis, % (as Sodium Oxide)	0.66	0.6	0.7	0.6
CaO/SiO_2	**3.17**	**1.74**	**2.48**	**2.04**

4.2.3. Experimental program

4.3.1.1. Mix Design

Mix design of FDRm-binder mixtures was performed using the PCA method to determine the optimum moisture content and optimum binder content of the mixes. The design was done for three FDR-BC, four FDR-NL and four FDR-Koss, totally for eleven mixes. FDR-NL and FDR-Koss mixes were prepared with all the four binders, while FDR-BC mixes were prepared with GU, HRB1 and HRB3 binders.

In the PCA method of mix design, the first step is the determination of optimum moisture content (OMC). This is done per ASTM D 558, Moisture-Density Relations of Soil-Cement Mixtures (56). Initial cement contents recommended for this test are obtained from PCA's Soil-Cement Laboratory Handbook (34) for different AASHTO soil classes. According to the handbook, for A-1-a and A-1-b soil classes, the recommended initial cement contents are 5% and 6% respectively. However, cement contents one or two percent above or below the initial cement contents do not significantly affect optimum moisture content (7,33,49). Consequently, initial cement contents of 5% and 6% were used to determine optimum moisture contents of the eleven mixes.

The second step in the mix design process is the determination of binder content that provides the required strength. This is done by making a series of duplicate or triplicate UCS specimens with different binder contents. UCS of the specimens is tested after 7 days of moist curing per ASTM D 1633. In this study, a strength range of 2.1 MPa (300psi) – 2.8 MPa (400 psi) was used to select optimum binder content (OBC). These strength thresholds are

recommended for balanced design which accounts both strength and durability of cement-treated materials (7).

The last step is evaluating the adequacy of the selected cement content based on durability criteria. For this purpose, the freeze-thaw test was performed according to ASTM D 560 (57), and the requirements specified in PCA Soil-Cement Laboratory Handbook was used. According to ASTM D 560, triplicate specimens with 101.6 mm diameter and 116.4 mm height should be prepared, moist cured for 7 days, and subjected to 12-cycles of freezing and thawing. After each cycle of freezing and thawing, the specimens should be rubbed along its sides and two faces by two strokes of purpose designed wire brush. At the end of the 12-cycles of freezing-thawing, the soil-cement loss (reduction in the weight) of a durable specimen should be within the specified limits. PCA's Soil-Cement Laboratory Handbook specified that for durable mixes the maximum soil-cement loss after 12-cycles of freezing and thawing shall not exceed 14% for A-1, A-2-4, A-2-5, and A-3 soil groups; 10% for A-2-6, A-2-7, A-4, and A-5 soil groups; and 7% for A-6 and A-7 soil groups (34).

4.3.1.2. Mechanical Characterization

- *Unconfined Compressive Strength (UCS)*

Unconfined compressive strength test was conducted on 7, 28 and 56 days moist cured specimens according to ASTM D 1633, method A. (58). The tests were performed on cylindrical specimens with 101.6 mm diameter and 116.4 mm height. The specimens were prepared by standard proctor test apparatus and compaction effort. After compaction, the specimens were kept at room temperature and humidity for 6 – 10 hours so that they set adequately. At this stage, the specimens were wetted manually to compensate for the moisture loss due to hydration and evaporation. The specimens were then moved to a curing room and

cured at 100% relative humidity and room temperature throughout the curing period. After curing for the desired number of days, the specimens were taken out of the curing room, capped with gypsum plaster and soaked in water for 4-hours prior to the test. While running the test, the specimens were wrapped with wet paper towel to keep the specimens moist. The UCS test was performed on displacement-controlled mode with a loading rate of 1.3 mm/minute. The test set-up and test specimens are shown in Figure 4.3.

Figure 4.3 a) UCS specimens; b) shapes of UCS specimens after the test; c) UCS test on progress

- *Modulus of Elasticity (MOE)*

The test method to determine the modulus of elasticity of chemically stabilized materials has not been in standardized in North America. However, the NCHRP guide for ME design recommends ASTM C469 (59) to test modulus of elasticity of chemically stabilized materials

(60). Accordingly, ASTM C469, which is a test method to determine the modulus of elasticity and Poisson's ratio of concrete, was used in this study. The test was conducted on 28 days moist cured specimens with 101.6 mm (4-in) diameter and 203.2 mm (8-in) height. The specimens were compacted in five layers with 25-blows of standard proctor hammer.

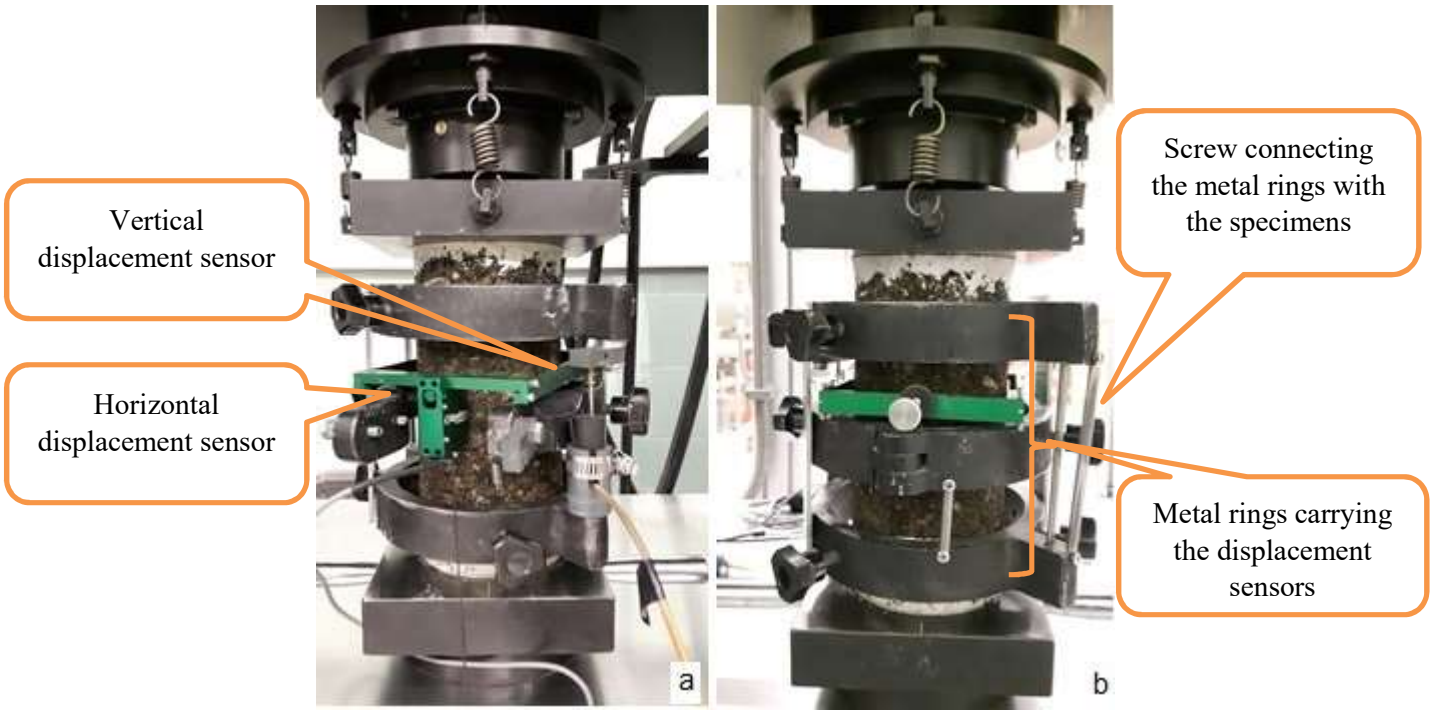

Figure 4.4 Modulus of elasticity test set-up: a) front view, b) rear view

ASTM C469 specifies test specimens shall be loaded at least three times with a load equivalent to 40% of the ultimate strength of the specimen. For this study, the specimens were loaded with six cycles of the 40% of UCS load. The load shall be applied continuously at a constant rate of 250 ± 50 kPa/s [35 ± 7 psi/s]. However, in this study, the test was run in displacement control mode with a loading rate of 1.44 mm/min. This was because the results of the test run in load control mode with the rate of 250 kPa/s was too noisy and did not show any good trend with the load increment. The specimens were capped with gypsum plaster and

soaked for 4-hours before the test and subjected to six cycles of loading and unloading at the specified loading rate. The MOE test set-up is shown in Figure 4.4.

Compared to concrete, cement treated specimens are weak and have softer surfaces. As a result, during the MOE test, cement treated specimens do not firmly hold the screws coming from the metallic frame carrying the displacement sensors. This often becomes the source of variability of the test data and makes the test a bit difficult to run on cement treated materials.

- *Indirect Tensile Strength (IDT)*

Similar to modulus of elasticity test, there is no standard test method to determine the indirect tensile strength of chemically stabilized materials in North America. Thus, in this research, the testing protocol specified in Austroads Technical Report, AP-T101/08, (61) was used. The test was performed on the 28 days moist cured cylindrical specimens with 150 mm diameter and 85 mm height. The load was applied using 19 mm (0.75-in) wide loading blocks that support the specimen along its diametral axis. AP-T101/08 specified a constant loading rate of 20 ± 2 kN/minute for the test. However, in this study, the test was performed on displacement-controlled mode by applying a monotonically increasing load at a rate of 1.3mm/min until no increase in force reading is observed. This was because the results of load-controlled test were noisy and did not show consistent trend with the applied load increment. The test specimens were prepared using gyratory compactor by setting the height as a control of the target level of compaction. As it is recommended to perform the test on saturated specimens, the test specimens were wrapped with plastic wrap right after they were taken out of the curing room.

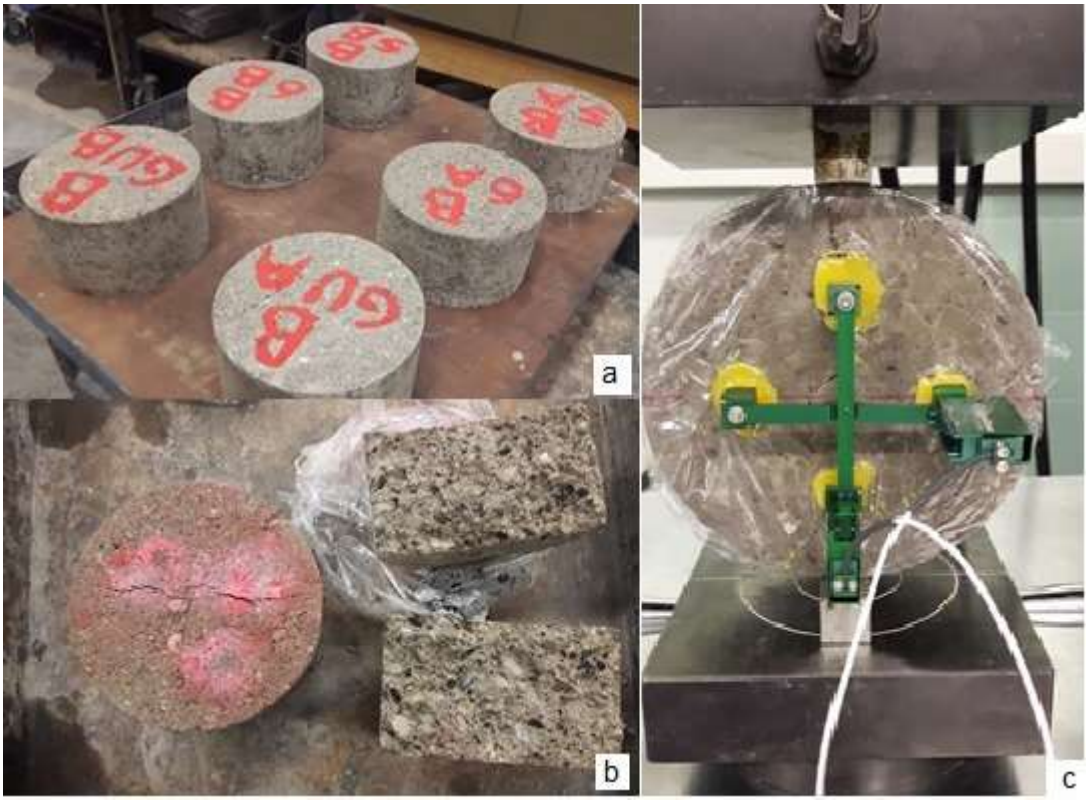

Figure 4.5 a) IDT specimens; b) IDT specimen after the test; c) IDT test on progress

4.3. Results and Discussion

4.3.1. Mix Design Results

4.3.1.1. Optimum Moisture Content (OMC)

Moisture-density relation curves are shown in Figure 6. It can be noted from the curves that the variations in the maximum dry densities and OMC of the different mixes of the same FDRm are not significant. This indicates the different binders used in the mixes have hardly any impact on the level of compaction and OMC. Nevertheless, the maximum dry density (MDD) and OMC of mixtures containing FDRm with higher RAP proportion is lower than the corresponding mixtures containing FDRm with lower RAP proportion. As shown in Figure 4.6, FDR-NL (20% RAP) mixes have the largest whereas FDR-Koss (60% RAP)

mixes have the smallest MDD and OMC. This agrees with the findings of the previous studies on the properties of mixes containing RAP (50,51,55,62) although, in this study, field samples with different types of aggregate were used.

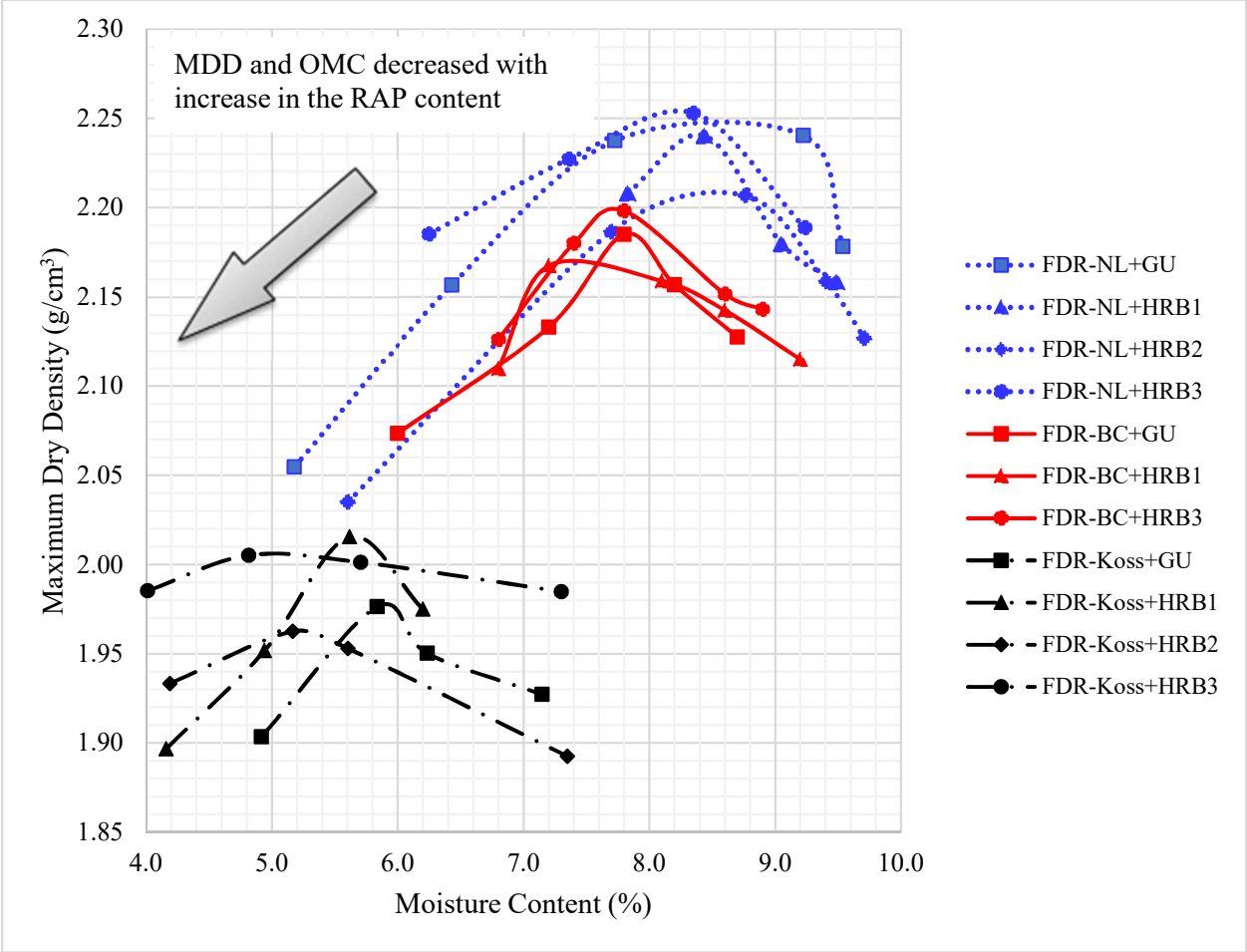

Figure 4.6 Moisture-density relation curves for the eleven FDRm-binder blends

4.3.1.2. Optimum Binder Content

Duplicate or triplicate UCS specimens were produced with different binder contents to identify the optimum binder content that would provide strength within the recommended threshold limit of 2.1 – 2.8 MPa. The optimum moisture contents that were determined by the standard proctor test were used to make all specimens. The average 7 days UCS of these

specimens are shown in Figure 4.7. In Figure 4.7, in the first row of the horizontal axis are binder contents, the second row show the binder types and the third row show the FDRm type. As shown in Figure 4.7, FDR-NL and FDR-BC mixes could attain the PCA's strength thresholds with binder contents 5% or less. However, FDR-Koss mixes could not attain the recommended strength limits even with 6% binder content. As higher binder content often causes shrinkage cracking in cement treated materials, the binder content of FDR-Koss mixes was not increased to more than 6% although the 7 days UCS requirement was not fulfilled.

The lowest binder contents that provided strength within the threshold limits were identified and another triplicate set of cylindrical specimens were made for freeze-thaw test. The average normalized cumulative soil-cement losses of the wet specimens throughout the 12-cycles of freezing and thawing are shown in Figure 4.8. As shown in Figure 4.8, the soil-cement losses of FDR-NL and FDR-Koss specimens were negligible after the first freeze-thaw cycle. In contrast, the soil-cement losses of FDR-BC were significant throughout the twelve cycles. This could be due to the relatively higher binder contents in FDR-NL and FDR-Koss specimens and lower binder contents of FDR-BC specimens. The total soil-cement loss after the 12-cycles of freezing and thawing was way below the threshold limit of 14% for all of the tested mixes.

The optimum binder contents (OBC) at which the mixes fulfill both strength and durability criteria are shown in Table 4.5 along with the optimum moisture content of each mixes. FDR-BC mixes require less binder than FDR-NL mixes for equivalent strength and durability. This is due to the higher amount of harmful clays and lower strength of coarse aggregates in FDR-NL, which were shown by Methylene Blue Value and Micro-Deval Abrasion Resistance tests, respectively. The strength and durability of the eleven mixes which

were prepared with the respective OMC and OBC are shown in Figure 4.9 in terms of UCS and soil-cement loss, respectively.

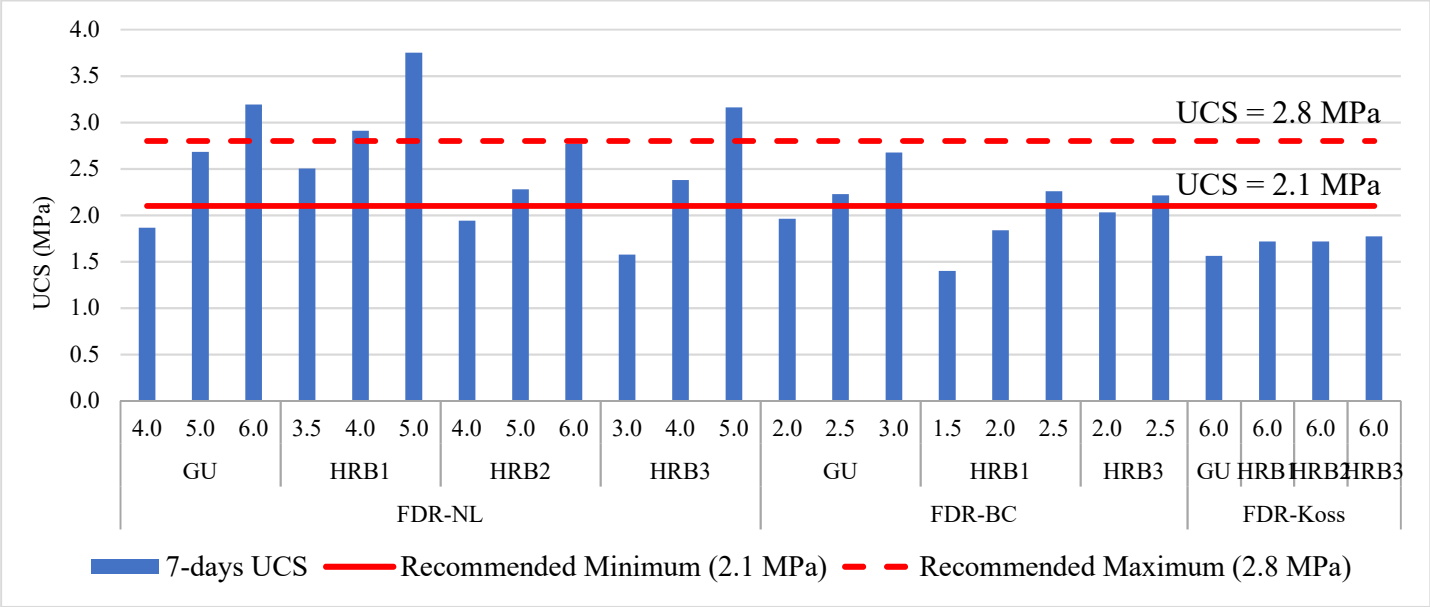

Figure 4.7 Average 7 days UCS of specimens with different binder contents

Table 4.5 Design Moisture and Binder Contents of Eleven Mixes

FDRm	Binder Type	MDD (g/cm^3)	OMC (%)	OBC (%)	Water/Binder (ratio)
FDR-NL	GU	2.25	8.6	5.0	1.7
	HRB1	2.24	8.4	3.5	2.4
	HRB2	2.21	8.5	5.0	1.7
	HRB3	2.26	8.2	4.0	2.1
FDR-BC	GU	2.19	7.8	2.5	3.1
	HRB1	2.17	7.4	2.5	3.0
	HRB3	2.20	7.7	2.5	3.1
FDR-Koss	GU	1.98	5.9	6.0	1.0
	HRB1	2.02	5.6	6.0	0.9
	HRB2	1.97	5.3	6.0	0.9
	HRB3	2.01	5.0	6.0	0.8

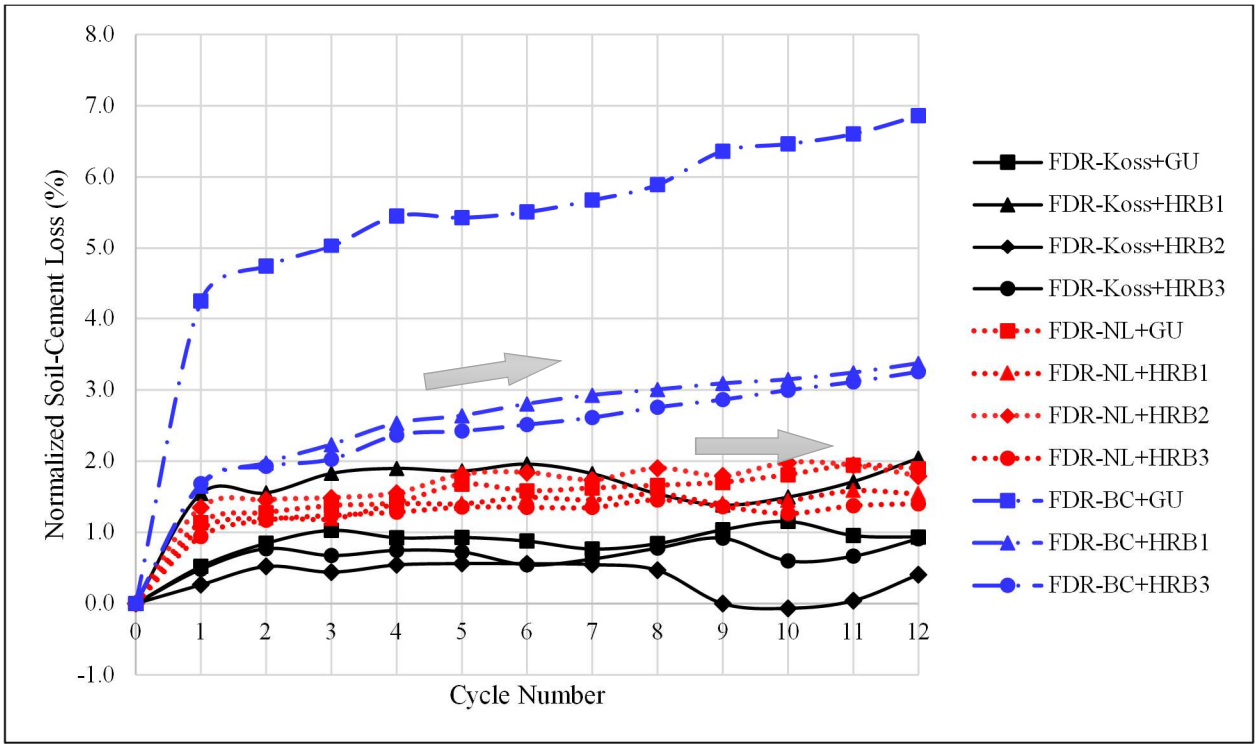

Figure 4.8 Average soil-cement loss of set specimens

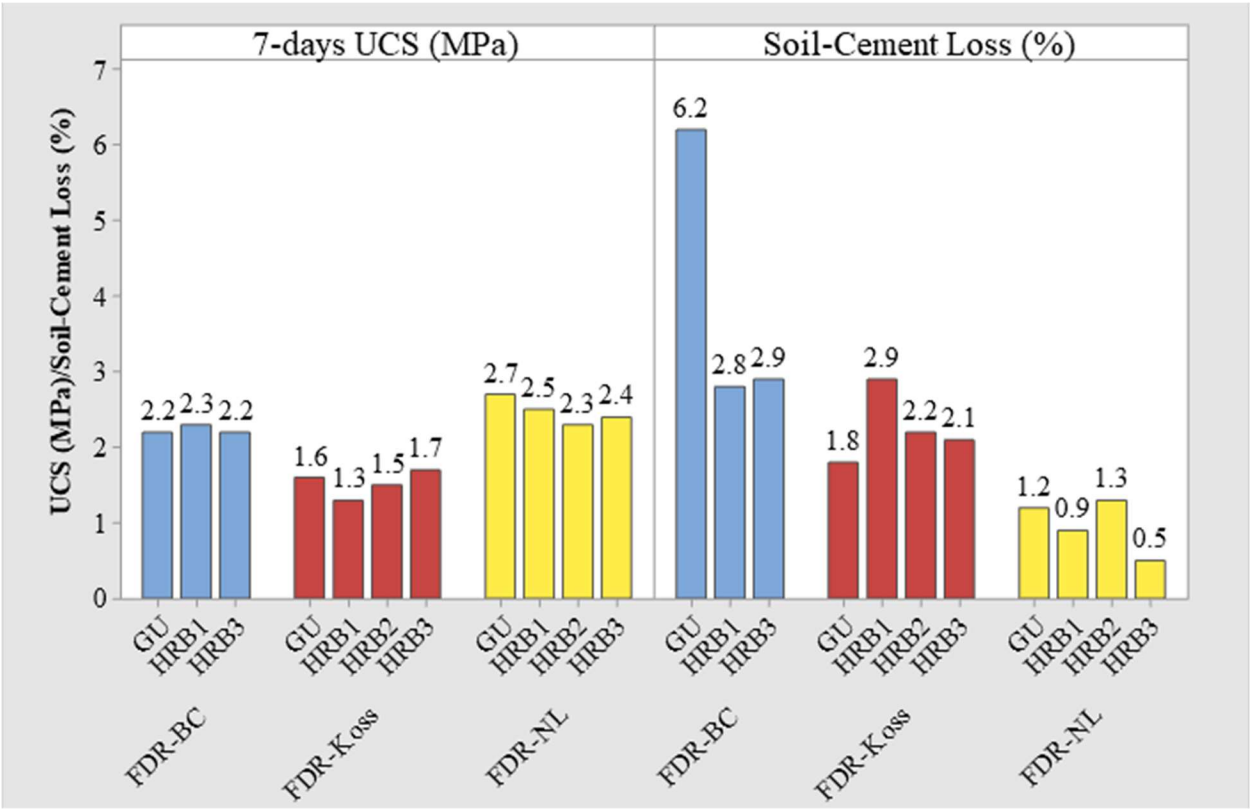

Figure 4.9 Strength and durability of mixes with OBCs

4.3.2. Unconfined Compressive Strength

The unconfined compressive strength of the eleven mixes after 7, 28 and 56 days of moist curing are shown in Figure 4.10. Exploring these data, one may observe the difference in UCS of all the mixes of respective ages is small regardless of the binder types. To prove whether the UCS values are significantly affected by the type of binders in the mixes, single factor ANOVA test was performed on the UCS data. The ANOVA was done using Minitab 18 with a significance level, $\alpha = 0.05$. The hypotheses of the ANOVA test were the following:

Null hypothesis Ho: Hydraulic road binders do not affect the strength of a mix

Alternative hypothesis H1: Hydraulic road binders significantly affect the strength

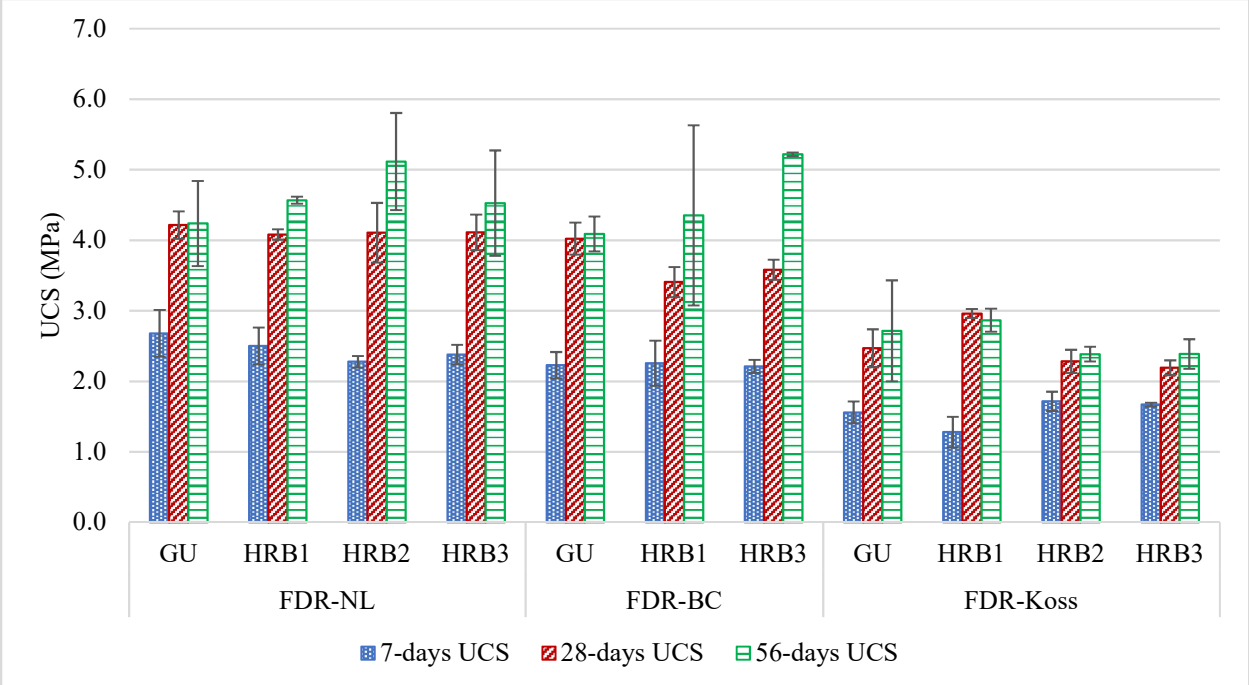

Figure 4.10 Unconfined compressive strength test results

The ANOVA tests were conducted on the overall UCS data and on the datasets split based on curing ages and FDRm types to assess the impact of the binders at different ages with different materials. The results of the ANOVA test are shown in Table 4.6.

The data in Table 4.6 indicated that based on the given dataset, there is no strong evidence to reject the null hypothesis in all but three datasets, namely, 28 days UCS of FDR-BC, 7 days UCS of FDR-Koss and 28 days UCS of FDR-Koss. The cause of the variation in the 28 days UCS of FDR-BC was the change in the test machine. The machine that had been used for UCS test was down on the day the 28 days UCS of FDR-BC+HRB1 and FDR-BC+HRB3 mixes was supposed to be tested. As a result, another heavy-duty machine with 1500 kN capacity was used by setting the loading rate to the same level, 1.3 mm/minute. Thus, the 28 days UCS data of FDR-BC cannot be used to evaluate the effect of the binders on the UCS values because of the experimental bias. To identify the source of variation in the 7 days and 28 days UCS of FDR-Koss specimens, Dunnett's multiple comparison test was performed with 95% confidence intervals (CIs). The Dunnett's test indicated that the difference in the 7 days UCS was statistically insignificant whereas the difference in the 28 days UCS was due to the higher UCS of mixes with HRB1 binder. The results of Dunnett's test on the 7 days and 28 days UCS of FDR-Koss mixes is shown in Figure 4.11.

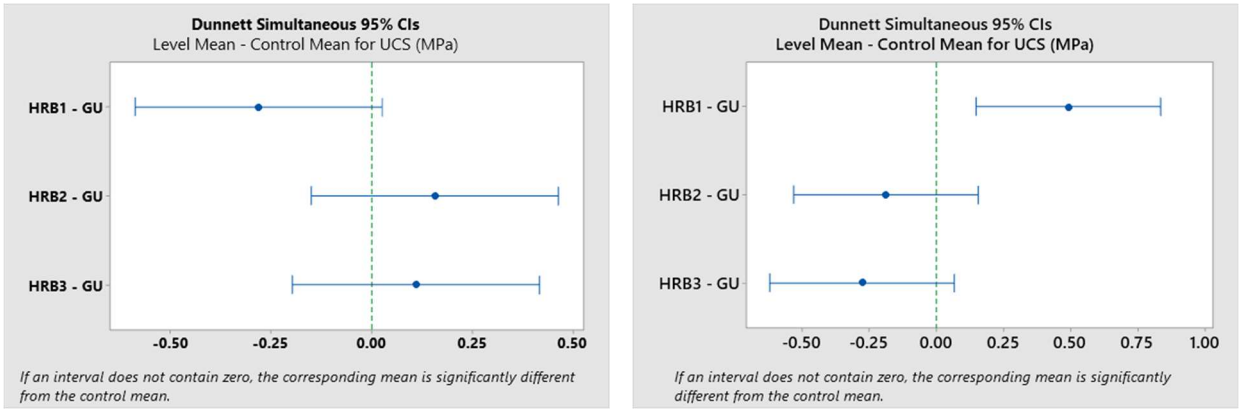

Figure 4.11 Dunnett's multiple comparison test on 7 days (left) and 28 days (right) UCS of FDR-Koss mixes

Dunnett's multiple comparisons test was also performed on the other datasets, shown in Table 4.6, to individually compare the UCS of HRB mixes with the corresponding GU mixes. As shown in Table 4.7, the results of Dunnett's multiple comparisons test perfectly match with the ANOVA results for all but the 7 days UCS of FDR-Koss datasets.

Table 4.6 Summary of ANOVA Test on UCS Data

FDR Material	Dataset	F-Value	P-Value
FDR-NL, FDR-BC, FDR-Koss	7 days UCS, 28 days UCS, 56 days UCS	0.05	0.986
FDR-NL	7 days UCS	2.36	0.147
	28 days UCS	0.19	0.898
	56 days UCS	1.53	0.279
	7, 28, 56 days UCS	0.04	0.989
FDR-BC	7 days UCS	0.04	0.958
	28 days UCS	10.32	**0.011**
	56 days UCS	2.48	0.231
	7, 28, 56 days UCS	0.12	0.883
FDR-Koss	7 days UCS	6.79	**0.014**
	28 days UCS	16.54	**0.001**
	56 days UCS	1.57	0.271
	7, 28, 56 days UCS	0.46	0.714

Assessment in the UCS growth pattern indicated that there was a substantial difference between the 7 days and 28 days strength of all mixes. However, the growth between 28 days and 56 days of curing was statistically insignificant for most of the mixes. The assessment was done using Dunnett's multiple comparison test and the results are shown in Table 4.8.

Overall, based on the statistical tests, both the early-age and long-term compressive strength of HRB mixes were equivalent to the strength of the corresponding GU mixes.

Table 4.7 Dunnett's Multiple Comparisons of UCS Data

FDR Material	Dataset	Difference of Levels (in UCS of mixes with different binder types)	T-Value	Adjusted P-Value
FDR-NL, FDR-BC, FDR-Koss	7,28,56 days UCS	HRB1 – GU	-0.01	1.000
		HRB2 - GU	-0.35	0.974
		HRB3 - GU	-0.12	0.999
FDR-NL	7 days UCS	HRB1 – GU	-1.12	0.571
		HRB2 - GU	-2.52	0.085
		HRB3 – GU	-1.89	0.213
	28 days UCS	HRB1 – GU	-0.70	0.824
		HRB2 – GU	-0.57	0.892
		HRB3 – GU	-0.54	0.908
	56 days UCS	HRB1 – GU	0.79	0.774
		HRB2 – GU	2.10	0.159
		HRB3 – GU	0.69	0.830
	7,28,56 days UCS	HRB1 – GU	0.01	1.000
		HRB2 – GU	0.25	0.989
		HRB3 - GU	-0.08	1.000
FDR-BC	7 days UCS	HRB1 – GU	0.18	0.976
		HRB2 - GU	-0.11	0.992
	28 days UCS	HRB1 – GU	-4.41	0.008
		HRB3 - GU	-3.16	0.034
	56 days UCS	HRB1 – GU	0.50	0.847
		HRB3 - GU	2.13	0.195
	7,28,56 days UCS	HRB1 – GU	-0.29	0.941
		HRB3 - GU	0.21	0.969
FDR-Koss	7 days UCS	HRB1 – GU	-2.64	0.072
		HRB2 - GU	1.48	0.375
		HRB3 – GU	1.03	0.623
	28 days UCS	HRB1 – GU	4.12	0.009
		HRB2 – GU	-1.58	0.328
		HRB3 – GU	-2.32	0.114
	56 days UCS	HRB1 – GU	0.55	0.901
		HRB2 – GU	-1.21	0.515
		HRB3 – GU	-1.20	0.520
	7,28,56 days UCS	HRB1 – GU	0.45	0.944
		HRB2 – GU	-0.45	0.943
		HRB3 - GU	-0.61	0.872

Table 4.8 Results of Dunnett's Multiple Comparisons on Strength Growth Patterns

FDR Material	Binder Type	Difference of Levels (Curing ages)	T-Value	Adjusted P-Value
FDR-NL	GU	7-28	-5.24	0.003
		56-28	0.08	**0.996**
	HRB1	7-28	-14.03	0.000
		56-28	4.32	0.009
	HRB2	7-28	-5.51	0.003
		56-28	3.04	0.040
	HRB3	7-28	-5.31	0.003
		56-28	1.27	**0.397**
FDR-BC	GU	7-28	-12.27	0.000
		56-28	0.41	**0.892**
	HRB1	7-28	-3.10	0.047
		56-28	2.28	**0.123**
	HRB3	7-28	-17.92	0.000
		56-28	19.15	0.000
FDR-Koss	GU	7-28	-2.86	0.050
		56-28	0.77	**0.677**
	HRB1	7-28	-14.67	0.000
		56-28	-0.83	**0.641**
	HRB2	7-28	-5.83	0.002
		56-28	1.07	**0.501**
	HRB3	7-28	-5.45	0.003
		56-28	2.03	**0.150**

4.3.3. Modulus of Elasticity

Typical plot of the modulus of elasticity test data from the six cycles loading is shown in Figure 4.12. The modulus of elasticity values were computed as the slope of the secant line joining the maximum stress point and the stress point corresponding to 50 micro-strain. ASTM C 469 suggests not to include the data from the first cycle in the modulus of elasticity calculation. Hence, the modulus of elasticity of a specimen was determined as the average of the secant moduli which were computed based on the second and subsequent cycles data.

The modulus of elasticity of 28 days moist cured specimens is shown in Figure 4.13. These values vary from 2400 MPa to 15,400 MPa. From Figure 4.13, it can be seen the

modulus of elasticities of FDR-Koss mixes are less than the corresponding FDR-NL and FDR-BC mixes due to the higher RAP content in the FDR-Koss mixes. In contrast, FDR-BC mixes contain more RAP than FDR-NL but the MOE of FDR-BC mixes are higher than the corresponding FDR-NL mixes. This was because of the weaker aggregates and higher injurious clay content of FDR-NL materials (as shown in Table 4.2). This indicates, in this case, the aggregate quality and clay content had more pronounced effect on the MOE than the RAP proportion had.

ANOVA and Dunnett's simultaneous tests were performed to assess the effects of the different binders on the MOE of the mixes. The results of the tests are shown in Table 4.9 and Table 4.10, respectively. The statistical tests on the overall MOE dataset (FDR-NL, FDR-BC and FDR-Koss, altogether) and on MOE of FDR-NL mixes indicated the MOE of the different mixes was not affected by the binder type. On the contrary, the MOE of FDR-BC and FDR-Koss were significantly affected by the binder type. Dunnett's 95% confidence interval showed the sources of the variation in the MOE of the FDR-BC and FDR-Koss mixes were HRB1 and HRB3 binders. As shown in Figure 4.14, the mixes treated with HRB3 binder had significantly higher MOE than the corresponding mixes treated with GU cement. The MOE of FDR-BC mix which were treated with HRB1 binder, however, was significantly lower than the corresponding GU mix. This effect of HRB1 binder, however, was not consistent on the other FDR materials (FDR-NL and FDR-Koss) which contained lower and higher, respectively, RAP than FDR-BC. Thus, the lower MOE of FDR-BC with HRB1 binder could be experimental anomaly.

Overall, the MOE test results indicated that HRB of similar properties as those used in this study could provide equivalent stiffness as GU binder without substantial difference in the binder content.

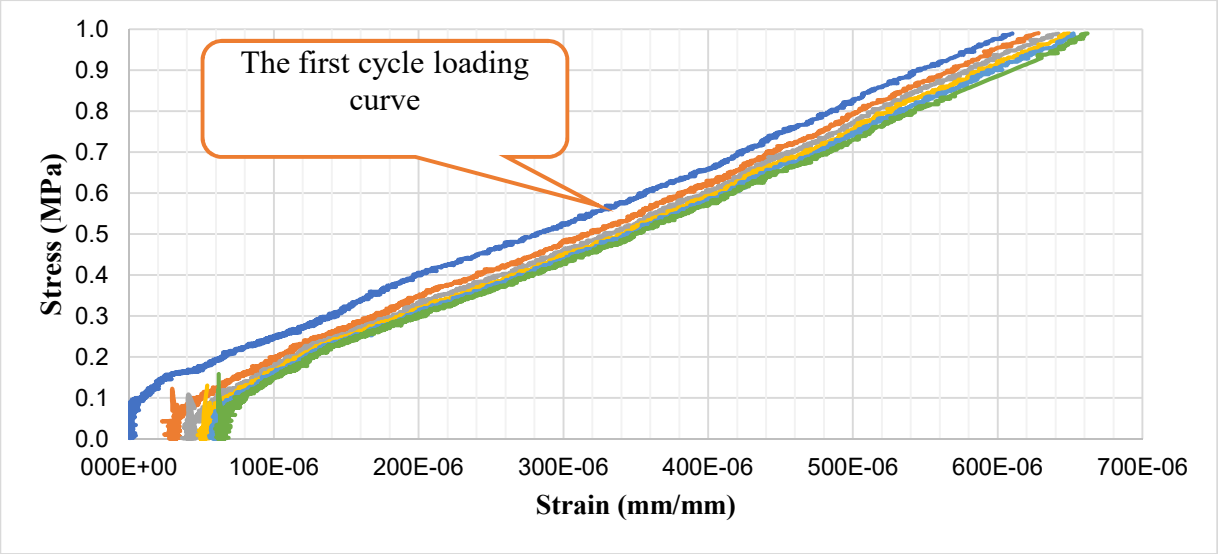

Figure 4.12 Typical plot of modulus of elasticity test data

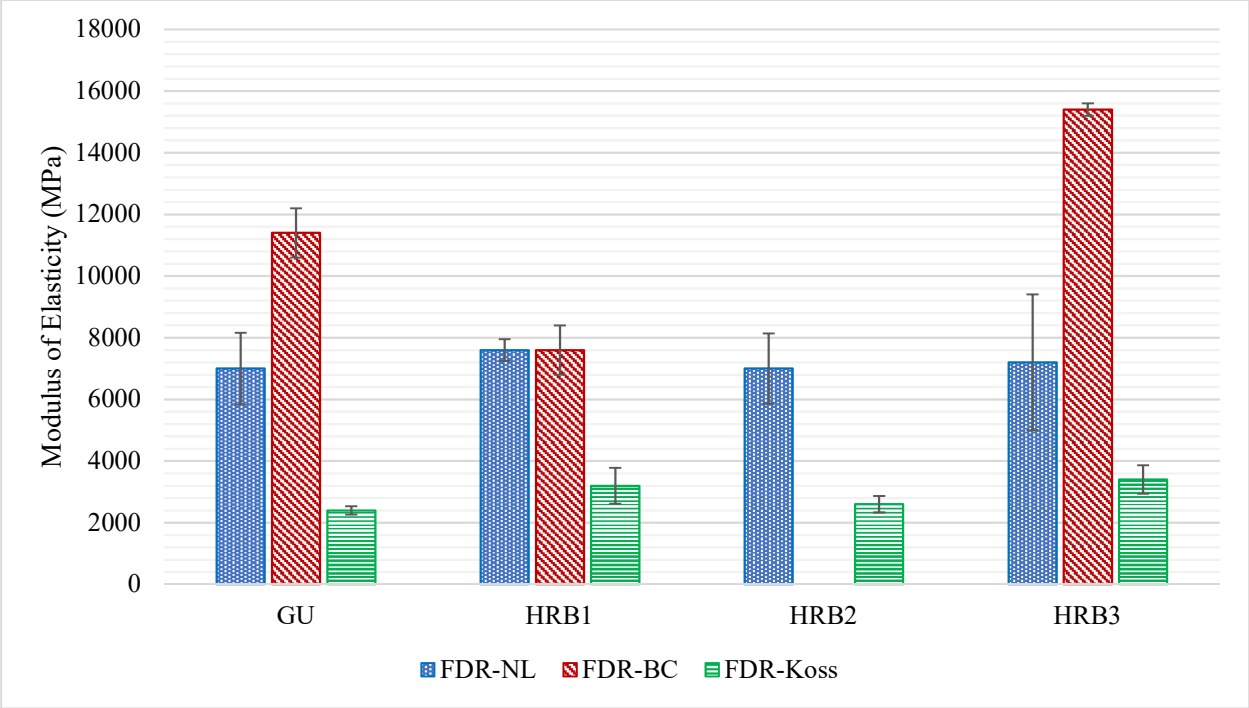

Figure 4.13 Modulus of Elasticity of 28 days cured specimens

Table 4.9 Summary of ANOVA Test on MOE Data

FDR Material	F-Value	P-Value
FDR-NL, FDR-BC, FDR-Koss	0.80	0.504
FDR-NL	0.17	0.914
FDR-BC	134.76	**0.001**
FDR-Koss	5.21	**0.028**

Table 4.10 Dunnett's Simultaneous Tests on MOE Data

FDR Material	Difference of Levels (in MOE of mixes with different binder types)	T-Value	Adjusted P-Value
FDR-NL, FDR-BC, FDR-Koss	HRB1 – GU	-0.26	0.988
	HRB2 – GU	-0.82	0.757
	HRB3 – GU	0.75	0.801
FDR-NL	HRB1 – GU	0.61	0.871
	HRB2 – GU	0.00	1.000
	HRB3 – GU	0.14	0.998
FDR-BC	HRB1 - GU	-8.10	**0.007**
	HRB3 - GU	8.31	**0.006**
FDR-Koss	HRB1 – GU	2.36	0.109
	HRB2 – GU	0.24	0.990
	HRB3 - GU	3.30	**0.027**

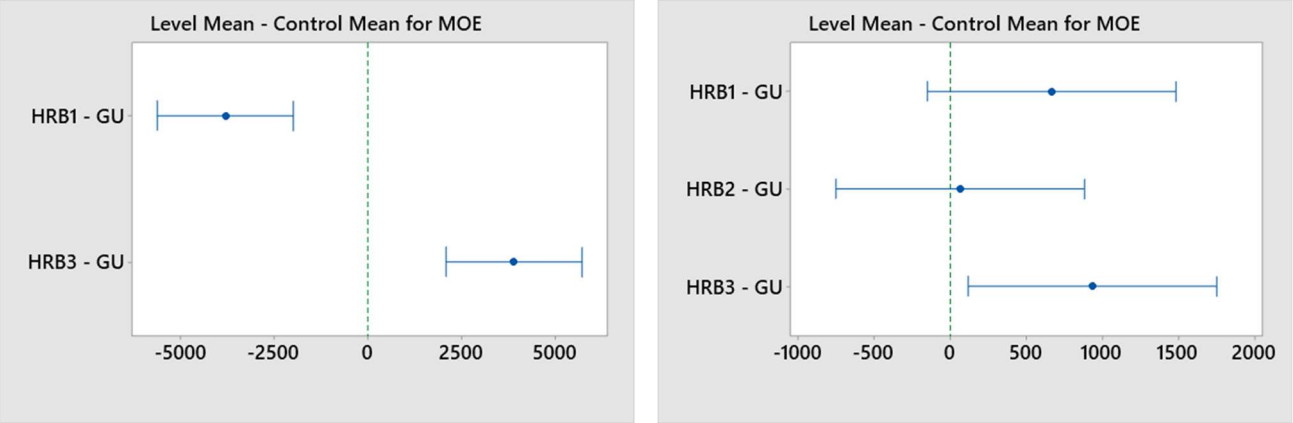

Figure 4.14 Dunnett's 95% confidence interval for MOE of FDR-BC (left) and FDR-Koss (right)

A regression analysis on the UCS and MOE data showed the correlation between the two parameters is significant. The empirical model, shown by Equation (4.1) was developed using the MOE and UCS data. The plot of the data points and the fitted line along with the

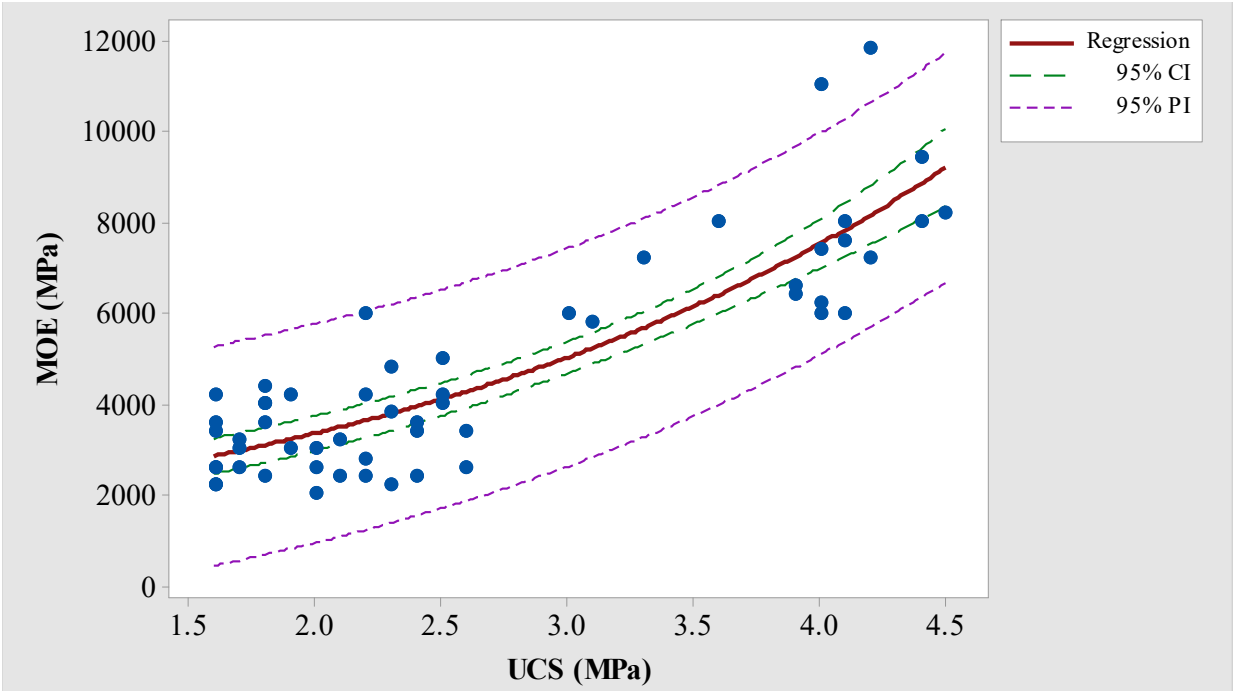

Figure 4.15 Plot of MOE test data and regression line

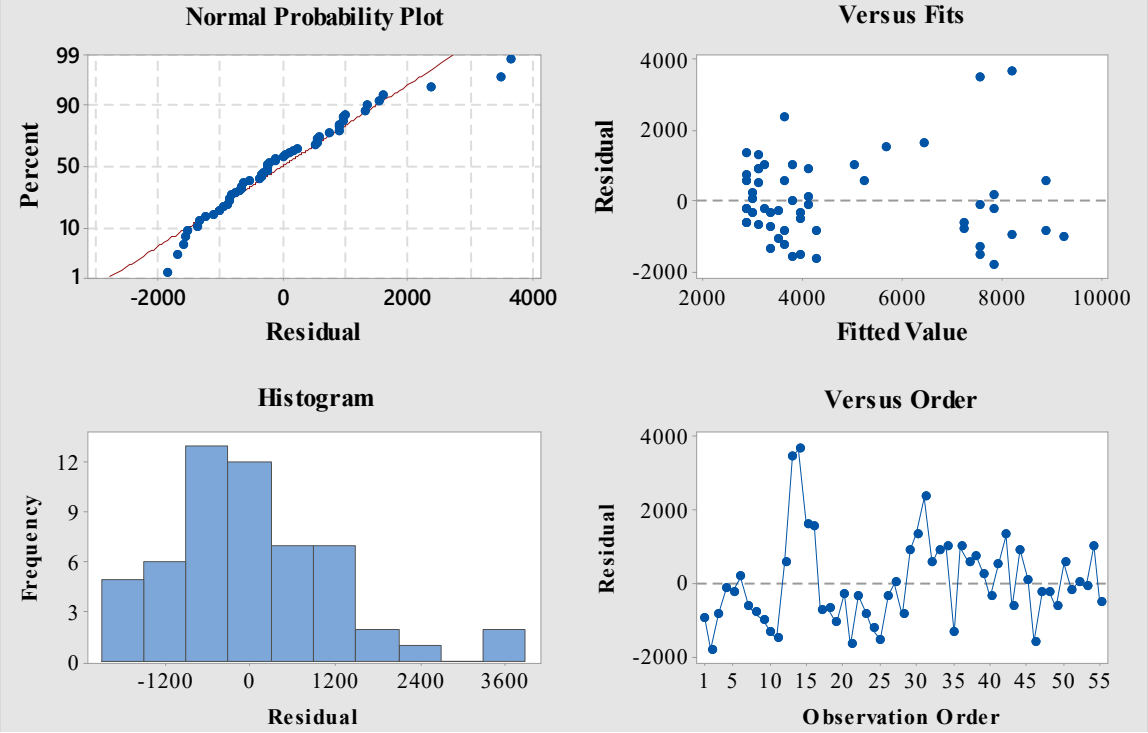

Figure 4.16 Residual plots of MOE model

95% confidence interval (CI) and 95% prediction interval (PI) is shown in Figure 4.15. The residual plots are shown in Figure 4.16.

$$MOE(MPa) = exp(7.312 + 0.403 * UCS(MPa)) \quad (4.1)$$

4.3.4. Indirect Tensile Strength

The tensile strength of cement-treated materials is equally important property as compressive strength is. In cement treated materials drying shrinkage cracking is often a major problem that causes premature pavement failure. Shrinkage cracking occurs when tensile stress developed due to drying exceeds the tensile strength of treated materials.

In this study, IDT was performed to evaluate typical values and assess the effects of HRB on the treated FDRm. The test results in Figure 4.17 show the 28 days IDT values of the eleven mixes are within the range of 0.40 MPa – 0.70 MPa. This shows the 28 days indirect tensile strength of the mixes is 10% - 20% of their 28 days unconfined compressive strength.

ANOVA and Dunnett's multiple comparisons were done on the IDT data to assess whether the observed differences in the IDT of the mixes are statistically significant. The tests were done on the whole dataset containing all the eleven mixes as well as on the datasets separated by FDRm types. Table 4.11 and Table 4.12 show the summary of the ANOVA and Dunnett's test results, respectively. All ANOVA tests indicated there is no significant variation in the IDT of the mixes. The Dunnett's test also confirmed the same except for the IDT of FDR-NL mix which were treated with HRB3 binder. Figure 4.18 shows this variation occurred because the IDT of HRB3 treated mixes was significantly higher than GU treated mixes. Based on the test data and statistical analyses, it can be concluded that the IDT HRB treated mixes is equivalent to the IDT of the corresponding GU treated mixes.

Table 4.11 Summary of ANOVA on IDT Data

FDR Material	F-Value	P-Value
FDR-NL, FDR-BC, FDR-Koss	1.86	0.161
FDR-NL	3.46	0.071
FDR-BC	1.02	0.459
FDR-Koss	0.92	0.472

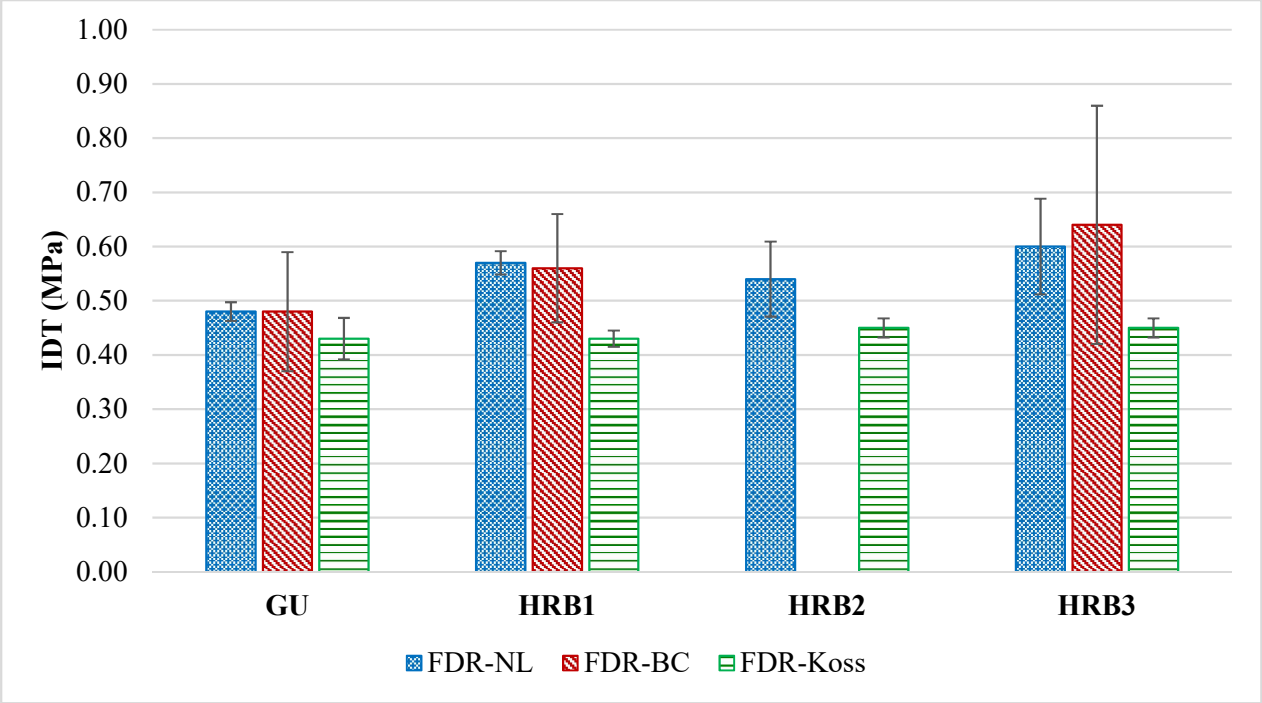

Figure 4.17 Average 28 days indirect tensile strength (IDT)

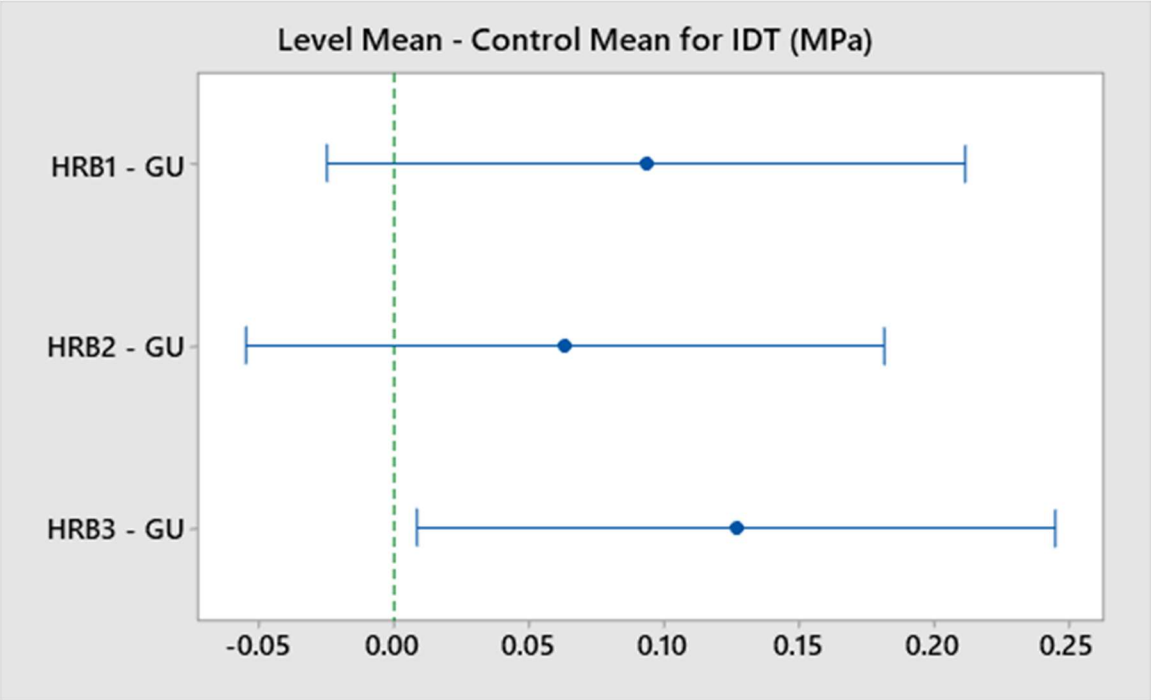

Figure 4.18 Dunnett's simultaneous 95% confidence interval for FDR-NL mixes

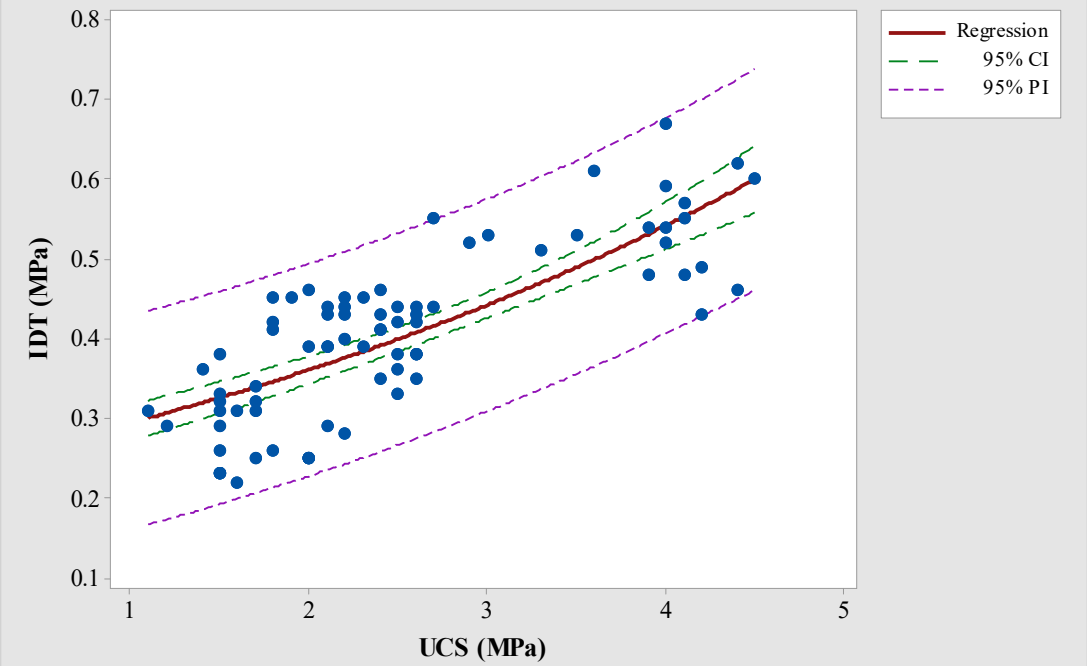

Figure 4.19 Plots of IDT data and regression line

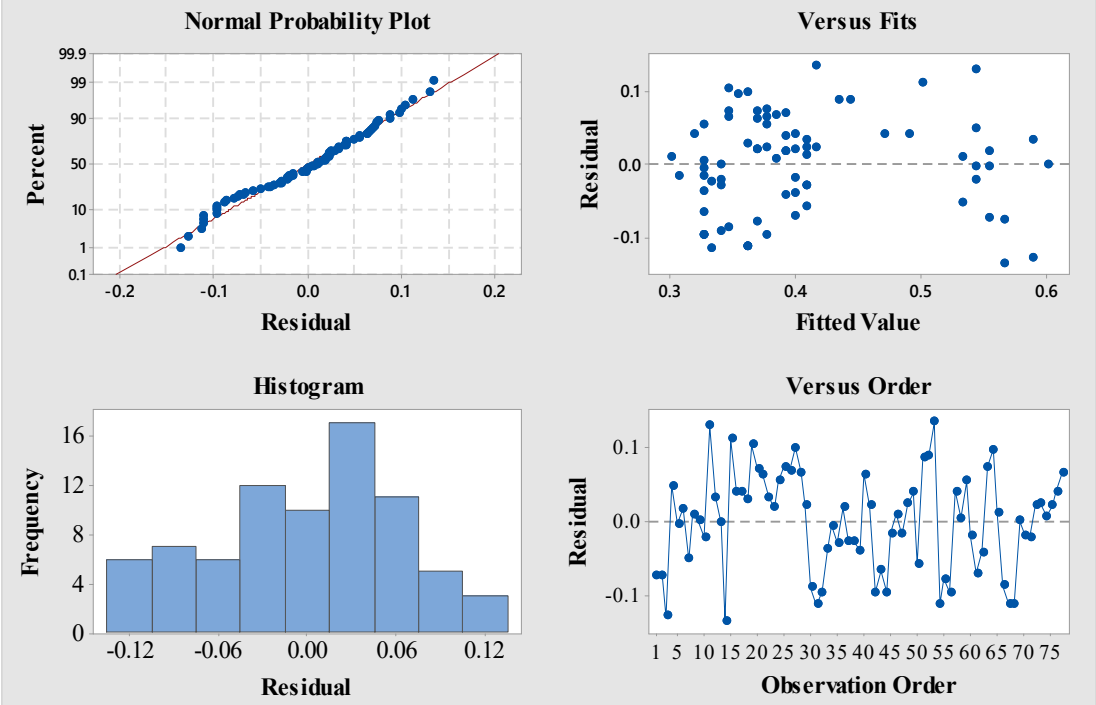

Figure 4.20 Residual plots for IDT model

The model in Equation (4.2) was developed based on the IDT and UCS test data by nonlinear regression analysis. The plots of the regression line and the residuals are shown in Figure 4.19 and Figure 4.20, respectively.

$$IDT(MPa) = exp(-1.4237 + 0.2028 * UCS(MPa)) \quad (4.2)$$

Table 4.12 Dunnett's simultaneous test on IDT Data

FDR Material	Difference of Levels (in IDT of mixes with different binder types)	T-Value	Adjusted P-Value
FDR-NL, FDR-BC, FDR-Koss	HRB1 – GU	1.33	0.424
	HRB2 – GU	0.76	0.792
	HRB3 – GU	2.32	0.074
FDR-NL	HRB1 – GU	2.28	0.122
	HRB2 – GU	1.55	0.342
	HRB3 – GU	3.09	**0.037**
FDR-BC	HRB1 – GU	0.69	0.738
	HRB3 - GU	1.43	0.378
FDR-Koss	HRB1 – GU	0.00	1.000
	HRB2 – GU	1.18	0.535
	HRB3 - GU	1.18	0.535

4.4. CONCLUSIONS

In this study, characterization of cement treated full-depth reclaimed pavement materials was performed using unconfined compressive strength, modulus of elasticity and indirect tensile strength tests. The study was conducted using reclaimed materials from three different sources and four different types of cement, namely, GU cement and three types of hydraulic road binders. Comparative assessment was conducted to identify the effects of the hydraulic road

binders on the mechanical properties of the mixes. The mixes with GU cement were used as a reference or control mixes to perform the comparative assessment. Based on the findings of the study, the following concluding remarks can be drawn:

- The optimum moisture content of the mixes treated with HRB did not vary significantly from the control mixes,
- The optimum binder content of the mixes treated with HRB was the same as, or less than, the corresponding mixes treated with GU cement,
- Hydraulic road binders could make mixes with equivalent early-age and long-term strength as GU cement,
- The stiffnesses of HRB mixes were equivalent to the corresponding stiffness of GU mixes;
- The tensile strengths of HRB mixes were equivalent to the corresponding GU mixes,

To summarize, the study findings revealed that HRB treated full-depth reclaimed pavement materials can have mechanical properties which are equivalent or even better than their GU counterparts. Therefore, hydraulic road binders could be a suitable sustainable alternative binder that can replace GU cement in FDR projects.

Based on the study findings, pavement structure with HRB treated FDRm base layer is expected to have similar or better performance than the corresponding structure with GU cement treated FDRm base. However, this should be confirmed through further research on test sections under actual field conditions.

5. FATIGUE BEHAVIOUR OF RECLAIMED PAVEMENT MATERIALS TREATED WITH HYDRAULIC ROAD BINDERS

Summary

Fatigue is one of the most common modes of failure in both flexible and rigid pavements. Several studies have been conducted to study this phenomenon for pavement materials such as bituminous mixes, Portland cement concrete, and cement treated aggregates and soils. The fatigue behaviour of **f**ully **r**eclaimed **p**avement **m**aterials treated with **c**ementitious binders (FRPMC), however, has barely been studied. FRPMC are composed of reclaimed asphalt pavement (RAP) aggregates, granular base course/ sub-base aggregate, fine grained soil particles and 3% – 6% cementitious binders. As a result, FRPMC have different properties than bituminous mixes and Portland cement concrete. In this study, the fatigue behaviour of FRPMC was assessed using four-point bending test, which was conducted in strain-control mode. The objectives of the study were to assess the fatigue life range of FRPMC at different strain levels, identify the effects of various cementitious stabilizer on the fatigue life and investigate the response of FRPMC to cyclic loadings. In total, eight mixtures and forty-eight beam specimens were prepared for the study using the two types of reclaimed materials and four types of binders. The findings of the study indicated that the type of cementitious stabilizers did not have significant effect on the fatigue life of FRPMC mixtures. It was also identified that FRPMC behaves mainly as quasi-brittle while possessing some properties of viscoelastic materials.

5.1. Introduction

For pavements with bound structural layers, fatigue is one of the governing factors that dictate the pavement performance. Fatigue is defined as a process of damage and failure of structures due to cycling loading (63). Fatigue process involves initiation and propagation of micro-cracks, and development of micro-cracks into macro-cracks (64). The occurrence of micro-cracks causes degradation of the modulus or rigidity of the structural layer. This is the decrease in the ability of the material to resist structural loads. Thus, understanding the fatigue behaviour of materials is of utmost importance to design and construct stable and durable structures.

Several studies have been conducted to study the fatigue characteristics of pavement materials like bituminous mixes (64–72), Portland cement concrete (73–76), and cement treated aggregates and soil (77–82). The fatigue behaviour of fully reclaimed pavement materials treated with cementitious binders (FRPMC), however, has barely been studied. FRPMC are composed of reclaimed asphalt pavement (RAP) aggregates, granular base course/ sub-base aggregate, fine grained soil particles and 3% – 6% cementitious binders. As a result, FRPMC have different properties than bituminous mixes and Portland cement concrete. Compared to both bituminous mixes and Portland cement concrete, FRPMC are characterised by lower strength and stiffness at room temperature. Typical cross-section of hot-mix asphalt, cement treated reclaimed pavement materials, and Portland cement concrete specimens are shown in Figure 5.1. FRPMC are also different from cement treated aggregates/soils due to the presence RAP aggregates in the reclaimed materials. The RAP aggregates contain aggregates coated with asphalt film and mastics (blend of asphalt and fine fractions). These provide FRPMC more flexibility as compared cement treated

aggregates/soils. Consequently, the fatigue behaviour of FRPMC could be different from the fatigue behaviour of cement treated aggregates/soils.

In this paper, the fatigue behaviour of FRPMC was investigated using four-point bending test. The objective of this study is to assess:

- the fatigue life range of FRPMC at different strain levels
- the effects of various cementitious binders on the fatigue life of FRPMC
- the behaviour of FRPMC under cycling loadings

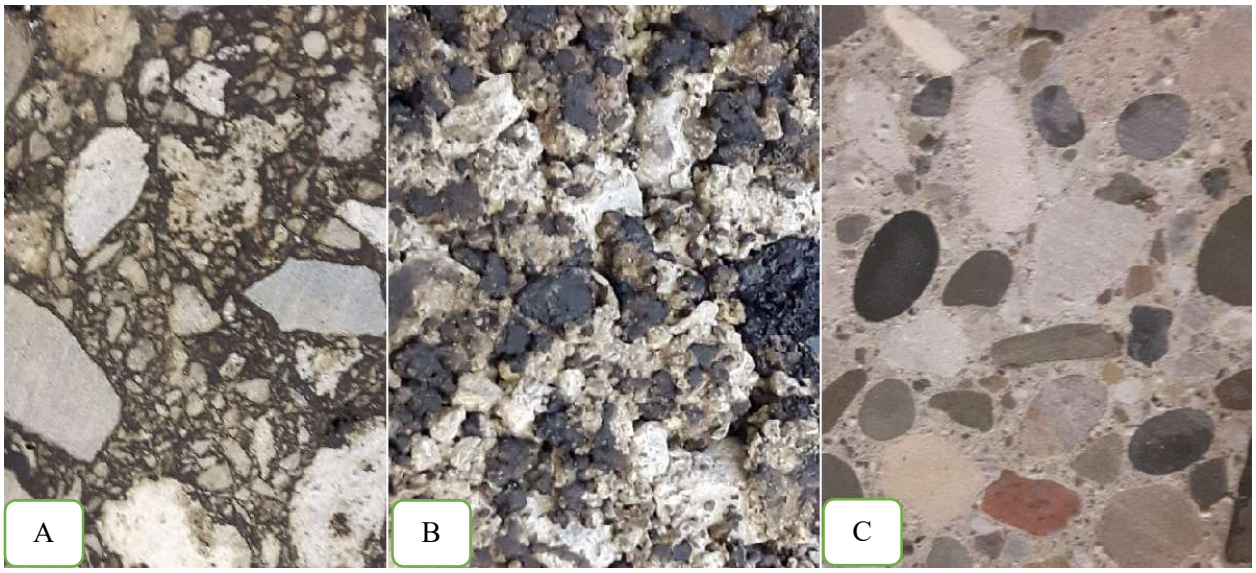

Figure 5.1 Cross-section of bound pavement material specimens: A) Hot-mix asphalt, B) FRPMC with 60% RAP content, C) Portland cement concrete

5.2. Materials and methods

5.2.1. Materials

Two types of fully reclaimed pavement materials and four types of cementitious binders were used for this study. The two reclaimed materials were collected from full-depth reclamation

project sites along Kossuth and Nafziger roads. Both projects were located in Ontario, Canada. The materials from Kossuth road contained 60% RAP and 40% granular material while the material from Nafziger road was composed of 80% RAP and 20% granular material. The properties of the two materials are shown in Figure 5.2 and Table 5.1.

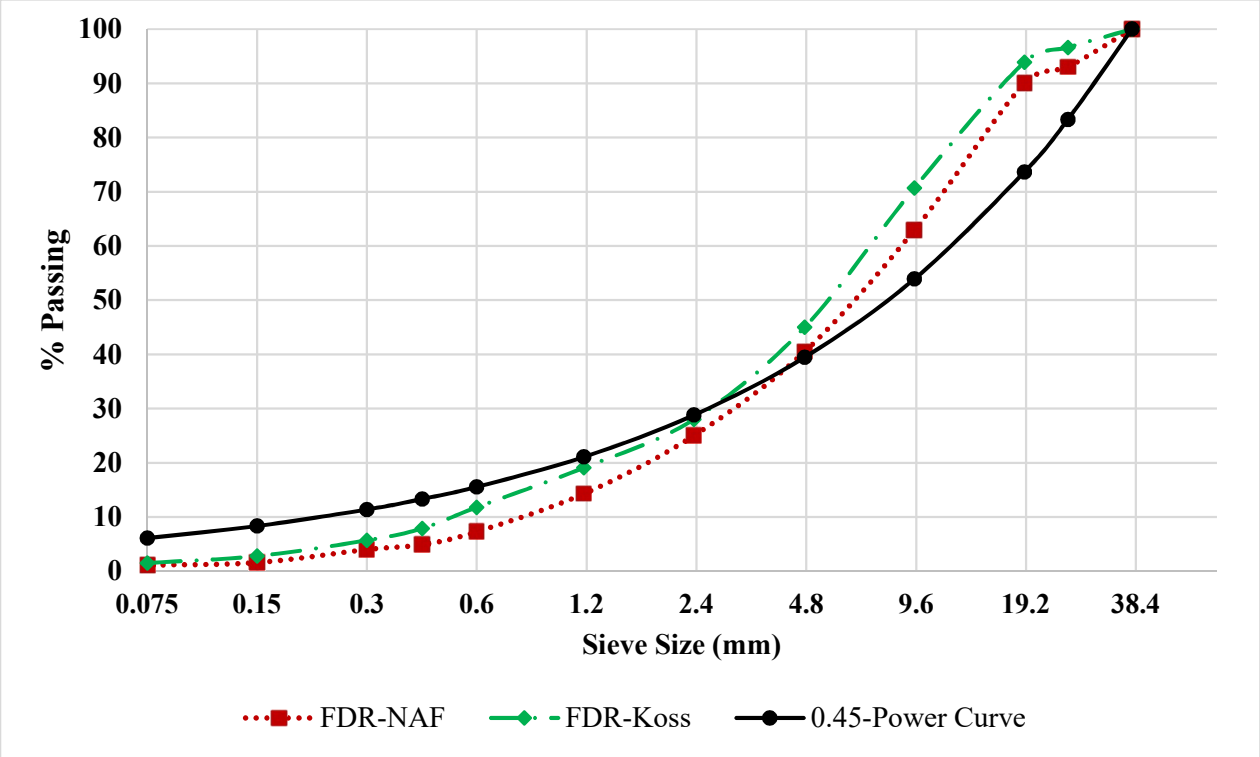

Figure 5.2 Particle size distribution of reclaimed pavement materials

Table 5.1 Physical Properties and Compositions of Reclaimed Materials

Test Description	Test Method	Test Results	
		FDR-Koss	FDR-NAF
Composition, RAP : Granular		60:40	80:20
Liquid Limit (%)	AASHTO T 89	Non-plastic	Non-plastic
Plasticity Index	AASHTO T 90	Non-plastic	Non-plastic
AASHTO Soil Class	AAHTO M 145	A-1-a	A-1-a
Micro-Deval Abrasion Loss (%)	ASTM D 6928	12.7	11.2
Methylene Blue Value (mg/g)	AASHTO TP 57	2.7	2.1

The cementitious binders used in this study are General Use (GU) cement and three different types of hydraulic road binders (HRB). Hydraulic road binders are factory made blends of GU cement and substantial amount of supplementary cementing materials (SCM). The chemical compositions and physical properties of the four binders are shown in Table 5.2 and Table 5.3, respectively.

Table 5.2 Chemical Compositions of Binders

Chemical Composition	GU	HRB1	HRB2	HRB3
SiO_2 (%)	19.6	28.4	22.3	26.2
Al_2O_3 (%)	5.0	7.6	5.7	7.0
Fe_2O_3 (%)	3.3	2.1	2.3	2.3
CaO (%)	62.2	49.4	55.4	53.4
MgO (%)	2.5	7.2	4.7	5.9
SO_3 (%)	3.9	3.3	3.7	3.6
Loss on ignition @ 950 (%)	2.3	1.5	4.3	1.7

Table 5.3 Physical Properties of Cementitious Binders

Physical Properties	GU	HRB1	HRB2	HRB3
Autocalve, % Expansion	0.05	0.0	0.0	0.0
Blaine Fineness, m^2/kg	383	465	497	389
Compressive Strength at 28 days, MPa	40.5	34.8	41.5	35.0
Fineness, 45μm sieve, % retained	4.0	5.0	1.9	4.1
Initial time of set, minutes	90	161	173	153
Sulphate Resistance, % expansion at 6 months	0.014	-	0.005	0.040

5.2.2. Methodology

There is no specific standard test protocol for fatigue assessment of cement treated reclaimed pavement materials. As a result, in this study, the fatigue assessment was made according to AASHTO T 321, which is a standard test method to determine fatigue life of compacted hot

mix asphalt. The test is performed on 380 mm long by 50 mm thick by 63 mm wide beam specimens.

Total of eight mixtures and forty-eight beam specimens were prepared for the study using the two reclaimed materials and the four binders. The mixtures were composed of the reclaimed materials, cementitious binders and water. The binder content in each mixture was fixed to be 6% regardless of the binder type. The optimum water contents (OMC) and maximum dry density (MDD) of each mixture were determined using standard proctor test. The test was performed according to ASTM D 558. The test results are shown in Figure 5.3 and Table 5.4. The results of the standard proctor test were used to proportion and calculate the amount of loose mixture required to make the beam with the specified dimensions.

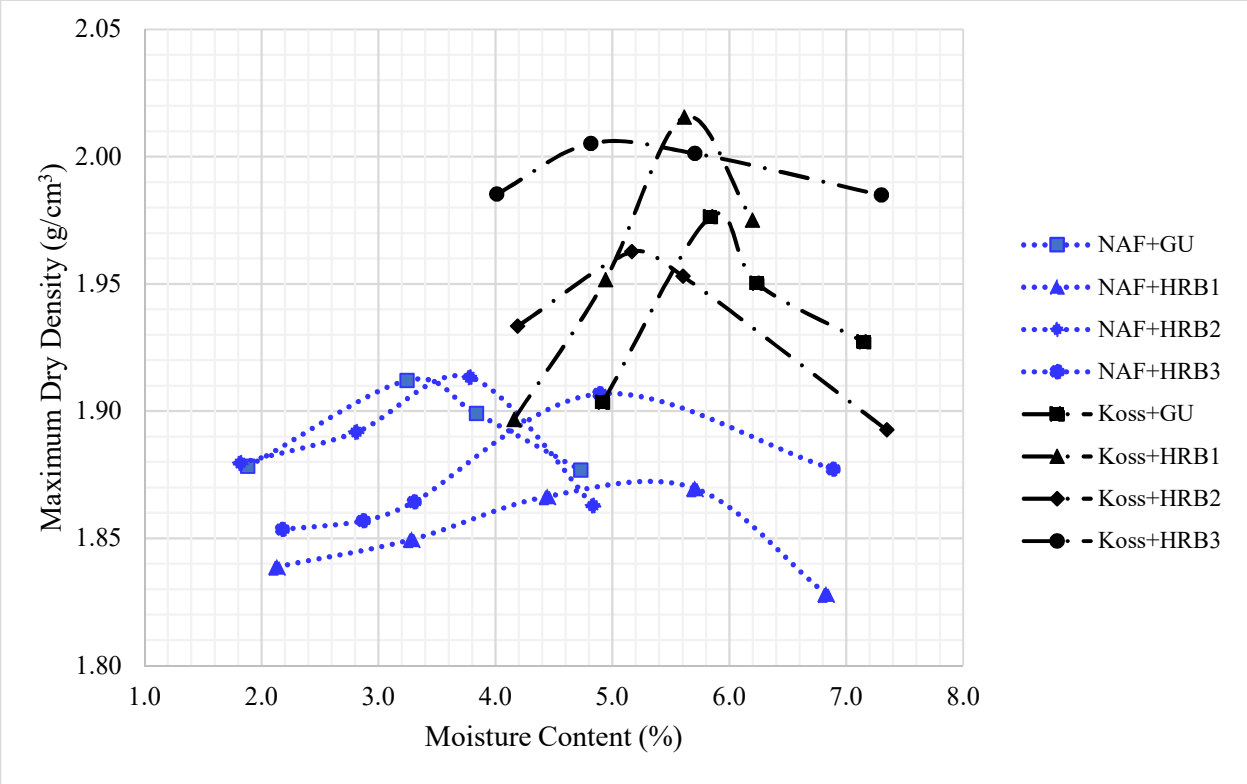

Figure 5.3 Moisture-density relationships

Table 5.4 Mixture Compositions

Reclaimed Material Type	Binder Type	Binder Content (%)	MDD (g/cm^3)	OMC (%)	Water/Binder (ratio)
FDR-Koss	GU	6	1.98	5.9	1.04
	HRB1	6	2.02	5.6	0.99
	HRB2	6	1.97	5.3	0.93
	HRB3	6	2.01	5.0	0.88
FDR-NAF	GU	6	1.91	3.4	0.60
	HRB1	6	1.87	5.2	0.92
	HRB2	6	1.91	3.7	0.65
	HRB3	6	1.91	5.0	0.88

- *Test Specimens Preparation*

The beam specimens were prepared using a purpose designed steel mould shown in Figure 5.4a. The internal dimensions of the steel mould were designed to have the standard beam dimensions specified in AASHTO T 321. To make a beam, the loose mixture was prepared and placed in the steel mould. Then the mixture was compacted first manually using a tamping rod and then using hydraulic compression machine, as shown in Figure 5.4b. The rate of loading of the compression machine was set to be 1 mm/minute to avoid the disintegration of the coarser fractions in the mix. The level of compaction was controlled by monitoring the displacement of the top plate. The target level of compaction would be attained when the edge of the top plate fully touches the mould. After compaction of the loose mixture is completed, the mould parts were disassembled and the freshly compacted specimen was left to set for 6 – 12 hours. The specimen was then moved to the humidity chamber where it was cured for 28 days at room temperature and relative humidity of 100%. After 28 days of curing the specimen was taken out of the humidity chamber and a nut was attached at the middle length along the neutral axis. The beam was then put into the environmental chamber of the testing

machine and conditioned at 20°C for a minimum of 2-hours before the test. The beams after 28 days of curing and a beam with the attached nut are shown in Figure 5.4d and Figure 5.4e, respectively.

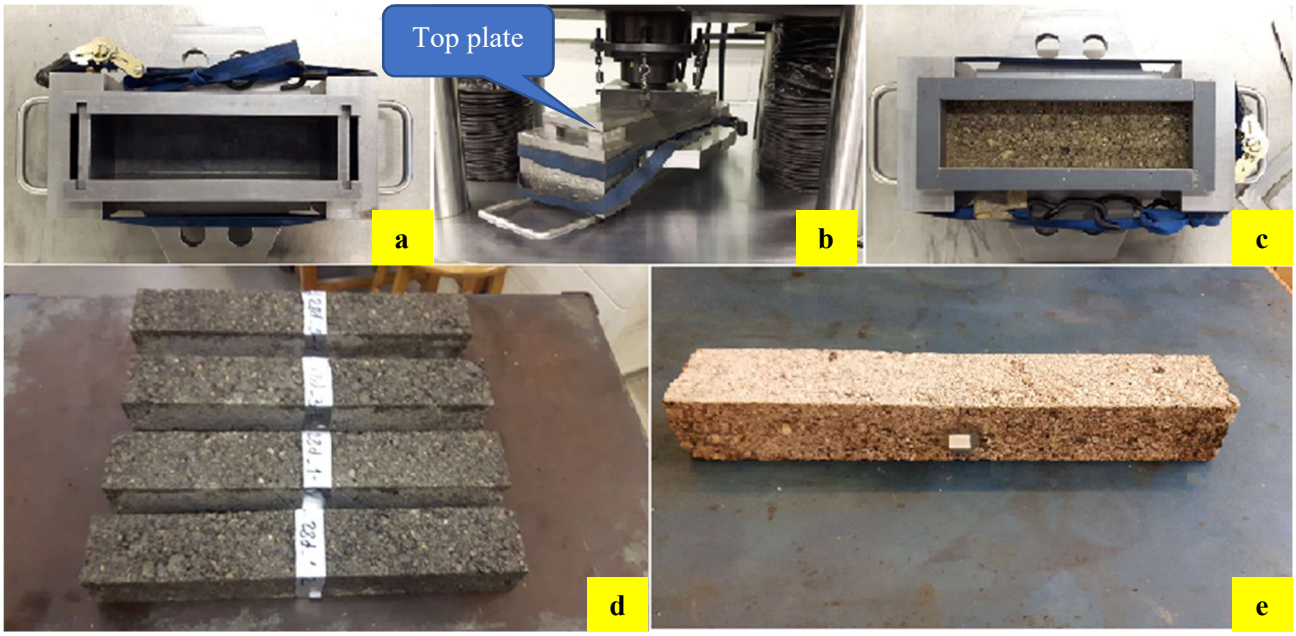

Figure 5.4 Preparation of beam specimens a) steel mould, b) compaction of loose mixtures, c) compacted mix in the mould, d) beam specimens after 28 days of curing, d) beam with a nut glued at the middle length along neutral axis

- *Four-point bending test*

After the two hours of conditioning, the test specimen was placed in the testing frame, shown in Figure 5.5. The test was performed at constant temperature of 20° C and constant loading frequency of 5 Hz in a strain-controlled mode. The test was conducted at three strain levels: 200, 250 and 300 micro- strains on duplicate specimens. These strain levels were selected after trial tests were conducted on dummy specimens, which were made with Kossuth mixtures. The strain-levels for the trial tests were 150, 200, 250, 300, 350, 400, 500 micro-strains. The test with 150 micro-strain was lengthy and could not be completed after 2.5-days.

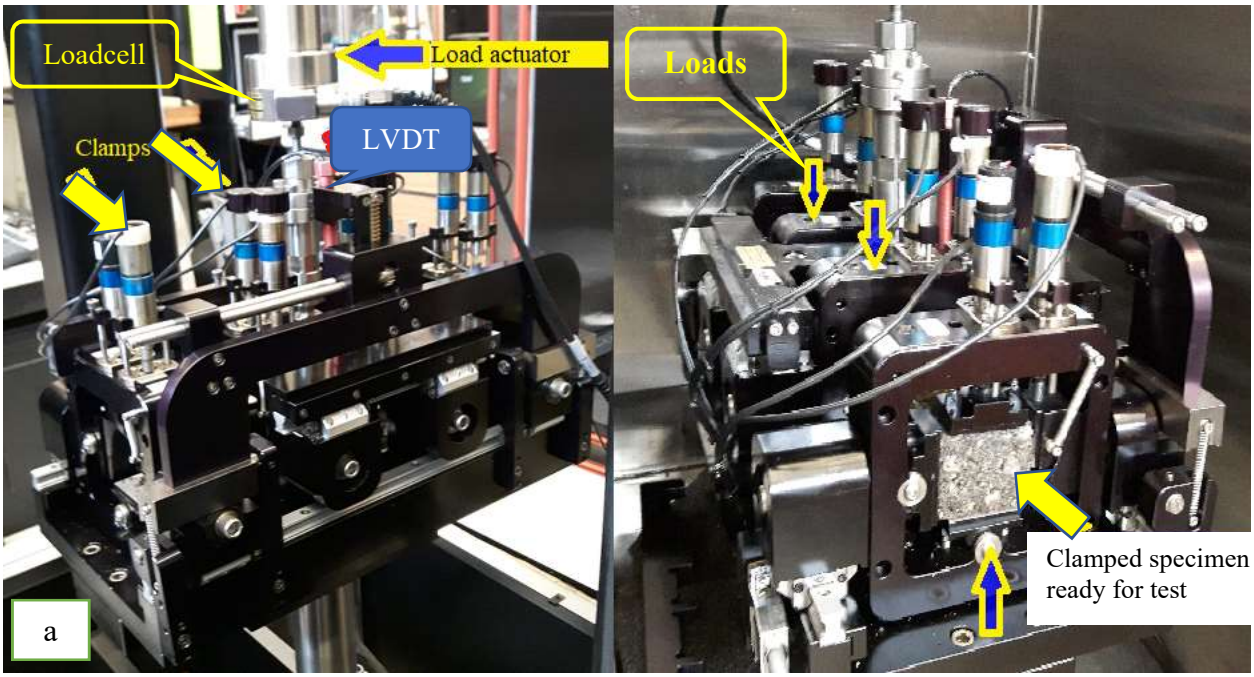

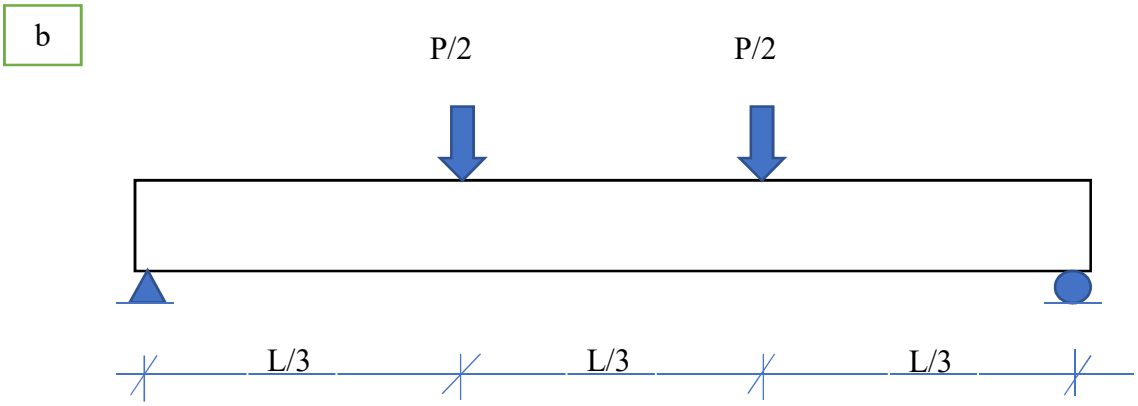

Figure 5.5 a) Four-point bending test frame, b) Schematic representation of four-point loading

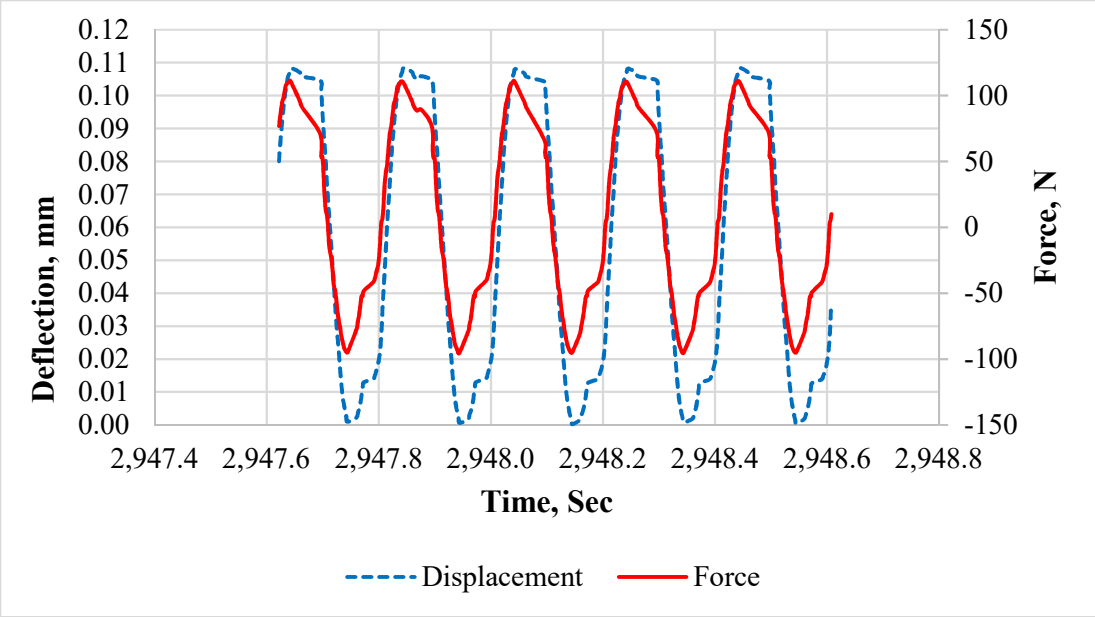

Figure 5.6 Typical force and displacement signals of a test ran at 200 micro-strain

In contrast, the tests with 350 micro-strain and higher strain levels were very short and completed rapidly indicating abrupt drop in the stiffness of the specimens. Therefore, the actual experiment was conducted within the mentioned narrow range of strains.

To be consistent, the same strain levels were used to conduct the test on Nafziger mixtures. At each strain level, duplicate specimens were tested from each mixture. Accordingly, 24 specimens with Kossuth mixtures and 24 specimens with Nafziger mixtures, total of 48 specimens were prepared for the test. The testing device was set to provide a repeated sinusoidal loading good enough to induce the specified tensile strain at the bottom of the test specimen. Here, it is worth noting that although a sinusoidal loading is applied, the specimens' response may not be perfectly sinusoidal due to non-linear behaviour of the test specimens and the non-homogeneity of the stress-strain field within the specimen (64). However, the response signals can be approximated with sinusoidal functions. The test set up,

and typical force and displacement (deflection) signal recorded during a test conducted at 200 micro-strain are shown in Figure 5.5 and Figure 5.6, respectively.

The stiffness of the test beam at the 50th load cycle was considered as the initial stiffness per AASHTO T 321 recommendation and used for the analysis. In this study, all of the fatigue tests were terminated once the initial stiffness of the test specimens was reduced by 60%.

5.3. Results and discussion

The first step in the data analysis was the computation of stress, tensile strain and flexural stiffness based on the amplitude of the force and the deflection of the specimen. This was done using Equation (5.1), Equation (5.2) and Equation (5.3) per AASHTO T 321 recommendation.

$$\sigma_t = \frac{0.357P}{bh^2} \tag{5.1}$$

where:

σ_t = tensile stress at bottom of beam

P = load applied by actuator, N

b = average specimen width, m

h = average specimen height, m

$$\varepsilon_t = \frac{12\delta h}{3L^2 - 4a^2} \tag{5.2}$$

where:

ε_t = tensile strain at bottom of beam

δ = deflection at center of beam, m

a = space between inside clamps = 0.119 m

L = length of beam between outside clamps = 0.357 m.

$$S = \frac{\sigma_t}{\varepsilon_t} \tag{5.3}$$

where:

S = flexural stiffness

5.3.1. Phenomenological fatigue analysis

In a phenomenological approach the relationship between the peak stress or peak strain and the number of load repetitions to failure is identified experimentally (65,66). The commonly known definition of fatigue life is the number of load repetition corresponding to 50 % reduction in the initial stiffness of the test specimens (64,66,83). The fatigue life of the eight mixtures, in this study, are shown in Table 5.5 and typical plot of the fatigue test data is shown in Figure 5.7. As shown in the test results, fatigue life of duplicate specimens had large variations at 200 and 250 micro-strain for some of the tests. This variation was smaller for the tests at 300 micro-strain.

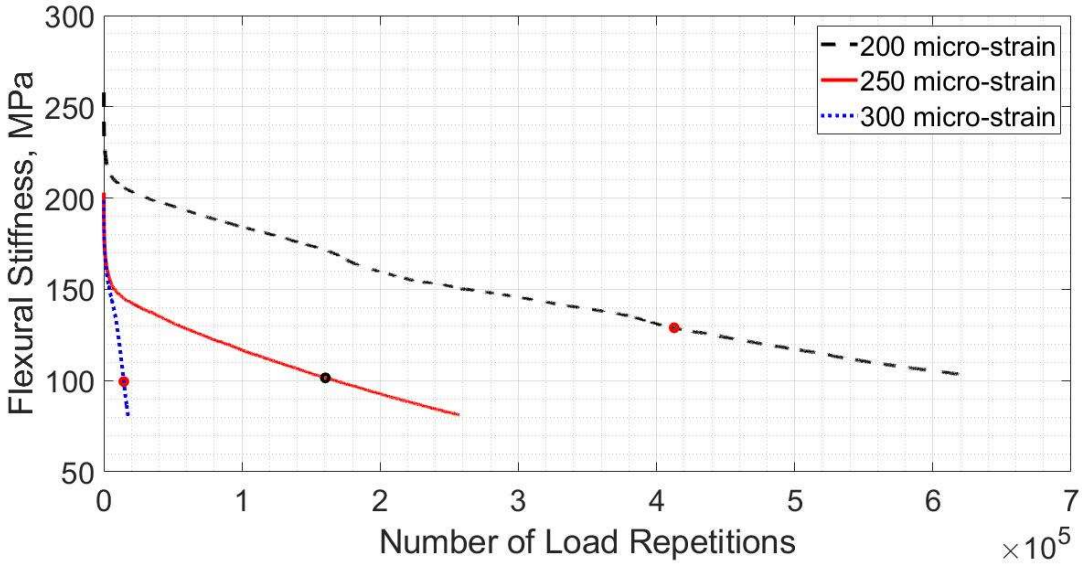

Figure 5.7 Typical flexural stiffness vs number of load repetition curves for the same mix

Table 5.5 Fatigue Test Results

Binder Type	Strain × 10^{-6} mm/mm	FDR-Koss		FDR-NAF	
		Initial Stiffness, MPa	N_f	Initial Stiffness, MPa	N_f
GU	200	208	431,290	140	11,850
	200	226	1,005,600	147	66,599
	250	212	76,999	164	8,050
	250	150	89,549	63	5,450
	300	175	11,100	88	5,900
	300	184	12,100	152	4,850
HRB1	200	218	1,055,000	162	64,299
	200	157	916,389	121	41,099
	250	203	160,350	81	16,200
	250	258	412,795	160	22,699
	300	199	14,500	61	3,950
	300	108	22,599	79	6,600
HRB2	200	206	116,848	192	25,099
	200	186	142,700	181	77,599
	250	206	9,450	162	10,400
	250	148	84,399	138	8,650
	300	195	6,000	178	3,450
	300	178	10,100	108	2,050
HRB3	200	242	706,490	186	130,148
	200	185	80,699	148	164,000
	250	211	28,249	73	45,849
	250	166	21,149	196	119,598
	300	160	7,416	157	5,600
	300	171	13,950	154	3,050

To evaluate the effect of the various binders and RAP content on the fatigue life, two-way analysis of variance (ANOVA) and multiple comparison with Dunnett's method were performed. The results of the ANOVA test, as shown in Table 5.6, indicated that the fatigue life was not significantly affected by the type binder used to stabilize the reclaimed materials. Dunnett's multiple comparisons indicated that the fatigue life of all of the HRB mixtures is equivalent to the fatigue life of GU mixtures. This indicates the hydraulic road binders of the type used in this study can make mixtures with the same fatigue performance as GU mixtures. The results of Dunnett's multiple comparison test are shown in Figure 5.8.

Table 5.6 ANOVA Test Result for Fatigue Life

Source	F-value	P-value
Reclaimed Materials	7.79	0.008
Binder Type	1.28	0.293
Reclaimed Materials*Binder Type	1.57	0.212

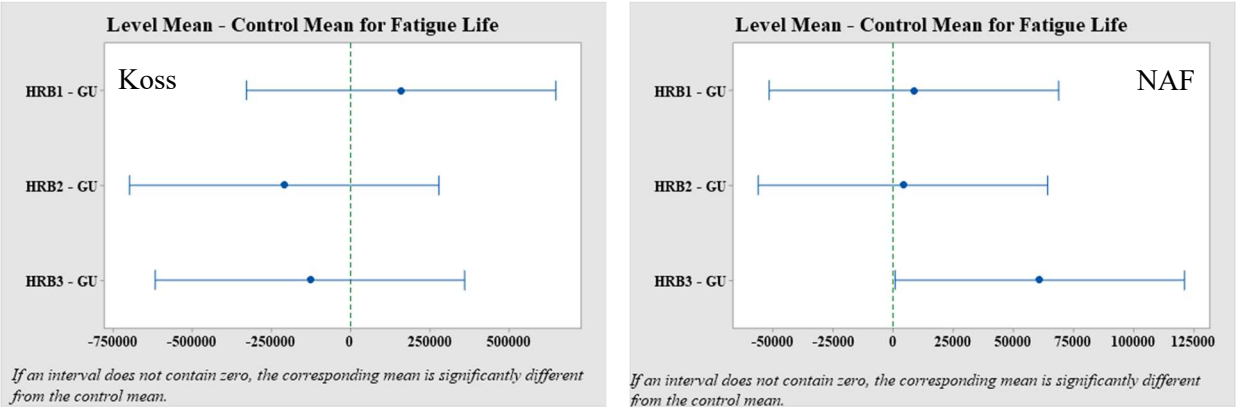

Figure 5.8 Results of Dunnett's multiple comparisons for simultaneous 95% confidence interval

On the other hand, the type of reclaimed materials had statistically significant effect on the fatigue life of the mixtures. As shown, in Figure 5.9, the fatigue life of all but one of

Nafziger mixtures are less than the fatigue life of the corresponding Kossuth mixtures. All Kossuth and Nafziger mixtures have the same binder content. The major difference between Kossuth and Nafziger mixtures is the RAP content. Nafziger material contained 20% more RAP than Kossuth material. According to this study, the mixture with higher RAP content had lower fatigue life. This contradicts with the findings of the previous works (84,85), which did not find a distinct trend between RAP content and fatigue life.

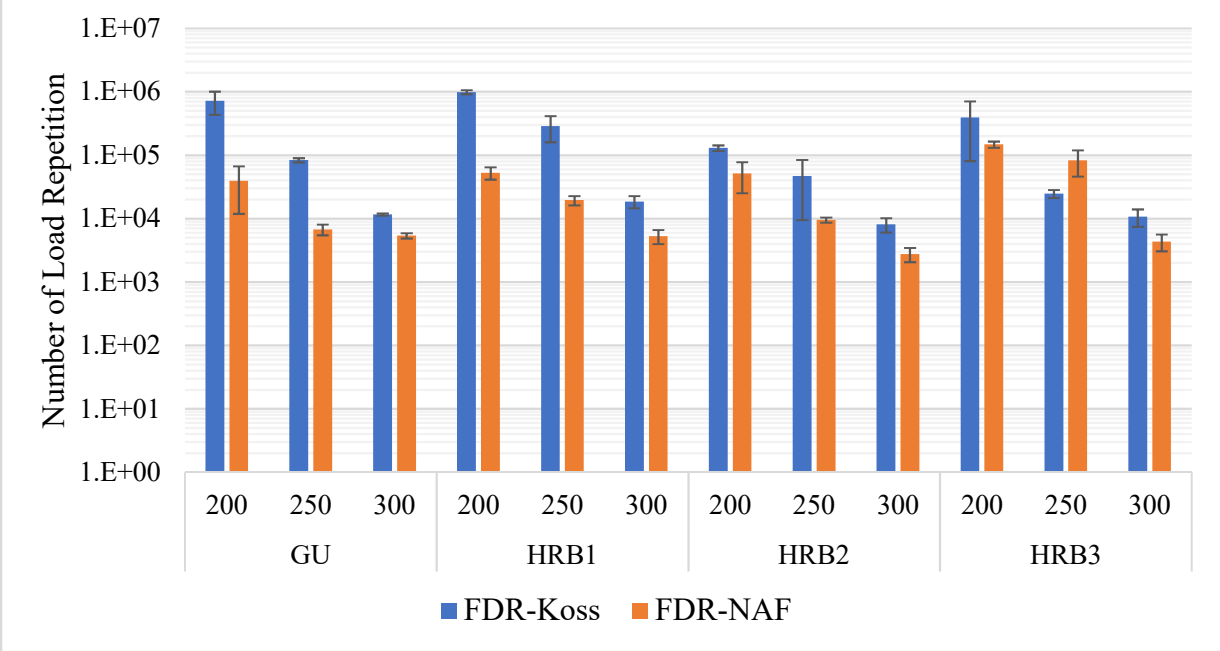

Figure 5.9 Comparison of fatigue life of FDR-Koss and FDR-NAF mixtures

The relationship between the fatigue life and peak tensile strain can be represented with one of the traditional fatigue models, shown in Equation (5.4). This is the model that fits well with the fatigue test results. The model parameters, shown in Table 5.7, were determined for the two reclaimed material mixtures using a regression analysis. The plots of load

repetition to failure versus peak tensile strain for Kossuth and Nafziger mixtures are shown in Figure 5.10 and Figure 5.11, respectively.

$$N_f = a * \varepsilon^b \tag{5.4}$$

where:

a and b = material constants (model parameters)

N_f = number of load repetition to failure

ε = peak tensile strain ($\times 10^{-6}$ mm/mm)

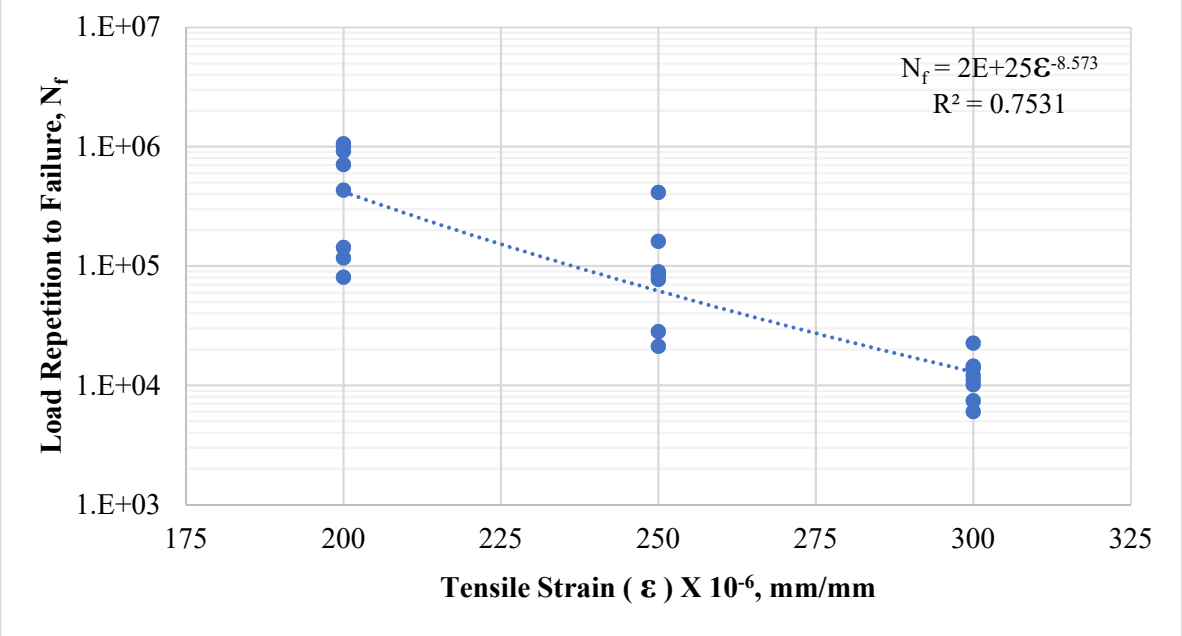

Figure 5.10 Fatigue curve for FDR-Koss mixtures

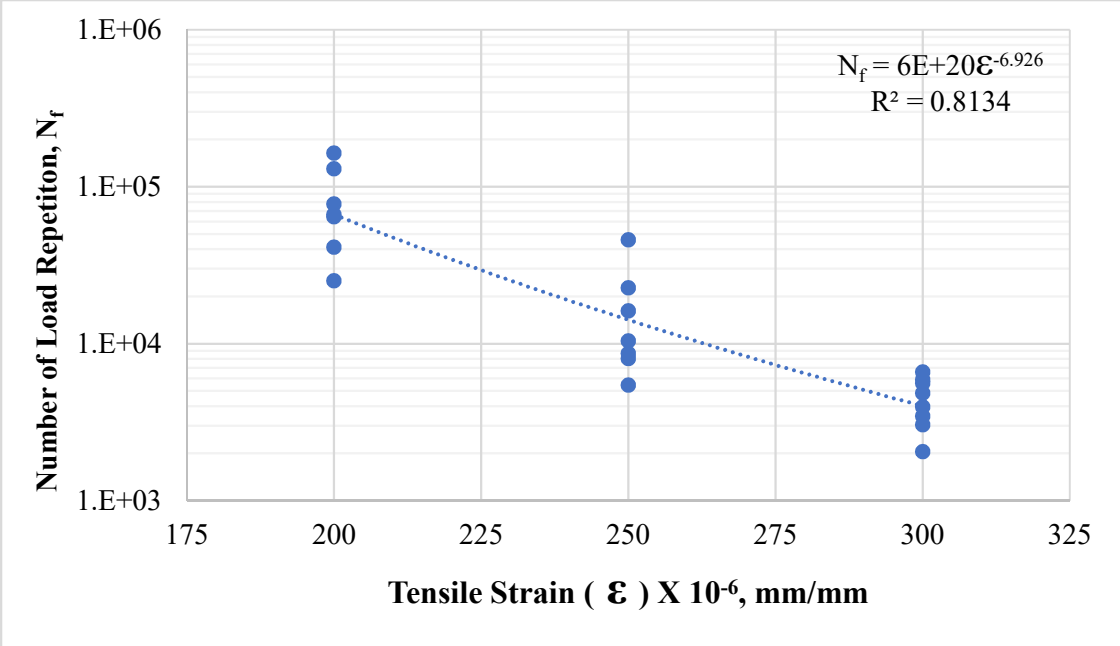

Figure 5.11 Fatigue curve for FDR-NAF mixtures

Table 5.7 Fatigue Model Parameters

Material Type	a	b	R^2
FDR-Koss	2E+25	-8.573	0.75
FDR-NAF	6E+20	-6.926	0.81

5.3.2. Energy-based methods

The fatigue test results indicated that there was a considerable phase lag between the load application and material response. The initial phase angles measured during the laboratory tests ranges 10 – 15 degrees. This indicated that part of the energy applied to the test specimens was dissipated in the process which is common for viscoelastic materials. Typical plots of the phase angle versus number of load repetitions and flexural stiffness versus phase angle are shown in Figure 5.12 and Figure 5.13. It has been shown that the fatigue life of bituminous mixtures and Portland cement concrete is related to the energy dissipated during

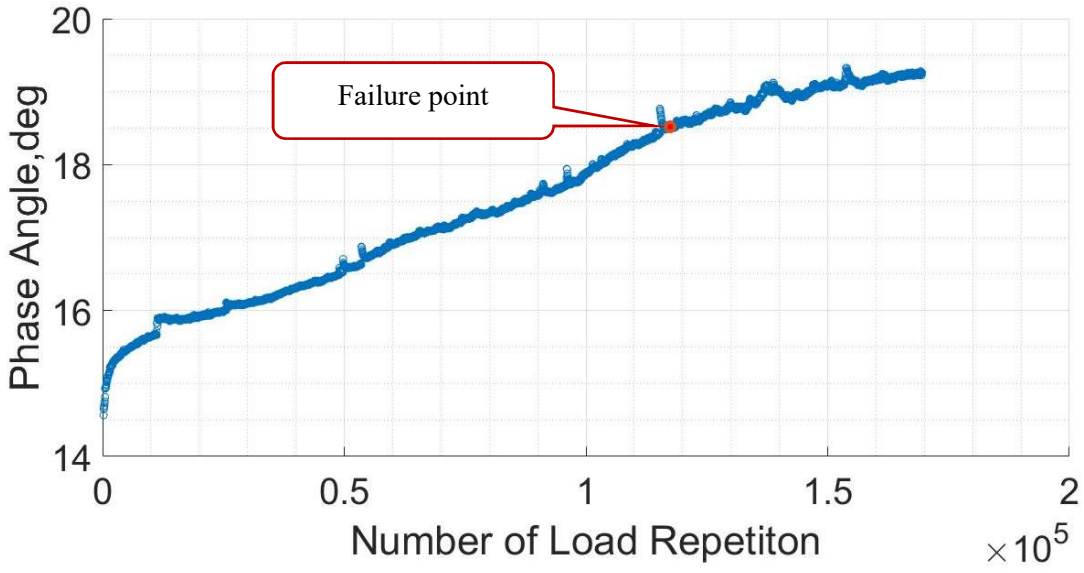

Figure 5.12 Evolution of phase-angle with number of load repetitions

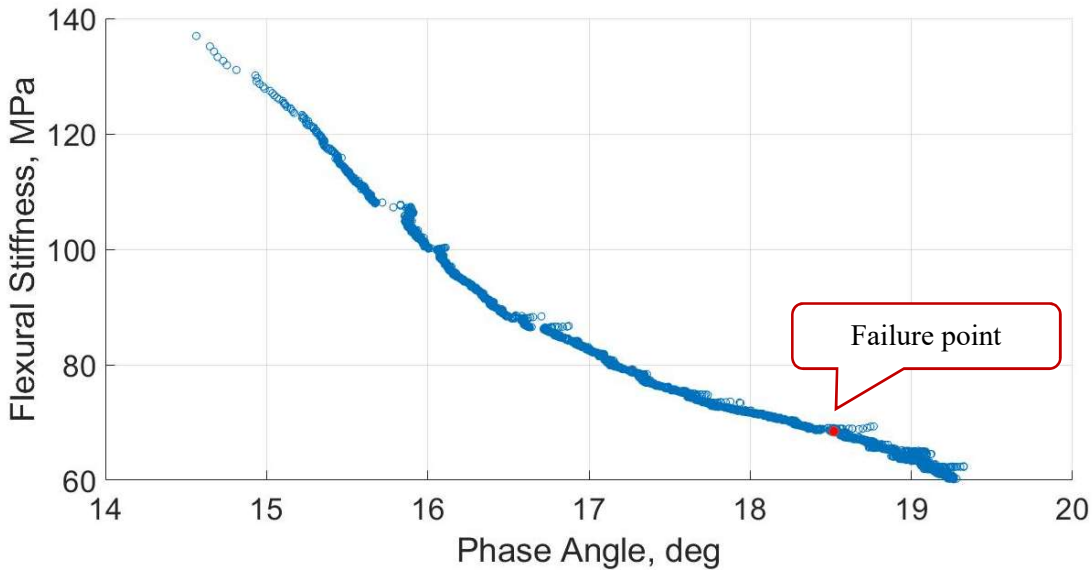

Figure 5.13 Evolution of phase-angle with flexural stiffness

the cycling loading (65,66,71,83,86). For a beam specimen tested under sinusoidal loading, the dissipated energy is computed as the area under the stress-strain hysteresis loop

(65,83,87,88). The typical hysteresis loop of a test in this study was illustrated in Figure 5.14. The area under a hysteresis loop can be approximated using the Equation (5.5) (65,71,83,87).

$$W_i = \pi \, \sigma_i \, \varepsilon_i \, sin\varphi \tag{5.5}$$

where,

W_i = dissipated energy at load cycle i

σ_i = stress amplitude at load cycle i

ε_i = strain amplitude at load cycle i

φ = phase shift between stress and strain at load cycle i

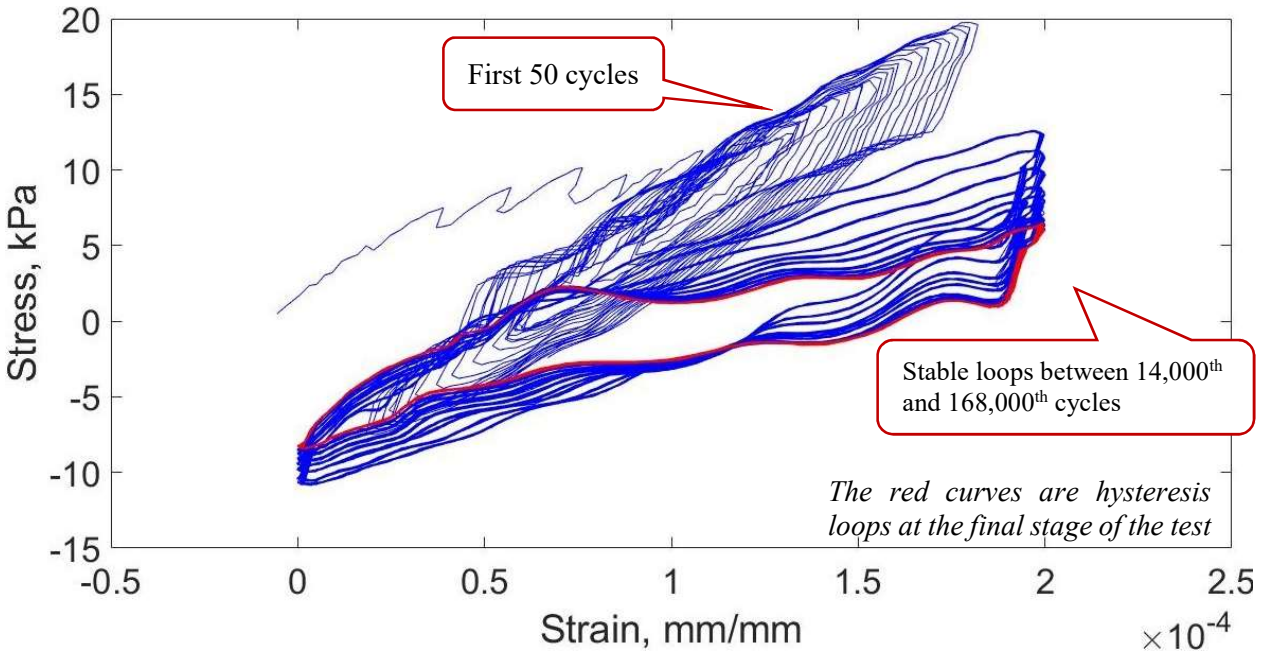

Figure 5.14 Hysteresis loop of the test on FDR-Koss + HRB1 mixture conducted at 250 micro-strain

The cumulative dissipated energy to failure of the test specimen is computed as the sum of the area of all the hysteresis loops. This is given by Equation (5.6).

$$W_{Nf} = \sum \pi \, \sigma_i \, \varepsilon_i \, sin\varphi \tag{5.6}$$

where,

W_{Nf} = cumulative dissipated energy

The relationship between fatigue life and cumulative dissipated energy can be characterised by the models shown by Equation (5.7) and Equation (5.8). These models were established for bituminous mixtures by Tayebali et. al (87). However, it was found out that the models can be used for the materials in this study, as well. The parameters for the model in Equation (5.7) were determined using non-linear regression analysis; whereas the parameters of the model in Equation 5.8 were determined using Excel's GRG Nonlinear optimization. The model parameters for the models in Equation (5.7) and Equation (5.8) are presented in Table 5.8 and Table 5.9.

$$CDE = A \left(N_f\right)^z \tag{5.7}$$

where,

CDE = cumulative dissipated energy

N_f = number load repetitions to failure

A, z = material constants

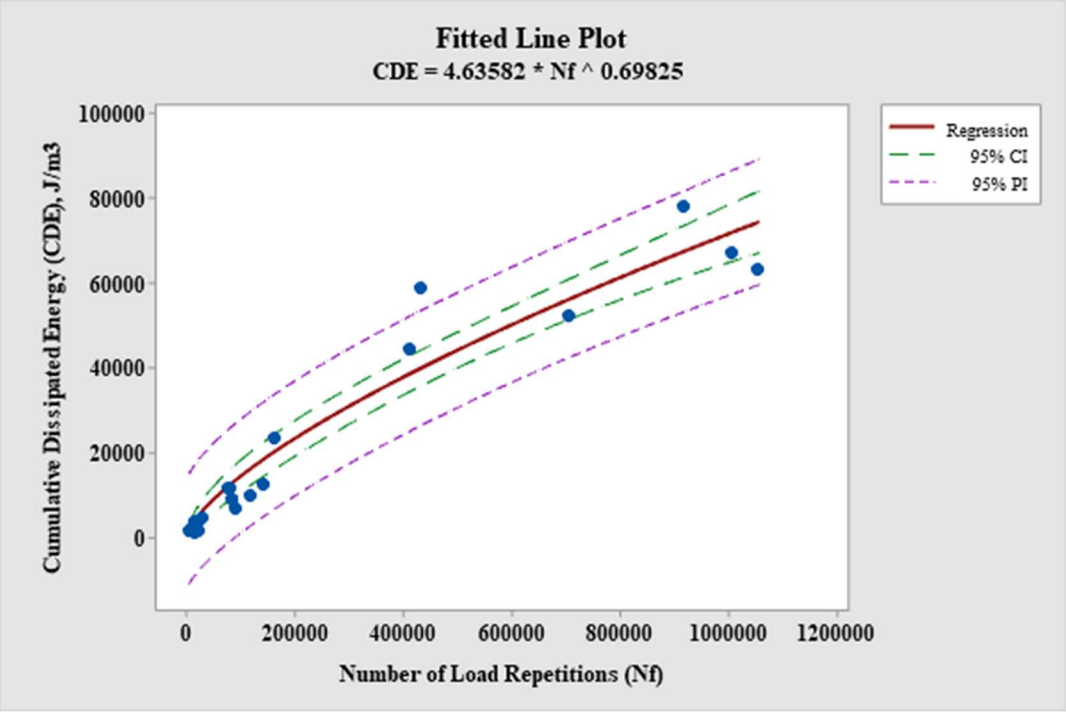

Figure 5.15 Fitted line and experimental data point of Kossuth mixtures

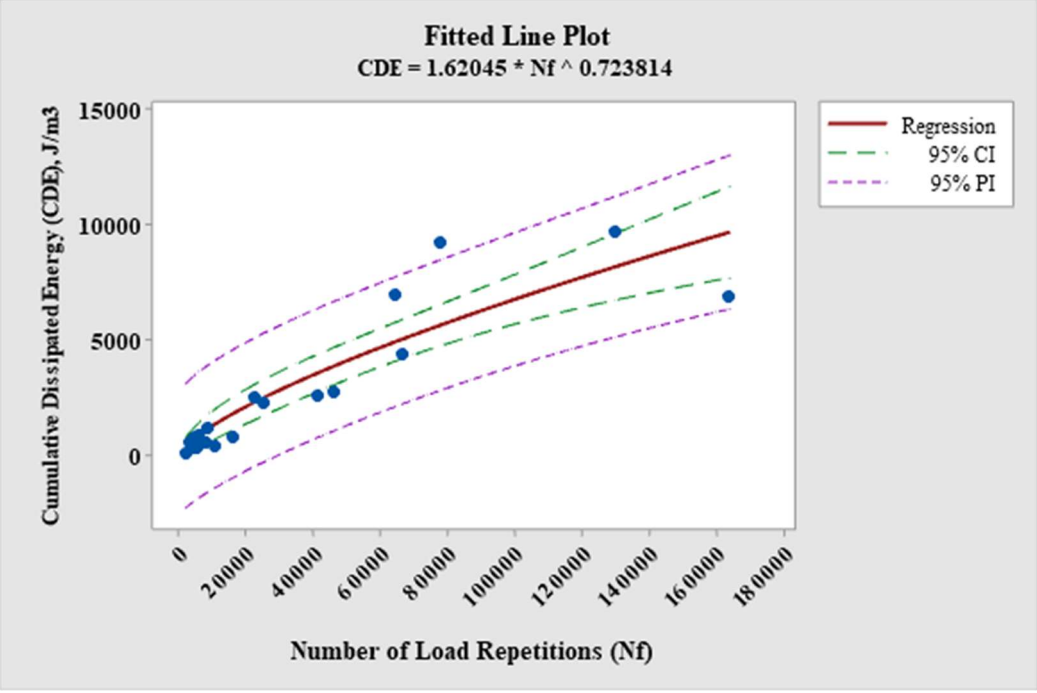

Figure 5.16 Fitted line and experimental data points of Nafziger mixtures

Table 5.8 Parameters of the Model in Equation (5.7)

Material Type	A	z
FDR-Koss	4.64	0.70
FDR-NAF	1.62	0.72

The plots of the experimental data and the fitted curves of the model in Equation (5.7) are shown in Figure 5.15 and Figure 5.16. In these figures, CI stands for confidence interval and PI stands for prediction interval. Figure 5.17 and Figure 5.18 illustrated the fatigue life measured experimentally and predicted by Equation (5.8) for FDR-Koss and FDR-NAF mixtures, respectively.

$$N_f = \left(\frac{A}{\pi\, \varepsilon_o^2\, S_o\, sin\varphi}\right)^{\frac{1}{1-z}} \tag{5.8}$$

where

N_f = Number of load repetitions to failure

ε_o = Initial applied strain

S_o = initial flexural stiffness,

φ = initial phase-angle

A, z = material constants

Table 5.9 Parameters of the Model in Equation (5.8)

Material Type	A	z	RMSE
FDR-Koss	1.75E-04	0.73	2.17E05
FDR-NAF	9.91E-04	0.48	3.08E04

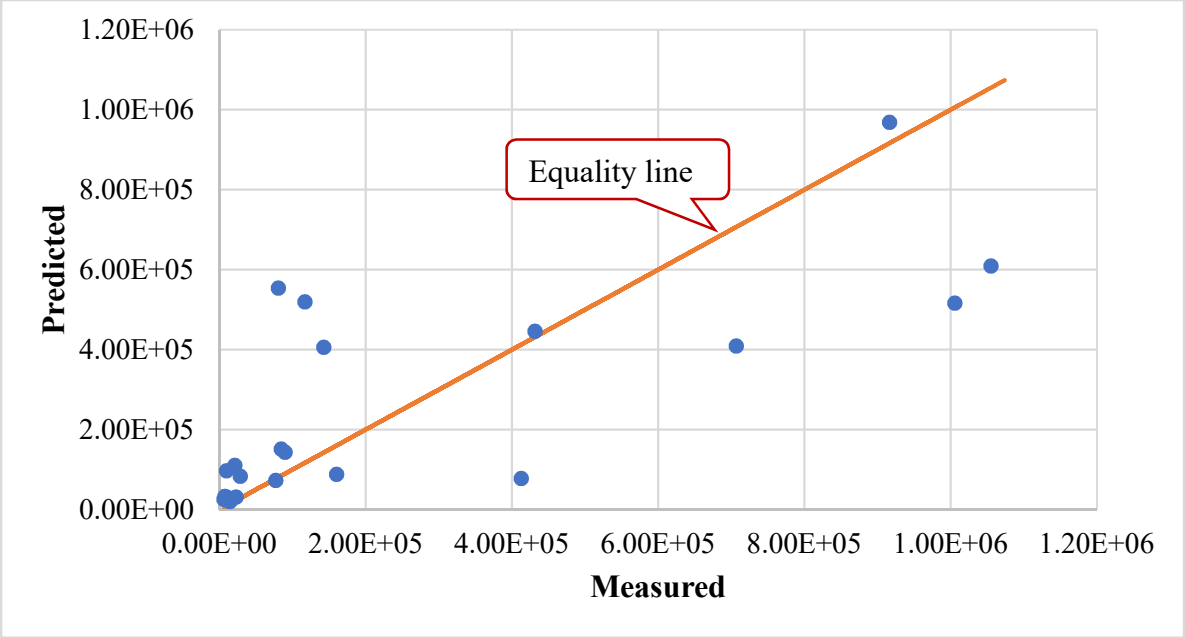

Figure 5.17 Measured and predicted fatigue life of Kossuth mixtures

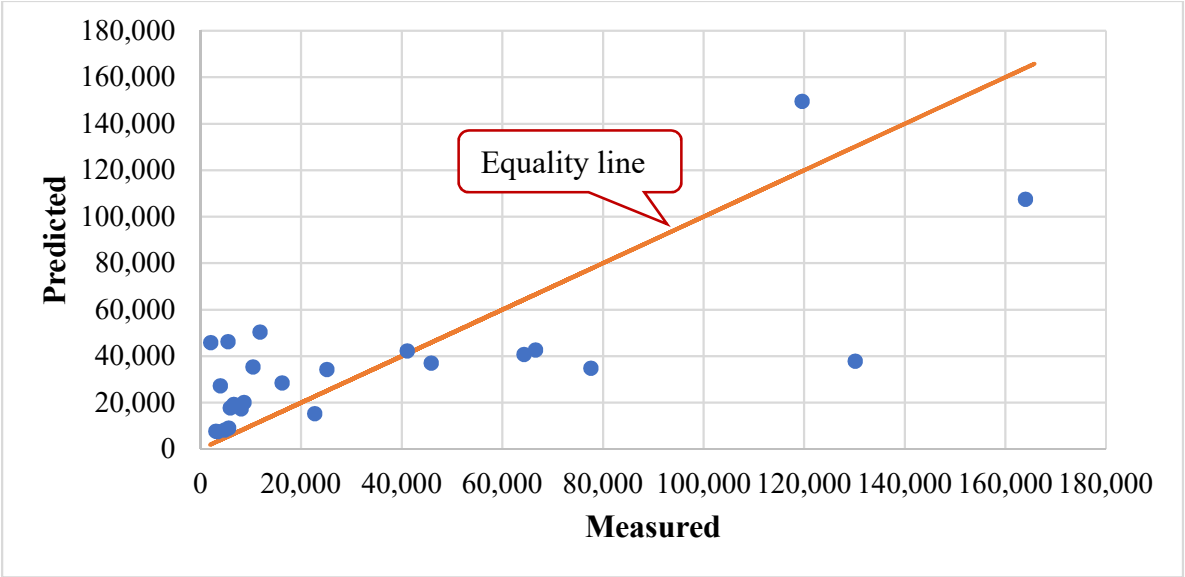

Figure 5.18 Measured and predicted fatigue life of Nafziger mixtures

The models based on cumulative dissipated energy are independent of test methods, loading modes, loading frequency and temperature (87,89,90). However, these models are

dependent on mixture formulation. Recent studies (65,66,83,86,88) suggested that the use of the Rate of Dissipated Energy Change (RDEC) approach to determine and predict the true fatigue life of the materials. The RDEC is computed as shown in Equation (5.9) and the typical plot of RDEC versus number of load repetitions is shown in Figure 5.19.

$$RDEC = \frac{|W_j - W_i|}{W_i\,(j-i)} \tag{5.9}$$

where,

W_j, W_i = dissipated energy of the i^{th} and j^{th} cycles (j > i), respectively.

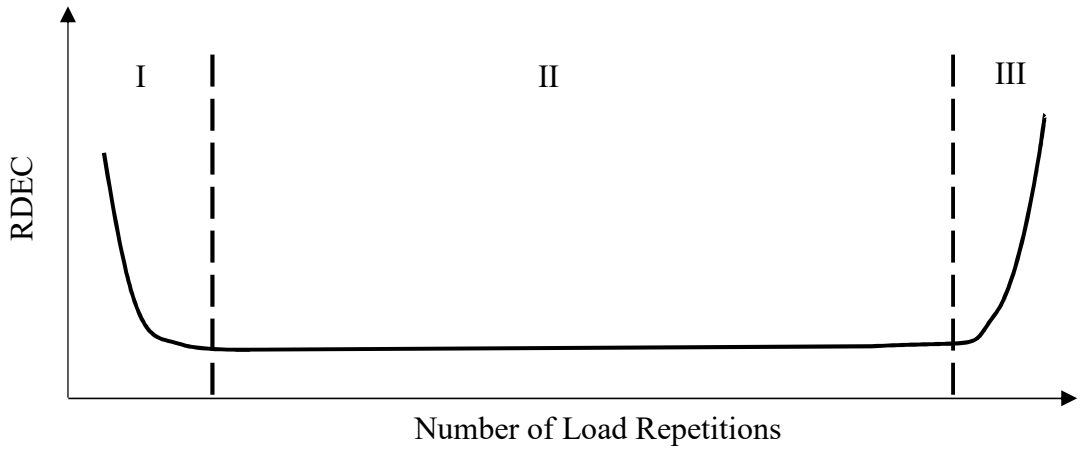

Figure 5.19 Typical evolution of RDEC with number of load repetitions (77,80,82)

As shown in Figure-5.19, RDEC curve was divided into three zones: I, II, III. Initially RDEC decreases (Zone-I), then remains stable for long time (Zone-II) and finally increases sharply (Zone-III) indicating fracture of the specimen. The RDEC in the stable zone

is called plateau value (PV). PV is considered to be independent of material type and loading method (65,86). For viscoelastic materials, PV was stated to have a unique relationship with fatigue life of various mixtures regardless of the mode of loading and the loading rate (65,83,91). The transition point between Zone-II and Zone-III of the RDEC curve is considered as the onset of the true fatigue failure (91).

However, the RDEC curve of all of the mixtures in this study did not show a sharp increase after Zone-II even after the initial stiffness was dropped by 60%. The typical RDEC curve of the mixtures was illustrated in Figure 5.20. This could be because the macroscopic cracks were not developed in the test specimens even after their initial stiffness was dropped by 60%. In all of the test specimens, visible cracks or fracture were not encountered at the end of the tests. The typical condition of the test specimens after fatigue test is shown in Figure 5.21.

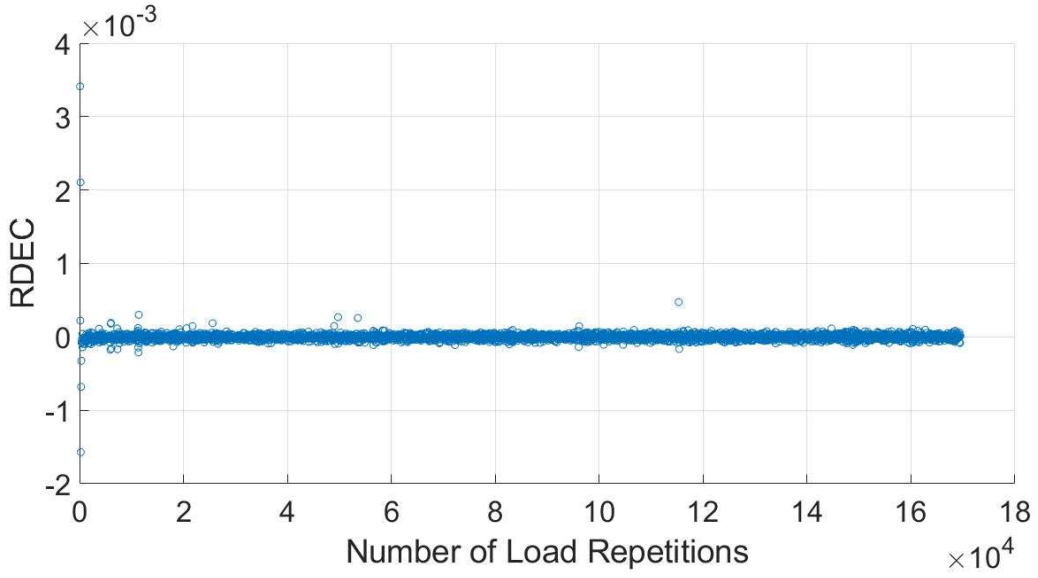

Figure 5.20 Typical plot of RDEC versus number of load repetitions

Figure 5.21 Condition of test specimens after fatigue test

The fact that the test specimens did not break after the test might not be surprising as the test was conducted on strain-controlled mode. In strain-controlled test the applied stress decreases with the loading cycle. As a result, the energy applied to the test specimen decreases with the number of load repetitions and hence clear fracture will not be developed in the specimen (83). The typical plots of stress-strain evolution and the evolution of dissipated energy with the number of load repetitions were shown in Figure 5.22 and Figure 5.23.

Another interesting point worth noting is the RDEC value of all mixtures in the study fluctuates around zero as shown in Figure 5.20. As a result, the PV value for the mixtures can not be recognized and hence the unique fatigue relationships can not be developed. D. Lei et al. (86) stated that the energy method based on RDEC is not applicable to quasi-brittle materials like concrete as the RDEC values are close to zero. According to D. Lei et al.(86)

for materials like concrete, the hysteretic energy is mainly dissipated causing a damage. For viscoelastic materials the hysteretic energy is dissipated mainly in the form of heat and only part of the dissipated energy causes damage to the test specimen. Accordingly, it can be inferred that the materials in the study possess the blended properties of viscoelastic and quasi-brittle materials.

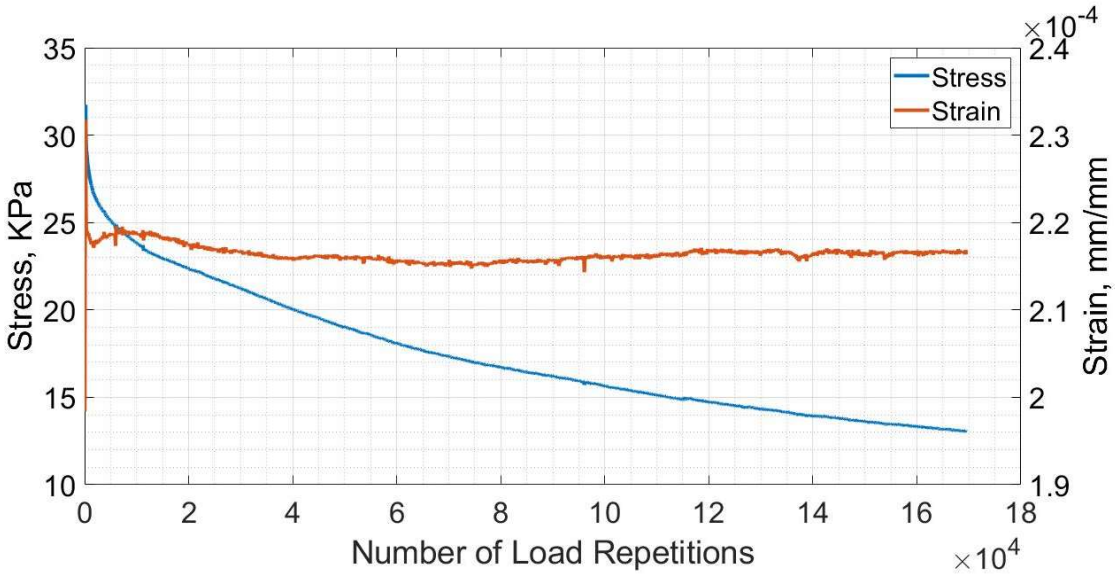

Figure 5.22 Typical stress and strain evolution with loading cycles

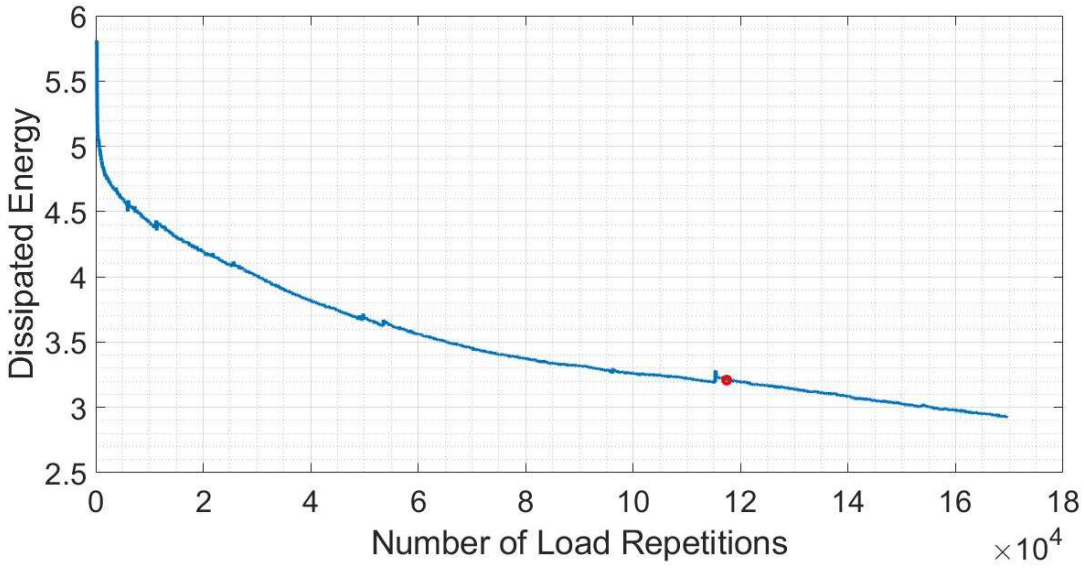

Figure 5.23 Evolution of dissipated energy (J/m^3) with number of load repetitions

5.3.3. Effects of binder types on phase-angle and cumulative dissipated energy

The plots of the initial phase-angle and cumulative dissipated energy for all of the eight mixtures were shown in Figure 5.24 and Figure 5.25. To assess the effects of the cementitious binders on the phase-angles and cumulative dissipated energy, two-way ANOVA and multiple comparison were performed. The ANOVA result in Table 5.10 indicated that the initial phase-angle was not affected by the binder type. This was supported by Dunnett's multiple comparison as shown in Figure 5.26. Also, the initial phase-angle of both FDR-Koss and FDR-NAF mixtures did not show significant variations.

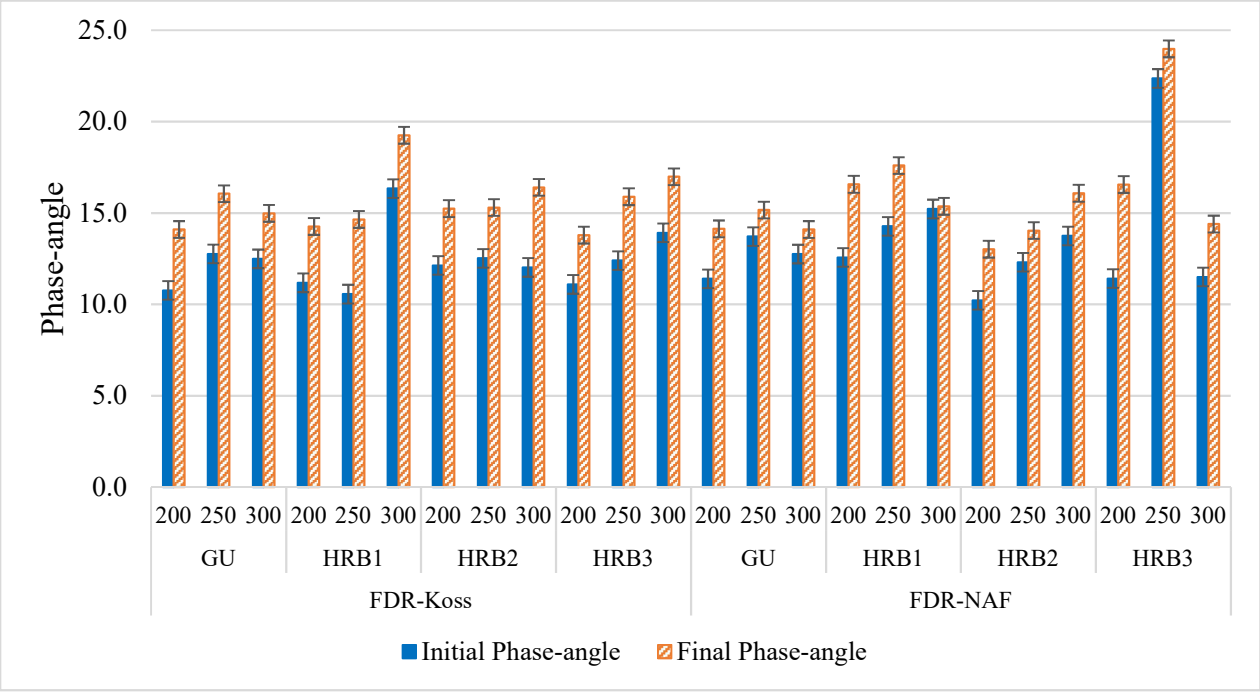

Figure 5.24 Initial and final phase-angle

The ANOVA and multiple comparison on the cumulative dissipated energy (CDE) also indicated the binder type did not have significant impact on the CDE. However, according to the results in Table 5.11, the CDE could vary significantly based on the type of reclaimed materials. The results of Dunnett's multiple comparison for CDE were shown in

Figure 5.27. According to the statistical analyses, the behaviour of hydraulic road binder mixtures to repeated loading were equivalent to those of GU mixtures.

Figure 5.25 Cumulative dissipated energy

Table 5.10 ANOVA for Phase-angle

Source	F-Value	P-Value
Binder Type	0.70	0.559
Material Type	1.37	0.248
Binder Type*Material Type	0.38	0.766

Table 5.11 ANOVA for Cumulative Dissipated Energy

Source	F-Value	P-Value
Binder Type	1.68	0.188
Material Type	12.28	0.001
Binder Type*Material Type	1.92	0.142

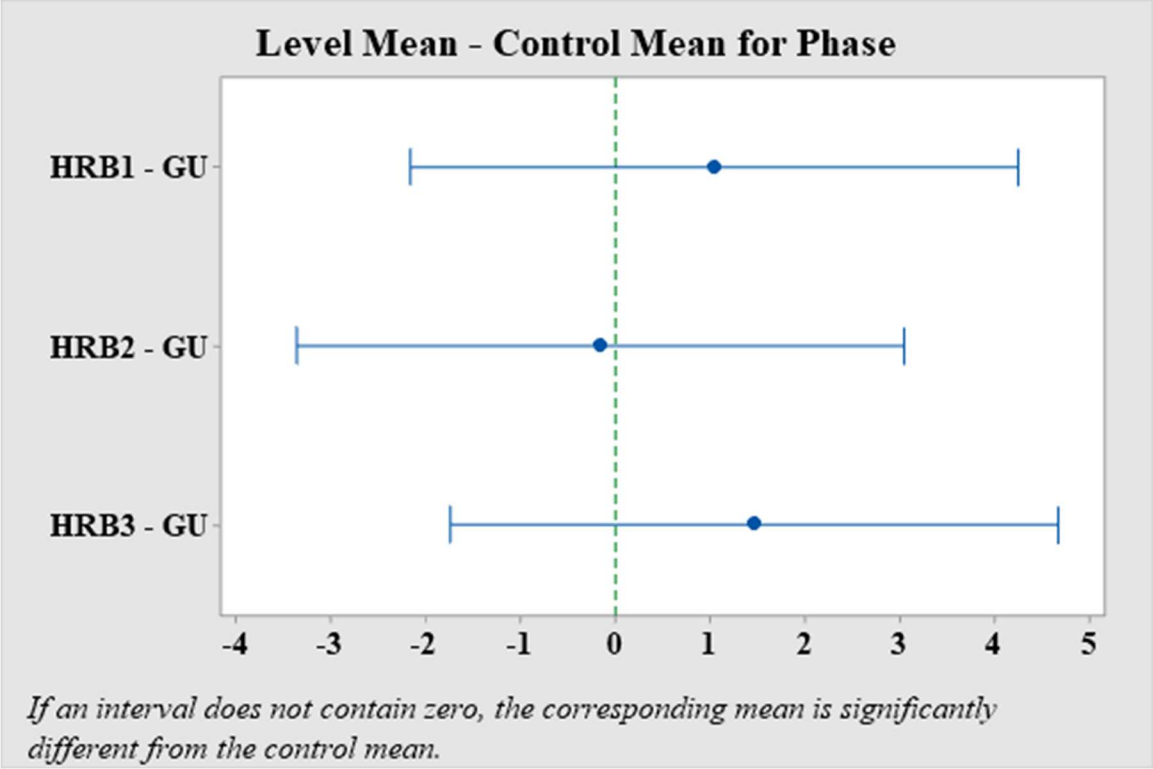

Figure 5.26 Dunnett's multiple comparison for phase-angle of FDR-Koss and FDR-NAF mixtures

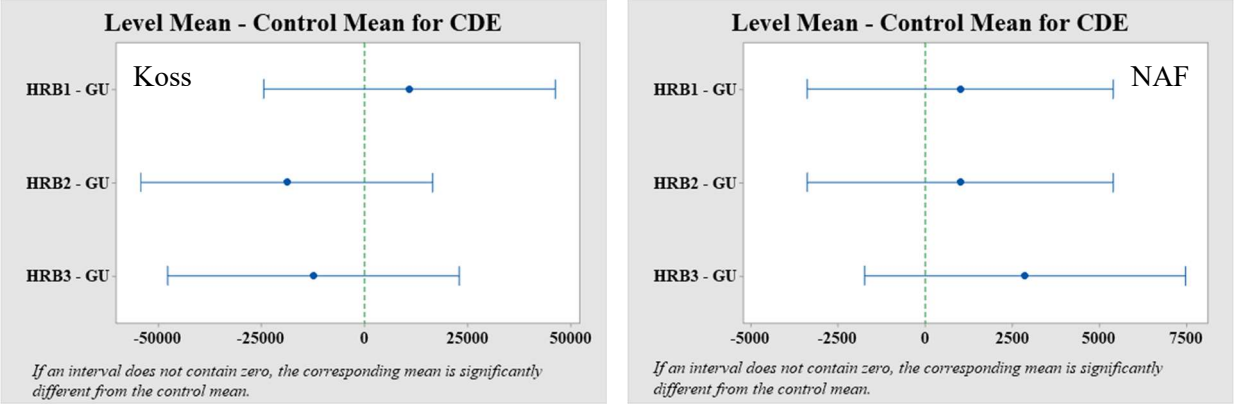

Figure 5.27 Dunnett's multiple comparison on CDE

5.4. Conclusions

The fatigue behaviour of FRPMC was investigated using four-point loading test. The assessment was done on eight different types of mixtures, which were composed of two types

of reclaimed pavement materials and four different types of cementitious stabilizers. Three of the four stabilizers were hydraulic road binders and the remaining one was GU cement.

The phenomenological and energy-based methods of fatigue analyses were performed, and the fatigue model parameters were determined based on the experimental results. These can be used to design semi-rigid pavements with FRPMC base layer. The study findings can be presented as:

- The type of stabilizers used in this study did not significantly affect the fatigue life of the mixtures indicating that the fatigue performance of HRB mixtures and GU mixtures would be equivalent
- Even though FRPMC are cement treated materials, they showed the properties of viscoelastic materials
- The rate of dissipated energy change of FRPMC was similar to that of quasi-brittle materials in Zone-II of the RDEC versus number of load repetition plot.
- The plot of RDEC versus number of load repetition of FRPMC mixtures did not indicate a sharp increase in Zone-III, which is not typical for bituminous mixtures neither for Portland cement concrete.

Further studies should be conducted to address the effects of binder content, temperature, loading rate, loading mode and testing methods on the fatigue performance of the FRPMC mixes. It is also recommended to verify the laboratory findings through field trial sections.

6. EFFECTS OF HYDRAULIC ROAD BINDERS ON LIFE-CYCLE IMPACTS OF FULL-DEPTH RECLAMATION

Summary

Approximately 5% of the global anthropogenic carbon dioxide (CO_2) emissions are generated from cement manufacturing. Production of 1 kg of ordinary Portland cement produces 0.81 – 0.87 kg CO_2. The main source of the emissions in the cement industry is the calcination process in which huge amount of fossil energy is consumed and limestone is decarbonized. To reduce the amount of CO_2 emission associated with cement production, various studies proposed different approaches. Among these is partial substitution of the clinker in the Portland cement with supplementary cementing materials (SCM). Cementitious binders containing SCM and specifically designed for application in road construction are called hydraulic road binders (HRB). In this study, comparative LCA was conducted to assess the effects of different HRB on the overall environmental impacts of full-depth reclamation process. The study was performed by integrating three major tasks: material characterization, pavement design and performance prediction, and life cycle assessment. Three different types of hydraulic road binders and general use cement were used to stabilize reclaimed pavement material containing 60% RAP. Pavement design and performance prediction was done using AASHTOWare Pavement ME and the life cycle impact assessment was performed with Athena Pavement LCA software. The results of the analysis indicated that using hydraulic road binders in full-depth reclamation process could reduce global warming potential by up to 27%.

6.1. Introduction

Approximately 5% of the global anthropogenic carbon dioxide (CO_2) emissions are generated from cement manufacturing (4,5). Production of 1 kg of ordinary Portland cement produces 0.81 – 0.87 kg CO_2 (92,93). The main source of the emissions in the cement industry is the calcination process in which huge amounts of fossil fuel is consumed and limestone is decarbonized. To reduce the amount of CO_2 emissions associated with cement production, various studies (6,12,40,41,94,95) have proposed different approaches. Among these is partial substitution of the clinker in the Portland cement with supplementary cementing materials (SCM). This process converts ordinary Portland cement to blended cement. Compared to ordinary Portland cement, blended cements have less environmental impact, requires less energy and consumes fewer material resources (42,43).

Blended cements that are specifically designed for applications in road construction works are known as hydraulic road binders (HRB). These are factory blends made for treatment of bases, sub-bases, capping layer and embankment materials (44,96). The standard requirements for composition and properties of HRB are given in the European standard EN 13282-1 and EN 13282-2 (44,96).

Previous works in similar topics mainly focused on the LCA of the pavement and pavement rehabilitation options (97–104), development of approaches for performing pavement LCA (105–107) and LCA of binders like cement and ground granulated blast furnace slag (93,94,108–113). Chiu et al. (103) conducted LCA to evaluate the eco-burden of different recycled materials used in pavement milling and overlay. The materials used were recycled hot mix asphalt, asphalt rubber and Glassphalt. The life cycle impact assessment

method used for the analysis was Eco-indicator 99. The findings of the analysis indicated that the use of recycled hot mix asphalt and asphalt rubber could reduce the eco-burden by 23% whereas Glassphalt increases the eco-burden 19%. Cross et al. (104) compared the environmental burdens associated with four types of pavement rehabilitation techniques using PaLATE (Pavement Life-Cycle Assessment Tool for Environmental and Economic Effects). The rehabilitation techniques considered in analysis were pavement cold in-place recycling (CIPR) with and without additional aggregates, mill and fill overlay, and two-course overlay. The results of the analysis indicated that CIPR without the addition of aggregates is the best and two-course overlay is the least preferred options from the life-cycle impact perspective. Giani et al. (98) conducted a cradle-to-grave analysis to identify the combined effect of using RAP and Warm Mix Asphalt (WMA) in pavement rehabilitation. The analysis was conducted on three pavement types in the form of comparative assessment. Each pavement type was composed of three layers: surface course, binder course and base course. The first pavement contains virgin materials and hot mix asphalt (HMA) in all of its three layers. This pavement was considered as a reference pavement or base case scenario. The second pavement type contained 10% and 20% RAP in its surfacing and binder layers, respectively. The surface and binder layer of the third pavement was the same as the second pavement but its base course was composed of 30% RAP and WMA. This analysis indicated that the use of RAP and WMA could result in 12% reduction of CO_2eq, 15% reduction in energy consumption and 15% reduction in water demand (98). Turk et al. (99) compared the environmental impacts associated with traditional pavement reconstruction and pavement rehabilitation with cold in-place recycling technique. In the cold in-place recycling process, Portland cement was used as a binder. The analysis indicated that the rehabilitation with cold in-place recycling would

reduce acidification potential, abiotic depletion of fossil fuels, and energy consumption by 15% - 18%. However, the global warming potential of both alternatives was similar. The higher global warming potential of cold in-place recycling was due to the huge amount of emissions related to the production of Portland cement (99). In general, all of the reviewed analyses indicated that the use of RAP and cold in-place recycling technologies would reduce the environmental impacts to a certain extent.

However, it was indicated that the use of Portland cement in cold in-place recycling process would increase the global warming potential (99). This problem could be overcome by using blended cements instead of Portland cement. Huntzinger and Eatmon (93) conducted an a cradle-to-gate LCA to compare the environmental impacts of three types of blended cement with the traditional Portland cement. The first blend was composed of natural pozzolans whereas the second and third blends contained cement kiln dust (CKD). The difference between the second and the third blend was that the third blend was produced using CKD to sequester portion of CO_2 emissions. The study findings indicated that substituting the clinker with natural pozzolans can reduce the impacts associated with clinker production by 21.6%. The sequestration of CO_2 by CKD would reduce CO_2 emissions and environmental impacts of cement by 5%. However, the use of CKD as a recycled material to produce blended cement of the second type have little environmental benefit (93). Li et al. (109) studied the environmental impact of utilizing blast furnace slag as an additional raw material in the manufacture of cement. In this study, the effects of incorporating 10% blast furnace slag was assessed by considering the slag as a co-product of pig-iron. The results of the study showed that slag-based cement could reduce the environmental impacts by 17%. Abiotic depletion potential and land use potential could also be reduced by 72% and 41%, respectively.

However, the human toxicity potential could increase by 9% as the blast furnace slag is not readily grindable.

The literature highlighted that certain level of environmental savings can be attained by using blended cements in lieu of Portland cement. However, more research is needed on a range of cement blends in different regions to have a broader and more comprehensive understanding of the environmental profile of these products. In this study, life cycle assessment (LCA) was used to evaluate the life cycle impacts associated with the use of HRB and GU cement in a full-depth reclamation (FDR) process.

6.2. Material and Methods

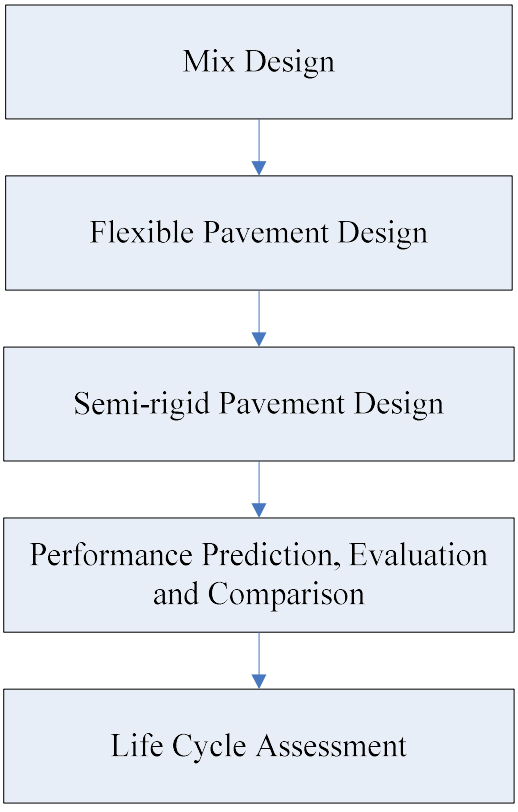

Figure 6.1 Life assessment methodology

The LCA approach followed in the study was indicated in the flow-chart in Figure 6.1. The first step was formulating the mixture proportions of the cement-treated reclaimed material to determine the maximum dry density and optimum moisture content. Next, a flexible pavement that represent an existing aged pavement was designed using AASHTOWare Pavement ME. Then semi-rigid pavements containing stabilized reclaimed material as a base layer were designed. Finally, life cycle assessment was used to compare the effects of the different stabilizers on the overall environmental impacts of the semi-rigid pavement. These are detailed in Section 6.2.2 and Section 6.2.3.

6.2.1. Material

- *Reclaimed material*

For the purpose of this study a reclaimed material with 60% reclaimed asphalt pavement (RAP) and 40% crushed coarse aggregate (Granular A) was collected from a full-depth reclamation project site in Ontario, Canada. The physical properties of the reclaimed material are shown in Figure 6.2 and Table 6.1.

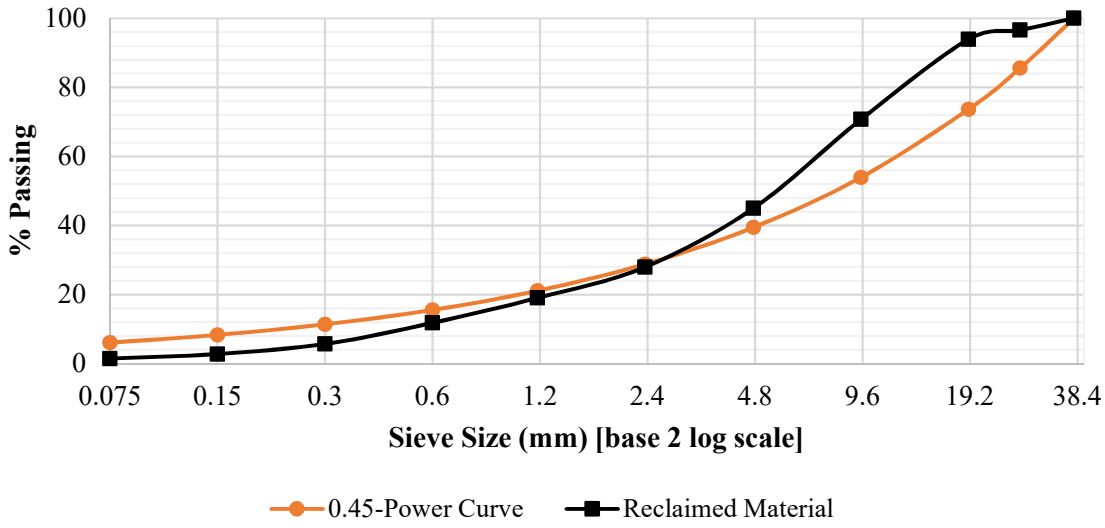

Figure 6.2 Particle size distribution of the reclaimed material

Table 6.1 Properties of Reclaimed Material

Description	Test Method	Results
Liquid limit (%)	AASHTO T 89	Non-plastic
Plasticity index	AASHTO T 90	Non-plastic
AASHTO Soil Class	AASHTTO M 145	A-1-a
Micro-deval Abrasion Loss (%)	ASTM D 6928	12.7

- *Cementitious binders*

Four different types of cementitious binders, three HRB and GU cement, were used for comparison. The three hydraulic road binders are designated as HRB1, HRB2, HRB3. The physical properties and chemical composition of the binders are shown in Table 6.2 and Table 6.3, respectively.

Table 6.2 Physical Properties of Cementitious Binders

Physical Properties	GU	HRB1	HRB2	HRB3
Autocalve, % Expansion	0.05	0.0	0.0	0.0
Blaine Fineness, m^2/kg	383	465	497	389
Compressive Strength at 28 days, MPa	40.5	34.8	41.5	35.0
Fineness, 45μm sieve, % retained	4.0	5.0	1.9	4.1
Initial time of set, minutes	90	161	173	153
Sulphate Resistance, % expansion at 6 months	0.014	-	0.005	0.040

Table 6.3 Chemical Composition of Binders

Chemical Composition	GU	HRB1	HRB2	HRB3
SiO_2 (%)	19.6	28.4	22.3	26.2
Al_2O_3 (%)	5.0	7.6	5.7	7.0
Fe_2O_3 (%)	3.3	2.1	2.3	2.3
CaO (%)	62.2	49.4	55.4	53.4
MgO (%)	2.5	7.2	4.7	5.9
SO_3 (%)	3.9	3.3	3.7	3.6
Loss on ignition @ 950 (%)	2.3	1.5	4.3	1.7

6.2.2. Methods

This study was conducted in three stages. The first stage was mixture design for the stabilization process. In this stage the optimum binder and moisture content required to stabilize the reclaimed material was determined. The second stage was pavement design and performance prediction. This was done to determine the pavement layer compositions and anticipated pavement performance. The sets of information from stage one and stage two were important to quantify the material requirement, set system boundary, and compute other life cycle inventory data. The details and findings of the first and second stages are discussed in the following two subsections of the manuscript. The final stage, which is the main focus of this study, is life cycle assessment. The life cycle assessment was conducted according to ISO 14040/14044 framework using Athena Pavement LCA software.

- *Mix design*

Mix design involves determination of the optimum mixing water and optimum binder (stabilizer) contents. The optimum mixing water content was determined by standard proctor test according to ASTM D 558. The optimum binder content is often determined as the minimum binder content that provides 7 days unconfined compressive strength (UCS) between 2.1 MPa – 2.8 MPa (7). However, with the reclaimed material used in this study, the minimum acceptable UCS value was not attained even with 6% binder content. As mixes with higher cementious binder content are often vulnerable to shrinkage cracking, the binder content was not increased beyond 6%. Thus, the binder content of 6% was used for the stabilization purpose. The optimum mixing water content (OMC), maximum dry density (MDD), wet density at optimum moisture content (MWD), optimum binder content (OBC), along with 7 days and 28 days UCS are shown in Table 6.4.

Table 6.4 Properties of Stabilized Mixtures [MDD = maximum dry density, MWD = wet density at optimum moisture content, OMC = optimum moisture content, OBC = optimum binder content]

Mixture Type	MDD (kg/m^3)	MWD (kg/m^3)	OMC (%)	OBC (%)	7 days UCS (MPa)	28 days UCS (MPa)
GU-Mix	1980	2100	5.9	6.0	1.6	2.5
HRB1-Mix	2020	2130	5.6	6.0	1.3	3.0
HRB2-Mix	2010	2106	5.0	6.0	1.5	2.8
HRB3-Mix	1970	2064	5.3	6.0	1.7	3.5

- *Pavement design and performance prediction*

It was assumed that full-depth reclamation was chosen to rehabilitate an aged two-way minor arterial road, which was designed and used for 20 years. The aged road was assumed to have initial annual average daily truck traffic (AADTT) of 900 with an annual growth rate of 3%. The pavement structure of the aged pavement was designed as a flexible pavement using AASHTOWare Pavement ME, version 2.2.5. Subgrade resilient modulus of 35 MPa was used to design the pavement structure. The designed pavement structure is shown in Table 6.5.

Table 6.5 Designed Pavement Structure for Existing Aged Pavement

Layer Type	Material Type	Thickness (mm)
Asphalt wearing course	Ontario SP 12.5 mm	80
Asphalt binder course	Ontario SP 19 mm	100
Granular base course	Granular A	400
Granular sub-base	Granular B	500

Then the pavement structures containing the stabilized reclaimed pavement as a base layer was designed for a design period of 15 years. These represent the pavement structure after the application of full-depth reclamation. The pavement design was done as semi-rigid

pavement again using AASHTOWare Pavement ME, version 2.2.5. The stabilized base is composed of the 180 mm bituminous layer and part of the underlying granular base of the existing aged pavement.

Typical properties of the granular base, granular sub-base and asphalt concrete recommended by Ministry of Transportation of Ontario (MTO) (114) were used to design the pavement structures. However, the properties of the stabilized reclaimed pavement materials were determined experimentally for all binder types. The laboratory test results are shown in Table 6.6.

Table 6.6 Stabilized Layer Properties for Semi-rigid Pavement Design

Mixture Type	Elastic Modulus (28 days, MPa)	Rupture Modulus (28 days, MPa)	Poisson's Ratio
GU-Mix	2420	0.66	0.24
HRB1-Mix	2834	0.67	0.20
HRB2-Mix	2420	0.69	0.24
HRB3-Mix	2664	0.60	0.20

The initial two-way AADTT used to design the semi-rigid pavement was 1,272. This was the anticipated traffic volume at the end of the design period (20 years) of the original flexible pavement with initial AADTT of 900. The annual traffic growth rate was assumed to remain the same, which is 3%, over the design period of the pavement. Since the properties of the four stabilized mixes are similar, the pavement structure that fulfills the design criteria is the same for all of the four binder mixes. The designed pavement structure is shown in Table 6.7 and summary of the predicted distress intensity at the end of the pavement design period (15 years) is shown in Table 6.8.

Considering a total analysis period of 50 years, the analysis period after the full-depth reclamation process was set to be 30 years. As a result, the performance of the pavements after rehabilitation was forecasted over a period of 30 years using AASHTOWare Pavement ME. This was done to assess whether the slight variations in the properties of the stabilized base of the four cementious mixes have significant effect on the progression of major distresses. As shown in Figure 6.3, the anticipated permanent deformation and transverse crack density are the same regardless of the type of binder used to stabilize the reclaimed material. The densities of bottom-up and top-down fatigue cracks, however, are slightly affected by the binder types. Likewise, Figure 6.4 shows the growth in the roughness of the pavements over the 30 years analysis period is the similar irrespective of the binder type.

Table 6.7 Designed Pavement Structure for the Rehabilitated Pavement

Layer Type	Material Type	Thickness (mm)
Asphalt concrete wearing course	Ontario SP 12.5	40
Cement bound base	Stabilized reclaimed pavement	300
Granular base course	Ontario Granular A	280
Granular sub-base	Ontario Granular B	500

Furthermore, the Pavement Condition Index (PCI) of the four pavements was computed using the pavement distress data forecasted by AASHTOWare Pavement ME over the period of 30 years. The PCI calculation was conducted using the formulae given in MTO's Pavement Design and Rehabilitation Manual (115), which are shown by Equation (6.1) and Equation (6.2).

$$PCI = Max\big(0, Min(100, 13.75 + 9 \times DMI - 7.5 \times IRI)\big) \quad (6.1)$$

where DMI = distress manifestation index, which is computed using Equation (6.2).

$$DMI = 10 * \frac{(208 - \sum_{k}^{N}(S_k + D_k) \times W_k)}{208} \quad (6.2)$$

where:

N = number of distress related to a given pavement type

S_k = severity rate of distress k

D_k = density rate of distress k

W_k = weighting factor of distress k

Table 6.8 Predicted Performance of Pavements with Stabilized Base

Distress Type	Target Reliability	Distress at Specified Reliability				
		Target	Predicted			
			GU	HRB1	HRB2	HRB3
Terminal IRI (m/km)	85	2.30	2.04	2.04	2.04	2.04
Permanent deformation - total pavement (mm)	85	13.00	5.50	5.47	5.50	5.50
AC total fatigue cracking: bottom up + reflective (% lane area)	85	50.00	1.98	2.36	1.98	1.98
AC total transverse cracking: thermal + reflective (m/km)	85	473.40	340.46	340.46	340.46	340.46
AC bottom-up fatigue cracking (%)	50	20.00	0.00	0.00	0.00	0.00
AC thermal cracking (m/km)	50	190.00	0.19	0.19	0.19	0.19
AC top-down fatigue cracking (m/km)	85	380.00	39.32	39.31	39.32	39.32
Permanent deformation - AC only (mm)	85	6.00	0.42	0.43	0.42	0.42
Chemically stabilized layer - fatigue fracture (percent lane area)	-	25.00	1.54	1.92	1.54	1.54

Using PCI as key pavement performance indicator, performance deterioration curves were plotted for the four pavement structures. As shown in Figure 6.5, performance deterioration trend of the pavements is not affected by the slight variation in the properties of the stabilized base layer.

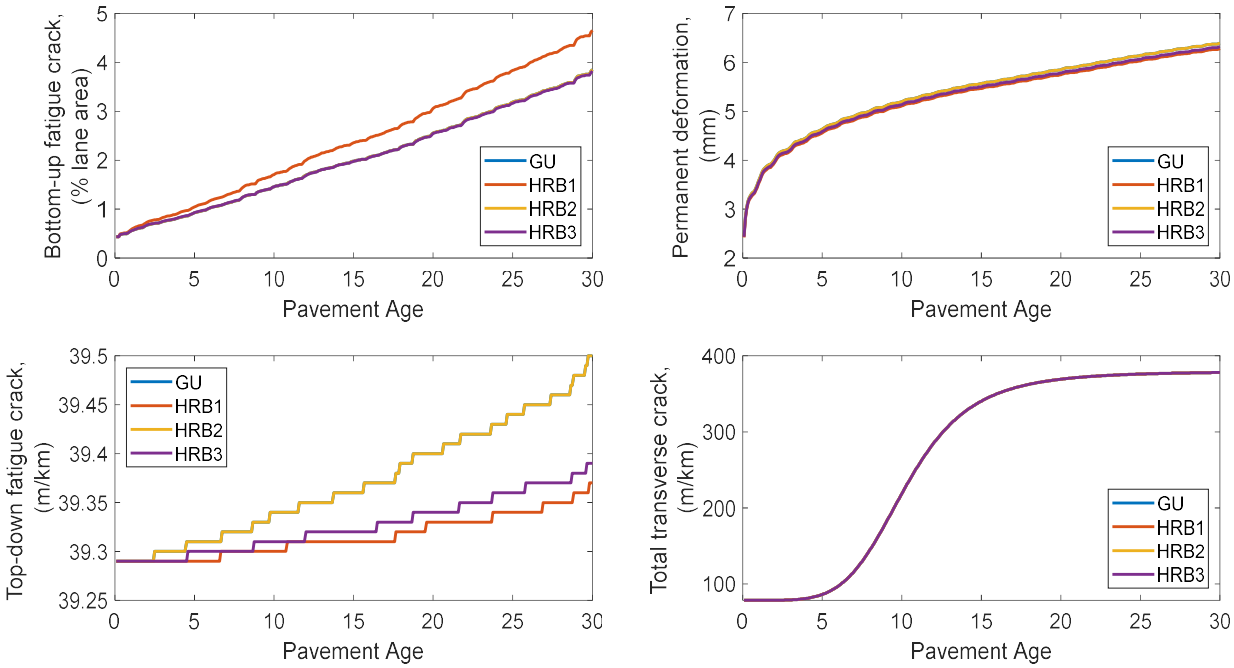

Figure 6.3 Distress progression over a period of 30 years after rehabilitation by full-depth reclamation

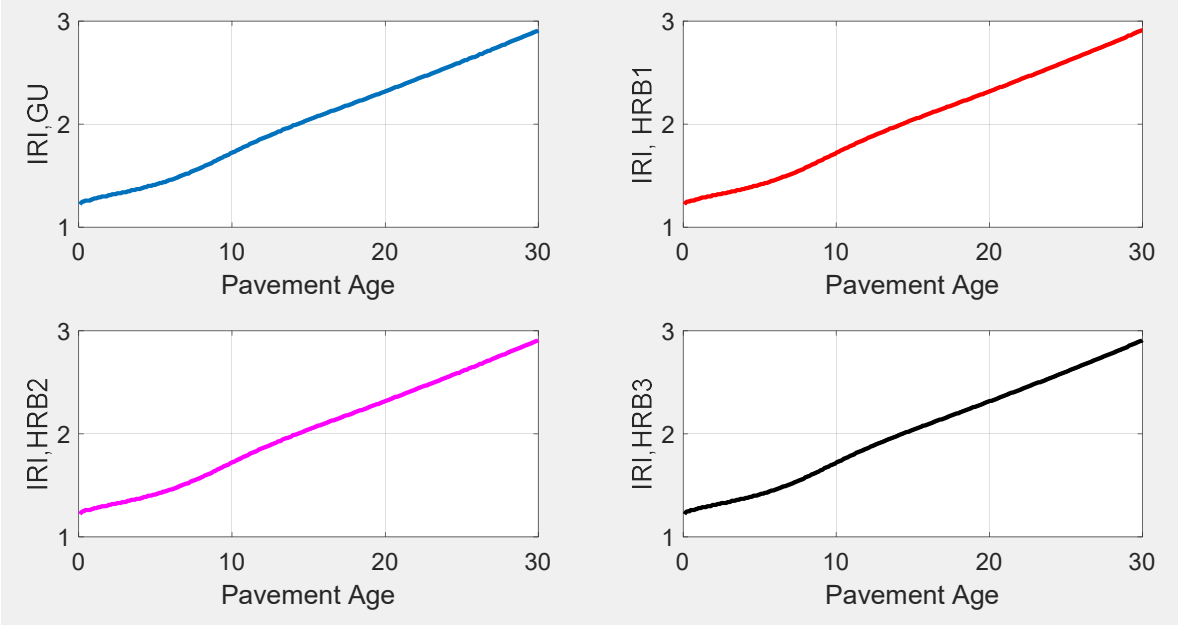

Figure 6.4 Growth trend in the severity of pavement roughness

Therefore, it is reasonable to assume that the performance of the pavement would be the same throughout the analysis period regardless of the binder type used to stabilize the base layer. Moreover, the remaining life and conditions of the pavement at the end of the analysis period could also be assumed to be the same irrespective of the binder type.

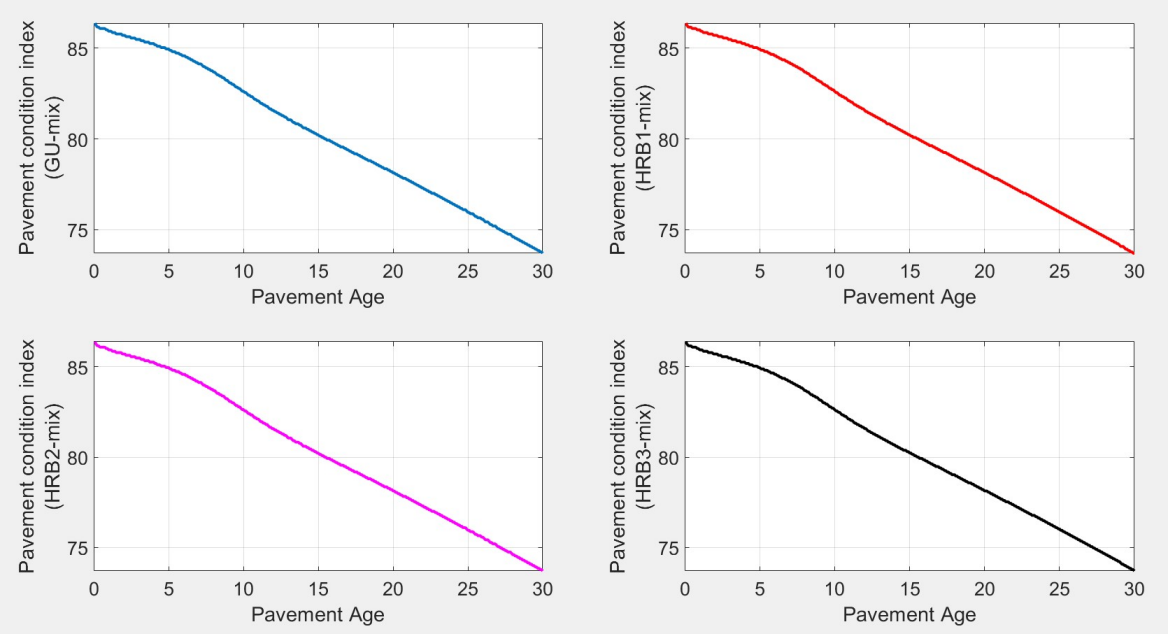

Figure 6.5 Performance deterioration curves

6.2.3. Goal and Scope of LCA

The goal of the LCA is to assess the environmental impacts associated with substituting GU cement with hydraulic road binders as stabilizers in full-depth reclamation process. The analysis also aims at evaluating viability of HRB as alternatives to GU cement from environmental impact perspectives. The analysis was performed with comparative LCA to identify the binder(s) with the least environmental impacts.

- *Product System*

The product system of this study entails pavement in-place recycling with full-depth reclamation using hydraulic road binder as a stabilizer for conditions in Ontario, Canada. In full-depth reclamation process, the existing aged road is pulverized in-place, blended with stabilizers (binders) and compacted to form a stable base layer. A thin hot mix asphalt (HMA) layer is often placed over the stabilized base to provide a smooth riding surface. A prime coat is applied between the stabilized base and the HMA layer to ensure good bond between the two layers. In this study, three different types of hydraulic road binders (HRB1, HRB2, HRB3) were considered. The HRB systems were compared to the reference system which uses GU cement, in lieu of HRB, as a stabilizer. The product system and reference system are shown in Figure 6.6.

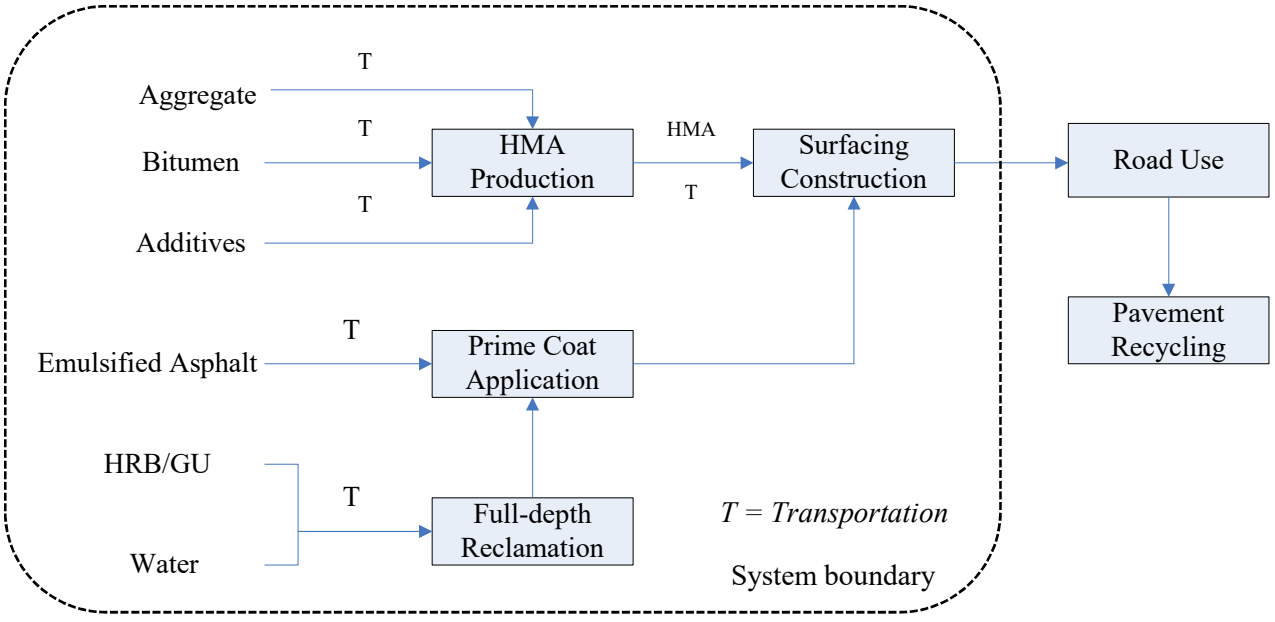

Figure 6.6 Cradle-to-construction gate boundary for life-cycle assessment of pavement systems using either HRB (hydraulic road binder) or GU (general use) cement

- *Alternate Scenarios for Pavement Structure*

Pavement design criteria varies across regions, as do other factors such as energy mix, transportation mode, manufacturing methods, and material extraction. To assess the consistency of the LCA results, a scenario analysis was conducted by considering road rehabilitation in both Manitoba and Quebec. This required verifying whether the pavement structure designed for Ontario is structurally adequate for Manitoba and Quebec. This was done with AASHTOWare Pavement ME by changing the climate data, material properties and design criteria. The material properties and design criteria were set up using the Canadian Guide: Default Parameters for AASHTOWare Pavement ME Design (116). The pavement structures used for the scenario analysis are shown in Table 6.9.

Table 6.9 Pavement Structure for Scenario Analysis

Layer Type	Material Type		Thickness (mm)
	Manitoba	Quebec	
Asphalt concrete wearing course	SP 12.5	ESG 10	40
Cement bound base	Stabilized reclaimed pavement		300
Granular base course	Granular A	MG 20	280
Granular sub-base	Granular B	MG 112	500

- *Functional Unit and Reference Flows*

The function of the systems is defined as providing a surface for vehicles to move over, which in this case is a rehabilitated minor arterial road. The functional unit of the analysis is 1 km-lane of a two-lane (3.75 m width per lane) minor arterial road with a design period of 15 years and first year AADTT of 1,272. The AADTT was assumed to have an annual growth rate of 3% over the design period of 15 years. The amount of materials required to meet the

functional unit (a.k.a reference flow) for the various pavement structures are shown in Table 6.7.

- *System Boundary*

The system boundary (i.e. stages of life cycle included) for this study is cradle-to-construction gate, and includes raw materials extraction, processing or manufacturing of construction materials, pavement rehabilitation, and all related transportation. The use, road maintenance and end-of-life stages are excluded from the system boundary because it was assumed that all the pavements have the same performance over the analysis period. There is no difference in the impacts at these stages. This assumption was based on the results of the pavement performance prediction discussed in Section 6.2.2.

6.2.4. Life Cycle Inventory

The materials quantity required per functional unit of the rehabilitated pavement was computed based on the pavement layer composition shown in Table 6.7 and mix design data shown in Table 6.4. The electricity and fossil fuel requirements of each process was set using the data in Athena Pavement LCA database. Similarly, the data for the emissions associated with each process were based on the database of Athena Pavement LCA. Transportation distances in Athena Pavement LCA database were found reasonable considering the locations of the asphalt plants and rock quarries from a hypothetical road in Ontario. Summary of the life cycle inventory are shown in Table 6.10.

Table 6.10 Life Cycle Inventory

Flow/Functional unit	Pavement containing base layer stabilized with:			
	GU	HRB1	HRB2	HRB3
Materials				
Asphalt concrete (kg)	369,000	369,000	369,000	369,000
Emulsified asphalt (kg)	13,460	13,460	13,460	13,460
RAP aggregate (kg)	1,254,488	1,274,805	1,260,441	1,235,304
Coarse aggregate crushed stone (kg)	836,325	850,669	841,084	824,310
Portland Cement (kg)	132,300	-	-	-
HRB1 (kg)	-	136,586	-	-
HRB2 (kg)	-	-	135,047	-
HRB3 (kg)	-	-	-	131,936
Water (Liter)	139,388	134,190	132,678	136,998
Energy				
Electricity	*From Athena Pavement LCA database*			
Fossil fuel	*From Athena Pavement LCA database*			
Transportation				
Distance of material processing plant to construction site (km)	30			
Distance of site to stockpile (km)	30			
Distance of equipment depot to site (km)	30			
Distance from aggregate extraction to crusher plant (km)	69			
Distance from bitumen manufacturing to HMA plant (km)	300			
Distance from fine aggregate extraction to HMA plant (km)	46			
Distance of GU cement and SCM	*In Athena Pavement LCA the cradle-to-gate transportation of these materials are included in LCI of the products and reported as Manufacturing Material effects*			
Performance year/Design period (years)	15			

6.2.5. Limitations of the Analysis

Athena Pavement LCA does not consider the energy input and emissions output related to the blending process, in which SCM is blended with GU cement. This was one of the limitations of this study. Because of this reason, the data related to the blending process were manually calculated using typical blending machine's specification and LCI data in Athena Institute publication (117). The emissions were first converted into global warming potential and then added to the global warming potential of the manufacturing stage directly obtained from the

software. Likewise, the energy calculated for this process was added to the total primary energy. The detailed calculation is shown in Appendix-2.

The other limitation was the absence of field performance data for the pavement types considered in this study. As a result, the pavement performance over the chosen design period was predicted using AASHTOWare Pavement LCA as explained in Section 6.2.2.

6.2.6. Life Cycle Impact Assessment (LCIA)

The LCIA methodology in Athena Pavement LCA is TRACI V 2.1, which is the US EPA Tool for Reduction and Assessment of Chemical and Other Environmental Impacts (118). The results of the LCIA are presented in terms of six mid-point impact categories, namely:

- Global warming potential
- Acidification potential
- Human health particulate
- Eutrophication potential
- Ozone depletion potential and
- Smog potential

All of these impact categories were used in the study to compare the environmental impacts of the pavement with each binder.

In addition to the impact categories, Athena Pavement LCA also provides the energy consumption of the life cycle stages in three forms as Total Primary Energy, Non-Renewable Energy, and Fossil Fuel Consumption. Total primary energy consumption shows all the direct and indirect energy involved throughout the whole life cycle stages (118). Based on its

description, the total primary energy is equivalent to the cumulative energy demand of the product system. Non-renewable energy consumption represents the consumption of energy that comes from fossil fuel and nuclear while Fossil fuel consumption indicates the energy that comes from fossil fuel only (118). Non-renewable and Fossil fuel consumption are subsets of the Total primary energy consumption. In this study, the energy consumption in all of the three forms are presented to identify and compare the energy demand of the products.

6.3. Results and discussion

The LCIA results were interpreted to identify the potential impacts of the HRB pavements and compare with the respective potential impacts of GU pavement. The interpretation was done considering the uncertainty on the LCIA data and the results of the scenario analysis. Further discussion on this is provided in the subsequent sections.

6.3.1. Comparison of HRB and GU full-depth reclamation

The results of life cycle impact assessment are shown in Table 6.11 and Figure 6.7. For simplicity, the pavements under comparison were designated by the prefix 'P' and type of binders used in the rehabilitation process. Accordingly, the designation of the four pavements became P-GU, P-HRB1, P-HRB2 and P-HRB3. In absolute values, the LCIA results indicated that P-GU have higher environmental impacts than the corresponding HRB pavements. This is true for all impact categories except Ozone depletion potential (ODP), in which HRB pavements have higher impacts.

In terms of energy consumption, P-GU consumes more energy than HRB pavements. A closer look at the energy consumptions indicates that more than 95% of the

energy comes from non-renewable sources (which includes fossil fuel and nuclear), mainly fossil fuel. According to the LCIA results, fossil fuel alone contributes about 90 % of the total primary energy consumed by the entire rehabilitation processes of each pavement type. Comparisons of the energy consumptions are shown in Table 6.11 and Figure 6.8.

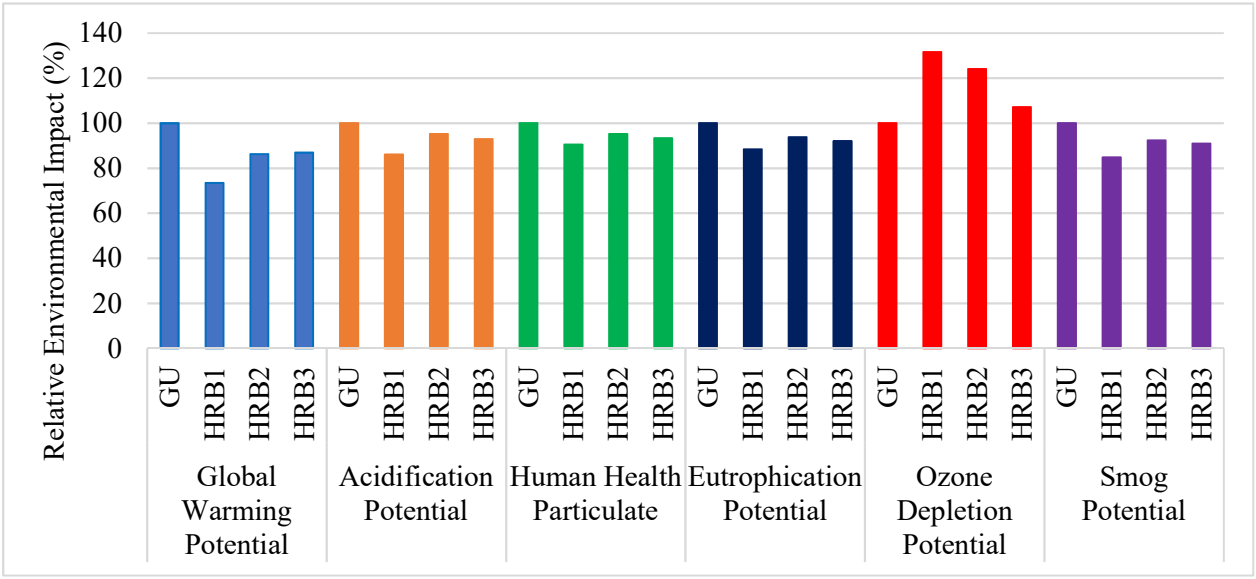

Figure 6.7 Comparison of life cycle impacts relative to impacts of GU pavement

The Athena Institute has declared that there is an uncertainty margin of 15% in LCIA results of Athena Pavement LCA, meaning the impact measures of two design scenarios are considered to be the same if the difference between them is less than 15% (118). As shown in Table 6.12, the differences between the impacts of P-GU and P-HRB3 pavements are less than 15% for all impact categories. This indicates that P-HRB3 would have the same level of potential impacts as P-GU pavement. The potential impacts of P-HRB2 are also equivalent to the corresponding impacts of P-GU pavement for all impact categories except ODP. The ODP of P-HRB2 is significantly higher than P-GU pavement. Similarly, the differences between P-HRB1 and P-GU pavements are insignificant for most impact categories, except global

warming potential and ODP. The ODP of P-HRB1 is higher than P-GU but the global warming potential of P-HRB1 is substantially lower than that of P-GU. This indicates that the global warming potential can be reduced by 27 % if HRB1 is used in lieu of GU cement in the rehabilitation process. HRB1 is the binder with the lowest Calcium/Silica ratio of all the four binders.

Table 6.11 Summary of Potential Environmental Impacts and Energy Consumptions

Impact Category	Unit	GU	HRB1	HRB2	HRB3
Global Warming Potential	kg CO_2 eq	244,270	179,331	210,519	212,115
Acidification Potential	kg SO_2 eq	1,307	1,125	1,244	1,214
Human Health Particulate	kg PM2.5 eq	178	161	170	166
Eutrophication Potential	kg N eq	86	76	81	79
Ozone Depletion Potential	kg CFC-11eq	1.54E-03	2.03E-03	1.91E-03	1.65E-03
Smog Potential	kg O_3 eq	20,723	17,573	19,139	18,857
Total Primary Energy	MJ	3,905,213	3,374,626	3,739,189	3,696,933
Non-Renewable Energy	MJ	3,781,804	3,298,235	3,644,601	3,592,944
Fossil Fuel Consumption	MJ	3,499,372	3,059,836	3,362,307	3,320,713

Overall, the LCIA results indicated that the environmental merits of the hydraulic road binders are not the same with all binder types. The environmental merits of some binders (like HRB2 and HRB3) might not be significant when used in full-depth reclamation process. However, binders like HRB1 could have significant saving in greenhouse emissions although their ODP is relatively high. To compare and rate the binders based on a single indicator, the potential impacts of each category should be summed up by using a weighting factor. The weighting factors corresponding to each impact category should be determined based on the level of damage they will inflict. Therefore, further analysis using end-point impact indicators should be conducted to determine the level of damages related to each impact category.

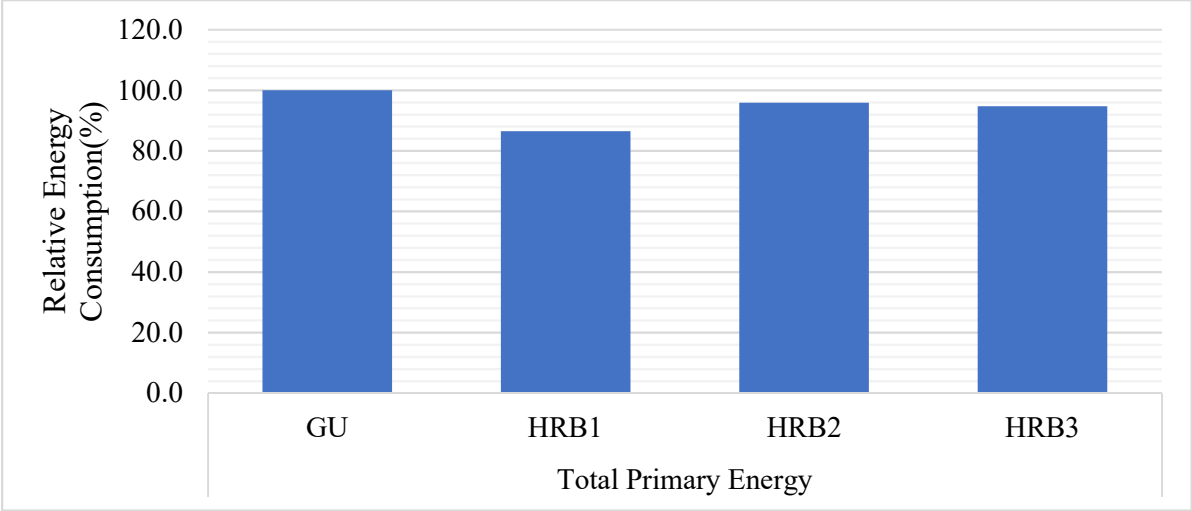

Figure 6.8 Comparison of energy consumptions relative to consumption of GU pavement

Table 6.12 Comparison of Differences in Impact Measures and Energy Consumptions

Impact Category	Unit	Difference in impact measures (%)		
		GU – HRB1	GU – HRB2	GU – HRB3
Global Warming Potential	% kg CO_2 eq	26.5	13.7	13.1
Acidification Potential	% kg SO_2 eq	13.9	4.8	7.1
Human Health Particulate	% kg PM2.5 eq	9.4	4.7	6.7
Eutrophication Potential	% kg N eq	11.6	6.2	8.0
Ozone Depletion Potential	kg CFC-11eq	-31.8	-24.0	-7.1
Smog Potential	% kg O_3 eq	15.2	7.6	9.0
Total Primary Energy	% MJ	13.5	4.2	5.3
Non-Renewable Energy	% MJ	12.8	3.6	5.0
Fossil Fuel Consumption	% MJ	12.6	3.9	5.1

- *Impact contribution analysis*

The impacts presented in this study are related to two major life cycle stages, namely, material manufacturing and pavement rehabilitation. The 'use' and end-of-life phases were excluded from the analysis for the reasons stated in Section 6.2.3. The impacts in the manufacturing stages are related to the manufacturing of industrial products like GU cement. The impacts

associated with the pavement rehabilitation stages include the environmental impacts due to extraction, processing and transportation of construction materials (like crushed coarse aggregate, processing of SCM), the full-depth reclamation, prime coat application and paving processes.

For the sake of comparison, the results of LCIA from the pavement rehabilitation stages were split into two groups, viz., 'materials and equipment' and 'transportation'. The 'materials and equipment' represents all the impacts related to the entire rehabilitation activities. 'Transportation' indicates the impacts due to all transportation activities involved in the pavement rehabilitation stage except for transportation of GU cement.

The results of contribution analysis indicate that pavement rehabilitation stage is the major source of the impacts for all categories (Figure 6.9 A-F). About 70% of global warming and acidification potentials and 90% of human health particulate, eutrophication potential and smog potentials are attributed to the pavement rehabilitation stage. Moreover, 70% of the total primary energy consumption is due to the activities in this stage (Figure 6.10A). The transportation in the pavement rehabilitation stage contributes to about 10% of global warming potential and human health particulates emissions. Transportation also contributes to 20% of acidification and eutrophication potentials, and 34 – 40% of smog potential. The energy consumed by the transportation activities accounts for 10% of the total primary energy consumption of the entire processes.

Comparing the impacts associated with the manufacturing stage, one may observe that the differences among all pavement types are insignificant. This could be because Athena Pavement LCA considers the SCM in the HRB as products with associated environmental

impacts, not as industrial by-products with no environmental loads. The summary of the impact contributions and energy consumption break down of the life cycle stages are shown in Table 6.13.

Table 6.13 Impact Contribution and Energy Consumption of Life Cycle Stages

Impact Category	Life Cycle Stage	Life Cycle Stage Subcategory	Contribution (%)			
			GU	HRB1	HRB2	HRB3
Global Warming Potential	Manufacturing	Manufacturing	29.5	32.9	35.1	33.5
	Pavement Rehabilitation	Material and Equipment	60.7	54.6	53.7	55.6
		Transportation	9.8	12.5	11.2	10.9
Acidification Potential	Manufacturing	Manufacturing	29.6	28.1	31.7	31.3
	Pavement Rehabilitation	Material and Equipment	52.7	52.6	49.9	50.3
		Transportation	17.7	19.3	18.4	18.4
Human Health Particulate	Manufacturing	Manufacturing	11.0	9.9	11.8	11.6
	Pavement Rehabilitation	Material and Equipment	81.8	82.7	80.8	81.0
		Transportation	7.2	7.4	7.4	7.4
Eutrophication Potential	Manufacturing	Manufacturing	9.8	9.0	10.6	10.4
	Pavement Rehabilitation	Material and Equipment	73.5	73.3	71.8	72.1
		Transportation	16.7	17.7	17.6	17.5
Ozone Depletion Potential	Manufacturing	Manufacturing	15.6	9.7	12.9	14.3
	Pavement Rehabilitation	Material and Equipment	84.3	90.3	87.1	85.6
		Transportation	0.1	0.0	0.0	0.1
Smog Potential	Manufacturing	Manufacturing	12.9	12.4	14.3	13.9
	Pavement Rehabilitation	Material and Equipment	51.7	48.5	48.0	48.7
		Transportation	35.4	39.1	37.7	37.4
Total Primary Energy	Manufacturing	Manufacturing	33.0	31.2	35.4	34.6
	Pavement Rehabilitation	Material and Equipment	58.0	58.8	55.1	56.0
		Transportation	9.0	10.0	9.5	9.4
Non-Renewable Energy	Manufacturing	Manufacturing	33.4	31.2	35.4	34.6
	Pavement Rehabilitation	Material and Equipment	57.4	58.8	55.1	56.0
		Transportation	9.2	10.0	9.5	9.4
Fossil Fuel Consumption	Manufacturing	Manufacturing	30.3	28.2	32.2	31.4
	Pavement Rehabilitation	Material and Equipment	59.7	61.1	57.6	58.5
		Transportation	10.0	10.7	10.2	10.1

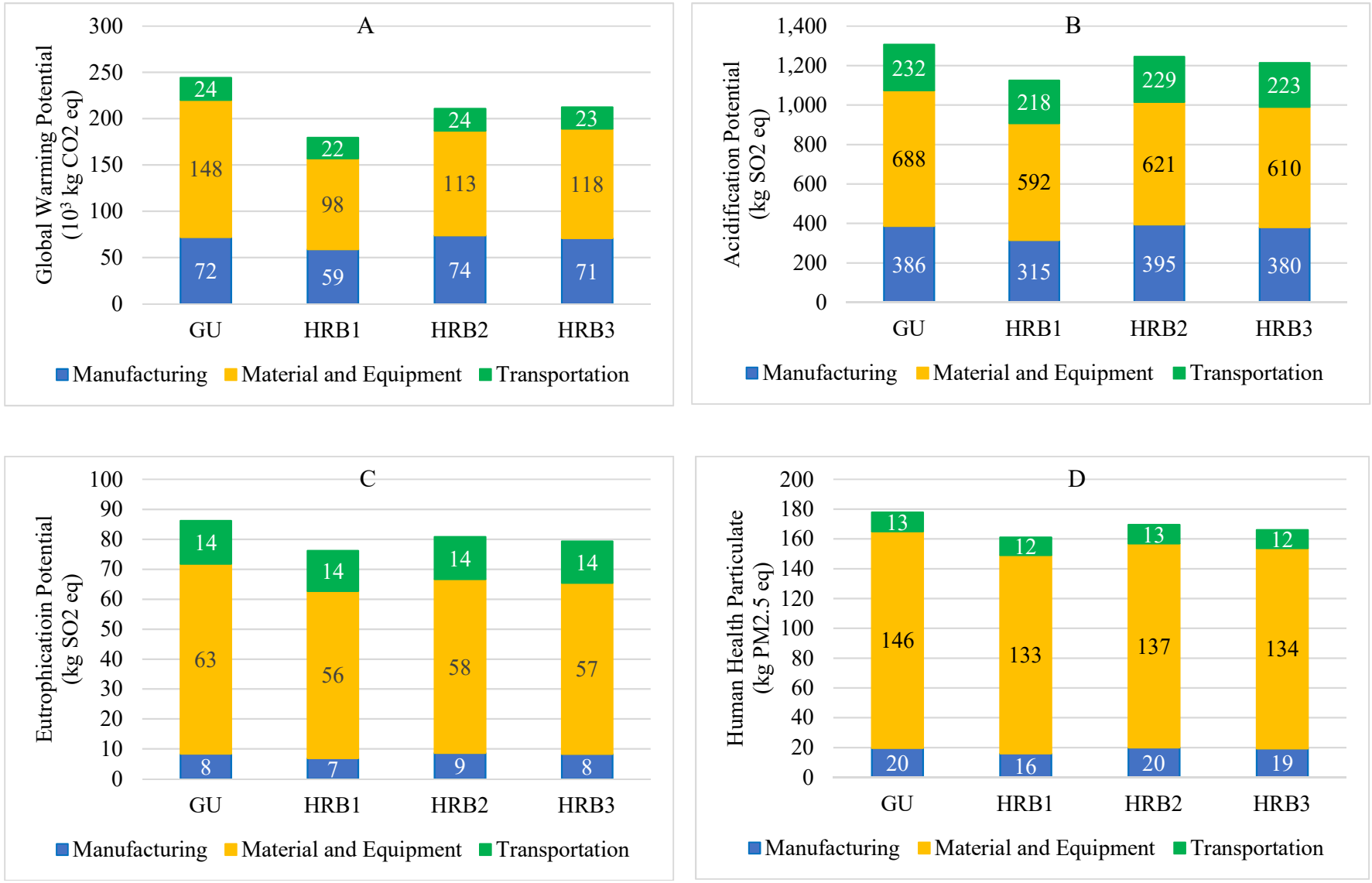

Figure 6.9 Life cycle stages contribution to A) global warming, B) acidification, C) eutrophication, D) human health particulate

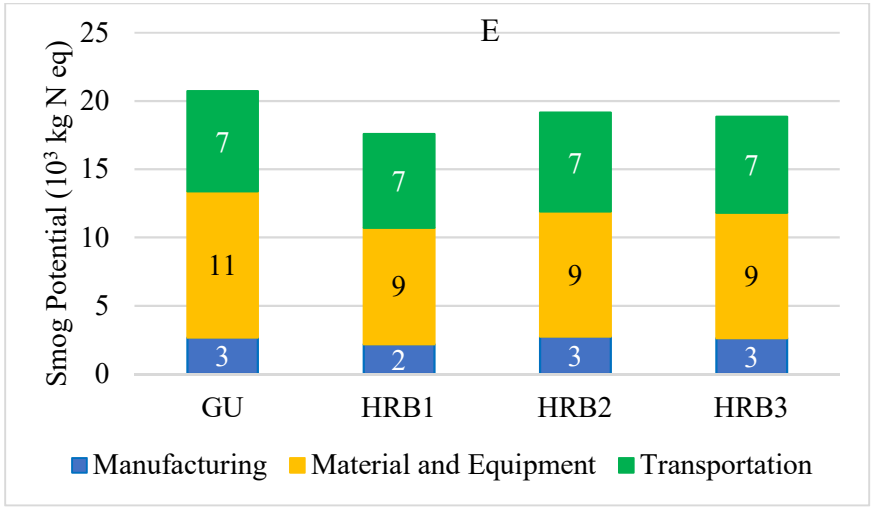

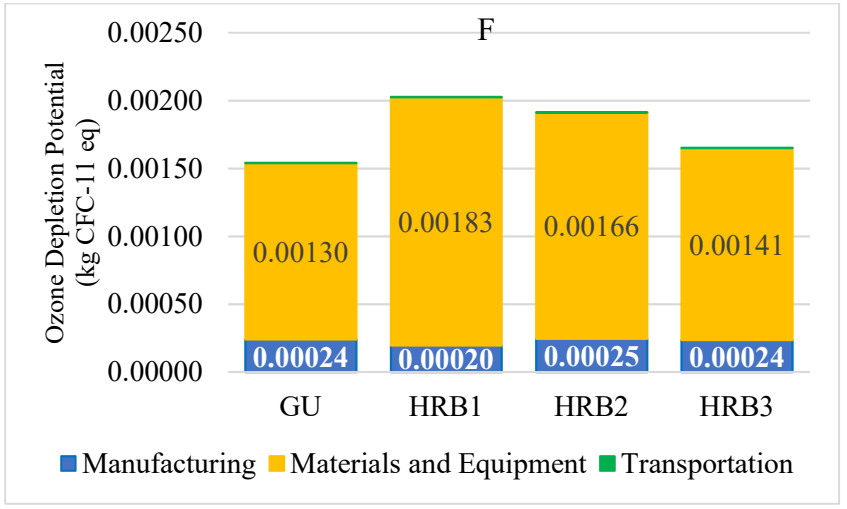

Figure 6.9 Life cycle stages contribution to E) smog potential, F) Ozone depletion

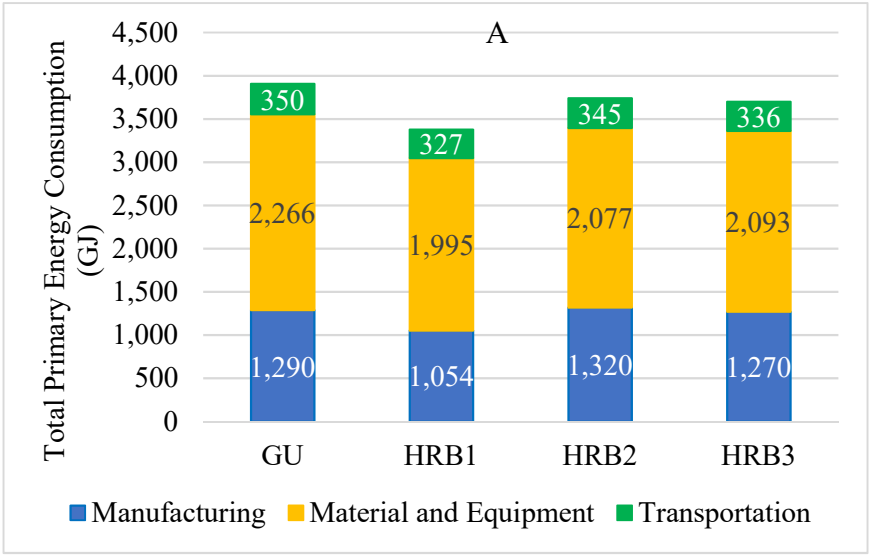

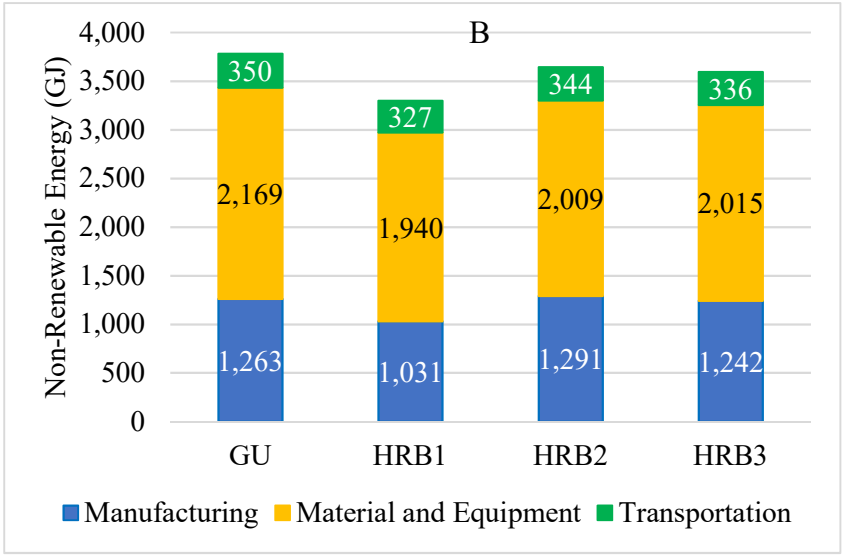

Figure 6.10 A) Total energy consumption break down, B) Non-renewable energy consumption break down

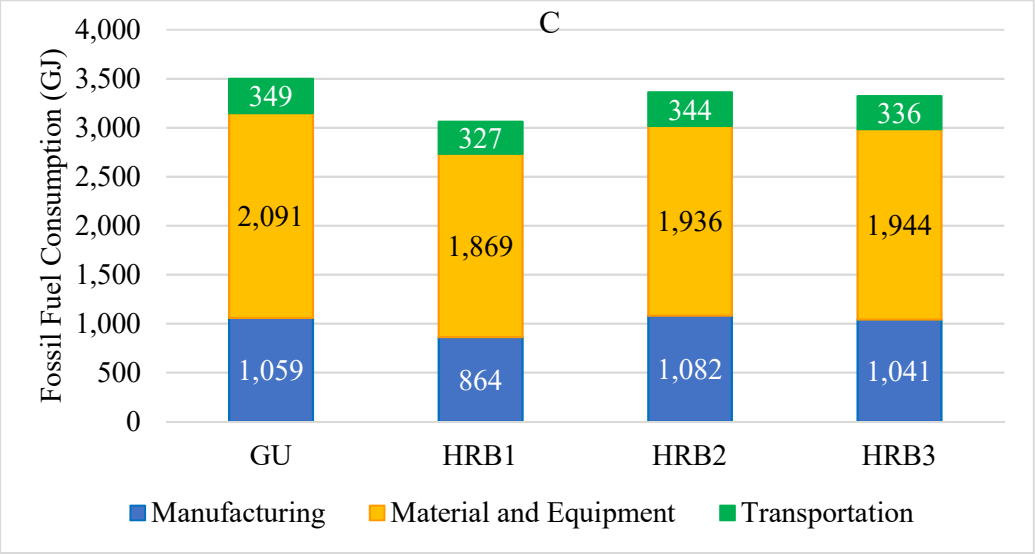

Figure 6.10 C) Fossil fuel consumption break down

- *Scenario Analysis*

The results of the scenario analysis are shown in Table 6.14 along with the original analysis results. The analysis results indicate the impacts and energy consumptions of pavements in Manitoba and Quebec have the same trend as Ontario. P-HRB1 is the only pavement type that have less environmental impact relative to P-GU in both cases. The global warming potential associated with P-HRB1 is less than that of P-GU by 21% in Manitoba and 20% in Quebec. The differences in the impact measures of all other categories are not significant for all pavement types.

Likewise, the contribution analysis on both Manitoba and Quebec pavements indicated that the impacts and energy consumptions due to 'material and equipment' are the highest for all impact categories except smog potential of Quebec pavements. 'Transportation' and 'Material and Equipment' of HRB pavements have the same contribution to potential smog in Quebec.

Table 6.14 Summary of Scenario Analysis

Impact Category	Unit	Location	GU	HRB1	HRB2	HRB3
Global Warming Potential	kg CO_2 eq	Ontario	244,270	179,331	210,519	212,115
		Manitoba	237,230	188,515	202,741	205,956
		Quebec	243,671	194,890	209,086	212,148
Acidification Potential	kg SO_2 eq	Ontario	1,307	1,125	1,244	1,214
		Manitoba	1,267	1,179	1,202	1,180
		Quebec	1,330	1,243	1,266	1,243
Human Health Particulate	kg PM2.5 eq	Ontario	178	161	170	166
		Manitoba	177	165	168	165
		Quebec	179	167	171	168
Eutrophication Potential	kg N eq	Ontario	86	76	81	79
		Manitoba	84	77	79	78
		Quebec	88	81	83	82
Ozone Depletion Potential	kg CFC-11eq	Ontario	1.54E-03	2.03E-03	1.91E-03	1.65E-03
		Manitoba	1.31E-03	1.84E-03	1.68E-03	1.43E-03
		Quebec	1.31E-03	1.84E-03	1.68E-03	1.42E-03
Smog Potential	kg O_3 eq	Ontario	20,723	17,573	19,139	18,857
		Manitoba	19,825	17,751	18,332	18,153
		Quebec	22,080	20,045	20,613	20,382
Total Primary Energy	MJ	Ontario	3,905,213	3,374,626	3,739,189	3,696,933
		Manitoba	3,779,538	3,530,284	3,597,522	3,586,652
		Quebec	3,764,636	3,514,807	3,581,468	3,568,188
Non-Renewable Energy	MJ	Ontario	3,781,804	3,298,235	3,644,601	3,592,944
		Manitoba	3,606,468	3,395,841	3,451,243	3,431,514
		Quebec	3,591,145	3,382,350	3,437,155	3,414,976
Fossil Fuel Consumption	MJ	Ontario	3,499,372	3,059,836	3,362,307	3,320,713
		Manitoba	3,524,852	3,320,605	3,374,211	3,356,676
		Quebec	3,510,009	3,307,601	3,360,602	3,340,609

Comparison of pavements of the same binder showed that Manitoba's P-GU, P-HRB2 and P-HRB3 pavements have 1 – 4 % less impacts and consume 1 – 5 % less energy than the Ontario counterparts. On the contrary, Manitoba's P-HRB1 has 1 – 5 % higher impact measures and consumes 5% more energy than Ontario's P-HRB1 pavement. The main source of the variations was the manufacturing stage.

Similarly, Quebec's P-HRB1 pavement causes 5 – 15% more impacts and consumes 4% more energy than Ontario's P-HRB1 pavement. However, the impact levels of the other pavement types (P-GU, P-HRB2 and P-HRB3) are equivalent in Ontario and Quebec. The

only exception is the smog potential, which is 7% more in Quebec pavements. Quebec's P-GU, P-HRB1 and P-HRB2 pavements consume 4% less energy than the Ontario counterparts. The impacts and energy consumptions associated with transportation are highest in Quebec pavements. Unlike Manitoba, the variations between the Ontario and Quebec pavements come from both transportation and manufacturing stage.

Overall, the scenario analysis indicated the ranking of the binders based on environmental impacts and energy consumption remains the same regardless of the project location. This indicates that the LCIA results would follow similar trend in Canada provided that the assumptions made regarding pavement performance and transportation distances do not vary substantially.

6.4. Conclusions

In this study, the environmental impacts associated with different cementitious stabilizers, which can be used in full-depth reclamation process, were assessed using LCA. The study was performed by integrating three major tasks, namely, material characterization, pavement design and performance prediction, and life cycle assessment. Three types of hydraulic road binders: HRB1, HRB2, HRB3, and GU cement were used for the analysis.

Comparison based on absolute values indicated that the potential environmental impacts and energy consumptions can be reduced by 4% – 25 % by using HRB in lieu of GU cement in full-depth reclamation process. However, due to the 15 % uncertainty margin, only HRB1 can be considered to have significant merit in reducing environmental impact. According to this study, using HRB1 instead of GU cement, can reduce the global warming

potential by 20 % – 27 %. In general, the following points can be drawn based on the study findings:

- Use of HRB1 in full-depth reclamation process would significantly reduce global warming potential,
- Hydraulic road binders used in this study had less environmental impact than GU cement for all categories except Ozone Depletion Potential,
- Ozone Depletion Potential of hydraulic road binders was higher than that of GU cement
- None of hydraulic road binder required more total energy demand than GU cement,
- Blending SCM with GU cement may not always reduce environmental impacts and energy demand significantly.

Based on the analysis, hydraulic road binders with a similar composition as HRB1 could be viable alternatives to GU cement for application in FDR process. But, the end-point impacts associated with Ozone depletion potential should be identified to make sure that the damage do not outweigh their other benefits. To confirm this further assessment should be conducted using end-point impact assessment methods.

7. CONCLUSIONS, RECOMMENDATIONS AND FUTURE WORK

7.1. General Summary

The research was conducted with the main purpose of evaluating hydraulic road binders as alternative stabilizers in full-depth reclamation process. The tasks undertaken to achieve the purpose can be broadly categorized in to four major groups. These are material characterization, fatigue performance assessment, pavement design and life cycle assessment.

The study was mainly conducted based on primary data collected from laboratory tests. To understand the effects of hydraulic road binders on the performance of FRPMC, a comparative assessment was conducted by using GU cement as a control binder that represents the base-case scenario.

Four different types of reclaimed pavement materials and four types of types of cementitious binders were used for the study. The four reclaimed materials were collected from four different full-depth reclamation projects in Ontario and each had different compositions. The RAP proportion of the reclaimed materials was in the range of 20% - 80%, representing low, medium and high RAP content materials.

The laboratory experiments were conducted on test specimens prepared from sixteen different soil-cement mixtures. The sixteen mixtures were made by blending each of the four reclaimed materials with the four binders. Therefore, the findings of the research could be reproduced for other types of reclaimed materials provided that the binders with similar compositions are utilized.

7.2. Major Findings and Conclusions

The major findings of this study can be summarized as follow:

- The optimum moisture content of the mixes treated with HRB did not vary significantly from the control mixes
- The optimum binder content of the mixes treated with HRB was the same as or less than the corresponding mixes treated with GU cement
- Hydraulic road binders could be used to make mixes with at least equivalent early-age and long-term compressive strength as GU cement mixes
- The stiffness and tensile strength of HRB mixes were equivalent to the corresponding stiffness and tensile strength of GU mixes
- The type of HRB used in this study did not have significant influence on the fatigue life of the mixtures indicating that fatigue performance of HRB mixtures and GU mixtures would be equivalent
- FRPMC possess the properties of viscoelastic materials even though they are cement treated materials
- The rate of dissipated energy change of FRPMC was similar to that of quasi-brittle materials in Zone-II of the RDEC versus number of load repetition plot
- The plot of RDEC versus number of load repetition of FRPMC mixtures did not indicate a sharp increase in Zone-III, which is not typical of both HMA and Portland cement concrete
- The use of HRB with the lowest Calcium/Silica ratio would significantly reduce global warming potential

- Hydraulic road binders used in this study had less environmental impact than GU cement for all categories except Ozone Depletion Potential (ODP)
- Ozone Depletion Potential of hydraulic road binders was higher than that of GU cement
- The total energy demand of HRB pavements were less than GU pavement
- Blending SCM with GU cement may not always significantly reduce environmental impacts and energy demand.

Based on the study findings it can be concluded that HRB with similar compositions can be used in full-depth reclamation process without compromising the strength and durability of the mixtures. However, not all HRB substantially reduce the environmental impacts and energy requirements. The LCA in this study indicated that only the HRB with the lowest Calcium/Silica ratio can significantly reduce the global warming potential.

7.3. Significant Contributions

The study touched an important but less-addressed area. As mentioned in the introductory parts, the use of hydraulic road binders in full-depth reclamation process is not common in Canada and many other countries. However, as the research findings indicated hydraulic road binders can be viable alternatives that can replace Portland cement in full-depth reclamation process. The followings are the major contributions of the study:

- Mechanical properties of HRB treated reclaimed materials were characterized,
- Influences of HRB on mechanical properties of stabilized reclaimed materials were evaluated
- Response of stabilized reclaimed materials to repeated loadings was studied

- Empirical models that can be used for mechanistic-empirical pavement design were established
- Fatigue performance models that can be used to predict pavement performance were calibrated
- Effects of HRB on the life cycle impacts were studied and reported.

7.4. Recommendations and Future Works

The use of alternative construction materials with less environmental impacts is among the actions that should be taken to mitigate the looming threat of climate change. Accordingly, the use of cementitious binders similar to HRB1, which would reduce environmental impact without affecting performance, should be encouraged.

The study indicated that hydraulic road binders with the right compositions can be suitable stabilizers for application in pavement rehabilitation works. However, the findings of the study should be verified and supported by further researches. Future researches should be conducted to:

- validate the findings of this study based on field trial sections
- establish appropriate laboratory test protocols that are specifically designed for FRPMC
- develop performance prediction models for pavement design
- modify the recipe of the binders for better performance and lower environmental impacts.

REFERENCES

1. Canadian Infrastructure Report Card 2019. 2019;56.

2. ARRA. Full Depth Reclamation [Internet]. Asphalt Recycling and Reclaiming Association; [cited 2017 Jan 25]. Available from: http://www.mdt.mt.gov/publications/docs/brochures/research/toolbox/ARRA/arrafull.pdf

3. Kearney E, Huffman J. Full-depth reclamation process. Transp Res Rec J Transp Res Board. 1999;(1684):203–209.

4. Damtoft JS, Lukasik J, Herfort D, Sorrentino D, Gartner EM. Sustainable development and climate change initiatives. Cem Concr Res. 2008 Feb;38(2):115–27.

5. Hendriks CA, Worrell E, Price L, Martin N, Ozawa Meida L, de Jager D, et al. Emission reduction of greenhouse gases from the cement industry. In: Greenhouse Gas Control Technologies 4 [Internet]. Elsevier; 1999 [cited 2019 May 17]. p. 939–44. Available from: https://linkinghub.elsevier.com/retrieve/pii/B9780080430188501508

6. Worrell E, Price L, Martin N, Hendriks C, Meida LO. Carbon Dioxide Emissions from the Global Cement Industry. Annu Rev Energy Environ. 2001;26(1):303–29.

7. Luhr DR, Adaska WS, Halsted GE. Guide to Full-Depth Reclamation (FDR) with Cement. 2008 [cited 2017 Jan 9]; Available from: https://trid.trb.org/view.aspx?id=836940

8. AFNOR. EN 13282-2 Hydraulic road binders - Part 2: Normal hardening hydraulic road binders - Composition, specifications and conformity criteria. 2015.

9. AFNOR. EN 13282-1 Hydraulic road binders - Part 1: Rapid hardening hydraulic road binders - Composition, specifications and conformity criteria. 2014.

10. Lothenbach B, Scrivener K, Hooton RD. Supplementary cementitious materials. Cem Concr Res. 2011 Dec;41(12):1244–56.

11. Snellings R, Mertens G, Elsen J. Supplementary Cementitious Materials. Rev Mineral Geochem. 2012 Jan 1;74(1):211–78.

12. Miller SA, John VM, Pacca SA, Horvath A. Carbon dioxide reduction potential in the global cement industry by 2050. Cem Concr Res. 2018 Dec;114:115–24.

13. Moretti L, Caro S. Critical analysis of the Life Cycle Assessment of the Italian cement industry. J Clean Prod. 2017 May 20;152:198–210.

14. The Loreti Group. Greenhouse Gas Emission Reductions from Blended Cement Production. Arlington; 2008.

15. BS 6100-0:2010 - Building and civil engineering. Vocabulary. Introduction and index. BSI; 2010.

16. ASTM. ASTM C219 Standard Terminology Relating to Hydraulic Cement.pdf. ASTM; 2014.

17. Abdo J, Serfass J-P, Pellevoisin P. Pavement cold in-place recycling with hydraulic binders: the state of the art in France. Road Mater Pavement Des [Internet]. 2013 Sep [cited 2017 Jan 9];14(3). Available from: https://trid.trb.org/view.aspx?id=1266121

18. DD ENV 13282-2000 Hydraulic road binders - Composition, specifications and conformity criteria - British Standards [Internet]. European Standards; 2000 [cited 2017 Jan 10]. Available from: http://www.worldstdindex.com/soft/277325.htm

19. Dodson VH. Concrete admixtures. Place of publication not identified: Springer; 2013.

20. Wang Y, Shao Y, Matovic MD, Whalen JK. Recycling combustion ash for sustainable cement production: A critical review with data-mining and time-series predictive models | Elsevier Enhanced Reader. Constr Build Mater. 2016 Jul;(123):683–9.

21. ARRA. Basic Asphalt Recycling Manual. Asphalt Recycling and Reclaiming Association; 2001.

22. Wirtgen. Cold Recycling: Wirtgen Cold Recycling Technology [Internet]. 3rd ed. Germany: Wirtgen GmbH; 2010 [cited 2017 Jan 25]. Available from: http://media.wirtgen-group.com/media/02_wirtgen/infomaterial_1/kaltrecycler/kaltrecycling_technologie/kaltrecycling_handbuch/Kaltrecycling_Handbuch_EN.pdf

23. Bergeron G. The Performance of Full-Depth Reclamation and Cold In-Place Recycling Techniques in Quebec. In 2005 [cited 2017 Jan 25]. Available from: https://trid.trb.org/view.aspx?id=798209

24. Diefenderfer BK, Apeagyei AK. Analysis of Full-Depth Reclamation Trial Sections in Virginia. 2011 Apr [cited 2017 Jan 25]; Available from: https://trid.trb.org/view.aspx?id=1108830

25. Senior SA, Gorman B, Szoke SI. Recycling road building materials and experience with full depth reclamation in the Ontario provincial highway system. In: Proceedings of the Transportation Association of Canada Annual Conference recycled materials and recycling processes for sustainable infrastructure session, Toronto, Ont [Internet]. 2008 [cited 2017 Jan 25]. Available from: http://conf.tac-atc.ca/english/resourcecentre/readingroom/conference/conf2008/docs/f1/Senior.pdf

26. Lewis AJN, Collings DC. Cold in place recycling: a relevant process for road rehabilitation and upgrading. 7th Conf Asph Pavements Dor South Afr. 1999;1–13.

27. Jones D, Fu P, Harvey JT, Halles F. Full-Depth Pavement Reclamation with Foamed Asphalt: Final Report [Internet]. University of California, Pavement Research Center; 2008

Apr [cited 2017 Jan 26]. Report No.: CA101069C. Available from: http://escholarship.org/uc/item/8378s3vk

28. Lewis AJN, Collings DC. Cold in place recycling: a relevant process for road rehabilitation and upgrading. In: Proceedings of the 7th conference on asphalt pavements for Southern Africa, Victoria Falls [Internet]. 1999 [cited 2017 Jan 10]. Available from: http://www.viastrade.it/letteratura/bitume/COLD%20IN%20PLACE%20RECYCLING%20A%20RELEVANT%20PROCESS%20FOR%20ROAD.pdf

29. Tang S, Cao Y, Labuz JF. Structural Evaluation of Asphalt Pavements with Full-Depth Reclaimed Base [Internet]. Minnesota Department of Transportation; 2012 Dec [cited 2017 Jan 25]. Available from: http://conservancy.umn.edu/handle/11299/146946

30. Kearney EJ, Huffman JE. Full-Depth Reclamation Process. Ransportation Res Rec J Transp Res Board 1684. 1999;(99):203–9.

31. Lewis DE, Jared DM, Torres H, Mathews M. Georgia's Use of Cement-Stabilized Reclaimed Base in Full-Depth Reclamation. Transp Res Rec. 2006;1952(1952):125–33.

32. Theyse H, Long F, Harvey JT, Monismith C. Discussion of Deep In-Situ Recycling (DISR). Pavement Research Center, Institue of Transportation Studies, University of California Berkeley and University of California Davis; 2004.

33. Reeder G, Harrington D, Ayers, Adaska W. Guide to Full-Depth Reclamation (FDR) with Cement [Internet]. Ames, IA: National Concrete Pavement Technology Center Institute for Transportation, Iowa State University; 2017 Mar [cited 2018 Jul 15]. Report No.: SR1006P. Available from: http://www.cement.org/docs/default-source/th-paving-pdfs/guide-to-full-depth-reclamation-(fdr)-with-cement.pdf?sfvrsn=2

34. Portland Cement Association. Soil-Cement Laboratory Handbook. Portland Cement Association; 1992.

35. Luhr BDR, Adaska WS, Halsted GE. Guide to Full-Depth Reclamation (FDR) with Cement. 2005;

36. Syed I. Full-Depth Reclamation With Portland Cement: a Study of Long-Term Performance. 2008.

37. PIARC. Pavement Recycling Guidelines for In-place Recycling with Cement; In-place Recycling with Emulsion or Foamed Bitumen; Hot Mix Recycling in Plant. PIARC Committee C7/8; 2003.

38. Halsted GE. Minimizing Reflective Cracking in Cement-Stabilized Pavement Bases. In Halifax, Nova Scotia; 2010. p. 10.

39. Supino S, Malandrino O, Testa M, Sica D. Sustainability in the EU cement industry: the Italian and German experiences. J Clean Prod. 2016 Jan 20;112:430–42.

40. Schneider M, Romer M, Tschudin M, Bolio H. Sustainable cement production—present and future. Cem Concr Res. 2011 Jul;41(7):642–50.

41. Scrivener KL, John VM, Gartner EM. Eco-efficient cements: Potential economically viable solutions for a low-CO2 cement-based materials industry. Cem Concr Res. 2018 Dec;114:2–26.

42. PCA. Environmental Product Declaration: Portland Cements [Internet]. 2016 [cited 2018 Apr 10]. Available from: http://www.cement.org/docs/default-source/sustainabilty2/pca-portland-cement-epd-062716.pdf

43. PCA. Environmental Product Declaration: Blended Cements [Internet]. 2016 [cited 2018 Apr 10]. Available from: http://www.cement.org/docs/default-source/sustainabilty2/pca-blended-cement-epd-062716-(002).pdf

44. NF EN 13282-1-2014 Hydraulic road binders - Part 1 : rapid hardening hydraulic road binders - Composition, specifications and conformity criteria [Internet]. AFNOR — French standard institute; 2015 [cited 2017 Apr 5]. Available from: http://www.freestd.us/soft4/4113537.htm

45. Aïtcin P-C. 4 - Supplementary cementitious materials and blended cements. In: Aïtcin P-C, Flatt RJ, editors. Science and Technology of Concrete Admixtures [Internet]. Woodhead Publishing; 2016 [cited 2019 Apr 6]. p. 53–73. Available from: http://www.sciencedirect.com/science/article/pii/B9780081006931000047

46. Isola M, Betti G, Marradi A, Tebaldi G. Evaluation of cement treated mixtures with high percentage of reclaimed asphalt pavement - ScienceDirect. Constr Build Mater. 2013 Nov;48:238–47.

47. Kolias S. Mechanical properties of cement-treated mixtures of milled bituminous concrete and crushed aggregates. Mater Struct. 1996 Aug 1;29(7):411–7.

48. Katsakou M, Kolias S. Mechanical properties of cement-bound recycled pavements. Proc Inst Civ Eng - Constr Mater. 2007 Nov;160(4):171–9.

49. Ghanizadeh AR, Rahrovan M, Bafghi KB. The effect of cement and reclaimed asphalt pavement on the mechanical properties of stabilized base via full-depth reclamation. Constr Build Mater. 2018 Feb 10;161:165–74.

50. Guthrie WS, Brown AV, Eggett DL. Cement Stabilization of Aggregate Base Material Blended with Reclaimed Asphalt Pavement. Transp Res Rec J Transp Res Board. 2007 Jan;2026(1):47–53.

51. Euch Khay Saloua El, Euch Ben Said Sawssen El, Loulizi Amara, Neji Jamel. Laboratory Investigation of Cement-Treated Reclaimed Asphalt Pavement Material. J Mater Civ Eng. 2015 Jun 1;27(6):04014192.

52. Tolbert J. Effect of High Percentages of Reclaimed Asphalt Pavement on Mechanical Properties of Cement-Treated Base Material. Theses Diss [Internet]. 2014 Jul 10; Available from: https://scholarsarchive.byu.edu/etd/4217

53. Louw S. Characterizing Cement Stabilized Base Material Containing Reclaimed Asphalt Pavement. [Davis]: University of California; 2014.

54. Yuan Nazarian, Hoyos L, Puppala AJ. Cement Treated RAP Mixes for Roadway Bases [Internet]. Texas, Austin: The University of Texas at El Paso; 2010 Oct [cited 2018 Jul 8]. Report No.: FHWA/TX-10/0-6084-1. Available from: http://ctis.utep.edu/reports/5TxDOT_Reoprt__0-6084-1_%28Final%29.pdf

55. Taha Ramzi, Al-Harthy Ali, Al-Shamsi Khalid, Al-Zubeidi Muamer. Cement Stabilization of Reclaimed Asphalt Pavement Aggregate for Road Bases and Subbases. J Mater Civ Eng. 2002 Jun 1;14(3):239–45.

56. D18 Committee. Test Methods for Moisture-Density (Unit Weight) Relations of Soil-Cement Mixtures [Internet]. ASTM International; [cited 2019 Apr 20]. Available from: http://www.astm.org/cgi-bin/resolver.cgi?D558-11

57. D18 Committee. Test Methods for Freezing and Thawing Compacted Soil-Cement Mixtures [Internet]. ASTM International; [cited 2019 Apr 20]. Available from: http://www.astm.org/cgi-bin/resolver.cgi?D560D560M-16

58. ASTM. ASTM D 1633-17 Compressive Strength of Molded Soil-Cement Cylinders. ASTM; 2017.

59. C09 Committee. Test Method for Static Modulus of Elasticity and Poissons Ratio of Concrete in Compression [Internet]. ASTM International; [cited 2019 Apr 20]. Available from: http://www.astm.org/cgi-bin/resolver.cgi?C469C469M-14

60. ARA Inc. Guide for Mechanistic-Empirical Design [Internet]. NCHRP; 2004 [cited 2017 Feb 21]. Report No.: Final Report 1-37A. Available from: http://onlinepubs.trb.org/onlinepubs/archive/mepdg/2appendices_FF.pdf

61. Yeo R. The development and evaluation of protocols for the laboratory characterisation of cemented materials [Internet]. 2008 [cited 2017 Feb 22]. Available from: https://trid.trb.org/view.aspx?id=882941

62. Guthrie WS, Cooley D, Eggett DL. Effects of Reclaimed Asphalt Pavement on Mechanical Properties of Base Materials. Transp Res Rec J Transp Res Board. 2007 Jan;2005(1):44–52.

63. Dowling N. Mechanical Behavior of Materials_Engineering Methods for Deformation, Fracture, and Fatigue. 4th ed. England: Pearson Education Limited; 2013. 977 p.

64. Di Benedetto H, de La Roche C, Baaj H, Pronk A, Lundström R. Fatigue of bituminous mixtures. Mater Struct. 2004 Apr;37(3):202–16.

65. Shen S, Airey GD, Carpenter SH, Huang H. A Dissipated Energy Approach to Fatigue Evaluation. Road Mater Pavement Des. 2006 Jan;7(1):47–69.

66. Ghuzlan KA, Carpenter SH. Fatigue damage analysis in asphalt concrete mixtures using the dissipated energy approach. Can J Civ Eng. 2006 Jul;33(7):890–901.

67. Carpenter SH, Ghuzlan KA, Shen S. Fatigue Endurance Limit for Highway and Airport Pavements. Transp Res Rec J Transp Res Board. 2003 Jan;1832(1):131–8.

68. Baaj H, Di Benedetto H, Chaverot P. Effect of Binder Characteristics on Fatigue of Asphalt Pavement Using an Instrinsic Damage Approach. Road Mater Pavement Des. 2005;6(2):147–74.

69. Castro M, Sánchez JA. Estimation of asphalt concrete fatigue curves – A damage theory approach. Constr Build Mater. 2008 Jun 1;22(6):1232–8.

70. Pramesti FP, Molenaar AAA, van de Ven MFC. The Prediction of Fatigue Life based on Four Point Bending Test. Procedia Eng. 2013 Jan 1;54:851–62.

71. Bhasin A, Castelo Branco VT, Masad E, Little DN. Quantitative Comparison of Energy Methods to Characterize Fatigue in Asphalt Materials. J Mater Civ Eng. 2009 Feb;21(2):83–92.

72. Kim J, Roque R, Birgisson B. Interpreting Dissipated Energy from Complex Modulus Data. Road Mater Pavement Des. 2006 Jan 1;7(2):223–45.

73. Hiller JE, Roesler JR. Determination of Critical Concrete Pavement Fatigue Damage Locations Using Influence Lines. J Transp Eng. 2005 Aug;131(8):599–607.

74. Tseng K-H. Fatigue Damage Properties of Asphaltic Concrete Pavements. :14.

75. Aglan HA, Bayomy FM. Innovative Approach to Fatigue Crack Propagation in Concrete Pavements. Transp Res Rec J Transp Res Board. 1997 Jan;1568(1):17–23.

76. Smith K, Roesler JR. Review of Fatigue Models for Concrete Airfield Pavement Design. Am Soc Civ Eng. 2004;231–58.

77. Raad L. A Mechanistic Model for Strength and Fatigue of Cement-Treated Soils. Geotech Test J. 1981;4(3):104.

78. Raad L, Monismith C, Mitchell JK. CRACK PROPAGATION IN SOIL-CEMENT BASES SUBJECTED TO REPEATED WHEEL LOADS. Transp Res Rec. 1978;(690):1–5.

79. Nusit K, Jitsangiam P. Damage Behavior of Cement-Treated Base Material | Elsevier Enhanced Reader. Adv Transp Geotech 3 3rd Int Conf Transp Geotech ICTG 2016. 2016;143:161–9.

80. Sobhan K, Das BM. Durability of Soil–Cements against Fatigue Fracture. J Mater Civ Eng. 2007 Jan;19(1):26–32.

81. Sounthararajah A, Bui HH, Nguyen N, Jitsangiam P, Kodikara J. Early-Age Fatigue Damage Assessment of Cement-Treated Bases under Repetitive Heavy Traffic Loading. J Mater Civ Eng. 2018 Jun;30(6):04018079.

82. Jitsangiam P, Nusit K, Chummuneerat S, Chindaprasirt P, Pichayapan P. Fatigue Assessment of Cement-Treated Base for Roads: An Examination of Beam-Fatigue Tests. J Mater Civ Eng. 2016 Oct;28(10):04016095.

83. Ghuzlan KA, Carpenter SH. Energy-Derived, Damage-Based Failure Criterion for Fatigue Testing. Transp Res Rec J Transp Res Board. 2000 Jan;1723(1):141–9.

84. Castañeda López MA, Fedrigo W, Kleinert TR, Matuella MF, Núñez WP, Ceratti JAP. Flexural fatigue evaluation of cement-treated mixtures of reclaimed asphalt pavement and crushed aggregates. Constr Build Mater. 2018 Jan 15;158:320–5.

85. Fedrigo W, Núñez WP, Schreinert GG, Kleinert TR, Matuella MF, Castañeda López MA, et al. Flexural strength, stiffness and fatigue of cement-treated mixtures of reclaimed asphalt pavement and lateritic soil. Road Mater Pavement Des. 2019 Sep 4;1–19.

86. Lei D, Zhang P, He J, Bai P, Zhu F. Fatigue life prediction method of concrete based on energy dissipation. Constr Build Mater. 2017;145:419–25.

87. Tayebali AA, Rowe GM, Sousa JB. FATIGUE RESPONSE OF ASPHALT-AGGREGATE MIXTURES (WITH DISCUSSION). In: Journal of the Association of Asphalt Paving Technologists [Internet]. 1992 [cited 2019 Nov 2]. Available from: https://trid.trb.org/view/486941

88. Miao-Miao Y, Xiao-Ning Z, Wei-Qiang C, Shun-Xian Z. Ratio of Dissipated Energy Change-based Failure Criteria of Asphalt Mixtures. Res J Appl Sci Eng Technol. 2013 Aug 10;6(14):2514–9.

89. Dijk W van. Practical Fatigue Characterization of Bituminous Mixes, Practical Applications. In: Proceedings, Association of Asphalt Pavement Technology. Phoenix, Arizona; 1975. p. 38–75.

90. Dijk W van, Visser W. The Energy Approach to Fatigue for Pavement Design. In: Proceedings, Association of Asphalt Pavement Technology. San Antonio, Texas; 1975. p. 40.

91. Shen S, Carpenter SH. Application of the Dissipated Energy Concept in Fatigue Endurance Limit Testing. Transp Res Rec. 1929;9.

92. Battelle. TOWARD A SUSTAINABLE CEMENT INDUSTRY [Internet]. World Business Council for Sustainable Development; 2002 [cited 2019 May 17]. Available from: http://citeseerx.ist.psu.edu/viewdoc/download?rep=rep1&type=pdf&doi=10.1.1.123.3145

93. Huntzinger DN, Eatmon TD. A life-cycle assessment of Portland cement manufacturing: comparing the traditional process with alternative technologies. J Clean Prod. 2009 May 1;17(7):668–75.

94. Zhang J, Liu G, Chen B, Song D, Qi J, Liu X. Analysis of CO2 Emission for the Cement Manufacturing with Alternative Raw Materials: A LCA-based Framework. Energy Procedia. 2014 Jan 1;61:2541–5.

95. Juenger MCG, Winnefeld F, Provis JL, Ideker JH. Advances in alternative cementitious binders. Cem Concr Res. 2011 Dec 1;41(12):1232–43.

96. NF EN 13282-2-2014 Hydraulic Road Binders - Part 2: Normal Hardening Hydraulic Road Binders - Composition, Specifications And Conformity Criteria - Freestd - Francaise de Normalisation(NF) [Internet]. AFNOR — French standard institute; 2014 [cited 2017 Apr 6]. Available from: http://www.freestd.us/soft4/4680877.htm

97. Santos J, Bryce J, Flintsch G, Ferreira A, Diefenderfer B. A life cycle assessment of in-place recycling and conventional pavement construction and maintenance practices. Struct Infrastruct Eng. 2015 Sep 2;11(9):1199–217.

98. Giani MI, Dotelli G, Brandini N, Zampori L. Comparative life cycle assessment of asphalt pavements using reclaimed asphalt, warm mix technology and cold in-place recycling. Resour Conserv Recycl. 2015 Nov 1;104:224–38.

99. Turk J, Mauko Pranjić A, Mladenovič A, Cotič Z, Jurjavčič P. Environmental comparison of two alternative road pavement rehabilitation techniques: cold-in-place-recycling versus traditional reconstruction. J Clean Prod. 2016 May 10;121:45–55.

100. Saboori A, Harvey J, Butt A, Jones D. Life cycle assessment and benchmarking of end of life treatments of flexible pavements in California. In: Pavement Life-Cycle Assessment [Internet]. Illinois, USA: CRC Press; 2017 [cited 2019 Sep 9]. p. 231–9. Available from: http://www.crcnetbase.com/doi/10.1201/9781315159324-24

101. Wang H, Gangaram R. Life Cycle Assessment of Asphalt Pavement Maintenance [Internet]. Rutgers: The State University of New Jersey; 2014 Jan [cited 2019 Sep 7] p. 67. Report No.: CAIT-UTC-013. Available from: https://rosap.ntl.bts.gov/view/dot/28057

102. Sudarno S, Purwanto P, Pratikso P. Life Cycle Assessment on Cement Treated Recycling Base (CTRB) Construction. Waste Technol. 2014 Oct 4;2(2):31–40.

103. Chiu C-T, Hsu T-H, Yang W-F. Life cycle assessment on using recycled materials for rehabilitating asphalt pavements. Resour Conserv Recycl. 2008 Jan 1;52(3):545–56.

104. Cross SA, Chesner WH, Justus HG, Kearney ER. Life-Cycle Environmental Analysis for Evaluation of Pavement Rehabilitation Options. Transp Res Rec J Transp Res Board. 2011 Jan;2227(1):43–52.

105. Santos J, Ferreira A, Flintsch G. A life cycle assessment model for pavement management: methodology and computational framework. Int J Pavement Eng. 2015 Mar 16;16(3):268–86.

106. Horvath A. A Life-Cycle Analysis Model and Decision-Support Tool for Selecting Recycled Versus Virgin Materials for Highway Applications [Internet]. University of California, Berkeley; 2004 Mar [cited 2019 Sep 9] p. 35. Report No.: RMRC Research Project No. 23. Available from: http://rmrc.wisc.edu/wp-content/uploads/2012/10/P23Final.pdf

107. Huang Y, Bird R, Heidrich O. Development of a life cycle assessment tool for construction and maintenance of asphalt pavements. J Clean Prod. 2009 Jan 1;17(2):283–96.

108. Saade MRM, Silva MG da, Gomes V. Appropriateness of environmental impact distribution methods to model blast furnace slag recycling in cement making. Resour Conserv Recycl. 2015 Jun 1;99:40–7.

109. Li Y, Liu Y, Gong X, Nie Z, Cui S, Wang Z, et al. Environmental impact analysis of blast furnace slag applied to ordinary Portland cement production. J Clean Prod. 2016 May 1;120:221–30.

110. Lee K-M, Park P-J. Estimation of the environmental credit for the recycling of granulated blast furnace slag based on LCA. Resour Conserv Recycl. 2005 May 1;44(2):139–51.

111. Stafford FN, Dias AC, Arroja L, Labrincha JA, Hotza D. Life cycle assessment of the production of Portland cement: a Southern Europe case study. J Clean Prod. 2016 Jul 10;126:159–65.

112. Li C, Cui S, Nie Z, Gong X, Wang Z, Itsubo N. The LCA of portland cement production in China. Int J Life Cycle Assess. 2015 Jan;20(1):117–27.

113. Marceau ML, Nisbet MA, VanGeem MG. Life Cycle Inventory of Portland Cement Manufacture. 2006;68.

114. Ministry of Transportation of Ontario. Ontario's Default Parameters for AASHTOWare Pavement ME Design-Interim Report 2019.pdf [Internet]. 2019 [cited 2019 Sep 11]. Available from: https://www.raqsb.mto.gov.on.ca/login/raqs.nsf/f7655a6959db3dd785256c1d0073eb7b/4365876106ab3bea85258411006bf14a/$FILE/ATTVSW69/Ontario's%20Default%20Parameters%20for%20AASHTOWare%20Pavement%20ME%20Design-Interim%20Report%202019.pdf

115. Ministry of Transportation of Ontario. Pavement Design and Rehabilitation Manual. Second Ed. Ontario, Canada: Materials Engineering and Research Office, Ministry of Transportation of Ontario; 2013.

116. Pavement ME User Group. Canadian Guide: Default Parameters for AASHTOWare Pavement ME Design [Internet]. Transportation Association of Canada; 2014 [cited 2019

Oct 1]. Available from: https://www.scribd.com/document/304718258/Canadian-Guide-Default-Parameters-for-AASHTOWare-Pavement-ME-Design

117. Athena Institute. A Life Cycle Perspective on Concrete and Asphalt Roadways: Embodied Primary Energy and Global Warming Potential [Internet]. Ottawa, Canada: Athena Institute; 2006 [cited 2019 Sep 27]. Available from: http://www.athenasmi.org/wp-content/uploads/2012/01/Athena_Update_Report_LCA_PCCP_vs_HMA_Final_Document_Sept_2006.pdf

118. Athena Sustainable Materials Institute. User Manual and Transparency Document_Pavement LCA v 3.1 - Web Application [Internet]. Athena Sustainable Materials Institute; 2018 [cited 2019 Sep 21]. Available from: https://calculatelca.com/wp-content/uploads/2016/04/PavementLCA_UserGuide.pdf

APPENDICES

APPENDICES-I

Sample AASHTOWare Pavement ME Outputs

Existing Flexible Pavement Structure

File Name: C:\Users\admin\Desktop\Eskedil_ME\Kossuth\Existing Flexible Pavement Structure.dgpx

Design Inputs

Design Life: 20 years
Design Type: FLEXIBLE

Base construction: May, 2000
Pavement construction: June, 2000
Traffic opening: July, 2000

Climate Data Sources (Lat/Lon) 43.5, -80.625
43, -80

Design Structure

Layer type	Material Type	Thickness(mm)
Flexible	Default asphalt concrete	80.0
Flexible	Default asphalt concrete	100.0
NonStabilized	Crushed stone	400.0
NonStabilized	Crushed gravel	500.0
Subgrade	A-6	Semi-infinite

Volumetric at Construction:	
Effective binder content (%)	11.8
Air voids (%)	7.0

Traffic

Age (year)	Heavy Trucks (cumulative)
2000 (initial)	900
2010 (10 years)	1,678,960
2020 (20 years)	3,801,700

Design Outputs

Distress Prediction Summary

Distress Type	Distress @ Specified Reliability		Reliability (%)		Criterion Satisfied?
	Target	Predicted	Target	Achieved	
Terminal IRI (m/km)	2.30	2.28	85.00	86.08	Pass
Permanent deformation - total pavement (mm)	13.00	7.55	85.00	100.00	Pass
AC bottom-up fatigue cracking (percent)	20.00	1.18	85.00	100.00	Pass
AC thermal cracking (m/km)	190.00	33.17	85.00	100.00	Pass
AC top-down fatigue cracking (m/km)	380.00	479.13	85.00	78.13	Fail
Permanent deformation - AC only (mm)	6.00	0.94	85.00	100.00	Pass

Distress Charts

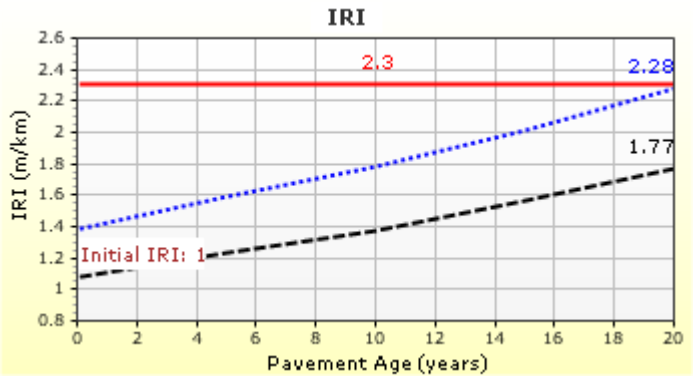

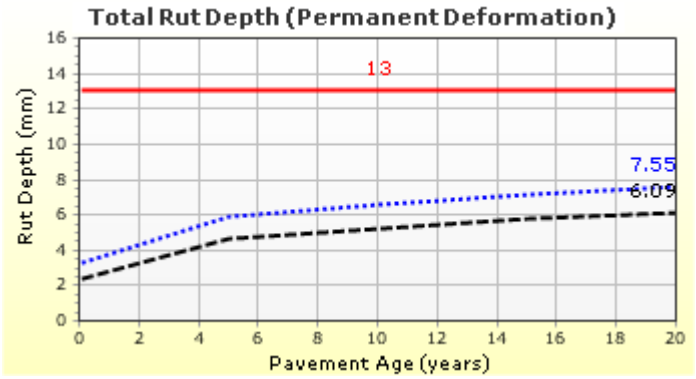

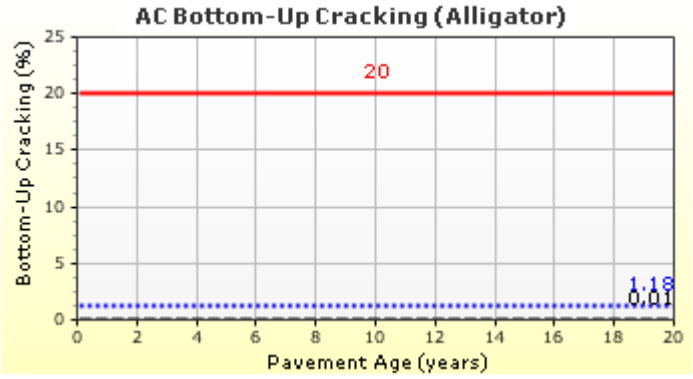

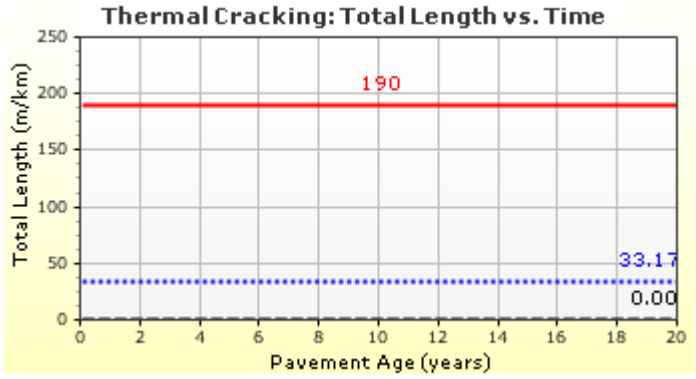

Traffic Inputs

Graphical Representation of Traffic Inputs

Initial two-way AADTT:	900	Percent of trucks in design direction (%):	50.0
Number of lanes in design direction:	2	Percent of trucks in design lane (%):	90.0
		Operational speed (kph)	100.0

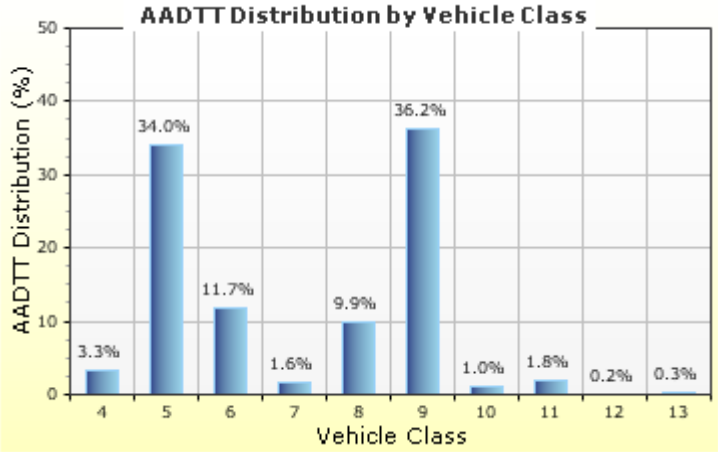

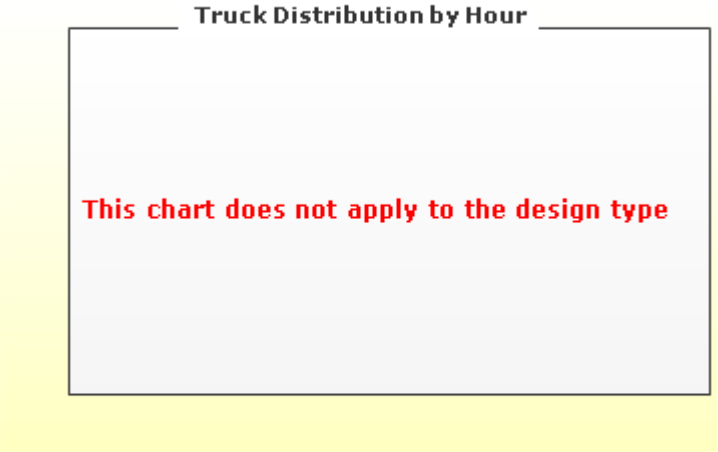

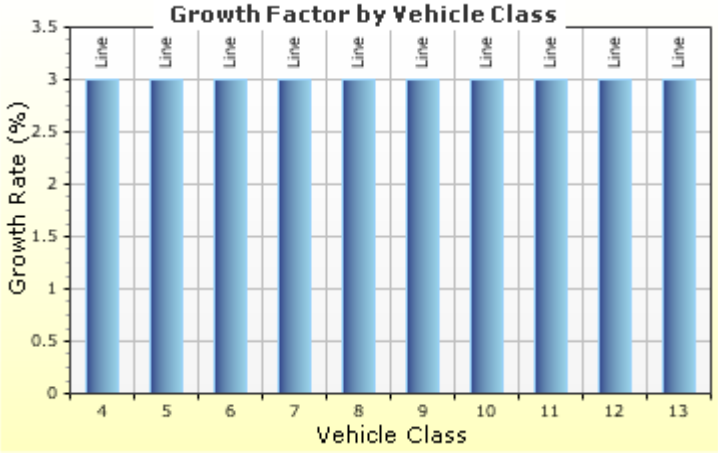

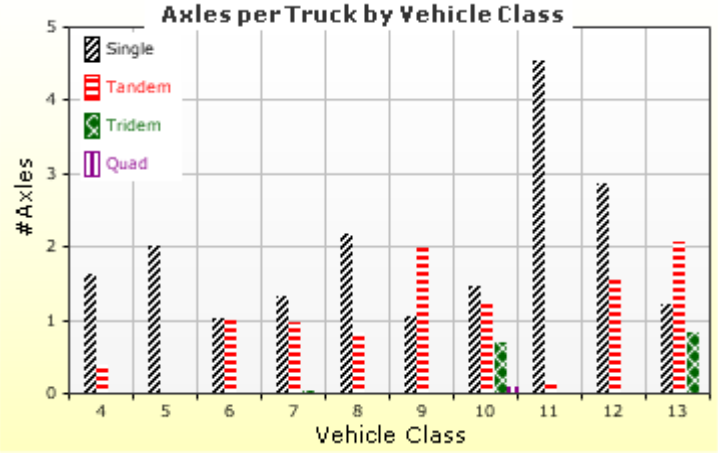

Traffic Volume Monthly Adjustment Factors

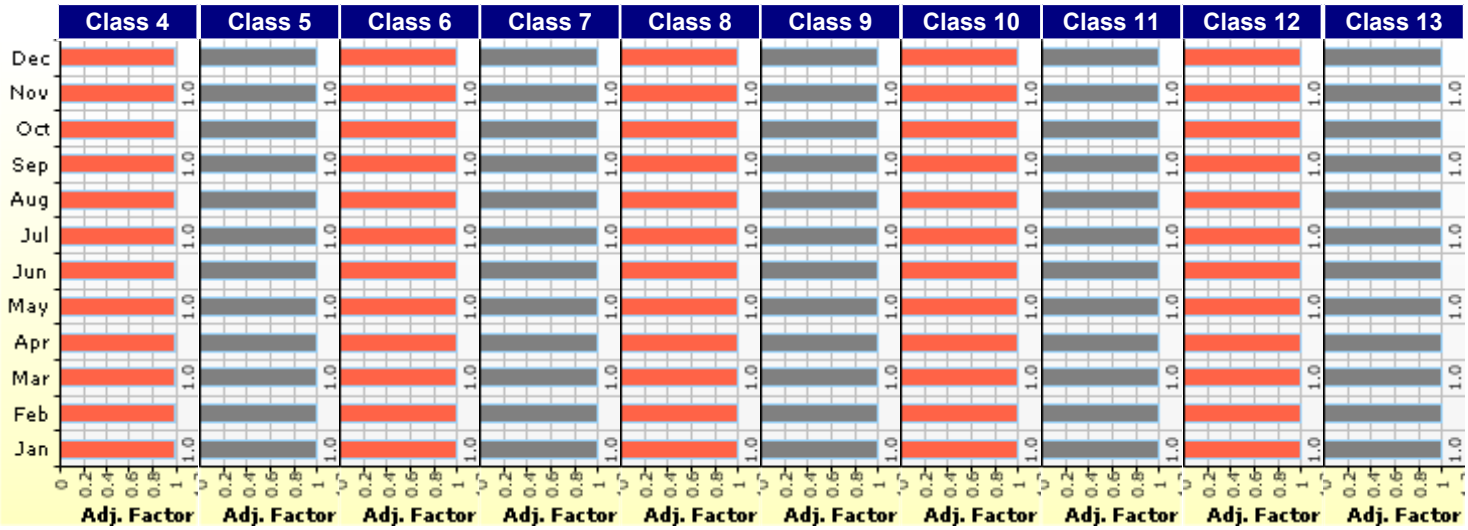

Tabular Representation of Traffic Inputs

Volume Monthly Adjustment Factors

Level 3: Default MAF

Month	Vehicle Class									
	4	5	6	7	8	9	10	11	12	13
January	1.0	1.0	1.0	1.0	1.0	1.0	1.0	1.0	1.0	1.0
February	1.0	1.0	1.0	1.0	1.0	1.0	1.0	1.0	1.0	1.0
March	1.0	1.0	1.0	1.0	1.0	1.0	1.0	1.0	1.0	1.0
April	1.0	1.0	1.0	1.0	1.0	1.0	1.0	1.0	1.0	1.0
May	1.0	1.0	1.0	1.0	1.0	1.0	1.0	1.0	1.0	1.0
June	1.0	1.0	1.0	1.0	1.0	1.0	1.0	1.0	1.0	1.0
July	1.0	1.0	1.0	1.0	1.0	1.0	1.0	1.0	1.0	1.0
August	1.0	1.0	1.0	1.0	1.0	1.0	1.0	1.0	1.0	1.0
September	1.0	1.0	1.0	1.0	1.0	1.0	1.0	1.0	1.0	1.0
October	1.0	1.0	1.0	1.0	1.0	1.0	1.0	1.0	1.0	1.0
November	1.0	1.0	1.0	1.0	1.0	1.0	1.0	1.0	1.0	1.0
December	1.0	1.0	1.0	1.0	1.0	1.0	1.0	1.0	1.0	1.0

Distributions by Vehicle Class

Truck Distribution by Hour does not apply

Vehicle Class	AADTT Distribution (%) (Level 3)	Growth Factor	
		Rate (%)	Function
Class 4	3.3%	3%	Linear
Class 5	34%	3%	Linear
Class 6	11.7%	3%	Linear
Class 7	1.6%	3%	Linear
Class 8	9.9%	3%	Linear
Class 9	36.2%	3%	Linear
Class 10	1%	3%	Linear
Class 11	1.8%	3%	Linear
Class 12	0.2%	3%	Linear
Class 13	0.3%	3%	Linear

Axle Configuration

Traffic Wander	
Mean wheel location (mm)	460.0
Traffic wander standard deviation (mm)	254.0
Design lane width (m)	3.7

Axle Configuration	
Average axle width (m)	2.6
Dual tire spacing (mm)	305.0
Tire pressure (kPa)	827.4

Average Axle Spacing	
Tandem axle spacing (m)	1.5
Tridem axle spacing (m)	1.7
Quad axle spacing (m)	1.3

Wheelbase does not apply

Number of Axles per Truck

Vehicle Class	Single Axle	Tandem Axle	Tridem Axle	Quad Axle
Class 4	1.62	0.39	0	0
Class 5	2	0	0	0
Class 6	1.014	0.993	0	0
Class 7	1.314	0.989	0.03	0
Class 8	2.163	0.845	0	0
Class 9	1.055	1.968	0.003	0
Class 10	1.446	1.234	0.7	0.088
Class 11	4.546	0.168	0	0
Class 12	2.857	1.526	0	0
Class 13	1.201	2.058	0.848	0.024

AADTT (Average Annual Daily Truck Traffic) Growth

*** Traffic cap is not enforced**

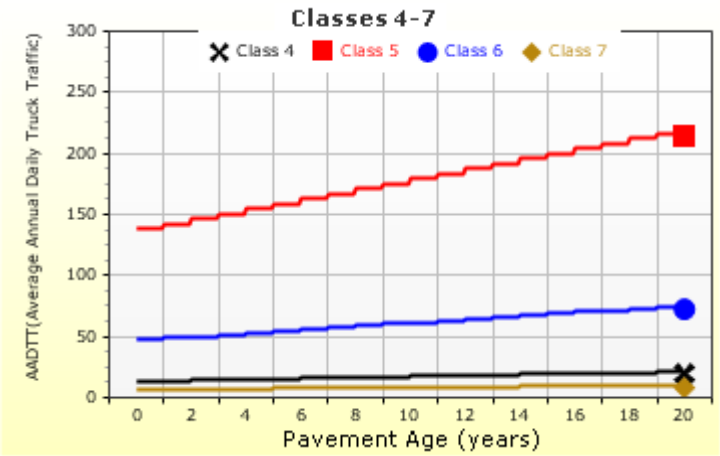

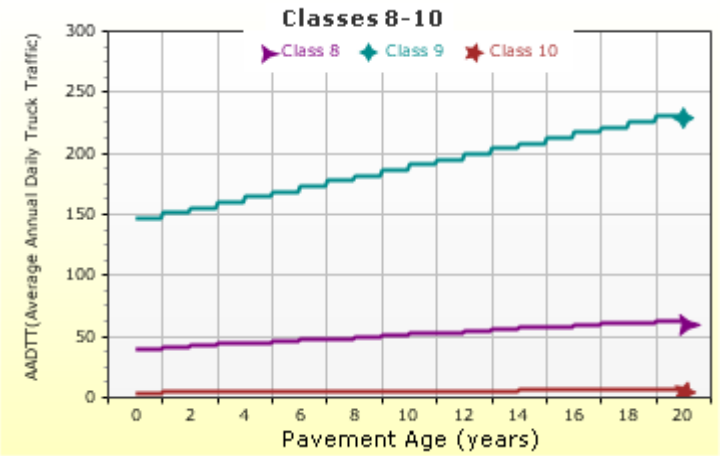

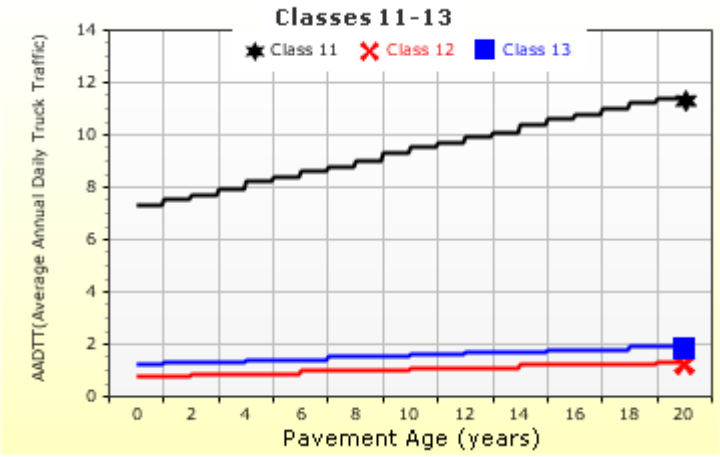

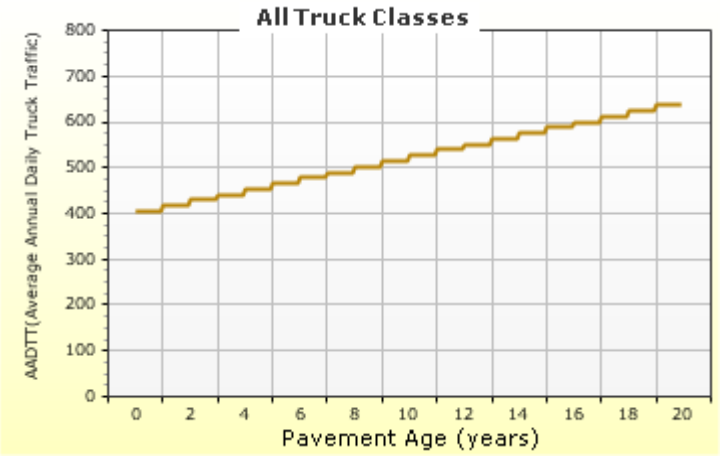

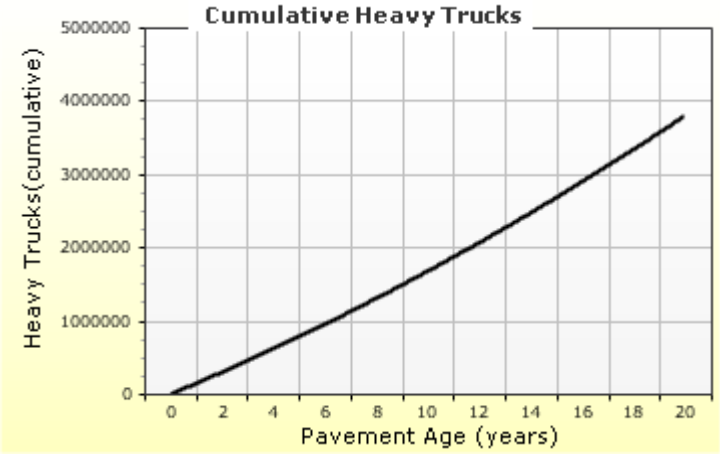

Climate Inputs

Climate Data Sources:

Climate Station Cities:	Location (lat lon elevation(m))
CA, ON	43.50000 -80.62500 369
CA, ON	43.00000 -80.00000 210

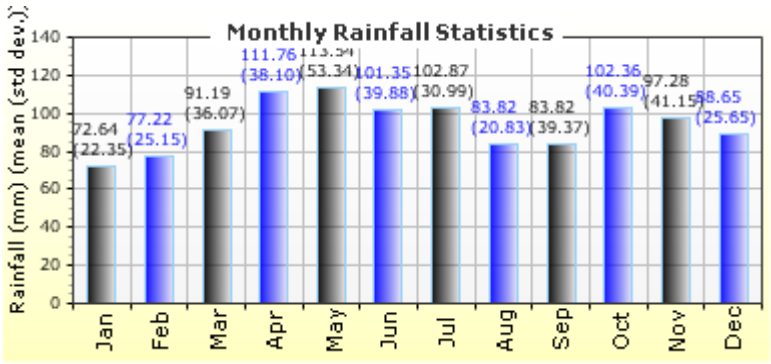

Annual Statistics:

Mean annual air temperature (°C)	8.18
Mean annual precipitation (mm)	1128.52
Freezing index (°C - days)	564.93
Average annual number of freeze/thaw cycles:	80.61

Water table depth (m)	10.00

Monthly Climate Summary:

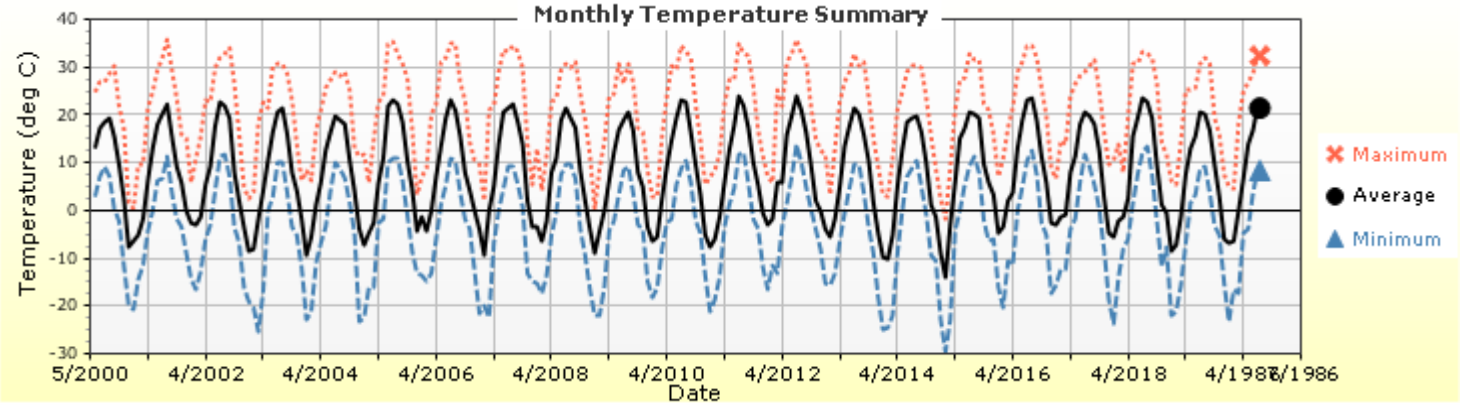

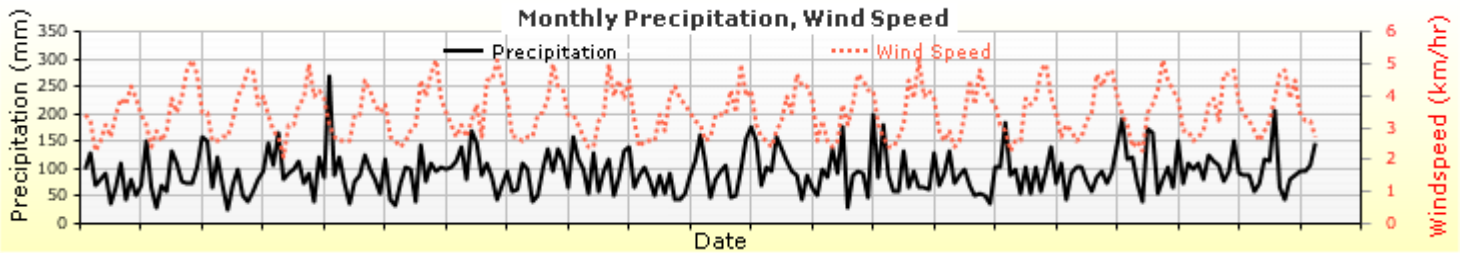

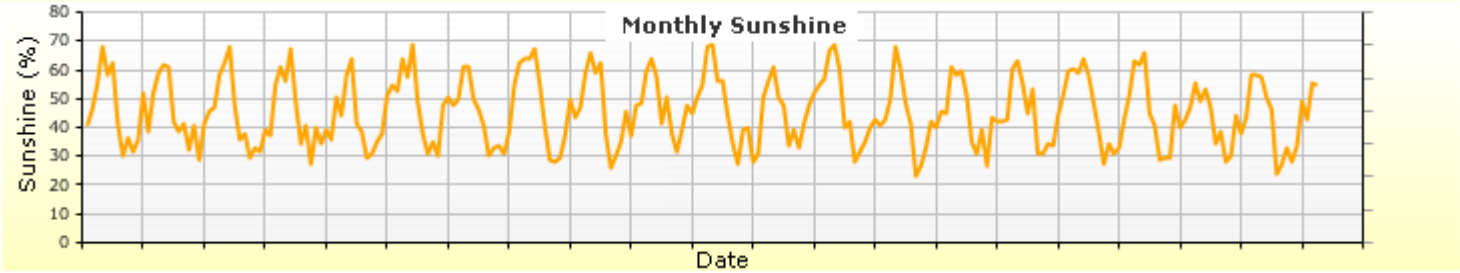

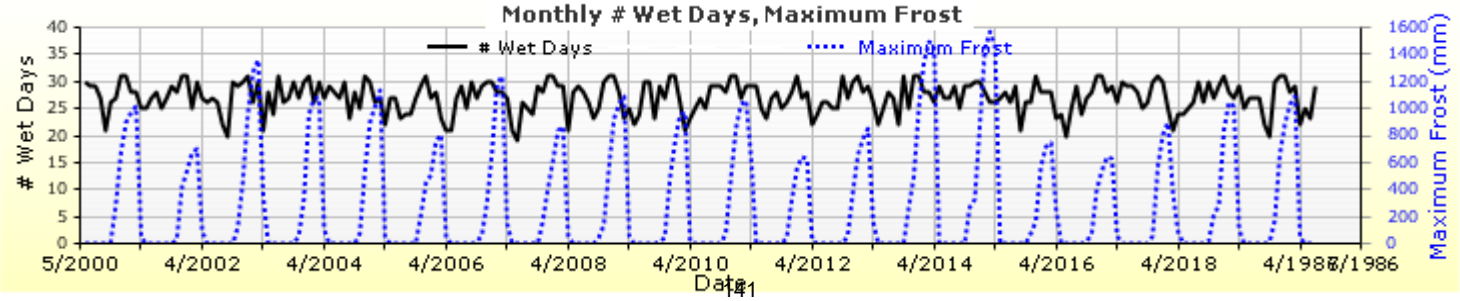

Hourly Air Temperature Distribution by Month:

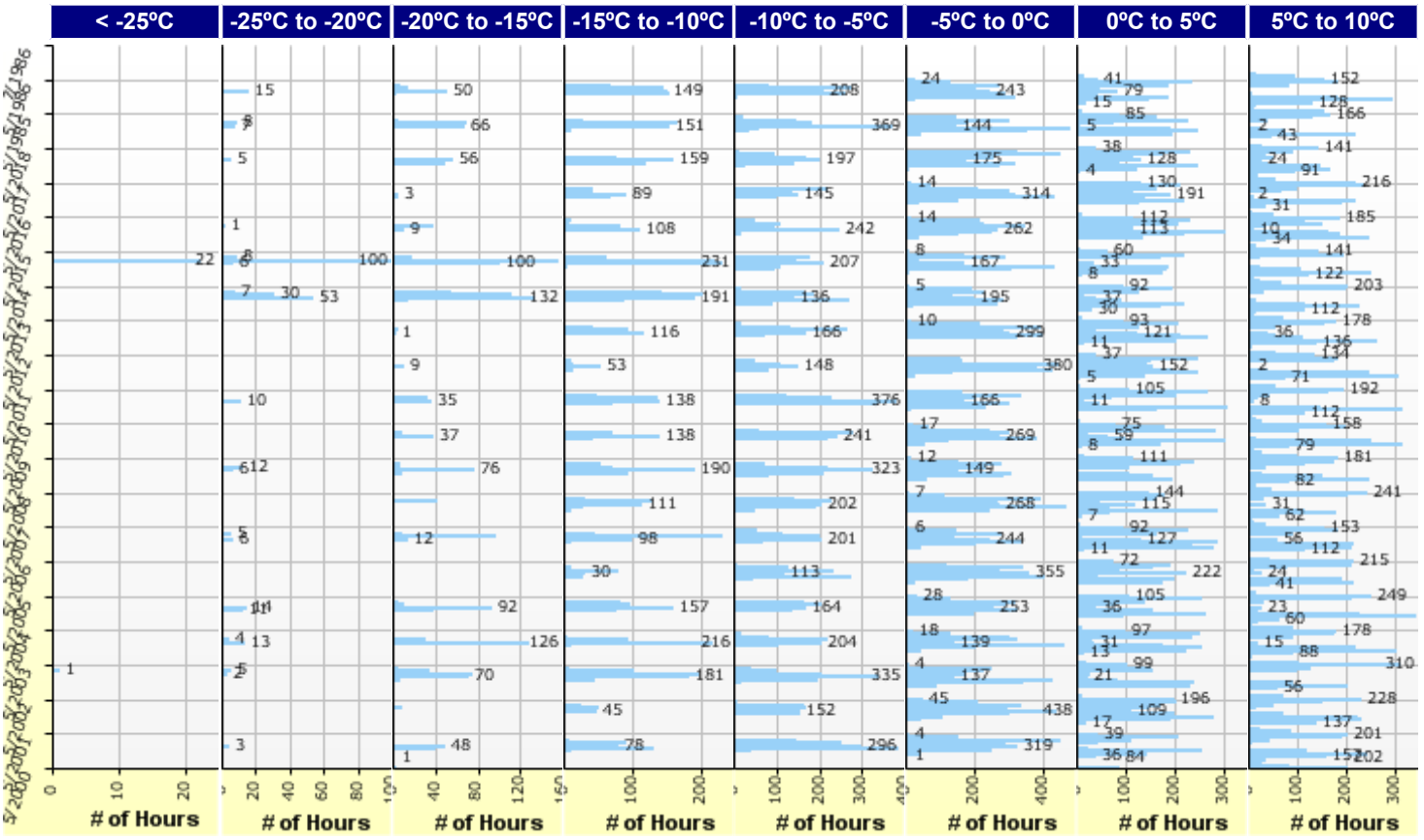

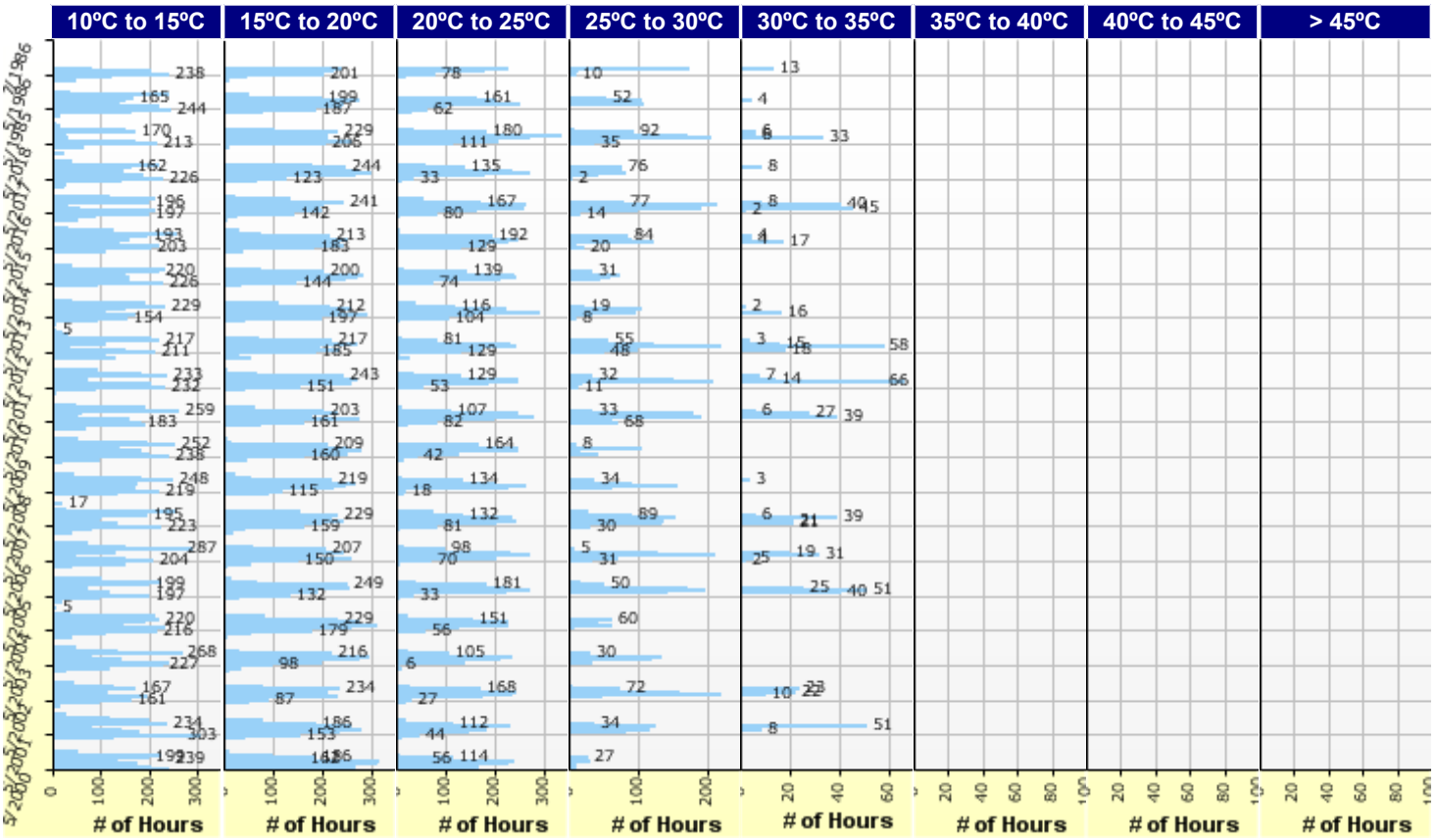

Design Properties

HMA Design Properties

Use Multilayer Rutting Model	False
Using G* based model (not nationally calibrated)	False
Is NCHRP 1-37A HMA Rutting Model Coefficients	True
Endurance Limit	-
Use Reflective Cracking	True

Structure - ICM Properties	
AC surface shortwave absorptivity	0.85

Layer Name	Layer Type	Interface Friction
Layer 1 Flexible : Default asphalt concrete	Flexible (1)	1.00
Layer 2 Flexible : Default asphalt concrete	Flexible (1)	1.00
Layer 3 Non-stabilized Base : Crushed stone	Non-stabilized Base (4)	1.00
Layer 4 Non-stabilized Base : Crushed gravel	Non-stabilized Base (4)	1.00
Layer 5 Subgrade : A-6	Subgrade (5)	-

Thermal Cracking

Thermal Contraction	
Is thermal contraction calculated?	True
Mix coefficient of thermal contraction (mm/mm/ºC)	-
Aggregate coefficient of thermal contraction (mm/mm/ºC)	9.0e-006
Voids in Mineral Aggregate (%)	18.8

Indirect Tensile Strength (Input Level: 3)	
Test Temperature (ºC)	**Indirect Tensilte Strength (Mpa)**
-10.0	2.79

Creep Compliance (1/GPa) (Input Level: 3)			
Loading time (sec)	**-20 ºC**	**-10 ºC**	**0 ºC**
1	5.57e-002	8.57e-002	1.16e-001
2	6.17e-002	1.01e-001	1.51e-001
5	7.07e-002	1.25e-001	2.15e-001
10	7.83e-002	1.48e-001	2.80e-001
20	8.68e-002	1.74e-001	3.65e-001
50	9.94e-002	2.16e-001	5.19e-001
100	1.10e-001	2.55e-001	6.77e-001

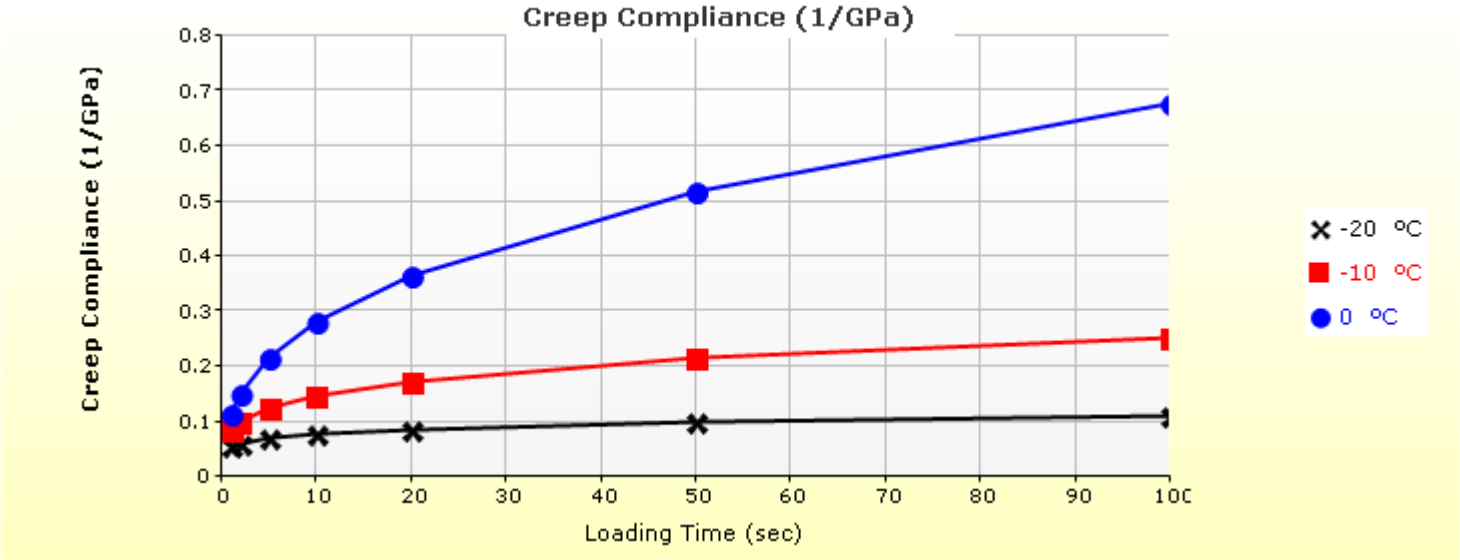

HMA Layer 1: Layer 1 Flexible : Default asphalt concrete

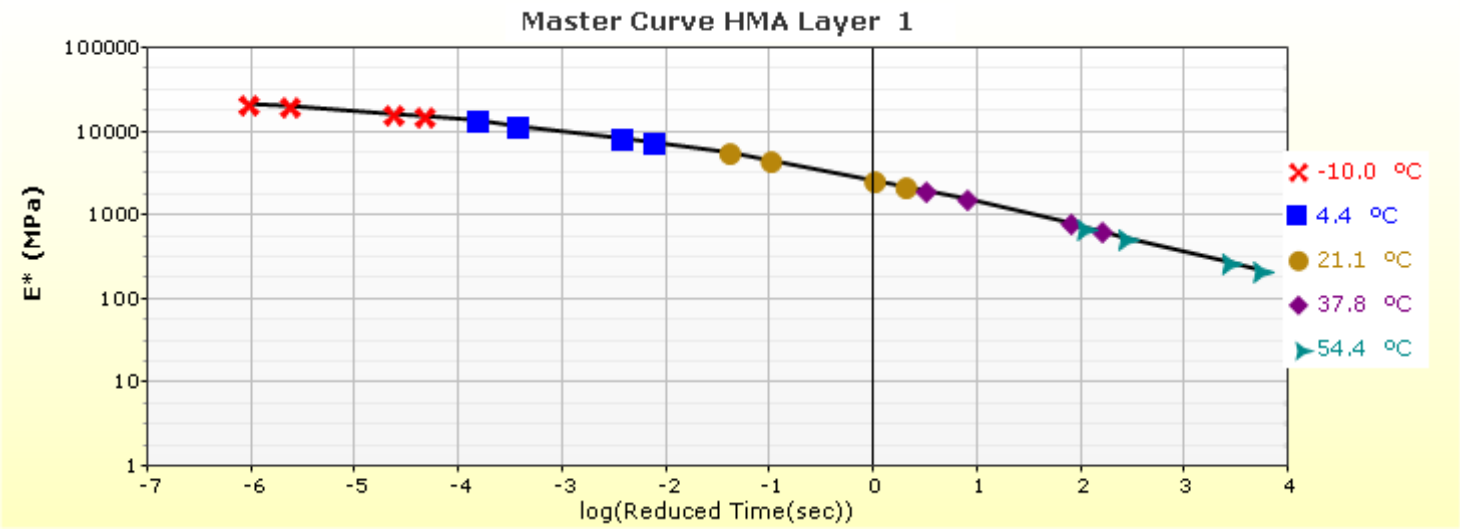

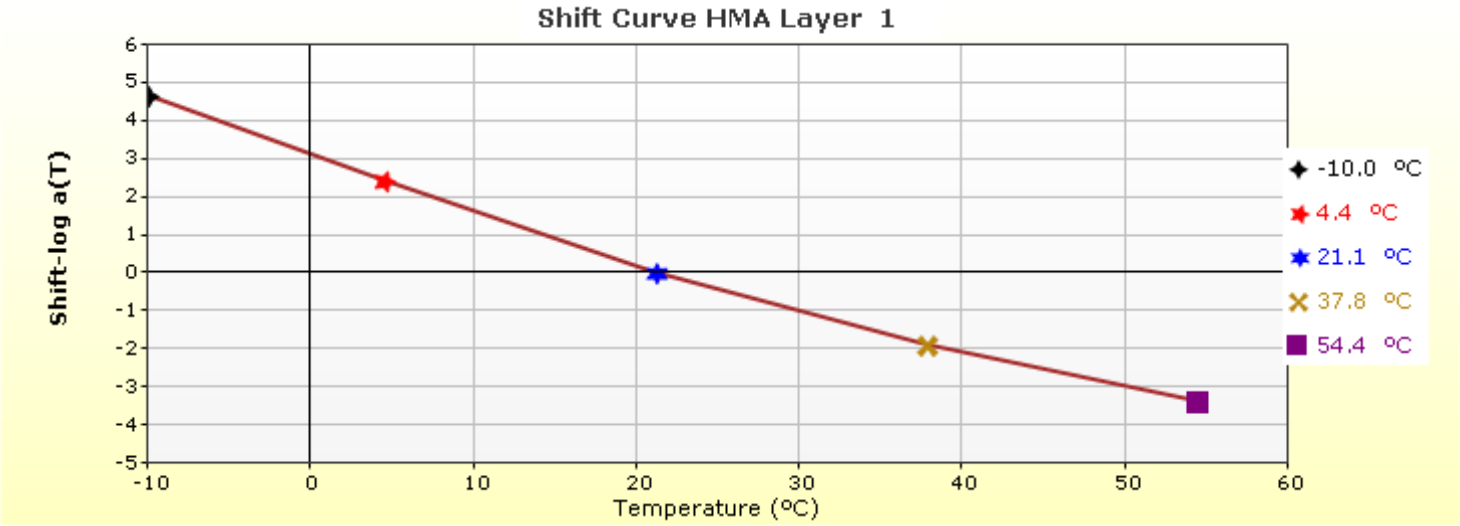

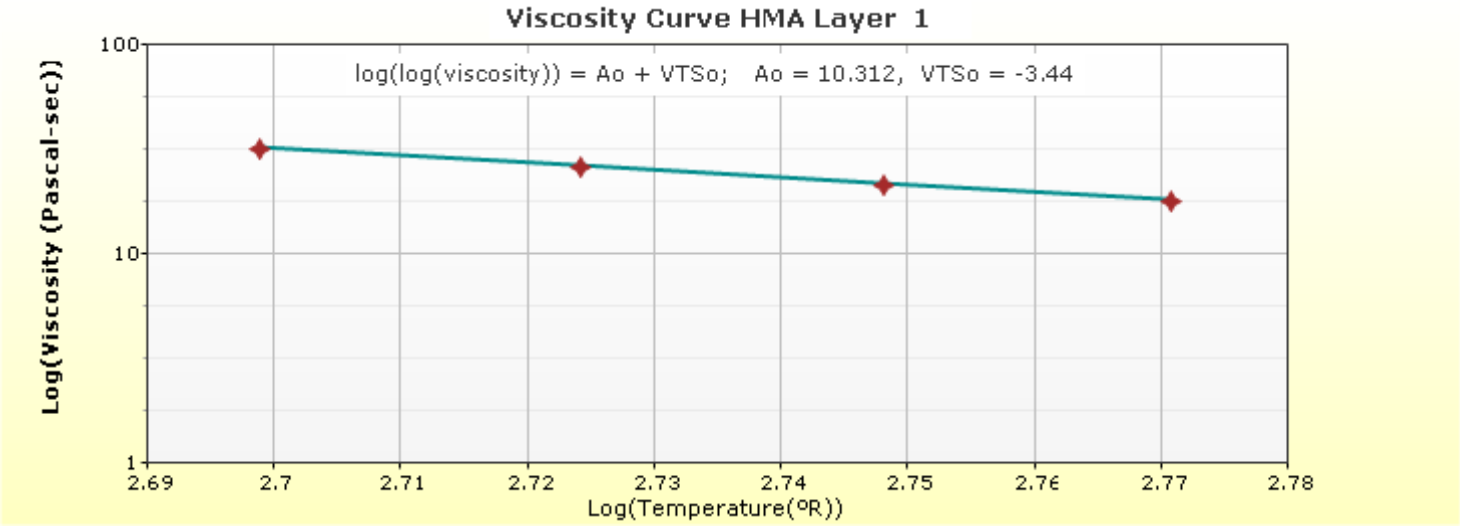

HMA Layer 2: Layer 2 Flexible : Default asphalt concrete

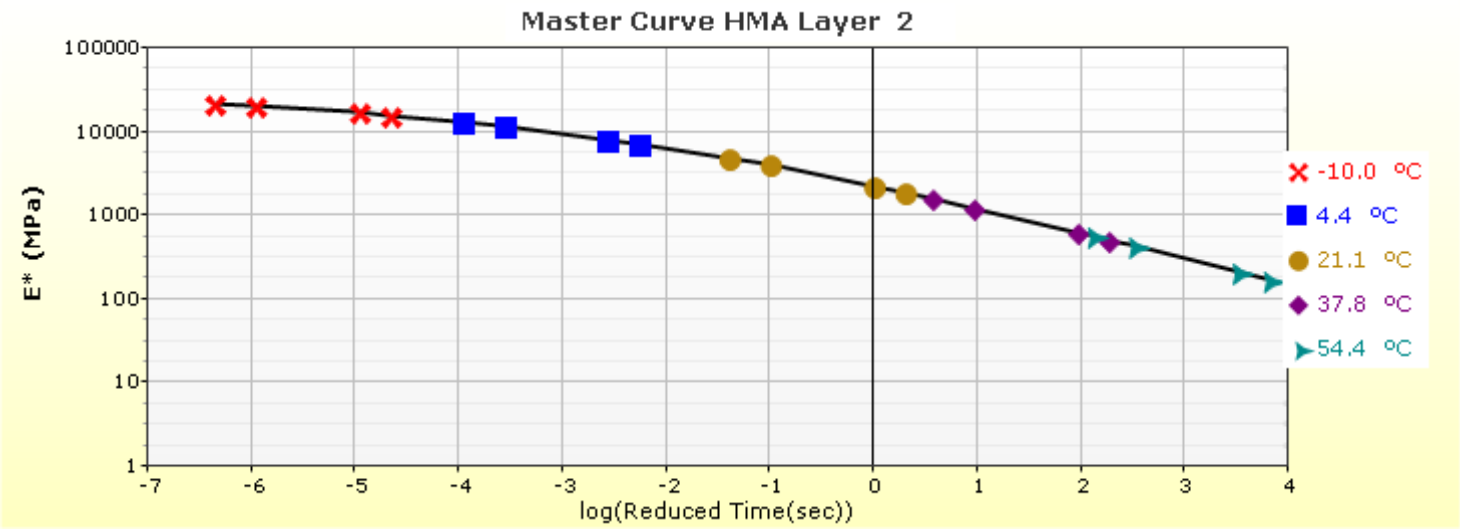

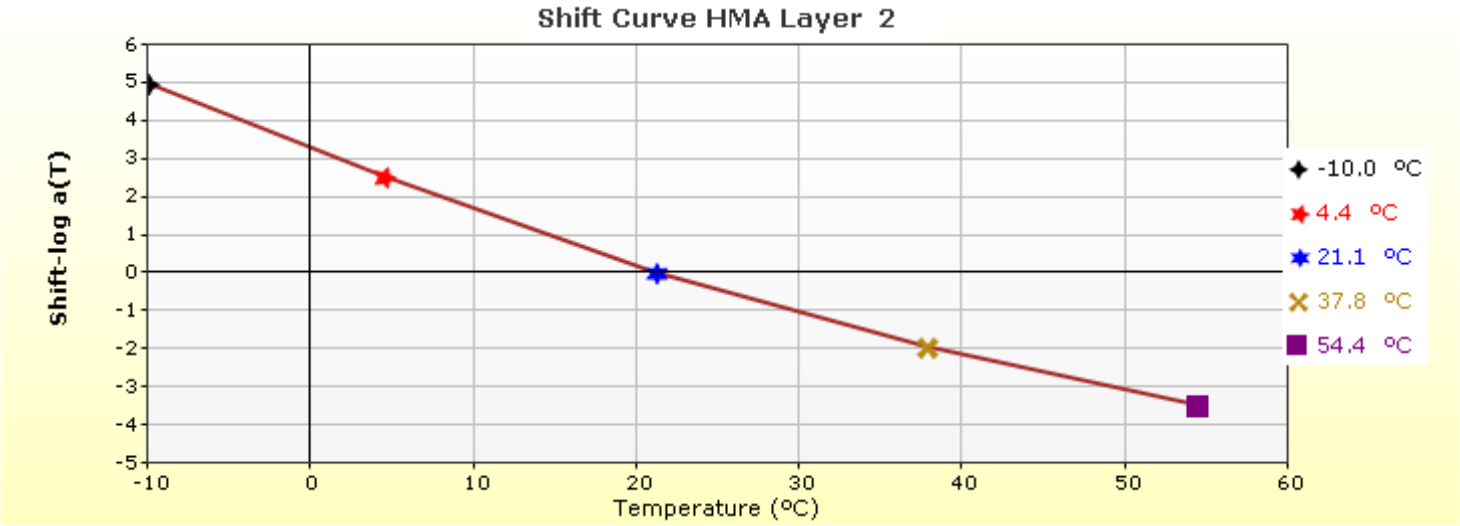

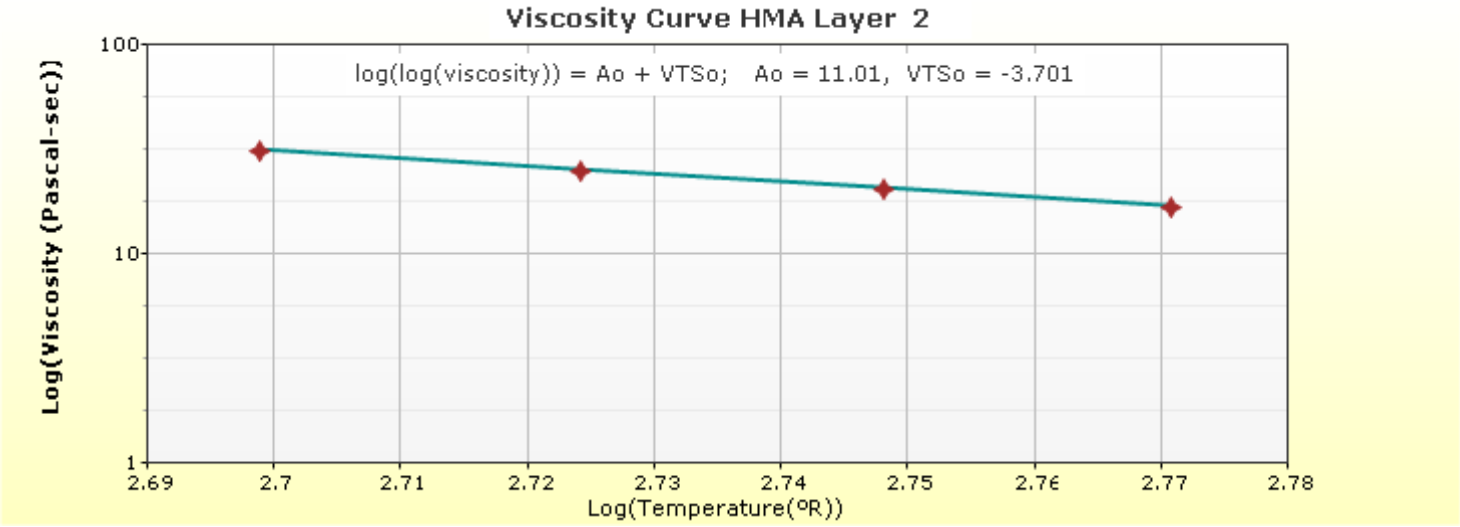

Analysis Output Charts

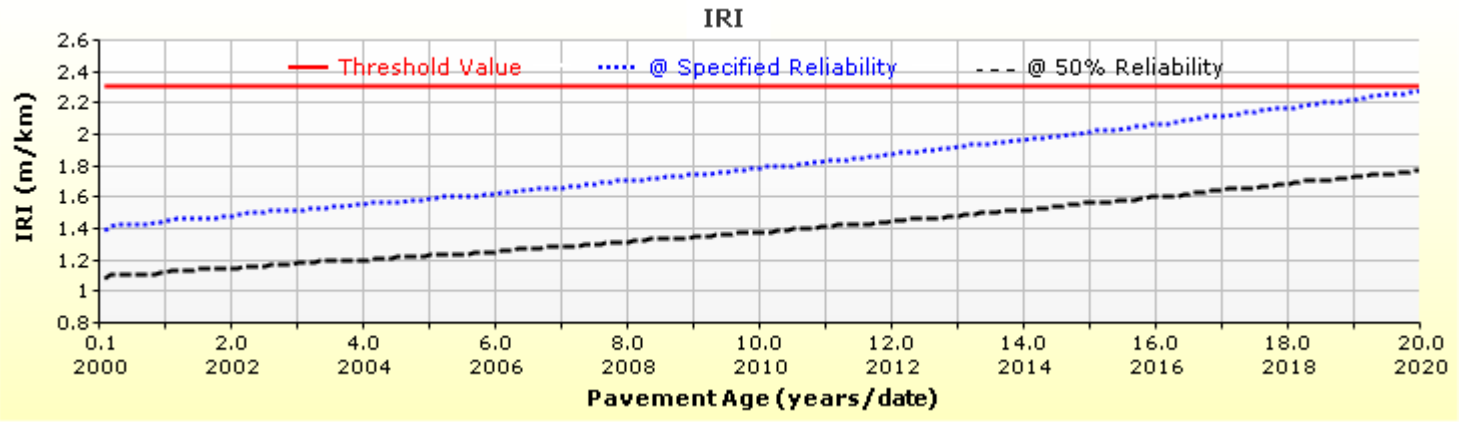

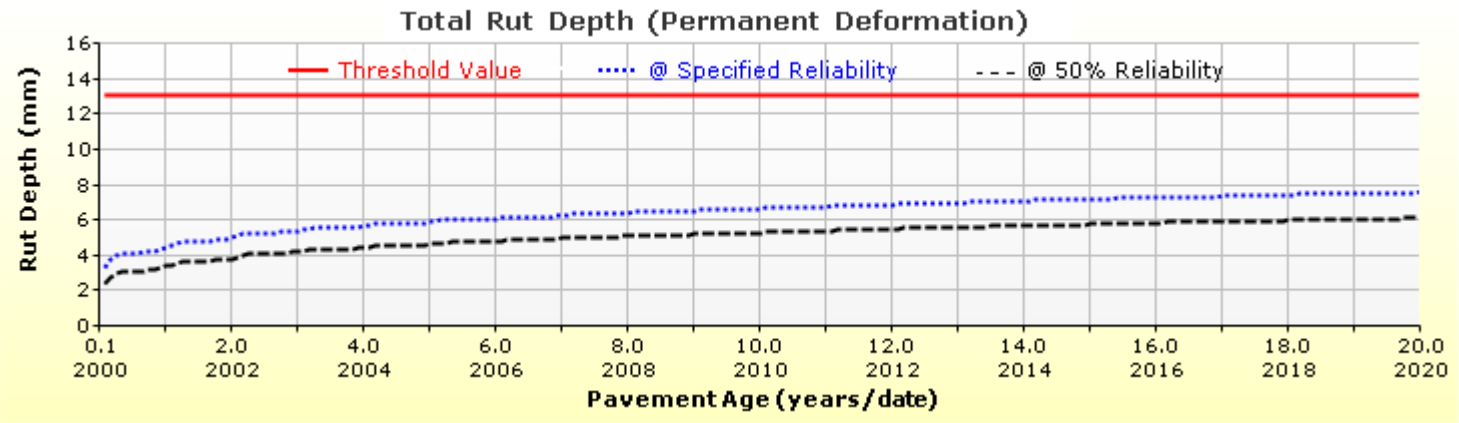

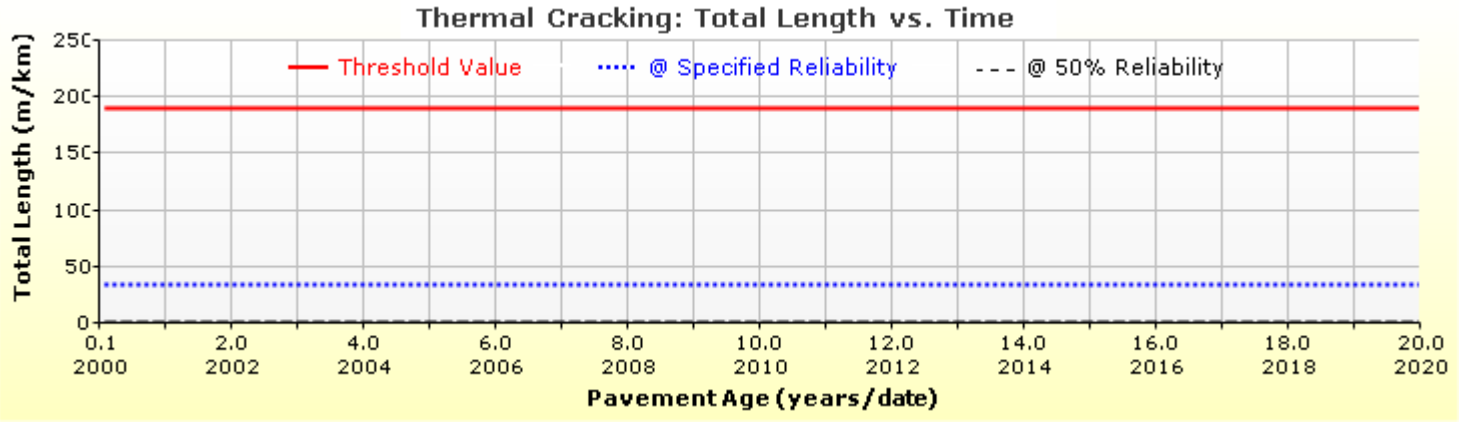

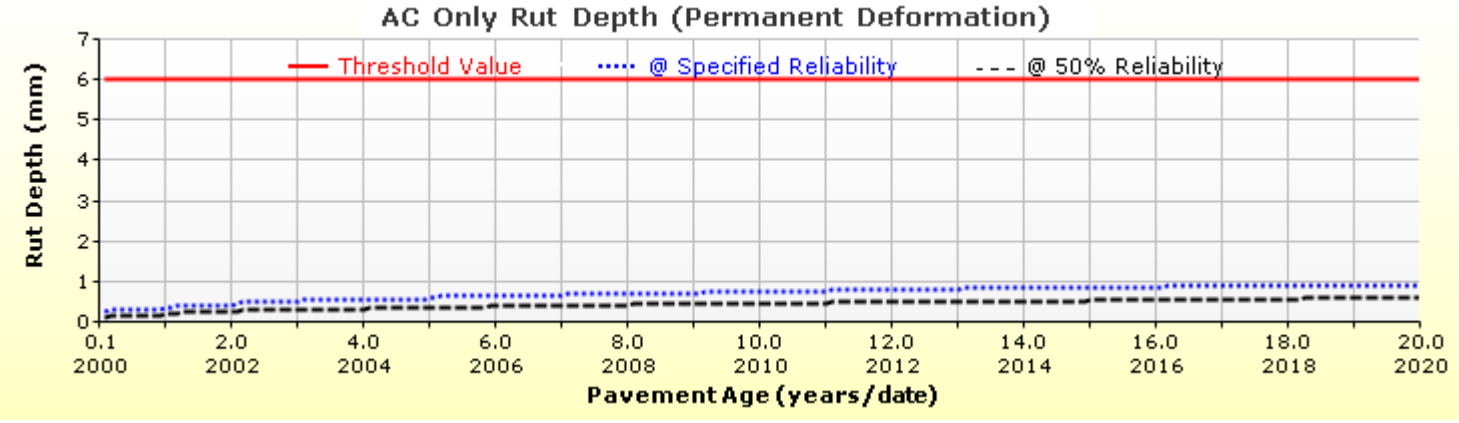

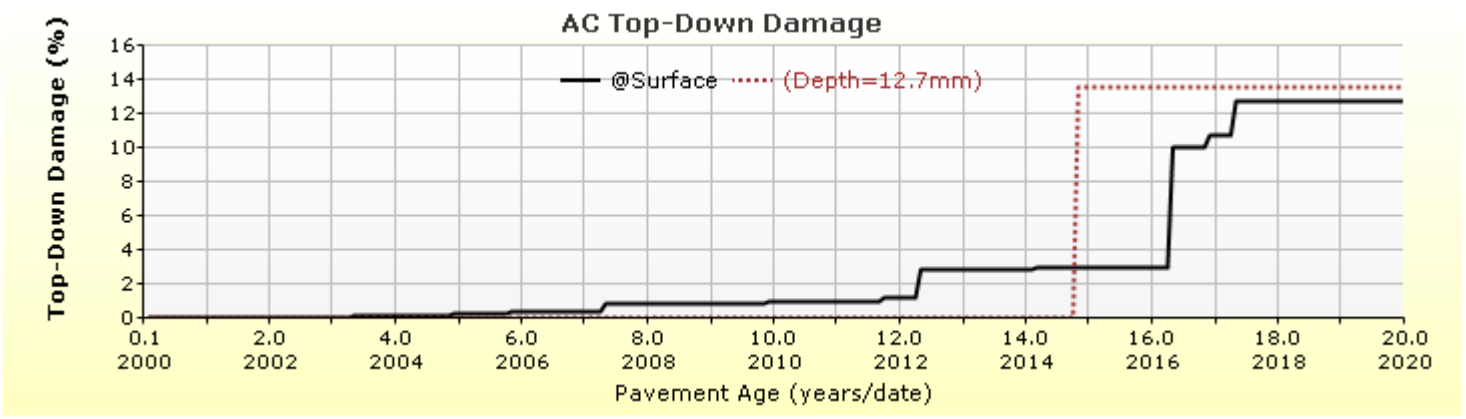
AC Top-Down Damage
Top-Down Damage (%)
@Surface
(Depth=12.7mm)
Pavement Age (years/date)

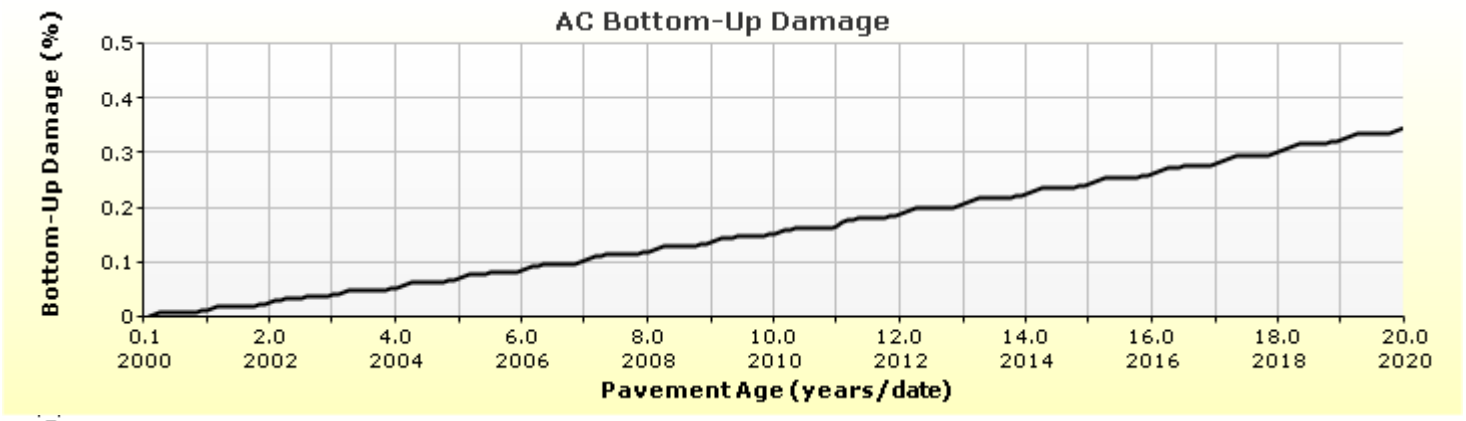
AC Bottom-Up Damage
Bottom-Up Damage (%)
Pavement Age (years/date)

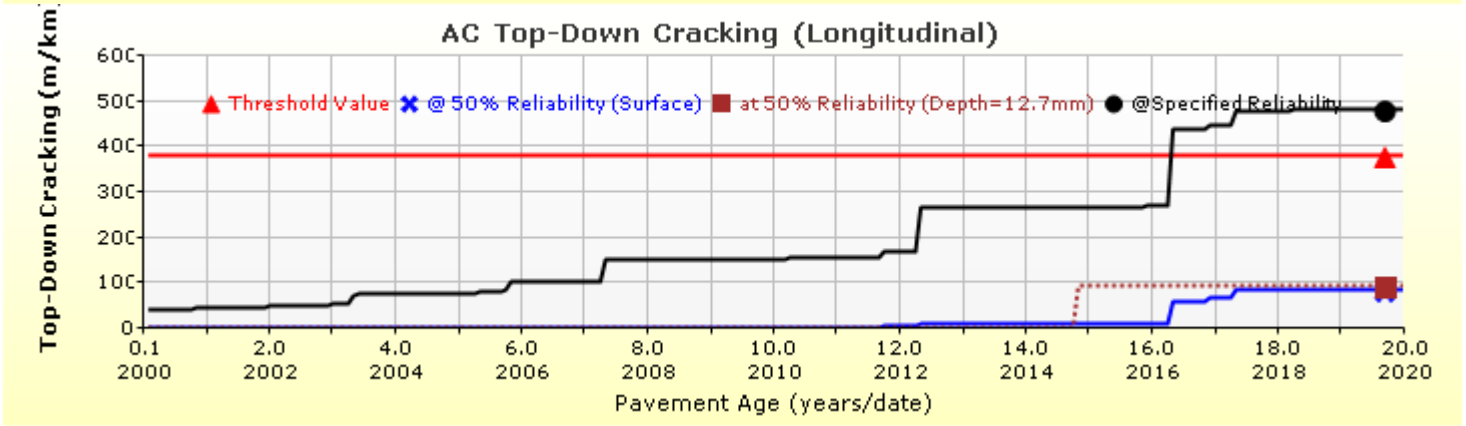
AC Top-Down Cracking (Longitudinal)
Top-Down Cracking (m/km)
Threshold Value
@ 50% Reliability (Surface)
at 50% Reliability (Depth=12.7mm)
@Specified Reliability
Pavement Age (years/date)

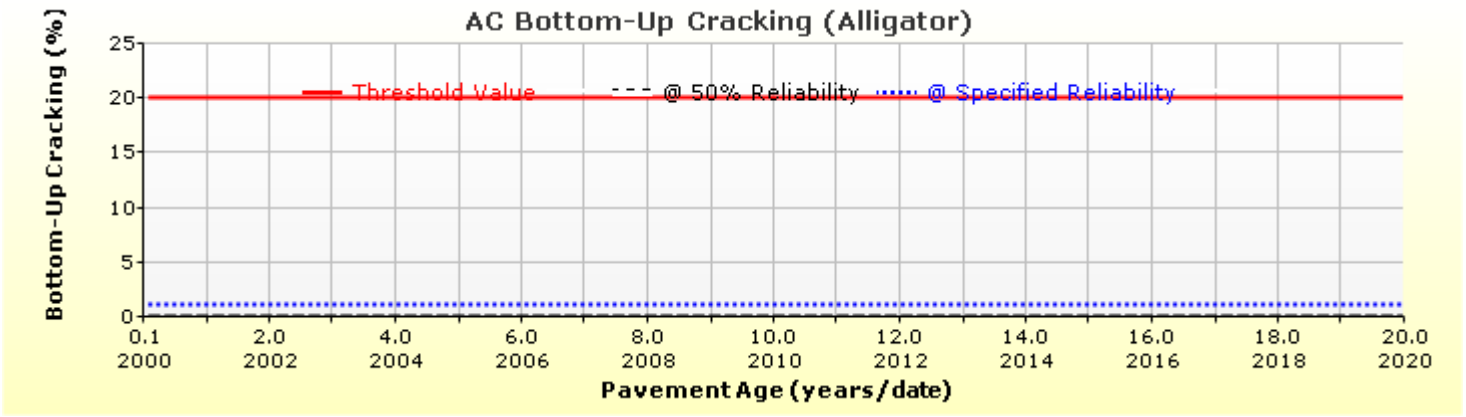
AC Bottom-Up Cracking (Alligator)
Bottom-Up Cracking (%)
Threshold Value
@ 50% Reliability
@ Specified Reliability
Pavement Age (years/date)

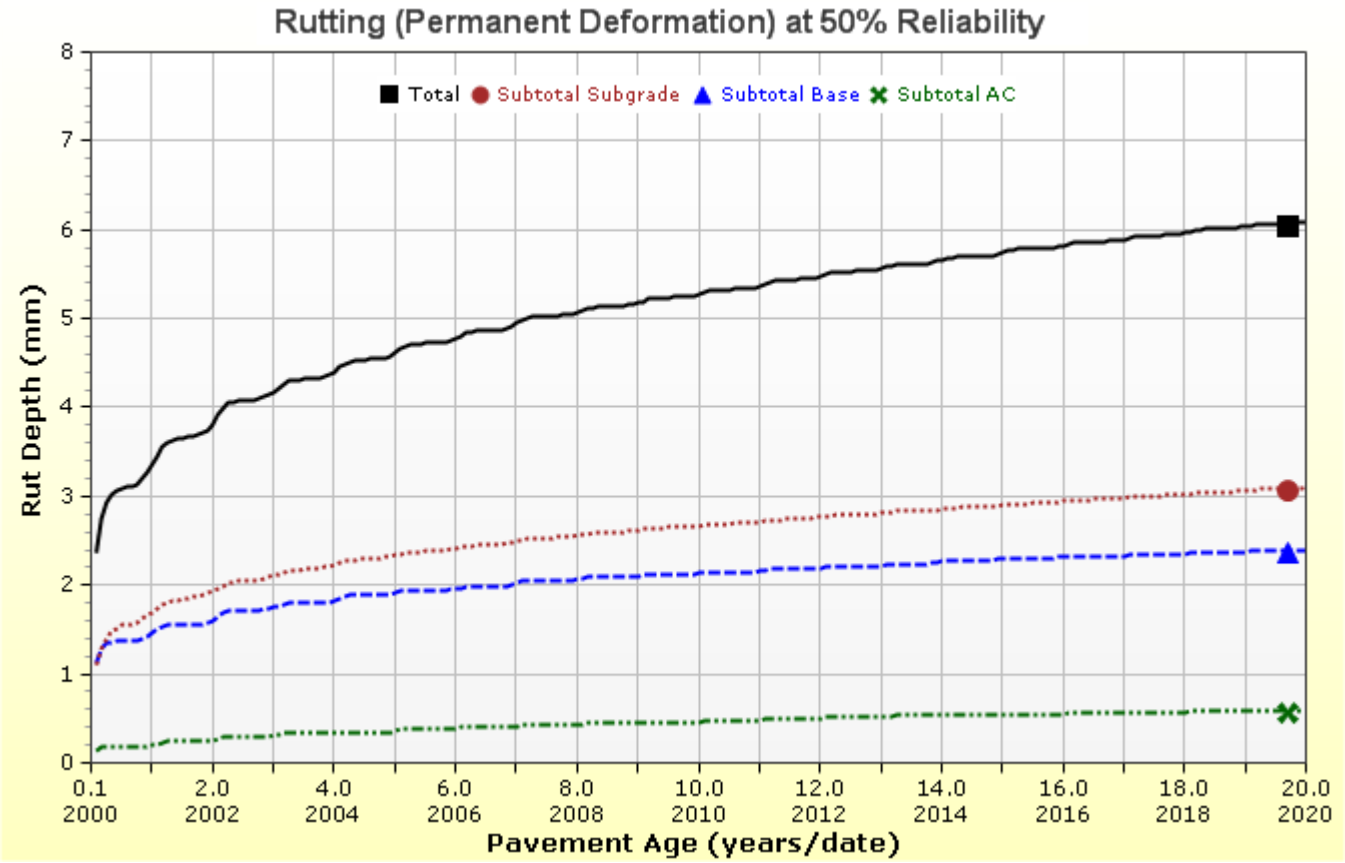
Rutting (Permanent Deformation) at 50% Reliability
Total
Subtotal Subgrade
Subtotal Base
Subtotal AC
Rut Depth (mm)
0
1
2
3
4
5
6
7
8
0.1
2000
2.0
2002
4.0
2004
6.0
2006
8.0
2008
10.0
2010
12.0
2012
14.0
2014
16.0
2016
18.0
2018
20.0
2020
Pavement Age (years/date)

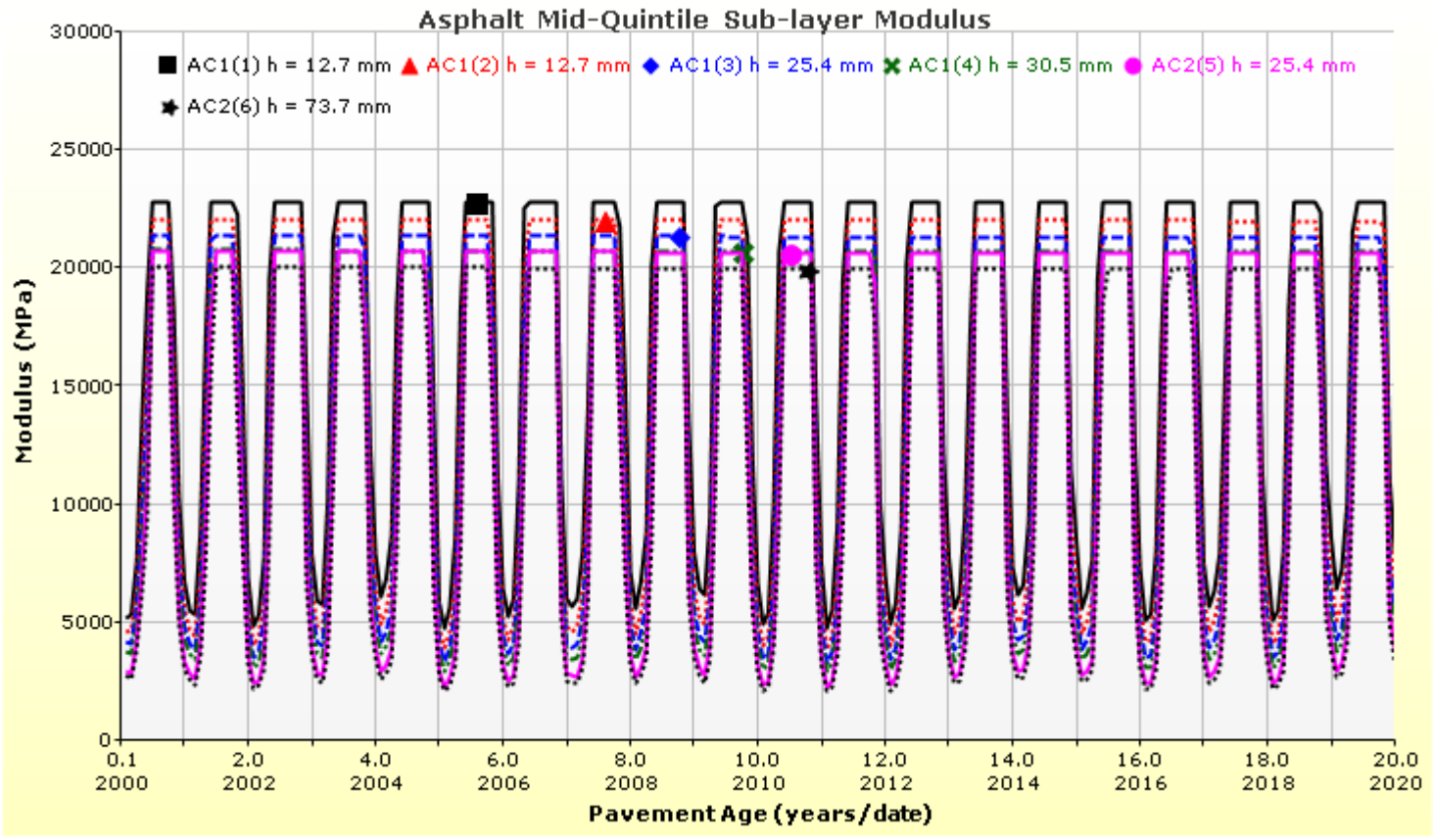
Asphalt Mid-Quintile Sub-layer Modulus
AC1(1) h = 12.7 mm
AC1(2) h = 12.7 mm
AC1(3) h = 25.4 mm
AC1(4) h = 30.5 mm
AC2(5) h = 25.4 mm
AC2(6) h = 73.7 mm
Modulus (MPa)
30000
25000
20000
15000
10000
5000
0
0.1
2000
2.0
2002
4.0
2004
6.0
2006
8.0
2008
10.0
2010
12.0
2012
14.0
2014
16.0
2016
18.0
2018
20.0
2020
Pavement Age (years/date)

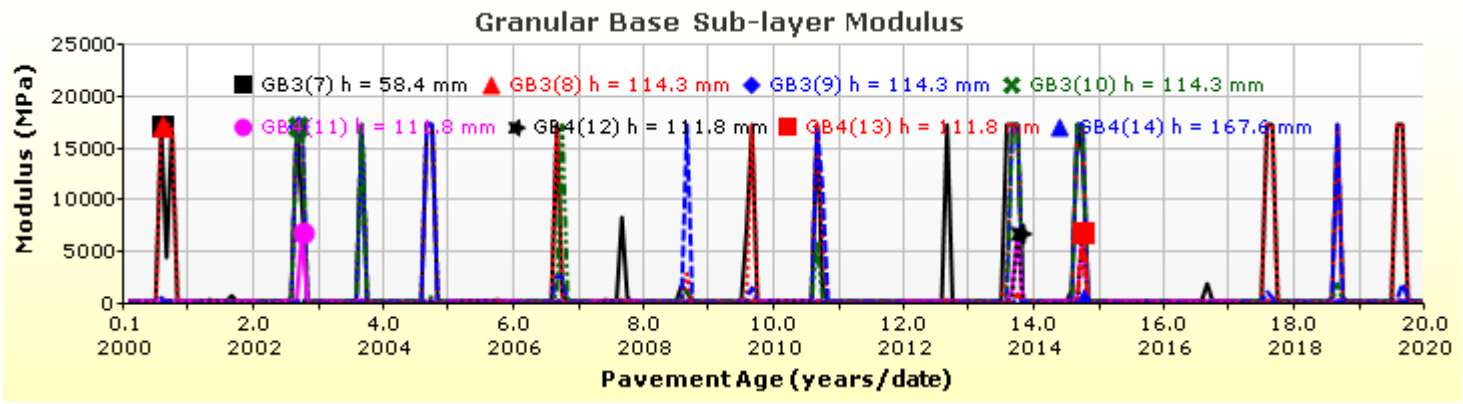
Granular Base Sub-layer Modulus
GB3(7) h = 58.4 mm
GB3(8) h = 114.3 mm
GB3(9) h = 114.3 mm
GB3(10) h = 114.3 mm
GB4(11) h = 111.8 mm
GB4(12) h = 111.8 mm
GB4(13) h = 111.8 mm
GB4(14) h = 167.6 mm
Modulus (MPa)
25000
20000
15000
10000
5000
0
0.1
2000
2.0
2002
4.0
2004
6.0
2006
8.0
2008
10.0
2010
12.0
2012
14.0
2014
16.0
2016
18.0
2018
20.0
2020
Pavement Age (years/date)

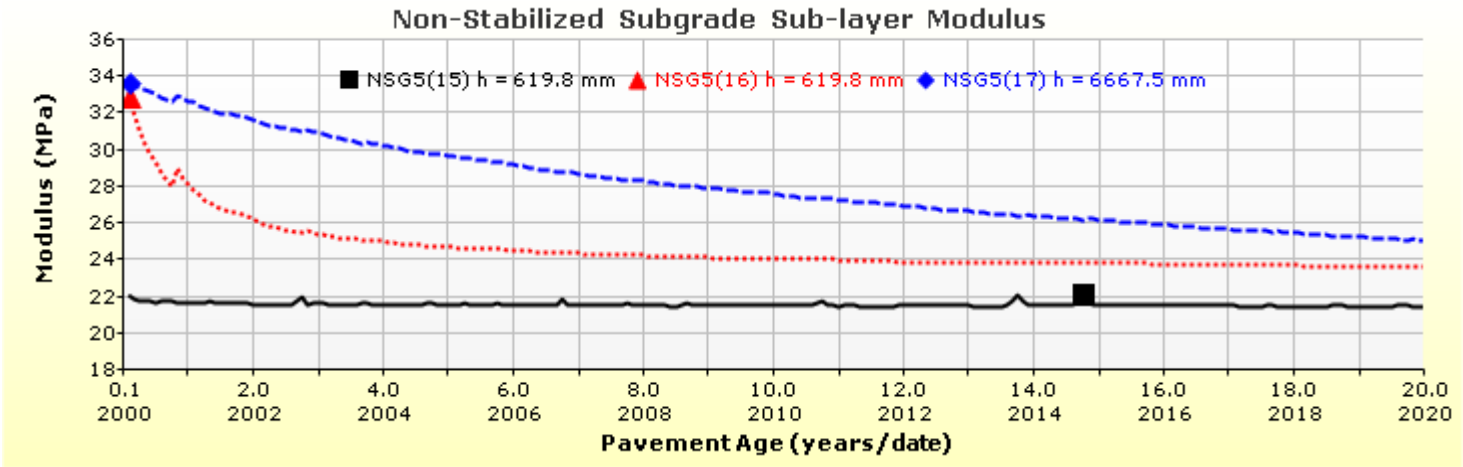
Non-Stabilized Subgrade Sub-layer Modulus
NSG5(15) h = 619.8 mm
NSG5(16) h = 619.8 mm
NSG5(17) h = 6667.5 mm
Modulus (MPa)
36
34
32
30
28
26
24
22
20
18
0.1
2000
2.0
2002
4.0
2004
6.0
2006
8.0
2008
10.0
2010
12.0
2012
14.0
2014
16.0
2016
18.0
2018
20.0
2020
Pavement Age (years/date)

Layer Information

Layer 1 Flexible : Default asphalt concrete

Asphalt		
Thickness (mm)	80.0	
Unit weight (kgf/m^3)	2390.0	
Poisson's ratio	Is Calculated?	False
	Ratio	0.35
	Parameter A	-
	Parameter B	-

Asphalt Dynamic Modulus (Input Level: 3)

Gradation	Percent Passing
19 mm sieve	100
9.5 mm sieve	77
4.75 mm sieve	60
0.075mm sieve	6

Asphalt Binder

Parameter	Value
Grade	Superpave Performance Grade
Binder Type	64-28
A	10.312
VTS	-3.44

General Info

Name	Value
Reference temperature (°C)	21.1
Effective binder content (%)	11.8
Air voids (%)	7
Thermal conductivity (watt/meter-kelvin)	1.16
Heat capacity (joule/kg-kelvin)	963

Identifiers

Field	Value
Display name/identifier	Default asphalt concrete
Description of object	
Author	
Date Created	9/16/2010 1:00:00 AM
Approver	
Date approved	9/16/2010 1:00:00 AM
State	
District	
County	
Highway	
Direction of Travel	
From station (km)	
To station (km)	
Province	
User defined field 1	
User defined field 2	
User defined field 3	
Revision Number	0

Layer 2 Flexible : Default asphalt concrete

Asphalt		
Thickness (mm)	100.0	
Unit weight (kgf/m^3)	2460.0	
Poisson's ratio	Is Calculated?	False
	Ratio	0.35
	Parameter A	-
	Parameter B	-

Asphalt Dynamic Modulus (Input Level: 3)

Gradation	Percent Passing
19 mm sieve	100
9.5 mm sieve	77
4.75 mm sieve	60
0.075mm sieve	6

Asphalt Binder

Parameter	Value
Grade	Superpave Performance Grade
Binder Type	58-28
A	11.01
VTS	-3.701

General Info

Name	Value
Reference temperature (ºC)	21.1
Effective binder content (%)	11.2
Air voids (%)	7
Thermal conductivity (watt/meter-kelvin)	1.16
Heat capacity (joule/kg-kelvin)	963

Identifiers

Field	Value
Display name/identifier	Default asphalt concrete
Description of object	
Author	
Date Created	9/16/2010 1:00:00 AM
Approver	
Date approved	9/16/2010 1:00:00 AM
State	
District	
County	
Highway	
Direction of Travel	
From station (km)	
To station (km)	
Province	
User defined field 1	
User defined field 2	
User defined field 3	
Revision Number	0

Layer 3 Non-stabilized Base : Crushed stone

Unbound	
Layer thickness (mm)	400.0
Poisson's ratio	0.35
Coefficient of lateral earth pressure (k0)	0.5

Modulus (Input Level: 3)

Analysis Type:	Modify input values by temperature/moisture
Method:	Resilient Modulus (MPa)

Resilient Modulus (MPa)
250.0

Use Correction factor for NDT modulus?	-
NDT Correction Factor:	-

Identifiers

Field	Value
Display name/identifier	Crushed stone
Description of object	Default material
Author	AASHTO
Date Created	1/1/2011 12:00:00 AM
Approver	
Date approved	1/1/2011 12:00:00 AM
State	
District	
County	
Highway	
Direction of Travel	
From station (km)	
To station (km)	
Province	
User defined field 1	
User defined field 2	
User defined field 3	
Revision Number	0

Sieve

Liquid Limit	6.0
Plasticity Index	0.0
Is layer compacted?	False

	Is User Defined?	Value
Maximum dry unit weight (kgf/m^3)	False	2048.3
Saturated hydraulic conductivity (m/hr)	False	2.376e-02
Specific gravity of solids	False	2.7
Water Content (%)	False	5.7

User-defined Soil Water Characteristic Curve (SWCC)	
Is User Defined?	False
af	3.0430
bf	2.5796
cf	0.7550
hr	100.0000

Sieve Size	% Passing
0.001mm	
0.002mm	
0.020mm	
0.075mm	5.0
0.150mm	
0.180mm	
0.250mm	
0.300mm	13.5
0.425mm	
0.600mm	
0.850mm	
1.18mm	27.5
2.0mm	
2.36mm	
4.75mm	45.0
9.5mm	61.5
12.5mm	
19.0mm	92.5
25.0mm	100.0
37.5mm	
50.0mm	
63.0mm	
75.0mm	
90.0mm	

Layer 4 Non-stabilized Base : Crushed gravel

Unbound	
Layer thickness (mm)	500.0
Poisson's ratio	0.35
Coefficient of lateral earth pressure (k0)	0.5

Modulus (Input Level: 3)

Analysis Type:	Modify input values by temperature/moisture
Method:	Resilient Modulus (MPa)

Resilient Modulus (MPa)
150.0

Use Correction factor for NDT modulus?	-
NDT Correction Factor:	-

Identifiers

Field	Value
Display name/identifier	Crushed gravel
Description of object	Default material
Author	AASHTO
Date Created	1/1/2011 12:00:00 AM
Approver	
Date approved	1/1/2011 12:00:00 AM
State	
District	
County	
Highway	
Direction of Travel	
From station (km)	
To station (km)	
Province	
User defined field 1	
User defined field 2	
User defined field 3	
Revision Number	0

Sieve

Liquid Limit	11.0
Plasticity Index	1.0
Is layer compacted?	False

	Is User Defined?	Value
Maximum dry unit weight (kgf/m^3)	False	2012.4
Saturated hydraulic conductivity (m/hr)	False	6.883e-03
Specific gravity of solids	False	2.7
Water Content (%)	False	8.2

User-defined Soil Water Characteristic Curve (SWCC)	
Is User Defined?	False
af	5.0935
bf	2.5668
cf	0.8576
hr	108.0000

Sieve Size	% Passing
0.001mm	
0.002mm	
0.020mm	
0.075mm	4.0
0.150mm	
0.180mm	
0.250mm	
0.300mm	33.5
0.425mm	
0.600mm	
0.850mm	
1.18mm	55.0
2.0mm	
2.36mm	
4.75mm	60.0
9.5mm	
12.5mm	
19.0mm	
25.0mm	75.0
37.5mm	
50.0mm	
63.0mm	
75.0mm	
90.0mm	

Layer 5 Subgrade : A-6

Unbound	
Layer thickness (mm)	Semi-infinite
Poisson's ratio	0.35
Coefficient of lateral earth pressure (k0)	0.5

Modulus (Input Level: 3)

Analysis Type:	Modify input values by temperature/moisture
Method:	Resilient Modulus (MPa)

Resilient Modulus (MPa)
35.0

Use Correction factor for NDT modulus?	-
NDT Correction Factor:	-

Identifiers

Field	Value
Display name/identifier	A-6
Description of object	Default material
Author	AASHTO
Date Created	1/1/2011 12:00:00 AM
Approver	
Date approved	1/1/2011 12:00:00 AM
State	
District	
County	
Highway	
Direction of Travel	
From station (km)	
To station (km)	
Province	
User defined field 1	
User defined field 2	
User defined field 3	
Revision Number	0

Sieve

Liquid Limit	42.0
Plasticity Index	15.0
Is layer compacted?	False

	Is User Defined?	Value
Maximum dry unit weight (kgf/m^3)	False	1693.8
Saturated hydraulic conductivity (m/hr)	False	3.012e-06
Specific gravity of solids	False	2.7
Water Content (%)	False	18.2

User-defined Soil Water Characteristic Curve (SWCC)	
Is User Defined?	False
af	114.8407
bf	0.6389
cf	0.1739
hr	500.0000

Sieve Size	% Passing
0.001mm	
0.002mm	25.0
0.020mm	
0.075mm	82.0
0.150mm	
0.180mm	91.0
0.250mm	
0.300mm	
0.425mm	95.0
0.600mm	
0.850mm	
1.18mm	
2.0mm	98.0
2.36mm	
4.75mm	100.0
9.5mm	100.0
12.5mm	100.0
19.0mm	100.0
25.0mm	100.0
37.5mm	
50.0mm	
63.0mm	
75.0mm	
90.0mm	100.0

Calibration Coefficients

AC Fatigue

$$N_f = 0.00432 * C * \beta_{f1} k_1 \left(\frac{1}{\varepsilon_1}\right)^{k_2\beta_{f2}} \left(\frac{1}{E}\right)^{k_3\beta_{f3}}$$

$$C = 10^M$$

$$M = 4.84\left(\frac{V_b}{V_a + V_b} - 0.69\right)$$

k1: 3.75	
k2: 2.87	
k3: 1.46	
Bf1: (5.014 * Pow(hac,-3.416)) * 1 + 0	
Bf2: 1.38	
Bf3: 0.88	

AC Rutting

$$\frac{\varepsilon_p}{\varepsilon_r} = k_z \beta_{r1} 10^{k_1 T^{k_2 \beta_{r2}} N^{k_3 \beta_{r3}}}$$

$$k_z = (C_1 + C_2 * depth) * 0.328196^{depth}$$

$$C_1 = -0.1039 * H_\alpha^2 + 2.4868 * H_\alpha - 17.342$$

$$C_2 = 0.0172 * H_\alpha^2 - 1.7331 * H_\alpha + 27.428$$

Where:

$$H_{ac} = total\ AC\ thickness(in)$$

$\varepsilon_p = plastic\ strain\left({}^{in}/_{in}\right)$
$\varepsilon_r = resilient\ strain\left({}^{in}/_{in}\right)$
$T = layer\ temperature(^{\circ}F)$
$N = number\ of\ load\ repetitions$

AC Rutting Standard Deviation	0.24 * Pow(RUT,0.8026) + 0.001	
AC Layer 1	K1:-2.45 K2:3.01 K3:0.22	Br1:0.128 Br2:0.52 Br3:1.36
AC Layer 2	K1:-2.45 K2:3.01 K3:0.22	Br1:0.4 Br2:0.52 Br3:1.36

Thermal Fracture

$$C_f = 400 * N\left(\frac{\log C / h_{ac}}{\sigma}\right)$$

$$\Delta C = (k * \beta t)^{n+1} * A * \Delta K^n$$

$$A = 10^{(4.389 - 2.52 * \log(E * \sigma_m * n))}$$

$C_f = observed\ amount\ of\ thermal\ cracking(ft/500ft)$
$k = refression\ coefficient\ determined\ through\ field\ calibration$
$N(\,) = standard\ normal\ distribution\ evaluated\ at(\,)$
$\sigma = standard\ deviation\ of\ the \log\ of\ the\ depth\ of\ cracks\ in\ the\ pavments$
$C = crack\ depth(in)$
$h_{ac} = thickness\ of\ asphalt\ layer(in)$
$\Delta C = Change\ in\ the\ crack\ depth\ due\ to\ a\ cooling\ cycle$
$\Delta K = Change\ in\ the\ stress\ intensity\ factor\ due\ to\ a\ cooling\ cycle$
$A, n = Fracture\ parameters\ for\ the\ asphalt\ mixture$
$E = mixture\ stiffness$
$\sigma_M = Undamaged\ mixture\ tensile\ strength$
$\beta_t = Calibration\ parameter$

Level 1 K: ((3 * Pow(10,-7)) * Pow(MAAT,4.0319)) * 1 + 0	Level 1 Standard Deviation: 0.14 * THERMAL + 168
Level 2 K: ((3 * Pow(10,-7)) * Pow(MAAT,4.0319)) * 1 + 0	Level 2 Standard Deviation: 0.20 * THERMAL + 168
Level 3 K: ((3 * Pow(10,-7)) * Pow(MAAT,4.0319)) * 1 + 0	Level 3 Standard Deviation: 0.289 * THERMAL + 168

CSM Fatigue

$$N_f = 10^{\left(\frac{k_1 \beta_{c1} \left(\frac{\sigma_s}{M_r}\right)}{k_2 \beta_{c2}}\right)}$$

$N_f = number\ of\ repetitions\ to\ fatigue\ cracking$
$\sigma_s = Tensile\ stress(psi)$
$M_r = modulus\ of\ rupture(psi)$

k1: 0.972	k2: 0.0825	Bc1: 1	Bc2:1

Unbound Layer Rutting

$$\delta_a(N) = \beta_{s_1} k_1 \varepsilon_v h \left(\frac{\varepsilon_0}{\varepsilon_r}\right) \left| e^{-\left(\frac{\rho}{N}\right)^{\beta}} \right|$$

$\delta_a = permanent\ deformation\ for\ the\ layer$
$N = number\ of\ repetitions$
$\varepsilon_v = average\ veritcal\ strain(in/in)$
$\varepsilon_0, \beta, \rho = material\ properties$
$\varepsilon_r = resilient\ strain(in/in)$

Base Rutting		Subgrade Rutting	
k1: 0.965	Bs1: 1	k1: 0.675	Bs1: 1
Standard Deviation (BASERUT) 0.1477 * Pow(BASERUT,0.6711) + 0.001		Standard Deviation (BASERUT) 0.1235 * Pow(SUBRUT,0.5012) + 0.001	

AC Cracking

AC Top Down Cracking

$$FC_{top} = \left(\frac{C_4}{1 + e^{(C_1 - C_2 * log_{10}(Damage))}}\right) * 10.56$$

c1: 7	c2: 3.5	c3: 0	c4: 1000

Top down AC Cracking Standard Deviation
200 + 2300/(1+exp(1.072-2.1654*LOG10(TOP+0.0001)))

AC Bottom Up Cracking

$$FC = \left(\frac{6000}{1 + e^{\left(C_1 * C_1' + C_2 * C_2' log_{10}(D * 100)\right)}}\right) * \left(\frac{1}{60}\right)$$

$$C_2' = -2.40874 - 39.748 * (1 + h_{ac})^{-2.856}$$

$$C_1' = -2 * C_2'$$

c1: 1.31	c2: (0.867 + 0.2583 * hac) * 1 + 0	c3: 6000

Bottom up AC Cracking Standard Deviation
1.13 + 13/(1+exp(7.57-15.5*LOG10(BOTTOM+0.0001)))

CSM Cracking

$$FC_{ctb} = C_1 + \frac{C_2}{1 + e^{C_3 - C_4 * log_{10}(Damage)}}$$

C1: 0	C2: 75	C3: 2	C4: 2

CSM Standard Deviation
CTB*1

IRI Flexible Pavements

C1 - Rutting
C2 - Fatigue Crack
C3 - Transverse Crack
C4 - Site Factors

C1: 55	C2: 0.4	C3: 0.008	C4: 0.015

Semi-Rigid Pavement_FDR+GU_ONTARIO

File Name: C:\Users\admin\Desktop\Eskedil_ME\Kossuth\Semi-Rigid Pavement_FDR+GU_ONTARIO.dgpx

Design Inputs

Design Life: 15 years
Design Type: SEMI_RIGID

Base construction: May, 2020
Pavement construction: June, 2020
Traffic opening: June, 2020

Climate Data Sources (Lat/Lon): 43.5, -80.625; 43, -80

Design Structure

Layer type	Material Type	Thickness(mm)
Flexible	Default asphalt concrete	40.0
Cement_Base	Soil cement	300.0
NonStabilized	Crushed stone	280.0
NonStabilized	Crushed gravel	500.0
Subgrade	A-6	Semi-infinite

Volumetric at Construction:	
Effective binder content (%)	11.8
Air voids (%)	7.0

Traffic

Age (year)	Heavy Trucks (cumulative)
2020 (initial)	1,272
2027 (7 years)	1,721,680
2035 (15 years)	3,794,600

Design Outputs

Distress Prediction Summary

Distress Type	Distress @ Specified Reliability		Reliability (%)		Criterion Satisfied?
	Target	Predicted	Target	Achieved	
Terminal IRI (m/km)	2.30	2.04	85.00	94.80	Pass
Permanent deformation - total pavement (mm)	13.00	5.50	85.00	100.00	Pass
AC total fatigue cracking: bottom up + reflective (% lane area)	50.00	1.98	85.00	100.00	Pass
AC total transverse cracking: thermal + reflective (m/km)	473.40	340.46	85.00	99.25	Pass
AC bottom-up fatigue cracking (percent)	20.00	0.00	50.00	100.00	Pass
AC thermal cracking (m/km)	190.00	0.19	50.00	100.00	Pass
AC top-down fatigue cracking (m/km)	380.00	39.32	85.00	100.00	Pass
Permanent deformation - AC only (mm)	6.00	0.42	85.00	100.00	Pass
Chemically stabilized layer - fatigue fracture (percent)	25.00	1.54	-	-	-

Distress Charts

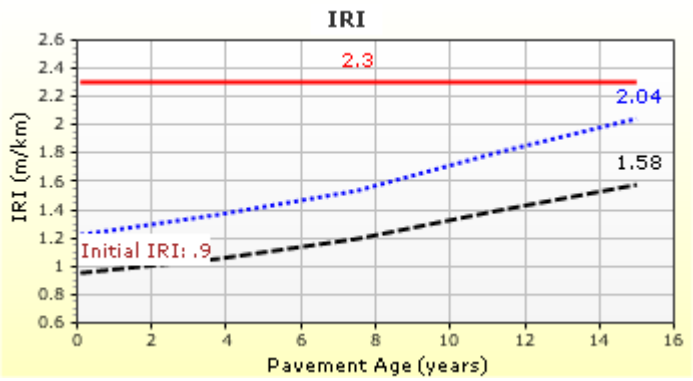

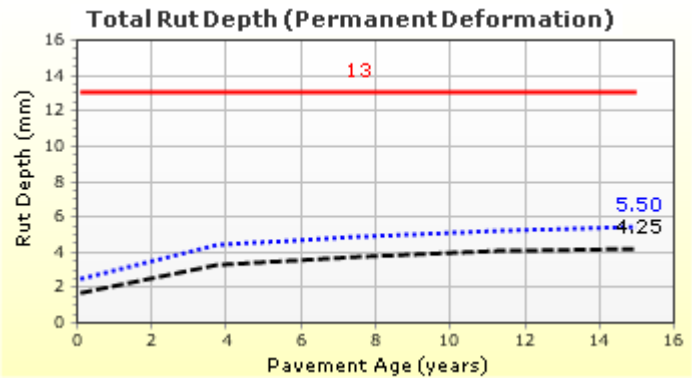

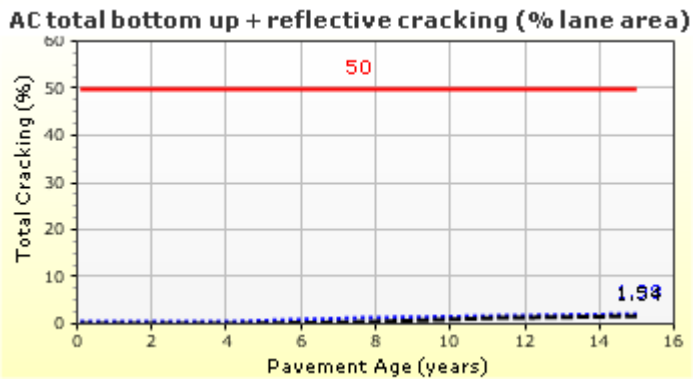

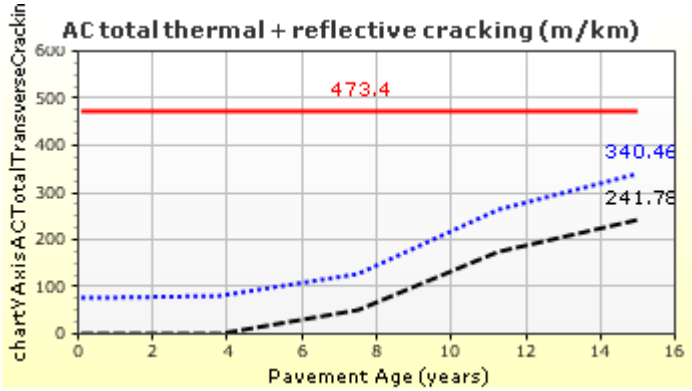

Traffic Inputs

Graphical Representation of Traffic Inputs

Initial two-way AADTT:	1,272	Percent of trucks in design direction (%):	50.0
Number of lanes in design direction:	2	Percent of trucks in design lane (%):	90.0
		Operational speed (kph)	100.0

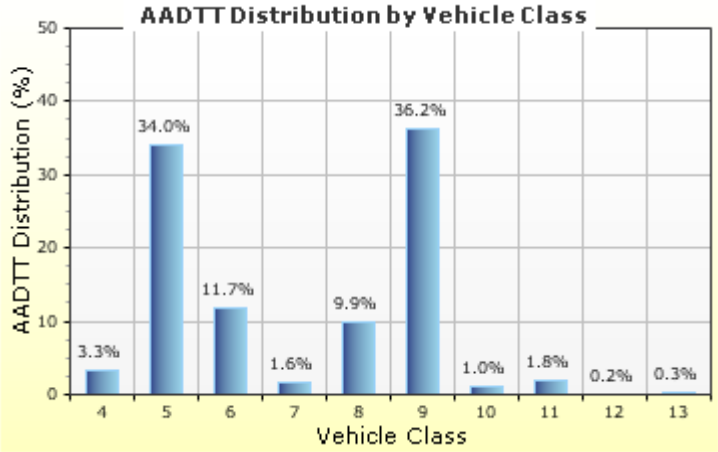

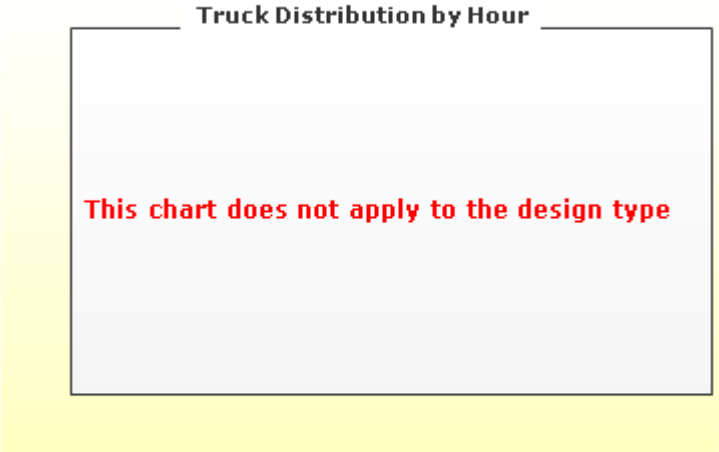

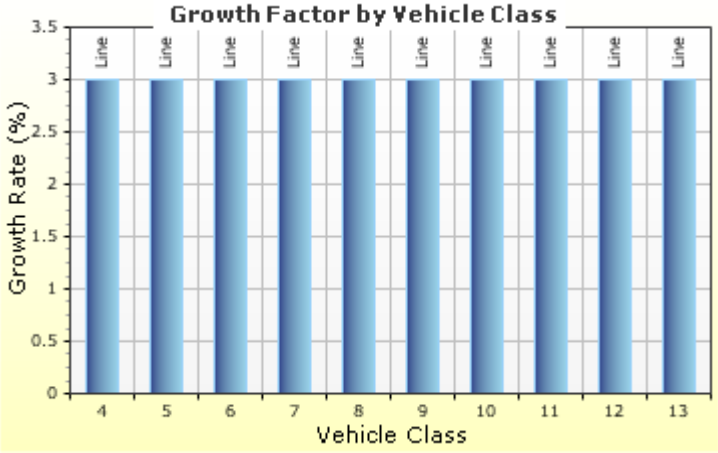

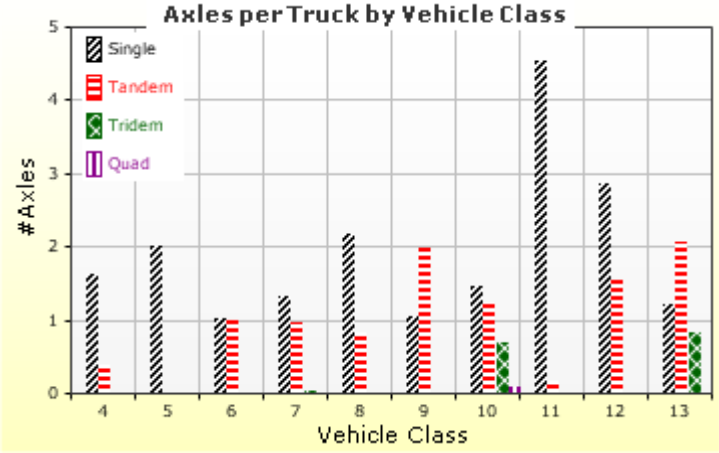

Traffic Volume Monthly Adjustment Factors

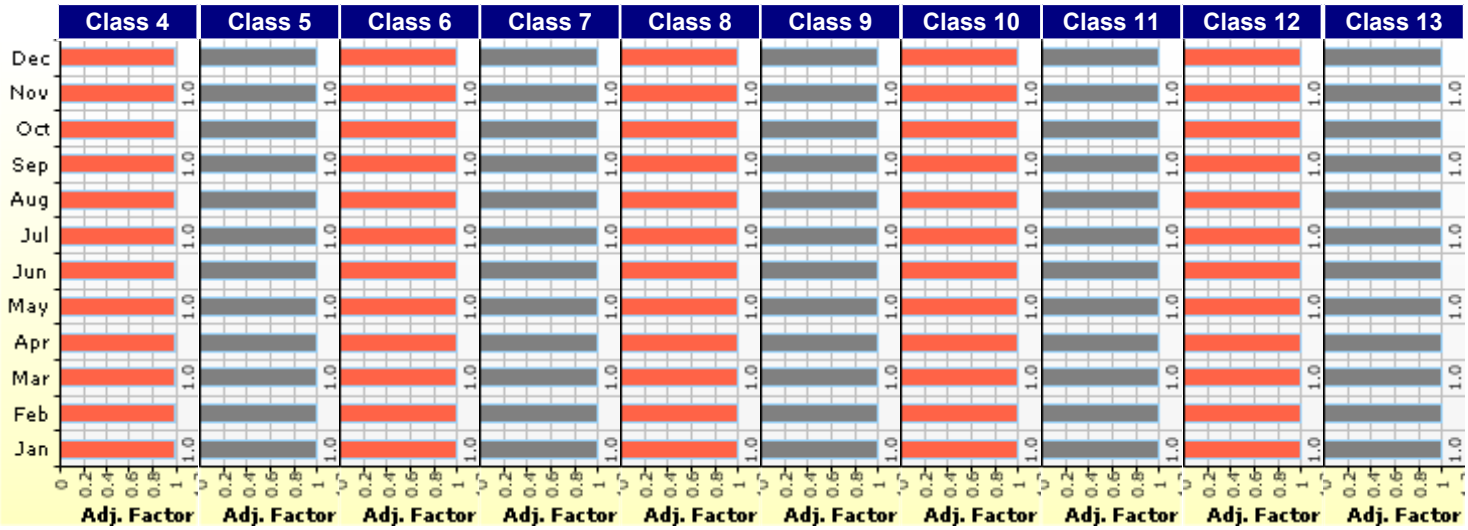

Tabular Representation of Traffic Inputs

Volume Monthly Adjustment Factors

Level 3: Default MAF

Month	Vehicle Class									
	4	5	6	7	8	9	10	11	12	13
January	1.0	1.0	1.0	1.0	1.0	1.0	1.0	1.0	1.0	1.0
February	1.0	1.0	1.0	1.0	1.0	1.0	1.0	1.0	1.0	1.0
March	1.0	1.0	1.0	1.0	1.0	1.0	1.0	1.0	1.0	1.0
April	1.0	1.0	1.0	1.0	1.0	1.0	1.0	1.0	1.0	1.0
May	1.0	1.0	1.0	1.0	1.0	1.0	1.0	1.0	1.0	1.0
June	1.0	1.0	1.0	1.0	1.0	1.0	1.0	1.0	1.0	1.0
July	1.0	1.0	1.0	1.0	1.0	1.0	1.0	1.0	1.0	1.0
August	1.0	1.0	1.0	1.0	1.0	1.0	1.0	1.0	1.0	1.0
September	1.0	1.0	1.0	1.0	1.0	1.0	1.0	1.0	1.0	1.0
October	1.0	1.0	1.0	1.0	1.0	1.0	1.0	1.0	1.0	1.0
November	1.0	1.0	1.0	1.0	1.0	1.0	1.0	1.0	1.0	1.0
December	1.0	1.0	1.0	1.0	1.0	1.0	1.0	1.0	1.0	1.0

Distributions by Vehicle Class

Truck Distribution by Hour does not apply

Vehicle Class	AADTT Distribution (%) (Level 3)	Growth Factor	
		Rate (%)	Function
Class 4	3.3%	3%	Linear
Class 5	34%	3%	Linear
Class 6	11.7%	3%	Linear
Class 7	1.6%	3%	Linear
Class 8	9.9%	3%	Linear
Class 9	36.2%	3%	Linear
Class 10	1%	3%	Linear
Class 11	1.8%	3%	Linear
Class 12	0.2%	3%	Linear
Class 13	0.3%	3%	Linear

Axle Configuration

Traffic Wander	
Mean wheel location (mm)	460.0
Traffic wander standard deviation (mm)	254.0
Design lane width (m)	3.7

Axle Configuration	
Average axle width (m)	2.6
Dual tire spacing (mm)	305.0
Tire pressure (kPa)	827.4

Average Axle Spacing	
Tandem axle spacing (m)	1.5
Tridem axle spacing (m)	1.7
Quad axle spacing (m)	1.3

Wheelbase does not apply

Number of Axles per Truck

Vehicle Class	Single Axle	Tandem Axle	Tridem Axle	Quad Axle
Class 4	1.62	0.39	0	0
Class 5	2	0	0	0
Class 6	1.01	0.993	0	0
Class 7	1.314	0.989	0.03	0
Class 8	2.163	0.845	0	0
Class 9	1.055	1.968	0.003	0
Class 10	1.446	1.234	0.7	0.088
Class 11	4.546	0.168	0	0
Class 12	2.857	1.526	0	0
Class 13	1.201	2.058	0.848	0.024

AADTT (Average Annual Daily Truck Traffic) Growth

*** Traffic cap is not enforced**

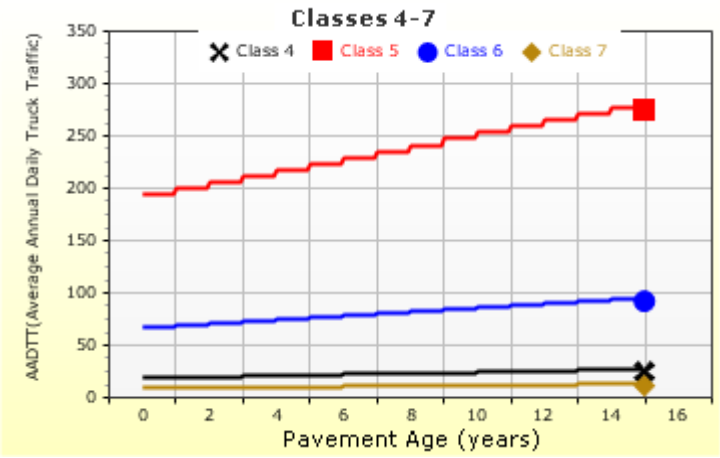

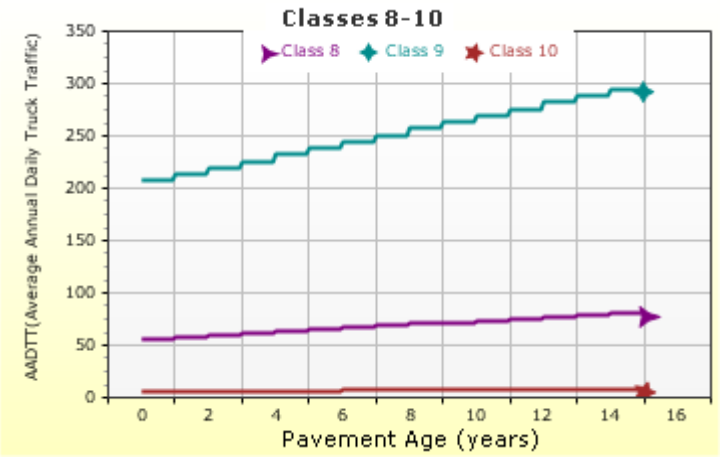

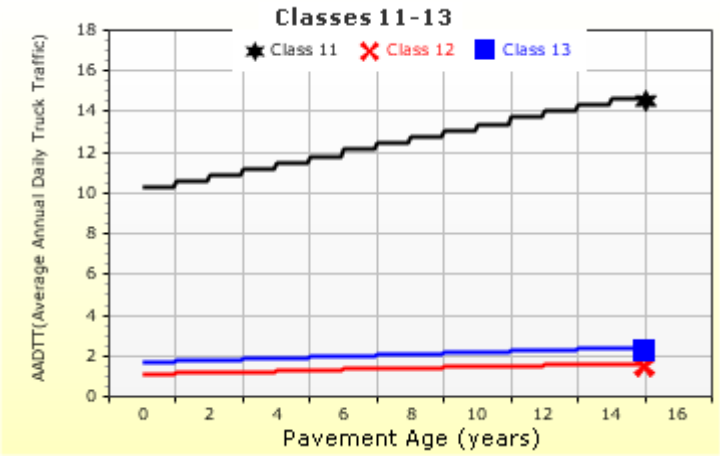

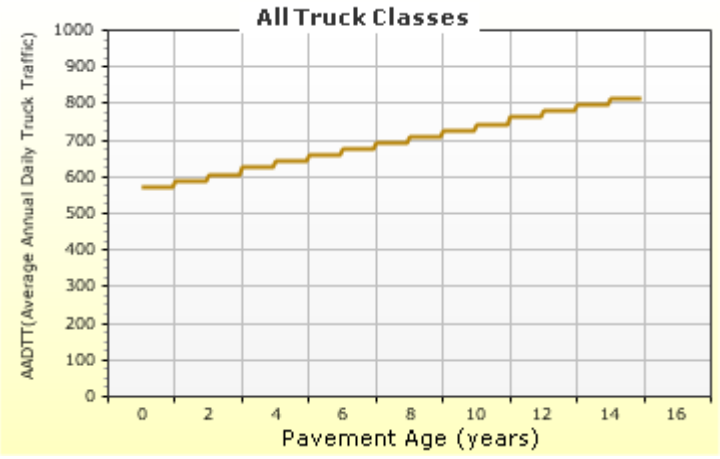

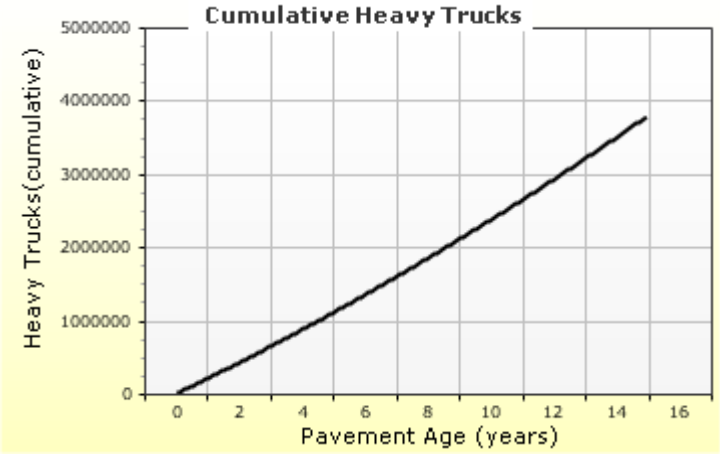

Climate Inputs

Climate Data Sources:

Climate Station Cities:	Location (lat lon elevation(m))
CA, ON	43.50000 -80.62500 369
CA, ON	43.00000 -80.00000 210

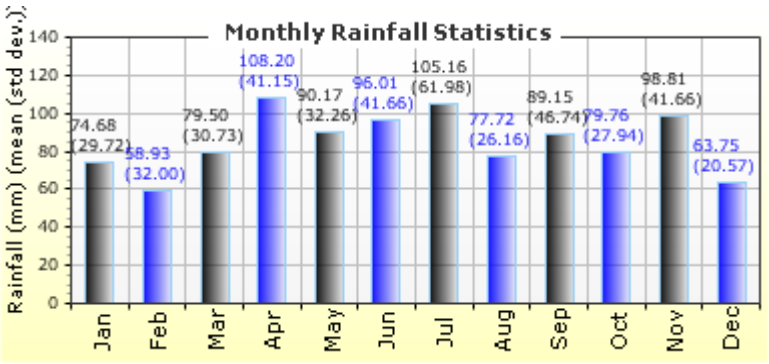

Annual Statistics:

Mean annual air temperature (°C)	7.96
Mean annual precipitation (mm)	1022.60
Freezing index (°C - days)	521.04
Average annual number of freeze/thaw cycles:	80.61

Water table depth (m)	10.00

Monthly Climate Summary:

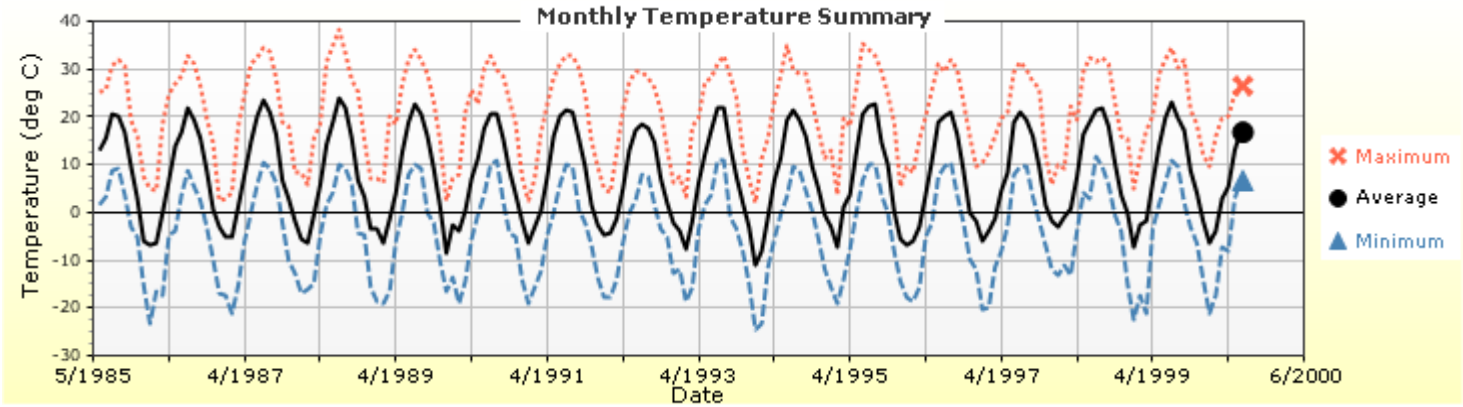

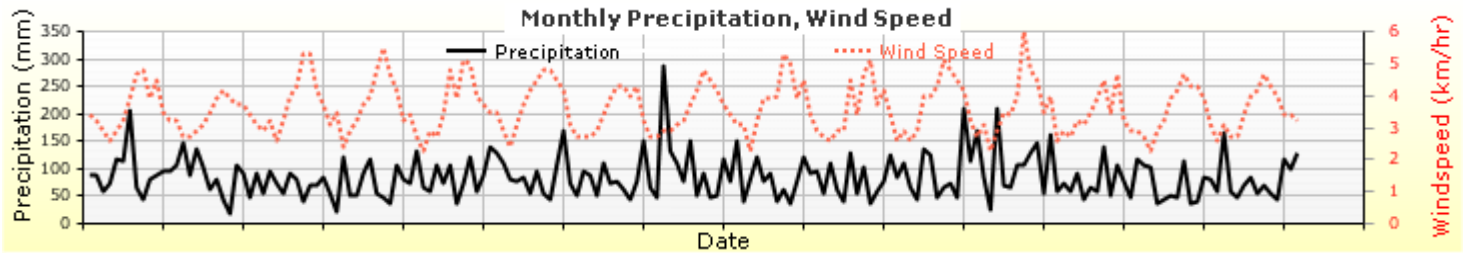

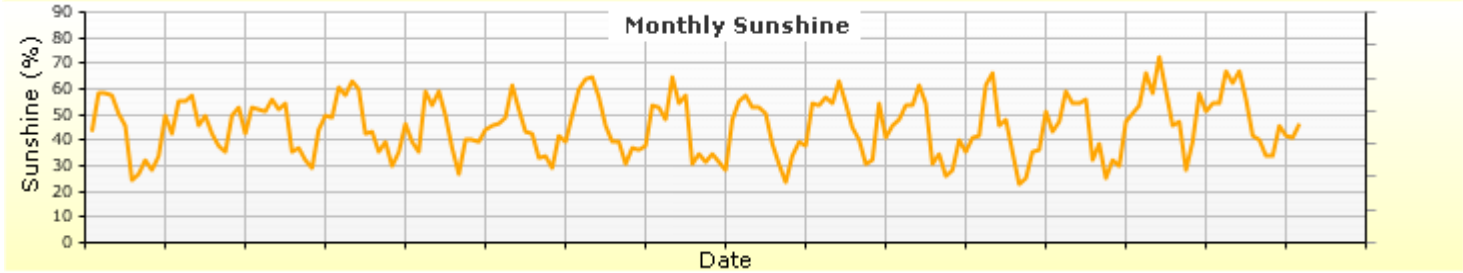

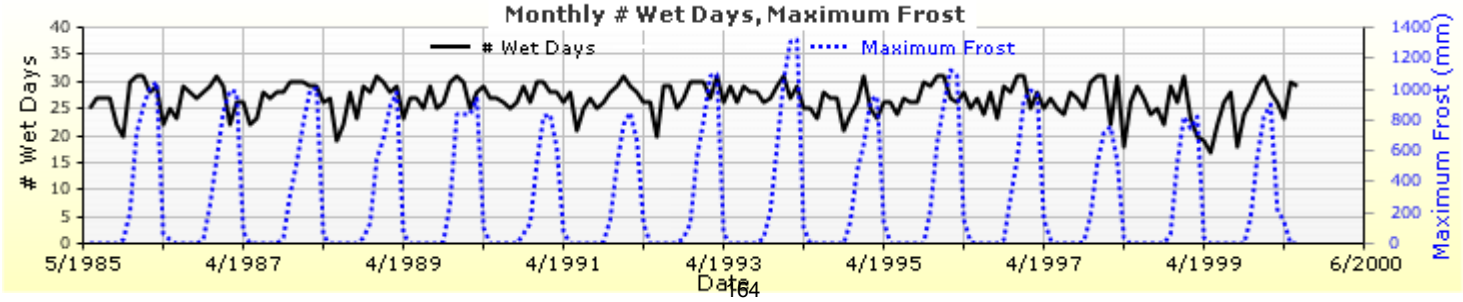

Hourly Air Temperature Distribution by Month:

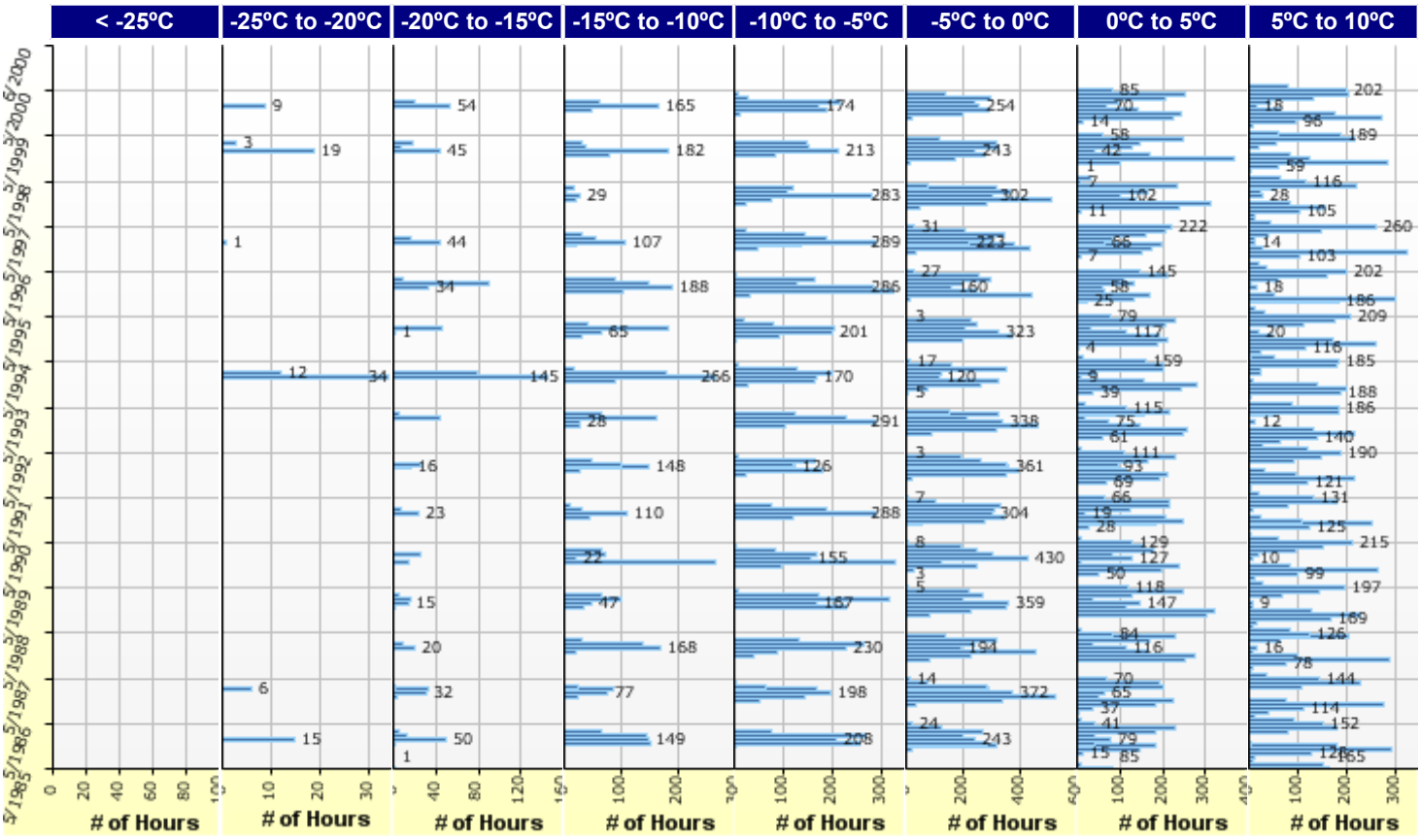

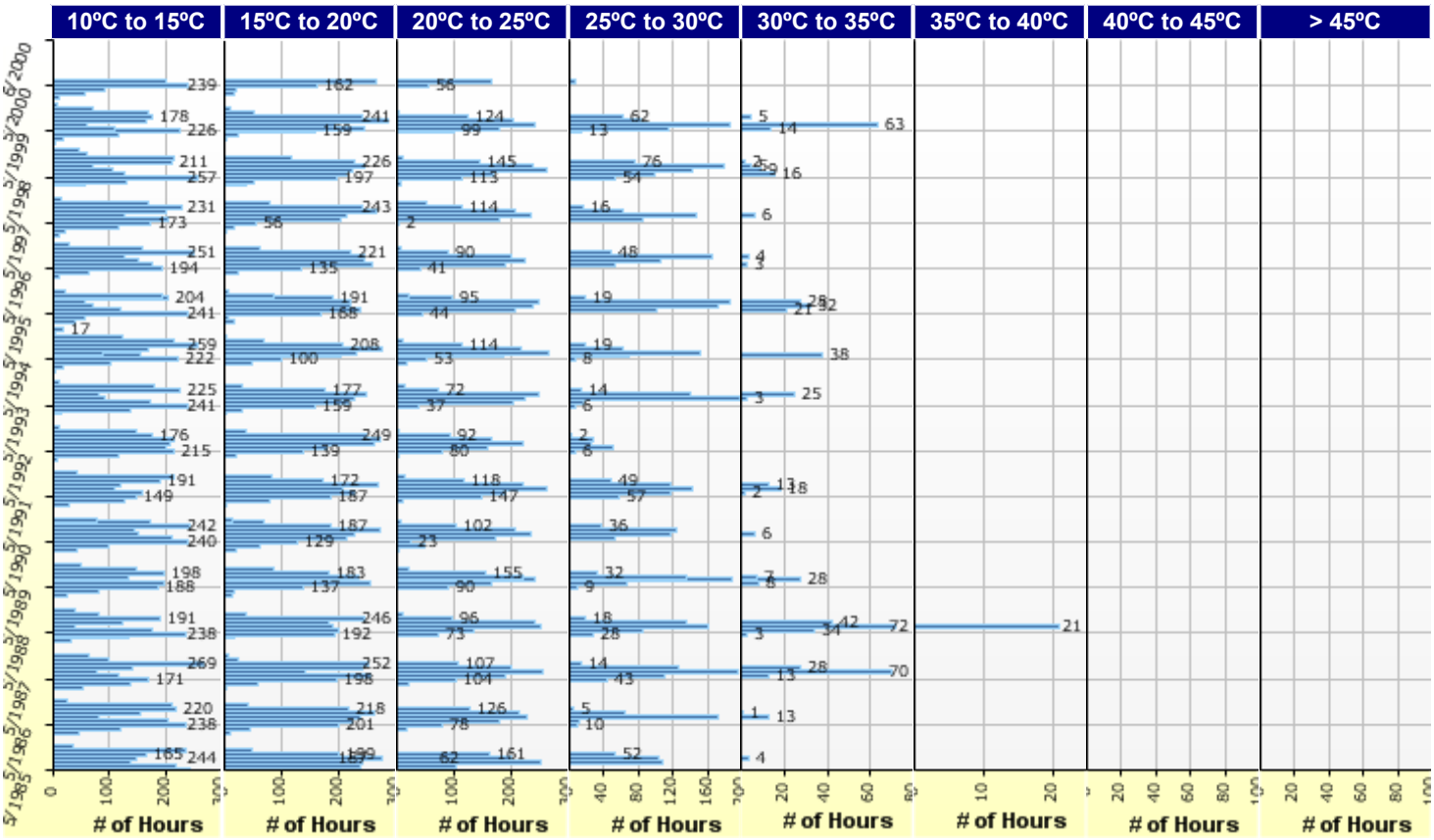

Design Properties

HMA Design Properties

Use Multilayer Rutting Model	False
Using G* based model (not nationally calibrated)	False
Is NCHRP 1-37A HMA Rutting Model Coefficients	True
Endurance Limit	-
Use Reflective Cracking	True

Structure - ICM Properties	
AC surface shortwave absorptivity	0.85

Layer Name	Layer Type	Interface Friction
Layer 1 Flexible : Default asphalt concrete	Flexible (1)	1.00
Layer 2 Chemically Stabilized : Soil cement	Chemically Stabilized (2)	1.00
Layer 3 Non-stabilized Base : Crushed stone	Non-stabilized Base (4)	1.00
Layer 4 Non-stabilized Base : Crushed gravel	Non-stabilized Base (4)	1.00
Layer 5 Subgrade : A-6	Subgrade (5)	-

Thermal Cracking

Thermal Contraction	
Is thermal contraction calculated?	True
Mix coefficient of thermal contraction (mm/mm/ºC)	-
Aggregate coefficient of thermal contraction (mm/mm/ºC)	9.0e-006
Voids in Mineral Aggregate (%)	18.8

Indirect Tensile Strength (Input Level: 3)	
Test Temperature (ºC)	**Indirect Tensilte Strength (Mpa)**
-10.0	2.79

Creep Compliance (1/GPa) (Input Level: 3)			
Loading time (sec)	**-20 ºC**	**-10 ºC**	**0 ºC**
1	5.57e-002	8.57e-002	1.16e-001
2	6.17e-002	1.01e-001	1.51e-001
5	7.07e-002	1.25e-001	2.15e-001
10	7.83e-002	1.48e-001	2.80e-001
20	8.68e-002	1.74e-001	3.65e-001
50	9.94e-002	2.16e-001	5.19e-001
100	1.10e-001	2.55e-001	6.77e-001

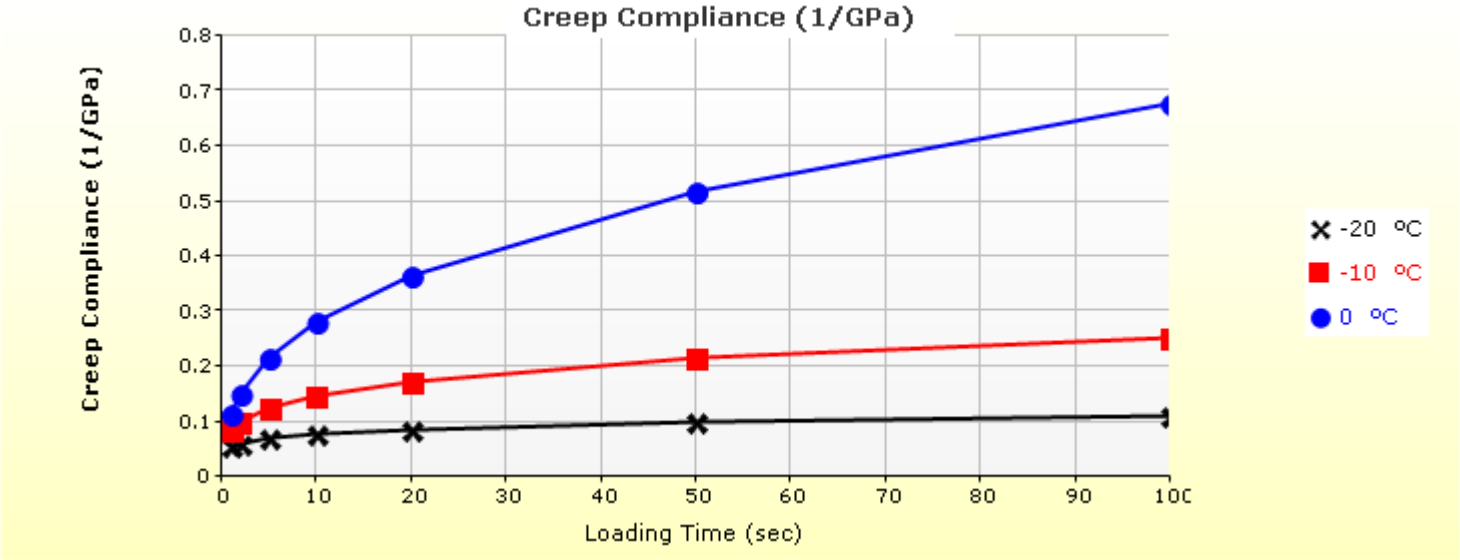

HMA Layer 1: Layer 1 Flexible : Default asphalt concrete

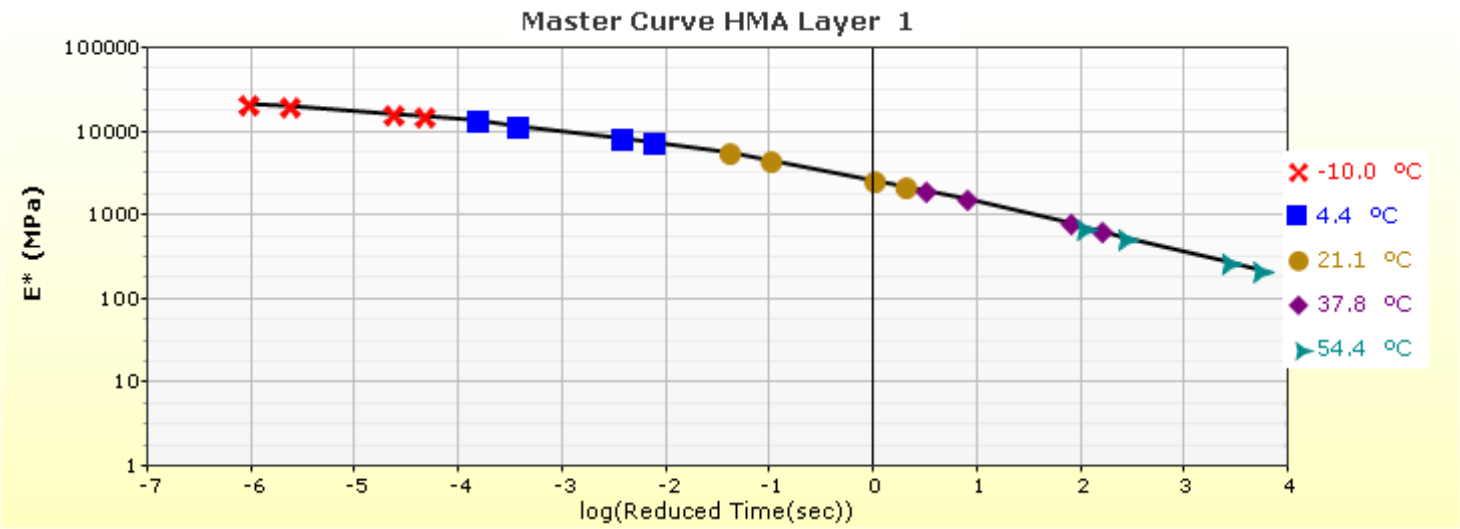

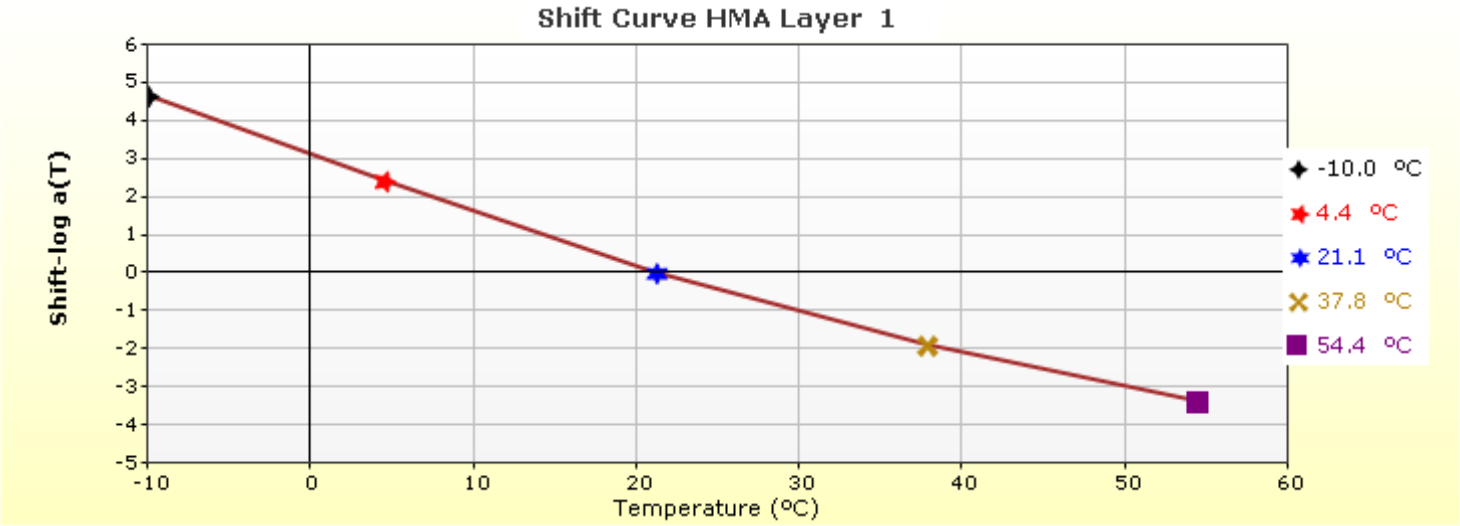

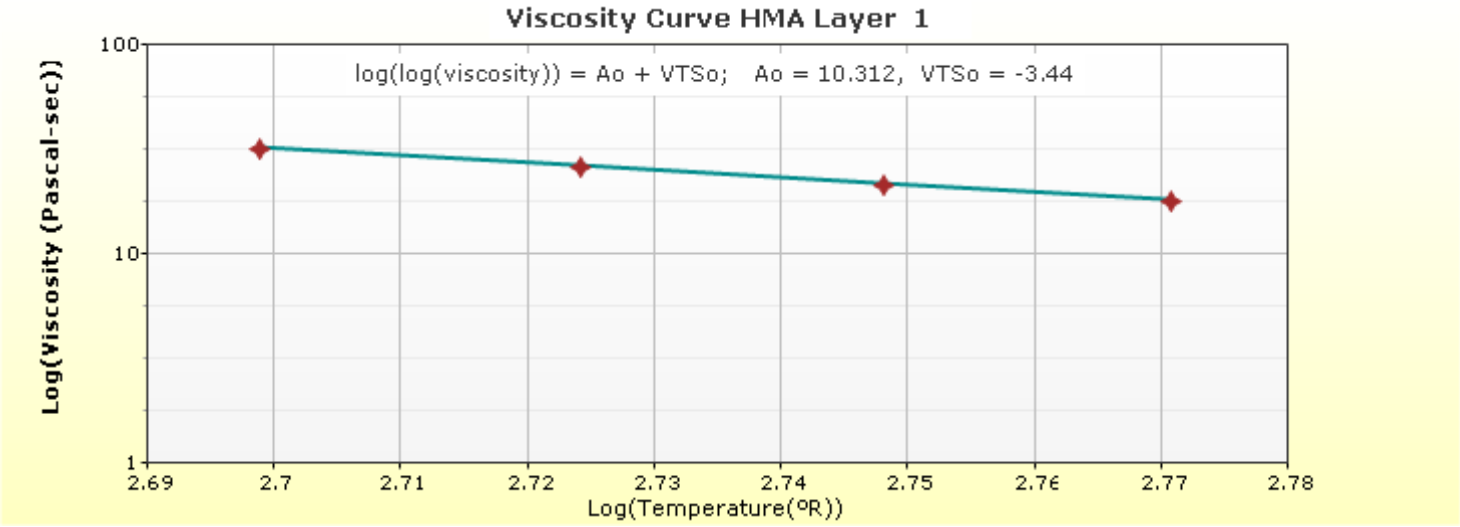

Analysis Output Charts

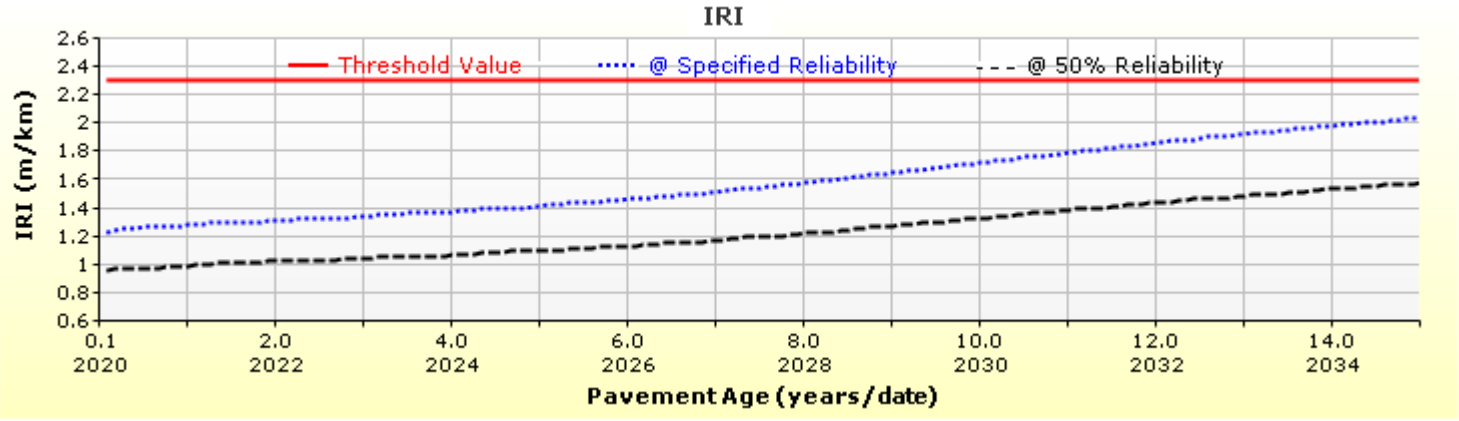

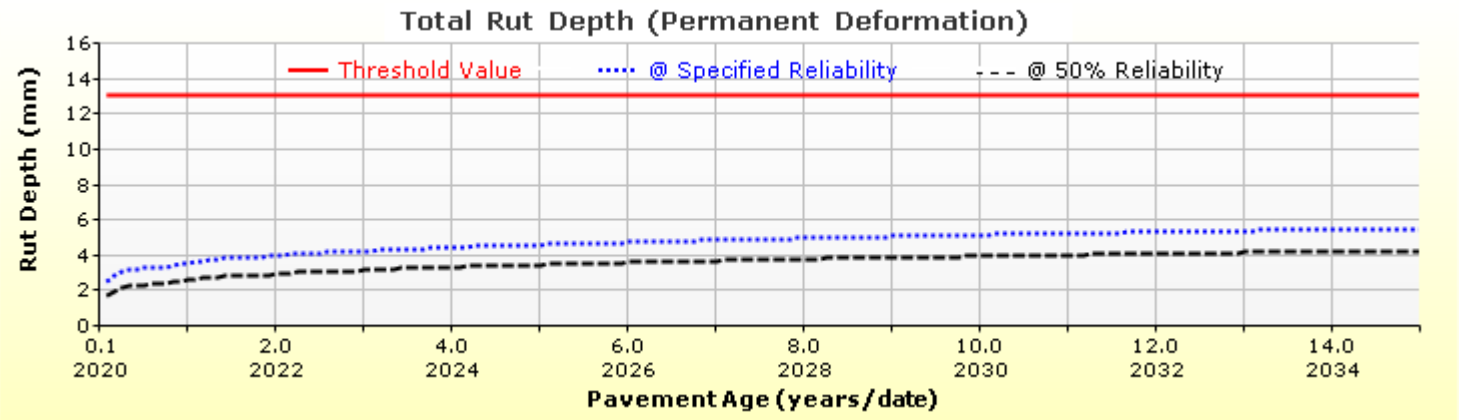

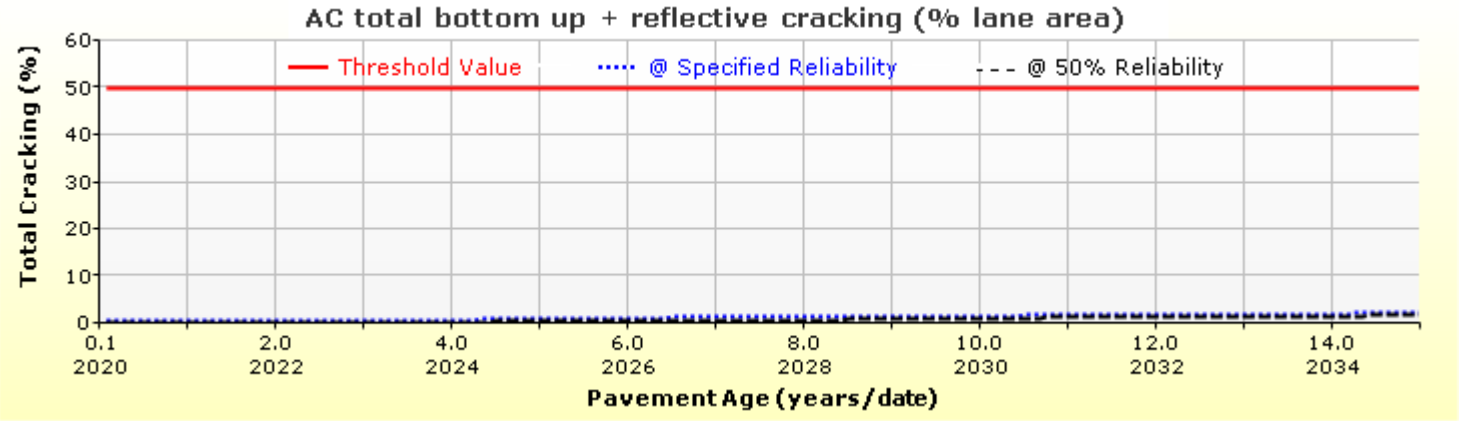

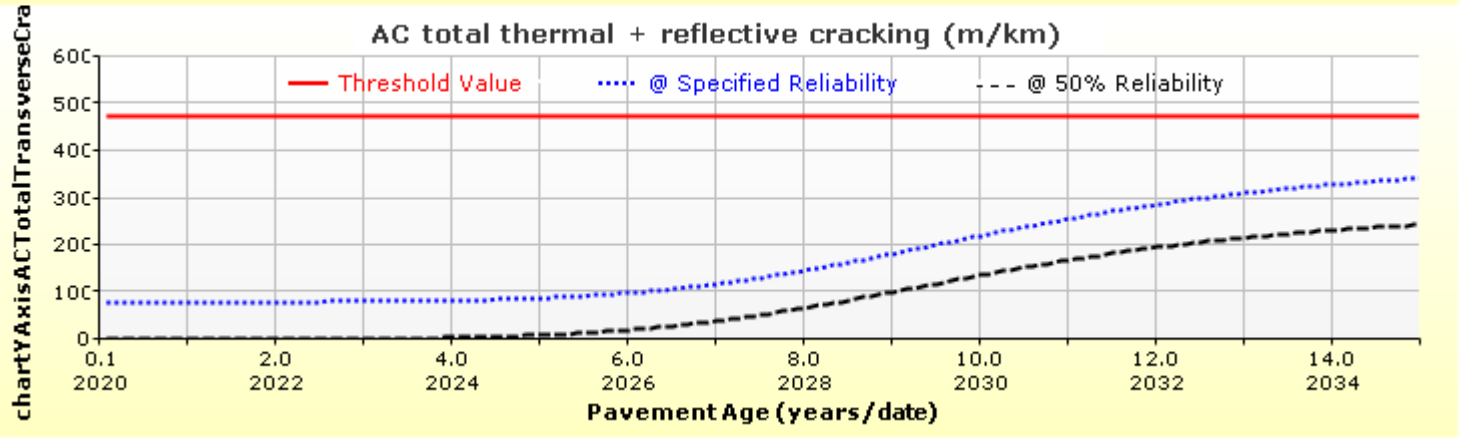

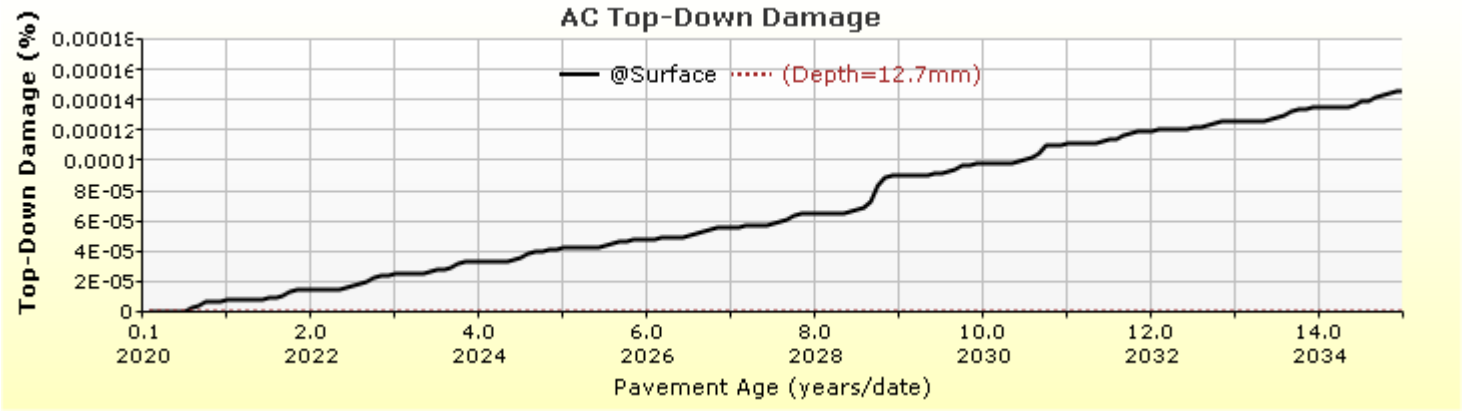
AC Top-Down Damage
Top-Down Damage (%)
@Surface
(Depth=12.7mm)
0.00018
0.00016
0.00014
0.00012
0.0001
8E-05
6E-05
4E-05
2E-05
0
0.1
2020
2.0
2022
4.0
2024
6.0
2026
8.0
2028
10.0
2030
12.0
2032
14.0
2034
Pavement Age (years/date)

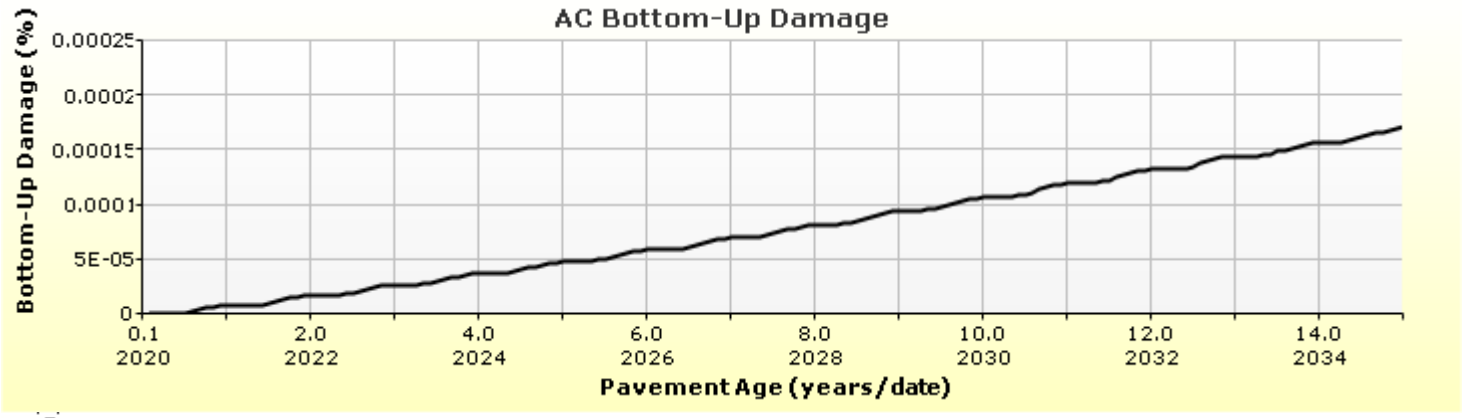
AC Bottom-Up Damage
Bottom-Up Damage (%)
0.00025
0.0002
0.00015
0.0001
5E-05
0
0.1
2020
2.0
2022
4.0
2024
6.0
2026
8.0
2028
10.0
2030
12.0
2032
14.0
2034
Pavement Age (years/date)

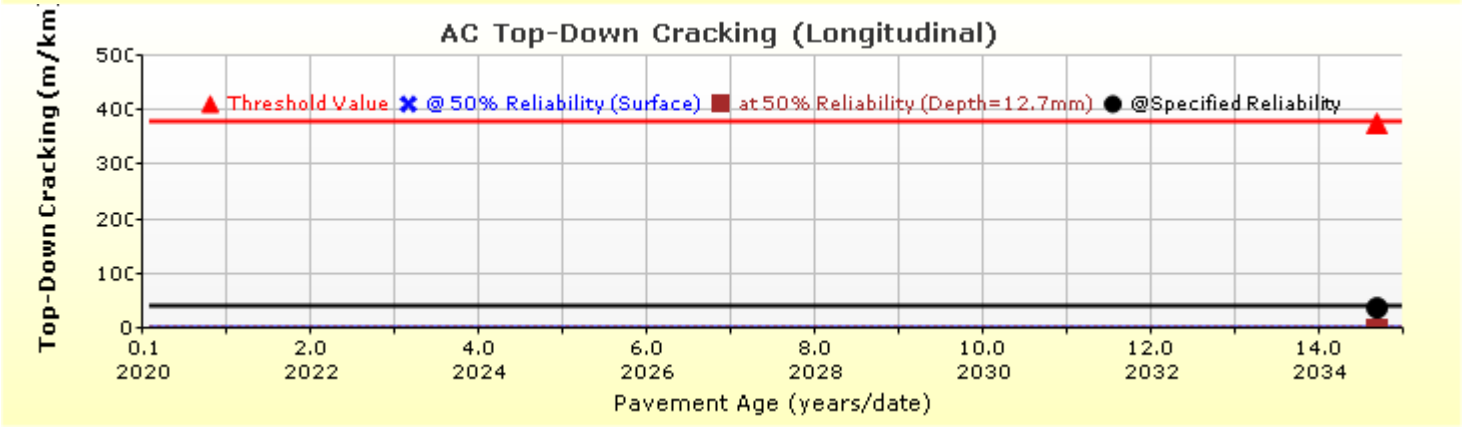
AC Top-Down Cracking (Longitudinal)
Top-Down Cracking (m/km)
Threshold Value
@ 50% Reliability (Surface)
at 50% Reliability (Depth=12.7mm)
@Specified Reliability
500
400
300
200
100
0
0.1
2020
2.0
2022
4.0
2024
6.0
2026
8.0
2028
10.0
2030
12.0
2032
14.0
2034
Pavement Age (years/date)

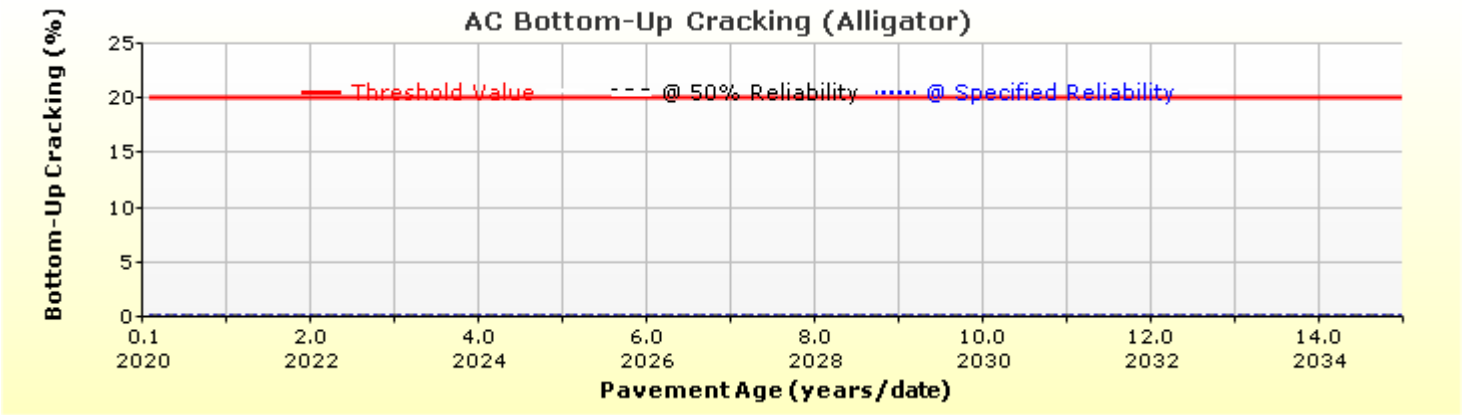
AC Bottom-Up Cracking (Alligator)
Bottom-Up Cracking (%)
Threshold Value
@ 50% Reliability
@ Specified Reliability
25
20
15
10
5
0
0.1
2020
2.0
2022
4.0
2024
6.0
2026
8.0
2028
10.0
2030
12.0
2032
14.0
2034
Pavement Age (years/date)

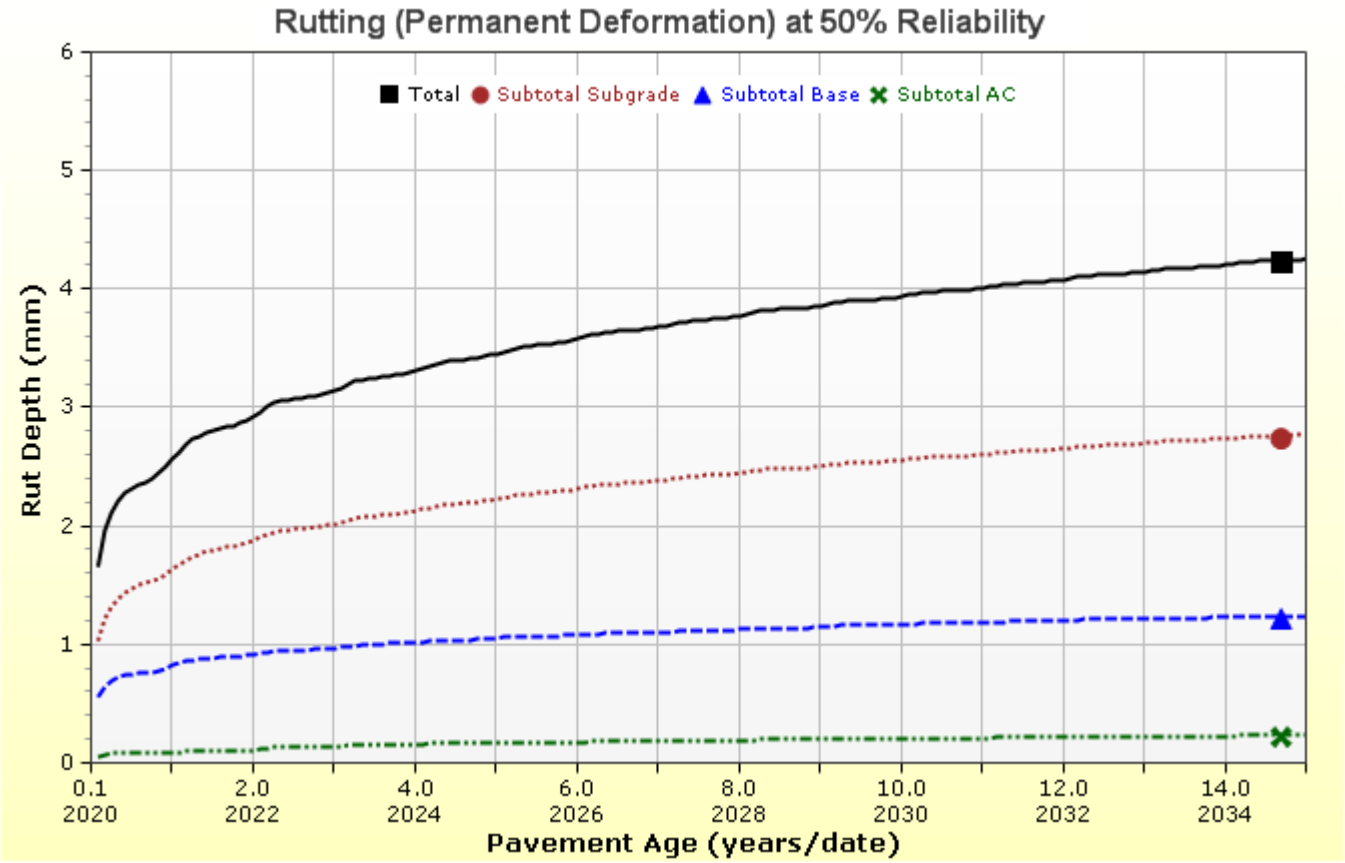
Rutting (Permanent Deformation) at 50% Reliability
Total
Subtotal Subgrade
Subtotal Base
Subtotal AC
Rut Depth (mm)
0
1
2
3
4
5
6
0.1
2020
2.0
2022
4.0
2024
6.0
2026
8.0
2028
10.0
2030
12.0
2032
14.0
2034
Pavement Age (years/date)

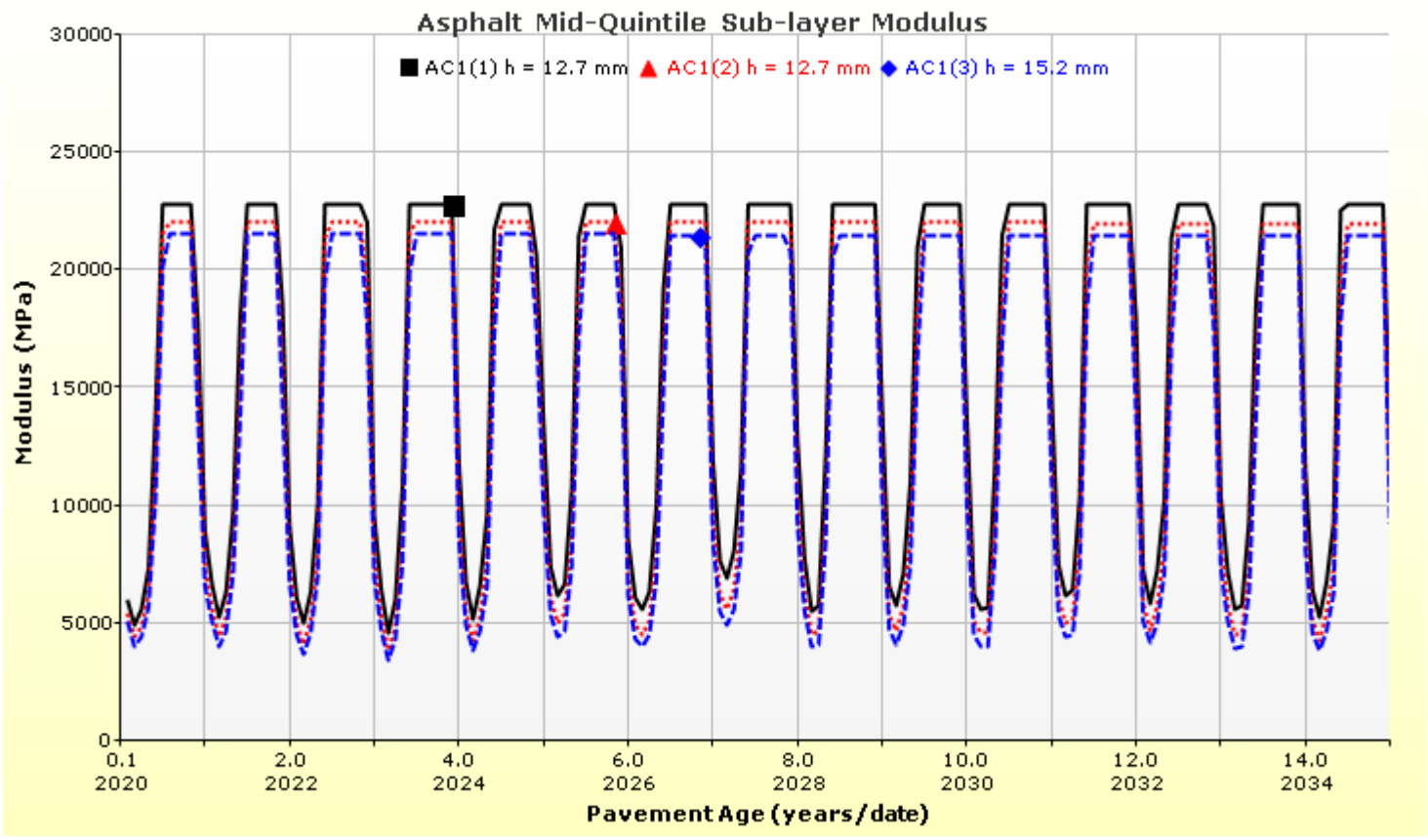
Asphalt Mid-Quintile Sub-layer Modulus
AC1(1) h = 12.7 mm
AC1(2) h = 12.7 mm
AC1(3) h = 15.2 mm
Modulus (MPa)
Pavement Age (years/date)

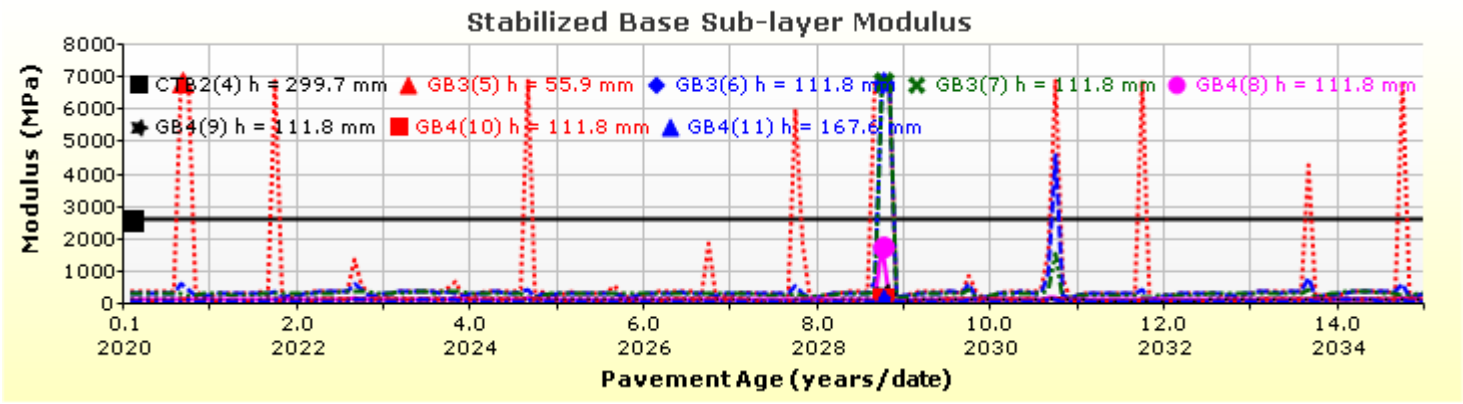
Stabilized Base Sub-layer Modulus
CTB2(4) h = 299.7 mm
GB3(5) h = 55.9 mm
GB3(6) h = 111.8 mm
GB3(7) h = 111.8 mm
GB4(8) h = 111.8 mm
GB4(9) h = 111.8 mm
GB4(10) h = 111.8 mm
GB4(11) h = 167.6 mm
Modulus (MPa)
Pavement Age (years/date)

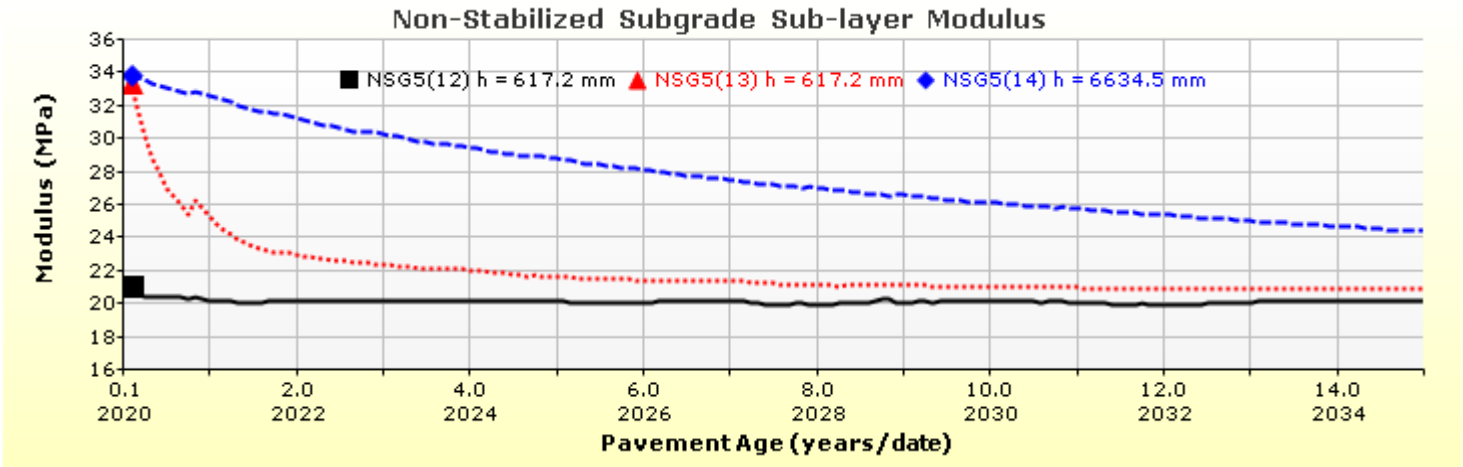
Non-Stabilized Subgrade Sub-layer Modulus
NSG5(12) h = 617.2 mm
NSG5(13) h = 617.2 mm
NSG5(14) h = 6634.5 mm
Modulus (MPa)
Pavement Age (years/date)

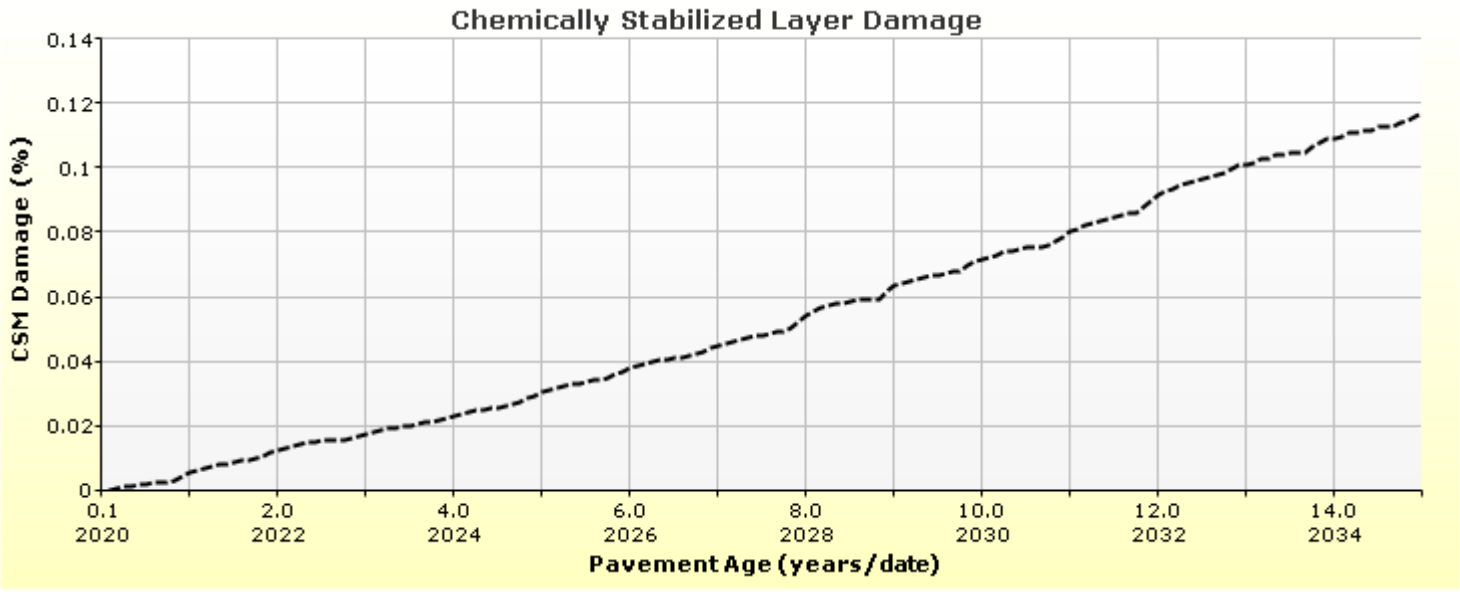
Chemically Stabilized Layer Damage
CSM Damage (%)
0.14
0.12
0.1
0.08
0.06
0.04
0.02
0
0.1
2020
2.0
2022
4.0
2024
6.0
2026
8.0
2028
10.0
2030
12.0
2032
14.0
2034
Pavement Age (years/date)

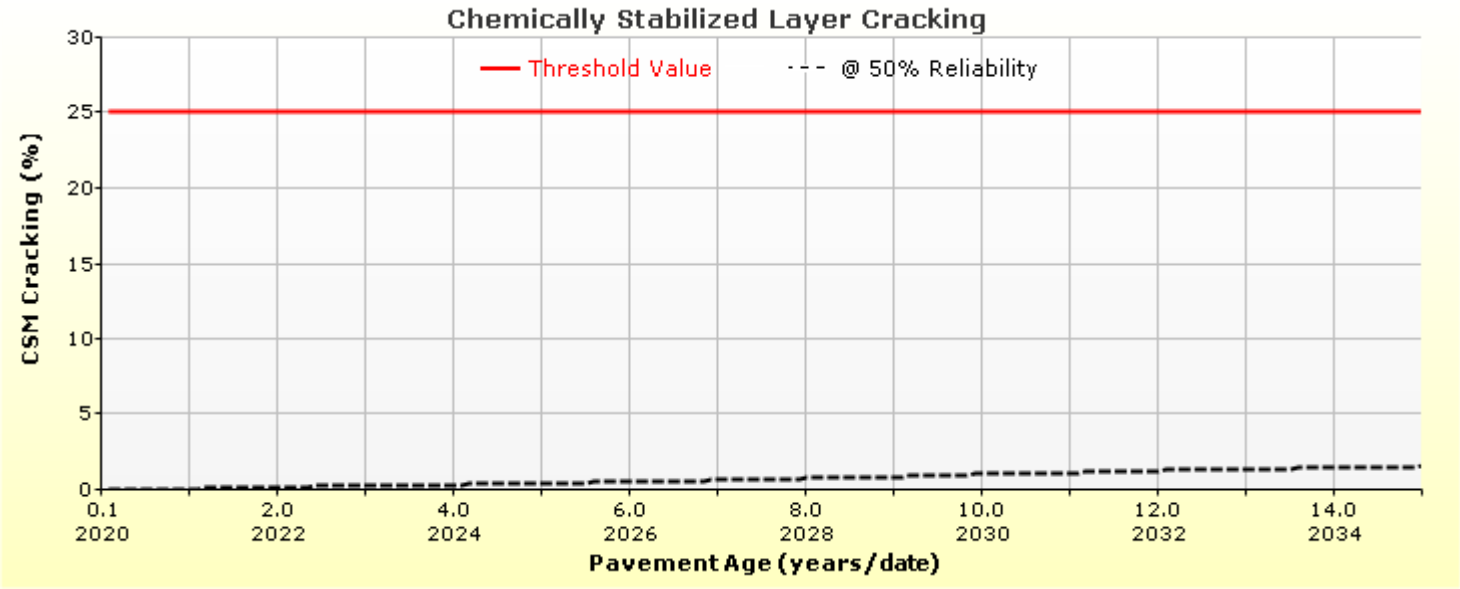
Chemically Stabilized Layer Cracking
Threshold Value
@ 50% Reliability
CSM Cracking (%)
30
25
20
15
10
5
0
0.1
2020
2.0
2022
4.0
2024
6.0
2026
8.0
2028
10.0
2030
12.0
2032
14.0
2034
Pavement Age (years/date)

Layer Information

Layer 1 Flexible : Default asphalt concrete

Asphalt		
Thickness (mm)	40.0	
Unit weight (kgf/m^3)	2460.0	
Poisson's ratio	Is Calculated?	False
	Ratio	0.35
	Parameter A	-
	Parameter B	-

Asphalt Dynamic Modulus (Input Level: 3)

Gradation	Percent Passing
19 mm sieve	100
9.5 mm sieve	77
4.75 mm sieve	60
0.075mm sieve	6

Asphalt Binder

Parameter	Value
Grade	Superpave Performance Grade
Binder Type	64-28
A	10.312
VTS	-3.44

General Info

Name	Value
Reference temperature (°C)	21.1
Effective binder content (%)	11.8
Air voids (%)	7
Thermal conductivity (watt/meter-kelvin)	1.16
Heat capacity (joule/kg-kelvin)	963

Identifiers

Field	Value
Display name/identifier	Default asphalt concrete
Description of object	
Author	
Date Created	9/16/2010 1:00:00 AM
Approver	
Date approved	9/16/2010 1:00:00 AM
State	
District	
County	
Highway	
Direction of Travel	
From station (km)	
To station (km)	
Province	
User defined field 1	
User defined field 2	
User defined field 3	
Revision Number	0

Layer 2 Chemically Stabilized : Soil cement

Semi-Rigid	
Chemically stabilized base crack spacing (m)	8
Chemically stabilized base transverse crack LTE (%)	50
Fatigue LTE (%)	50

Chemically Stabilized	
Layer thickness (mm)	300
Poisson's ratio	0.2
Unit weight (kgf/m^3)	2100

Strength	
Elastic/resilient modulus (MPa)	2664

Thermal	
Heat capacity (joule/kg-kelvin)	1172.3
Thermal conductivity (watt/meter-kelvin)	2.16

Identifiers

Field	Value
Display name/identifier	Soil cement
Description of object	Default material
Author	AASHTO
Date Created	1/1/2011 12:00:00 AM
Approver	
Date approved	1/1/2011 12:00:00 AM
State	
District	
County	
Highway	
Direction of Travel	
From station (km)	
To station (km)	
Province	
User defined field 1	
User defined field 2	
User defined field 3	
Revision Number	0

Layer 3 Non-stabilized Base : Crushed stone

Unbound	
Layer thickness (mm)	280.0
Poisson's ratio	0.35
Coefficient of lateral earth pressure (k0)	0.5

Modulus (Input Level: 3)

Analysis Type:	Modify input values by temperature/moisture
Method:	Resilient Modulus (MPa)

Resilient Modulus (MPa)
250.0

Use Correction factor for NDT modulus?	-
NDT Correction Factor:	-

Identifiers

Field	Value
Display name/identifier	Crushed stone
Description of object	Default material
Author	AASHTO
Date Created	1/1/2011 12:00:00 AM
Approver	
Date approved	1/1/2011 12:00:00 AM
State	
District	
County	
Highway	
Direction of Travel	
From station (km)	
To station (km)	
Province	
User defined field 1	
User defined field 2	
User defined field 3	
Revision Number	0

Sieve

Liquid Limit	6.0
Plasticity Index	1.0
Is layer compacted?	False

	Is User Defined?	Value
Maximum dry unit weight (kgf/m^3)	False	2048.3
Saturated hydraulic conductivity (m/hr)	False	2.257e-02
Specific gravity of solids	False	2.7
Water Content (%)	False	7

User-defined Soil Water Characteristic Curve (SWCC)	
Is User Defined?	False
af	3.0919
bf	2.6074
cf	0.7701
hr	110.0000

Sieve Size	% Passing
0.001mm	
0.002mm	
0.020mm	
0.075mm	5.0
0.150mm	
0.180mm	
0.250mm	
0.300mm	13.5
0.425mm	
0.600mm	
0.850mm	
1.18mm	27.5
2.0mm	
2.36mm	
4.75mm	45.0
9.5mm	61.5
12.5mm	
19.0mm	92.5
25.0mm	100.0
37.5mm	
50.0mm	
63.0mm	
75.0mm	
90.0mm	

Layer 4 Non-stabilized Base : Crushed gravel

Unbound	
Layer thickness (mm)	500.0
Poisson's ratio	0.35
Coefficient of lateral earth pressure (k0)	0.5

Modulus (Input Level: 3)

Analysis Type:	Modify input values by temperature/moisture
Method:	Resilient Modulus (MPa)

Resilient Modulus (MPa)
150.0

Use Correction factor for NDT modulus?	-
NDT Correction Factor:	-

Identifiers

Field	Value
Display name/identifier	Crushed gravel
Description of object	Default material
Author	AASHTO
Date Created	1/1/2011 12:00:00 AM
Approver	
Date approved	1/1/2011 12:00:00 AM
State	
District	
County	
Highway	
Direction of Travel	
From station (km)	
To station (km)	
Province	
User defined field 1	
User defined field 2	
User defined field 3	
Revision Number	0

Sieve

Liquid Limit	11.0
Plasticity Index	1.0
Is layer compacted?	False

	Is User Defined?	Value
Maximum dry unit weight (kgf/m^3)	False	2012.4
Saturated hydraulic conductivity (m/hr)	False	6.883e-03
Specific gravity of solids	False	2.7
Water Content (%)	False	8.2

User-defined Soil Water Characteristic Curve (SWCC)	
Is User Defined?	False
af	5.0935
bf	2.5668
cf	0.8576
hr	108.0000

Sieve Size	% Passing
0.001mm	
0.002mm	
0.020mm	
0.075mm	4.0
0.150mm	
0.180mm	
0.250mm	
0.300mm	33.5
0.425mm	
0.600mm	
0.850mm	
1.18mm	55.0
2.0mm	
2.36mm	
4.75mm	60.0
9.5mm	
12.5mm	
19.0mm	
25.0mm	75.0
37.5mm	
50.0mm	
63.0mm	
75.0mm	
90.0mm	

Layer 5 Subgrade : A-6

Unbound	
Layer thickness (mm)	Semi-infinite
Poisson's ratio	0.35
Coefficient of lateral earth pressure (k0)	0.5

Modulus (Input Level: 3)

Analysis Type:	Modify input values by temperature/moisture
Method:	Resilient Modulus (MPa)

Resilient Modulus (MPa)
35.0

Use Correction factor for NDT modulus?	-
NDT Correction Factor:	-

Identifiers

Field	Value
Display name/identifier	A-6
Description of object	Default material
Author	AASHTO
Date Created	1/1/2011 12:00:00 AM
Approver	
Date approved	1/1/2011 12:00:00 AM
State	
District	
County	
Highway	
Direction of Travel	
From station (km)	
To station (km)	
Province	
User defined field 1	
User defined field 2	
User defined field 3	
Revision Number	0

Sieve

Liquid Limit	42.0
Plasticity Index	15.0
Is layer compacted?	False

	Is User Defined?	Value
Maximum dry unit weight (kgf/m^3)	False	1693.8
Saturated hydraulic conductivity (m/hr)	False	3.012e-06
Specific gravity of solids	False	2.7
Water Content (%)	False	18.2

User-defined Soil Water Characteristic Curve (SWCC)	
Is User Defined?	False
af	114.8407
bf	0.6389
cf	0.1739
hr	500.0000

Sieve Size	% Passing
0.001mm	
0.002mm	25.0
0.020mm	
0.075mm	82.0
0.150mm	
0.180mm	91.0
0.250mm	
0.300mm	
0.425mm	95.0
0.600mm	
0.850mm	
1.18mm	
2.0mm	98.0
2.36mm	
4.75mm	100.0
9.5mm	100.0
12.5mm	100.0
19.0mm	100.0
25.0mm	100.0
37.5mm	
50.0mm	
63.0mm	
75.0mm	
90.0mm	100.0

Calibration Coefficients

AC Fatigue

$$N_f = 0.00432 * C * \beta_{f1} k_1 \left(\frac{1}{\varepsilon_1}\right)^{k_2\beta_{f2}} \left(\frac{1}{E}\right)^{k_3\beta_{f3}}$$

$$C = 10^M$$

$$M = 4.84\left(\frac{V_b}{V_a + V_b} - 0.69\right)$$

k1: 3.75	
k2: 2.87	
k3: 1.46	
Bf1: 0.02054	
Bf2: 1.38	
Bf3: 0.88	

AC Rutting

$$\frac{\varepsilon_p}{\varepsilon_r} = k_z \beta_{r1} 10^{k_1 T^{k_2\beta_{r2}} N^{k_3\beta_{r3}}}$$

$$k_z = (C_1 + C_2 * depth) * 0.328196^{depth}$$

$$C_1 = -0.1039 * H_\alpha^2 + 2.4868 * H_\alpha - 17.342$$

$$C_2 = 0.0172 * H_\alpha^2 - 1.7331 * H_\alpha + 27.428$$

Where:

$$H_{ac} = total\ AC\ thickness(in)$$

$\varepsilon_p = plastic\ strain\left({}^{in}/_{in}\right)$
$\varepsilon_r = resilient\ strain\left({}^{in}/_{in}\right)$
$T = layer\ temperature(^{\circ}F)$
$N = number\ of\ load\ repetitions$

AC Rutting Standard Deviation	0.24 * Pow(RUT,0.8026) + 0.001	
AC Layer 1	K1:-2.45 K2:3.01 K3:0.22	Br1:0.128 Br2:0.52 Br3:1.36

Thermal Fracture

$$C_f = 400 * N\left(\frac{\log C / h_{ac}}{\sigma}\right)$$

$$\Delta C = (k * \beta t)^{n+1} * A * \Delta K^n$$

$$A = 10^{(4.389 - 2.52 * \log(E * \sigma_m * n))}$$

$C_f = observed\ amount\ of\ thermal\ cracking(ft/500ft)$
$k = refression\ coefficient\ determined\ through\ field\ calibration$
$N(\,) = standard\ normal\ distribution\ evaluated\ at(\,)$
$\sigma = standard\ deviation\ of\ the \log\ of\ the\ depth\ of\ cracks\ in\ the\ pavments$
$C = crack\ depth(in)$
$h_{ac} = thickness\ of\ asphalt\ layer(in)$
$\Delta C = Change\ in\ the\ crack\ depth\ due\ to\ a\ cooling\ cycle$
$\Delta K = Change\ in\ the\ stress\ intensity\ factor\ due\ to\ a\ cooling\ cycle$
$A, n = Fracture\ parameters\ for\ the\ asphalt\ mixture$
$E = mixture\ stiffness$
$\sigma_M = Undamaged\ mixture\ tensile\ strength$
$\beta_t = Calibration\ parameter$

Level 1 K: ((3 * Pow(10,-7)) * Pow(MAAT,4.0319)) * 1 + 0	
Level 2 K: ((3 * Pow(10,-7)) * Pow(MAAT,4.0319)) * 1 + 0	
Level 3 K: ((3 * Pow(10,-7)) * Pow(MAAT,4.0319)) * 1 + 0	

CSM Fatigue

$$N_f = 10^{\left(\frac{k_1 \beta_{c1} \left(\frac{\sigma_s}{M_r}\right)}{k_2 \beta_{c2}}\right)}$$

$N_f = number\ of\ repetitions\ to\ fatigue\ cracking$
$\sigma_s = Tensile\ stress(psi)$
$M_r = modulus\ of\ rupture(psi)$

k1: 0.972	k2: 0.0825	Bc1: 1	Bc2:1

Unbound Layer Rutting

$$\delta_a(N) = \beta_{s_1} k_1 \varepsilon_v h \left(\frac{\varepsilon_0}{\varepsilon_r}\right) \left| e^{-\left(\frac{\rho}{N}\right)^{\beta}} \right|$$

$\delta_a = permanent\ deformation\ for\ the\ layer$
$N = number\ of\ repetitions$
$\varepsilon_v = average\ veritcal\ strain(in/in)$
$\varepsilon_0, \beta, \rho = material\ properties$
$\varepsilon_r = resilient\ strain(in/in)$

Base Rutting		Subgrade Rutting	
k1: 0.965	Bs1: 1	k1: 0.675	Bs1: 1
Standard Deviation (BASERUT) 0.1477 * Pow(BASERUT,0.6711) + 0.001		Standard Deviation (BASERUT) 0.1235 * Pow(SUBRUT,0.5012) + 0.001	

AC Cracking

AC Top Down Cracking

$$FC_{top} = \left(\frac{C_4}{1 + e^{(C_1 - C_2 * log_{10}(Damage))}}\right) * 10.56$$

c1: 7	c2: 3.5	c3: 0	c4: 1000

Top down AC Cracking Standard Deviation

200 + 2300/(1+exp(1.072-2.1654*LOG10(TOP+0.0001)))

AC Bottom Up Cracking

$$FC = \left(\frac{6000}{1 + e^{(C_1 * C_1' + C_2 * C_2' log_{10}(D * 100))}}\right) * \left(\frac{1}{60}\right)$$

$$C_2' = -2.40874 - 39.748 * (1 + h_{ac})^{-2.856}$$

$$C_1' = -2 * C_2'$$

c1: 1.31	c2: 2.1585	c3: 6000

Bottom up AC Cracking Standard Deviation

1.13 + 13/(1+exp(7.57-15.5*LOG10(BOTTOM+0.0001)))

CSM Cracking

$$FC_{ctb} = C_1 + \frac{C_2}{1 + e^{C_3 - C_4 * log_{10}(Damage)}}$$

C1: 0	C2: 75	C3: 2	C4: 2

CSM Standard Deviation

CTB*1

IRI Flexible Pavements

C1 - Rutting
C2 - Fatigue Crack
C3 - Transverse Crack
C4 - Site Factors

C1: 55	C2: 0.4	C3: 0.008	C4: 0.015

Reflective Cracking

$$\Delta C = k_1 \Delta_{bending} + k_2 \Delta_{shaering} + k_3 \Delta_{thermal}$$

$$\Delta D = \frac{C_1 k_1 \Delta_{bending} + C_2 k_2 \Delta_{shearing} + C_3 k_3 \Delta_{thermal}}{h_{OL}}$$

$$\Delta_{Bending} = A(SIF)_B^n$$

$$\Delta_{Shearing} = A(SIF)_S^n$$

$$\Delta_{Thermal} = A(SIF)_T^n$$

$$D = \sum_{i=1}^{N} \Delta D$$

$$RCR = \left(\frac{100}{C4 + e^{C5 \log D}}\right) * EX\_CRK$$

Where

ΔC	=	Crack length increment, in
ΔD	=	Incremental damage ratio
$k_1, k_2, k_3, C_1, C_2, C_3, C_4, C_5$	=	Calibration factors (local and global)
$\Delta_{bending}, \Delta_{shearing}, \Delta_{thermal}$	=	Crack length increments caused by bending, shearing, and thermal loading
A, n	=	HMA material fracture properties
N	=	Total number of days
$(SIF)_B, (SIF)_S, (SIF)_T$	=	Stress intensity factors caused by bending, shearing, and thermal loading
D	=	Damage ratio
h_{OL}	=	Overlay thickness, in
RCR	=	Cracks in the underlying layers reflected, %
EX_CRK	=	Transverse cracking in underlying pavement layers, ft/mile (transverse cracking) Alligator cracking in underlying pavement layers, % lane area (alligator cracking)

Pavement Type	Distress Type	k1	k2	k3	C1	C2	C3	C4	C5	Standard Deviation
Semi-Rigid	Transverse	0.45	0.05	1	0.1	0.9809	0.19	165.3	-5.1048	0.000027 * Pow (TRANSVERSE,2.1187) + 399.9
Semi-Rigid	Fatigue	0.45	0.05	1	1.64	1.1	0.19	62.1	-404.6	1.3897 * Pow (FATIGUE,0.2960) + 0.4212

Semi-Rigid Pavement_FDR+HRB1_ONTARIO

File Name: C:\Users\admin\Desktop\Eskedil_ME\Kossuth\Semi-Rigid Pavement_FDR+HRB1_ONTARIO.dgpx

Design Inputs

Design Life: 15 years
Design Type: SEMI_RIGID

Base construction: May, 2020
Pavement construction: June, 2020
Traffic opening: June, 2020

Climate Data Sources (Lat/Lon): 43.5, -80.625; 43, -80

Design Structure

Layer type	Material Type	Thickness(mm)
Flexible	Default asphalt concrete	40.0
Cement_Base	Soil cement	300.0
NonStabilized	Crushed stone	280.0
NonStabilized	Crushed gravel	500.0
Subgrade	A-6	Semi-infinite

Volumetric at Construction:	
Effective binder content (%)	11.8
Air voids (%)	7.0

Traffic

Age (year)	Heavy Trucks (cumulative)
2020 (initial)	1,272
2027 (7 years)	1,721,680
2035 (15 years)	3,794,600

Design Outputs

Distress Prediction Summary

Distress Type	Distress @ Specified Reliability		Reliability (%)		Criterion Satisfied?
	Target	Predicted	Target	Achieved	
Terminal IRI (m/km)	2.30	2.04	85.00	94.75	Pass
Permanent deformation - total pavement (mm)	13.00	5.47	85.00	100.00	Pass
AC total fatigue cracking: bottom up + reflective (% lane area)	50.00	2.36	85.00	100.00	Pass
AC total transverse cracking: thermal + reflective (m/km)	473.40	340.46	85.00	99.25	Pass
AC bottom-up fatigue cracking (percent)	20.00	0.00	50.00	100.00	Pass
AC thermal cracking (m/km)	190.00	0.19	50.00	100.00	Pass
AC top-down fatigue cracking (m/km)	380.00	39.31	85.00	100.00	Pass
Permanent deformation - AC only (mm)	6.00	0.43	85.00	100.00	Pass
Chemically stabilized layer - fatigue fracture (percent)	25.00	1.92	-	-	-

Distress Charts

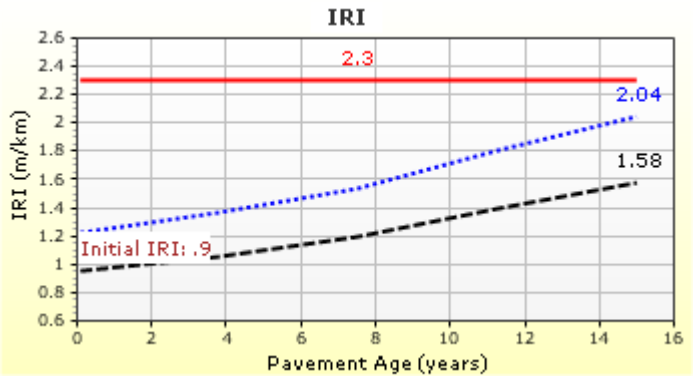

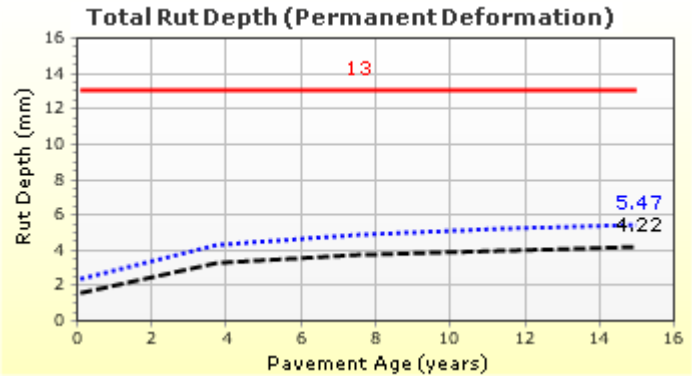

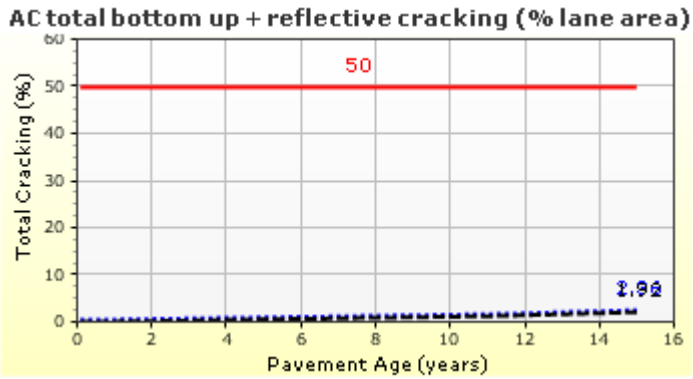

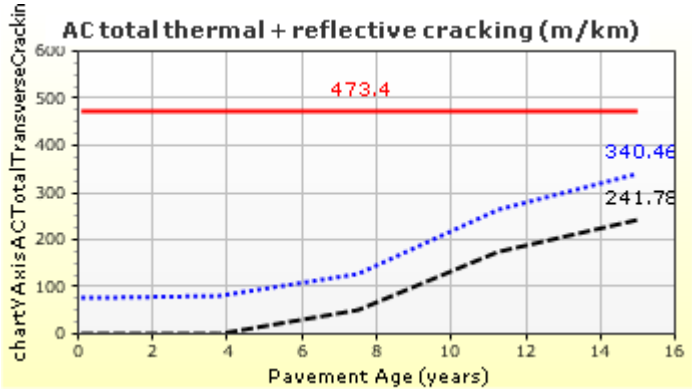

Traffic Inputs

Graphical Representation of Traffic Inputs

Initial two-way AADTT:	1,272	Percent of trucks in design direction (%):	50.0
Number of lanes in design direction:	2	Percent of trucks in design lane (%):	90.0
		Operational speed (kph)	100.0

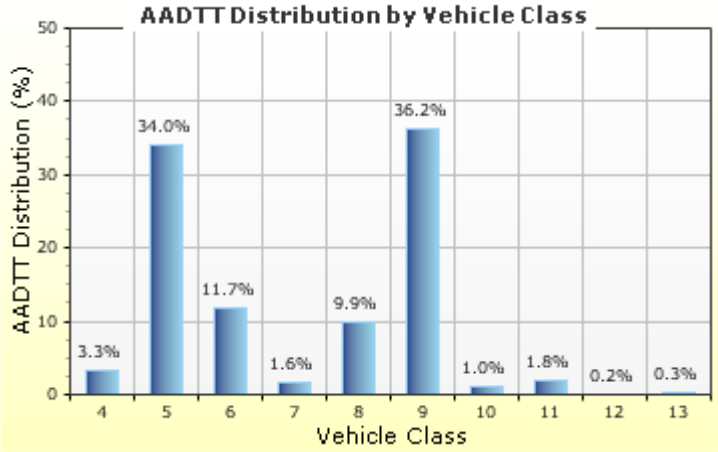

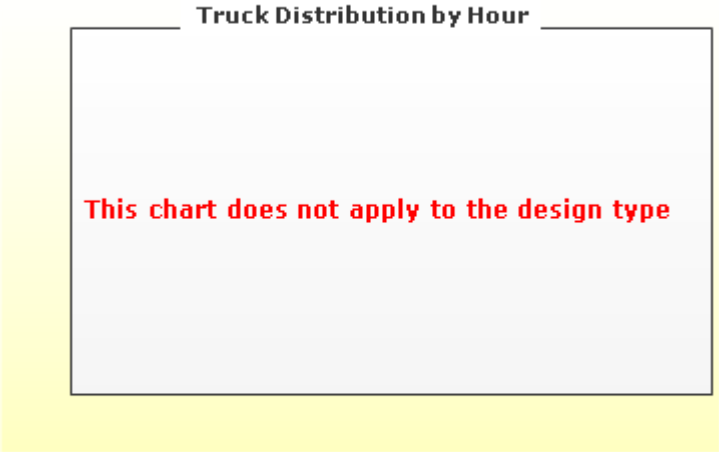

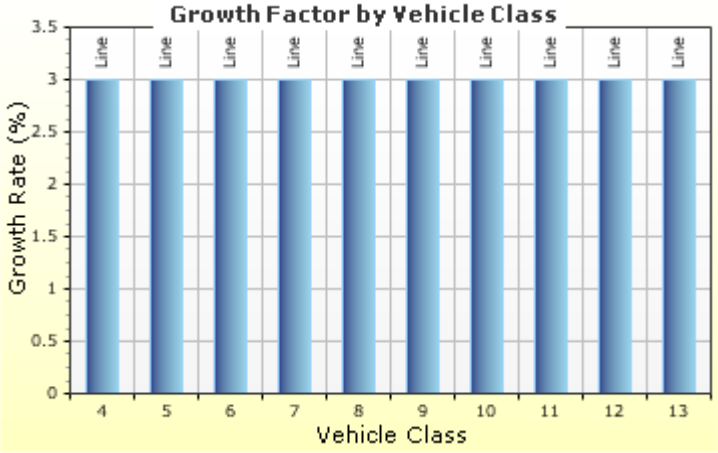

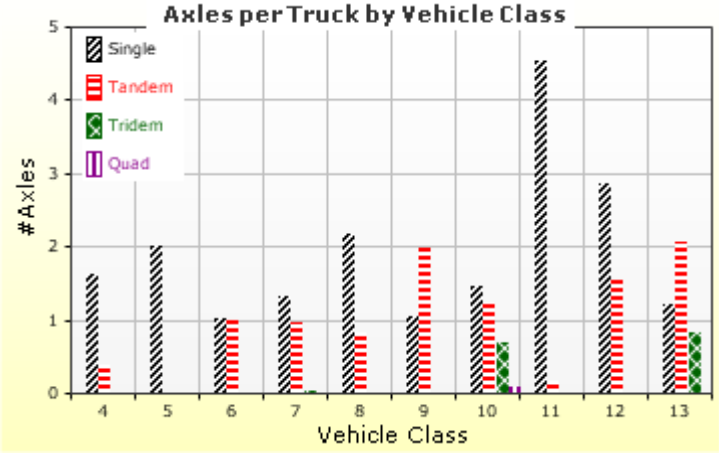

Traffic Volume Monthly Adjustment Factors

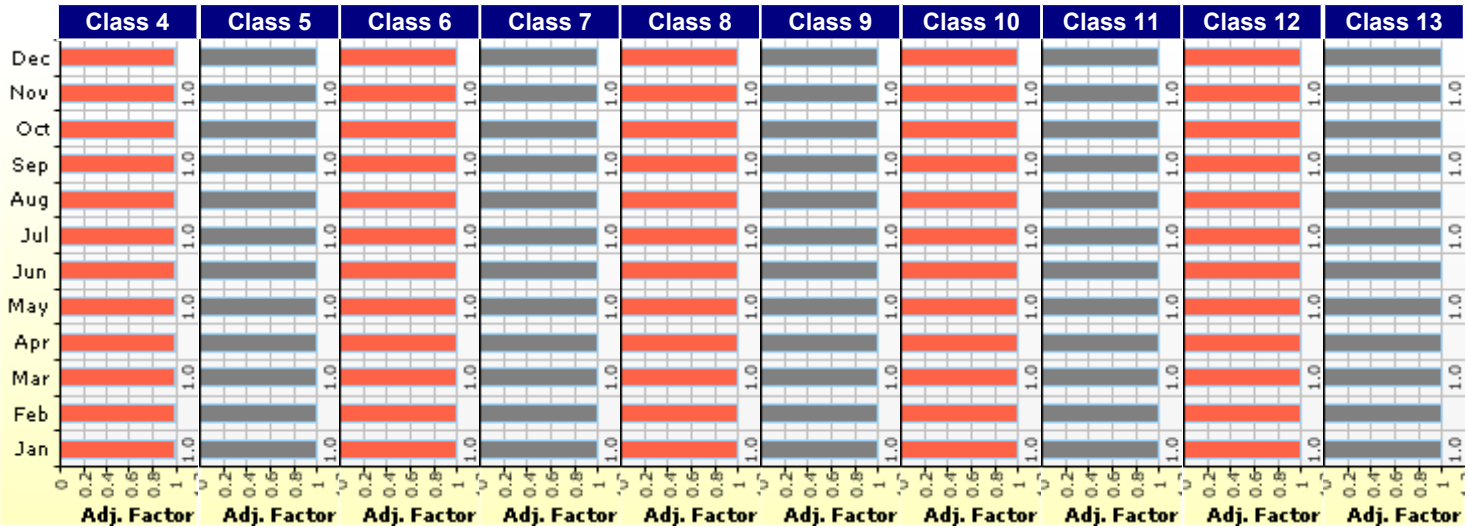

Tabular Representation of Traffic Inputs

Volume Monthly Adjustment Factors

Level 3: Default MAF

Month	Vehicle Class									
	4	5	6	7	8	9	10	11	12	13
January	1.0	1.0	1.0	1.0	1.0	1.0	1.0	1.0	1.0	1.0
February	1.0	1.0	1.0	1.0	1.0	1.0	1.0	1.0	1.0	1.0
March	1.0	1.0	1.0	1.0	1.0	1.0	1.0	1.0	1.0	1.0
April	1.0	1.0	1.0	1.0	1.0	1.0	1.0	1.0	1.0	1.0
May	1.0	1.0	1.0	1.0	1.0	1.0	1.0	1.0	1.0	1.0
June	1.0	1.0	1.0	1.0	1.0	1.0	1.0	1.0	1.0	1.0
July	1.0	1.0	1.0	1.0	1.0	1.0	1.0	1.0	1.0	1.0
August	1.0	1.0	1.0	1.0	1.0	1.0	1.0	1.0	1.0	1.0
September	1.0	1.0	1.0	1.0	1.0	1.0	1.0	1.0	1.0	1.0
October	1.0	1.0	1.0	1.0	1.0	1.0	1.0	1.0	1.0	1.0
November	1.0	1.0	1.0	1.0	1.0	1.0	1.0	1.0	1.0	1.0
December	1.0	1.0	1.0	1.0	1.0	1.0	1.0	1.0	1.0	1.0

Distributions by Vehicle Class

Truck Distribution by Hour does not apply

Vehicle Class	AADTT Distribution (%) (Level 3)	Growth Factor	
		Rate (%)	Function
Class 4	3.3%	3%	Linear
Class 5	34%	3%	Linear
Class 6	11.7%	3%	Linear
Class 7	1.6%	3%	Linear
Class 8	9.9%	3%	Linear
Class 9	36.2%	3%	Linear
Class 10	1%	3%	Linear
Class 11	1.8%	3%	Linear
Class 12	0.2%	3%	Linear
Class 13	0.3%	3%	Linear

Axle Configuration

Traffic Wander	
Mean wheel location (mm)	460.0
Traffic wander standard deviation (mm)	254.0
Design lane width (m)	3.7

Axle Configuration	
Average axle width (m)	2.6
Dual tire spacing (mm)	305.0
Tire pressure (kPa)	827.4

Average Axle Spacing	
Tandem axle spacing (m)	1.5
Tridem axle spacing (m)	1.7
Quad axle spacing (m)	1.3

Wheelbase does not apply

Number of Axles per Truck

Vehicle Class	Single Axle	Tandem Axle	Tridem Axle	Quad Axle
Class 4	1.62	0.39	0	0
Class 5	2	0	0	0
Class 6	1.01	0.993	0	0
Class 7	1.314	0.989	0.03	0
Class 8	2.163	0.845	0	0
Class 9	1.055	1.968	0.003	0
Class 10	1.446	1.234	0.7	0.088
Class 11	4.546	0.168	0	0
Class 12	2.857	1.526	0	0
Class 13	1.201	2.058	0.848	0.024

AADTT (Average Annual Daily Truck Traffic) Growth

*** Traffic cap is not enforced**

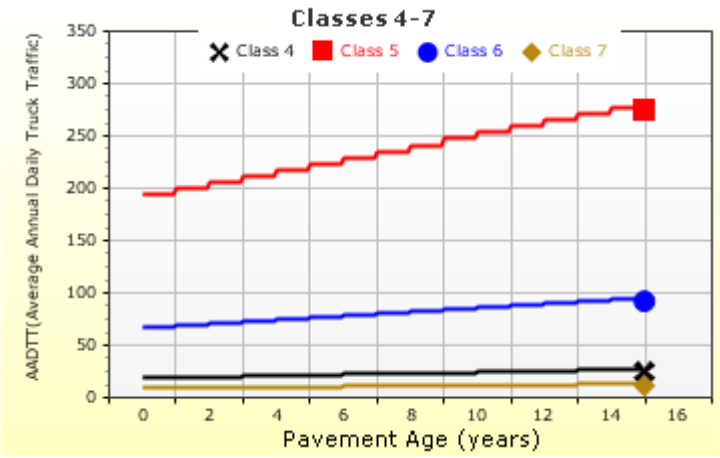

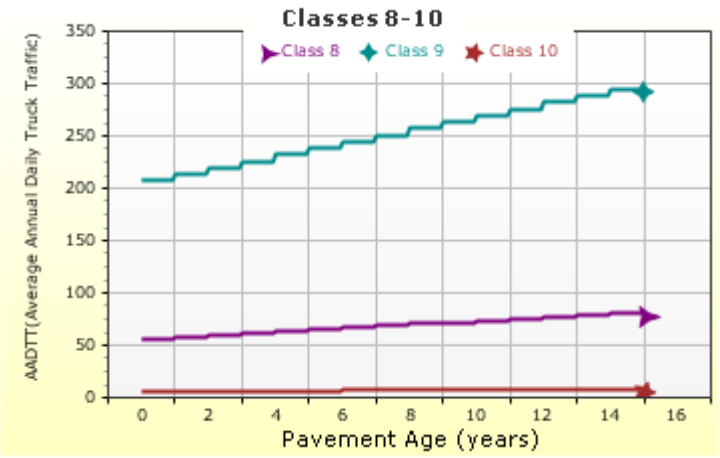

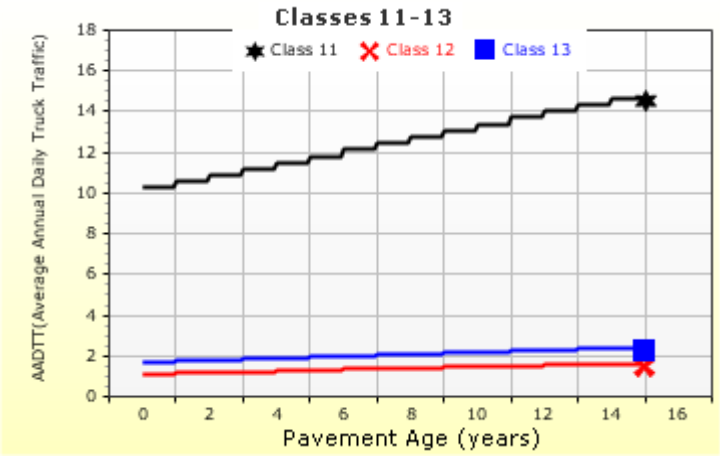

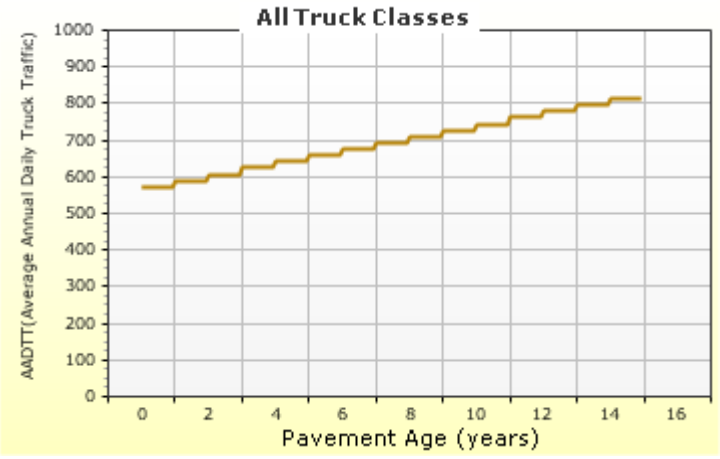

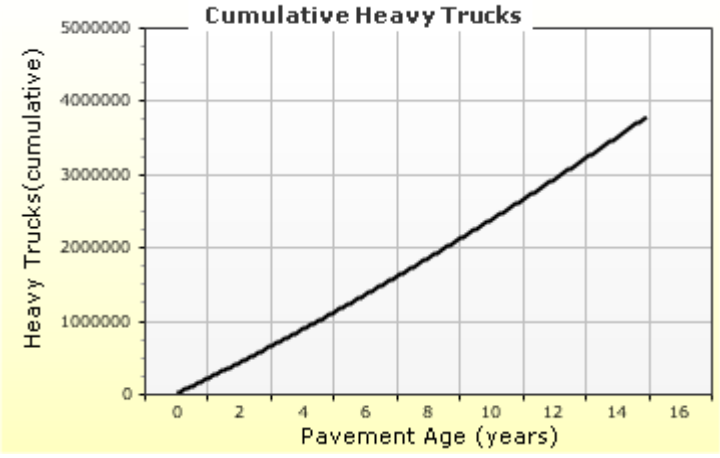

Climate Inputs

Climate Data Sources:

Climate Station Cities:	Location (lat lon elevation(m))
CA, ON	43.50000 -80.62500 369
CA, ON	43.00000 -80.00000 210

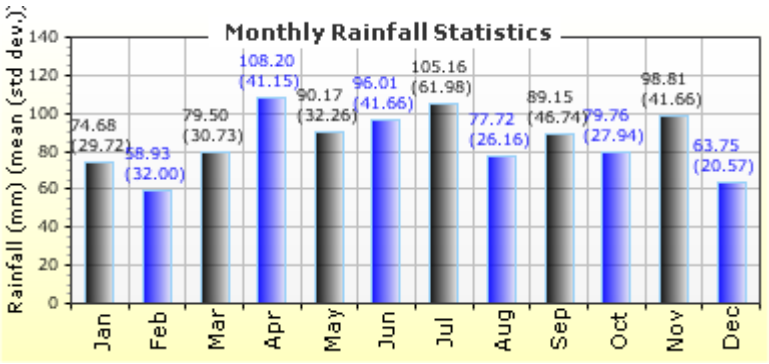

Annual Statistics:

Mean annual air temperature (°C)	7.96
Mean annual precipitation (mm)	1022.60
Freezing index (°C - days)	521.04
Average annual number of freeze/thaw cycles:	80.61

Water table depth (m)	10.00

Monthly Climate Summary:

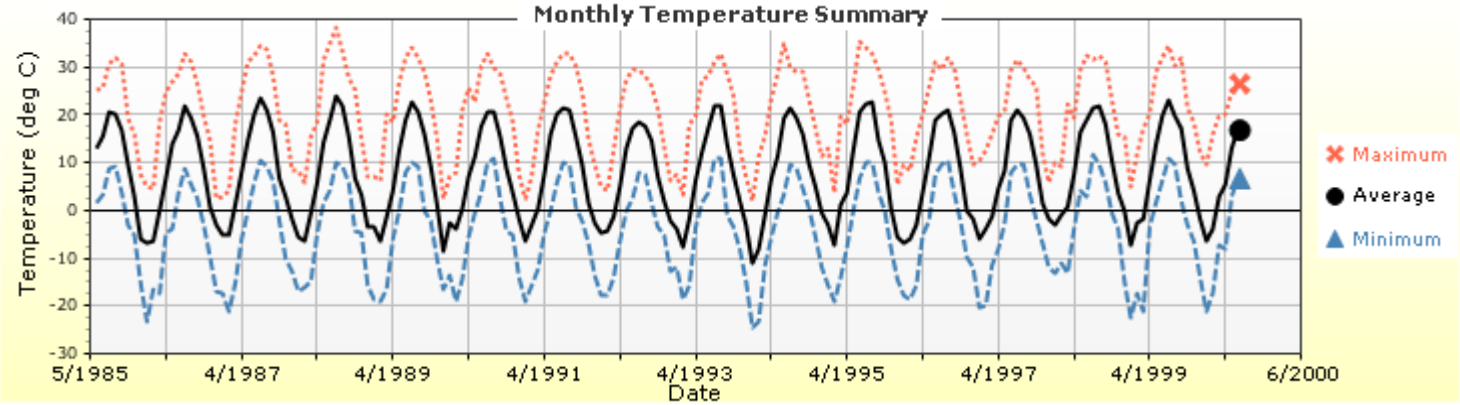

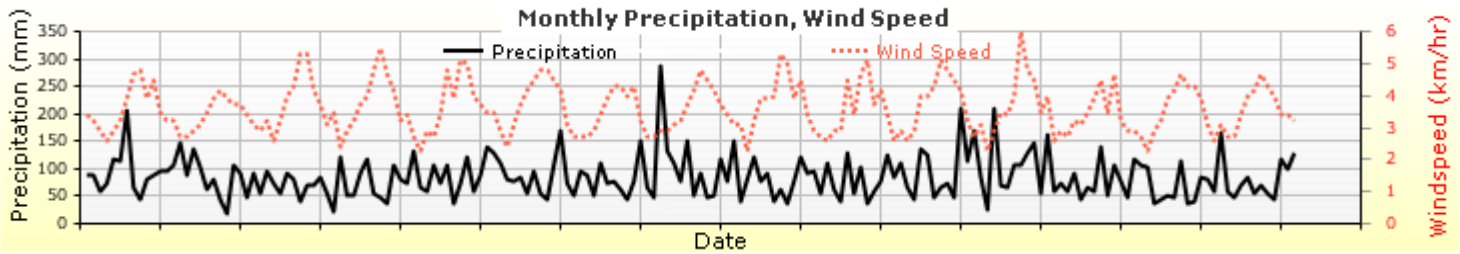

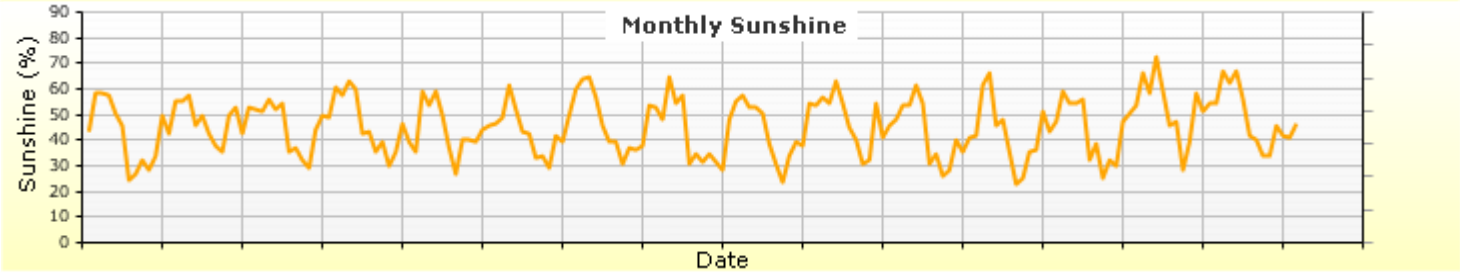

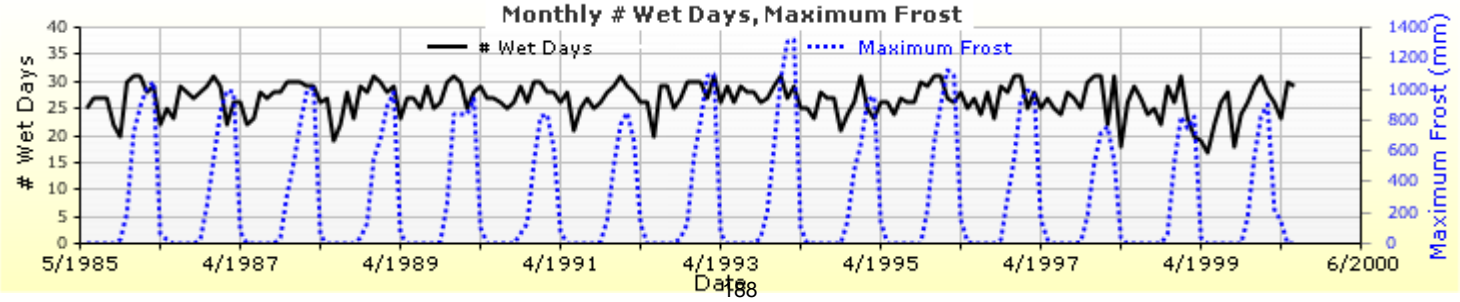

Hourly Air Temperature Distribution by Month:

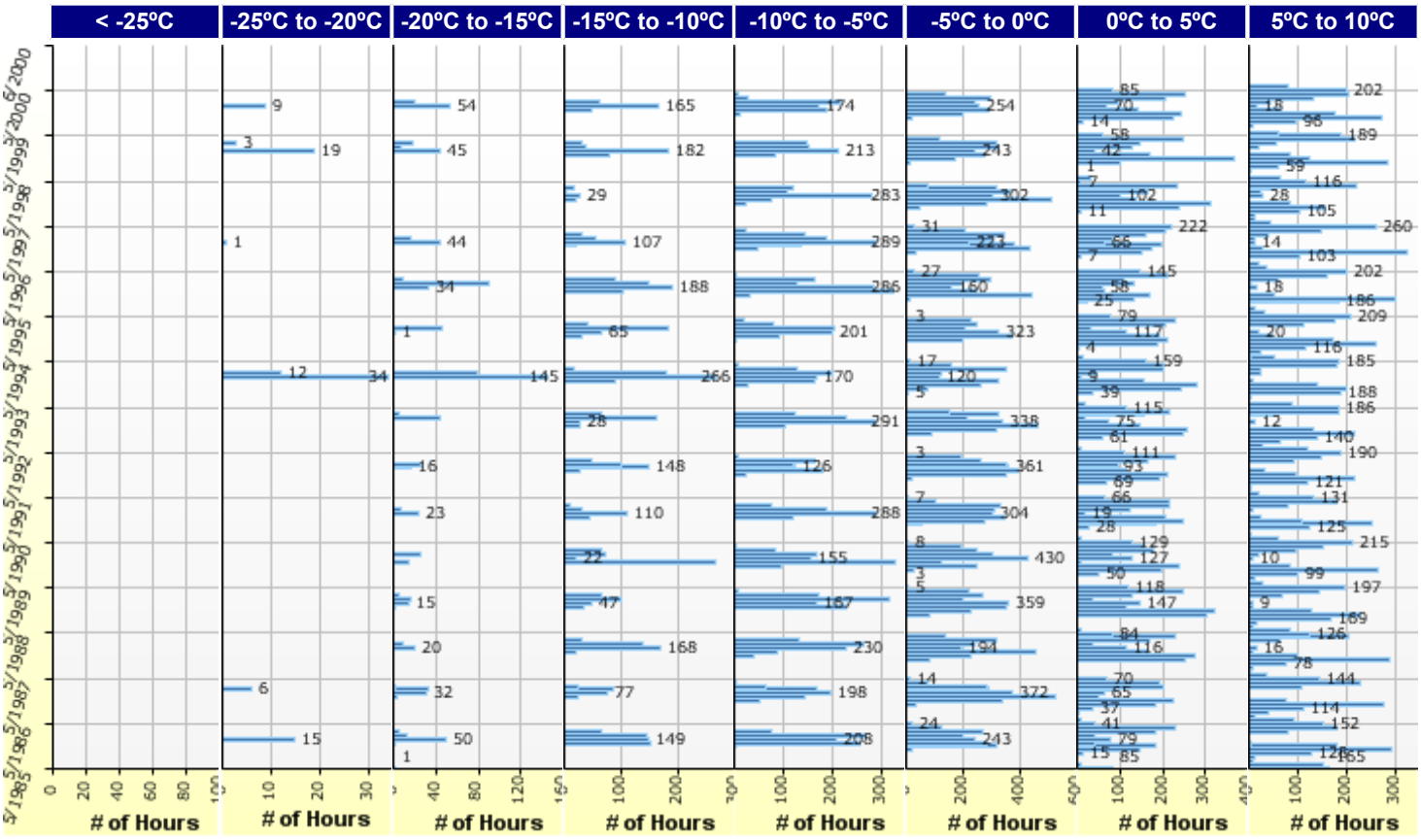

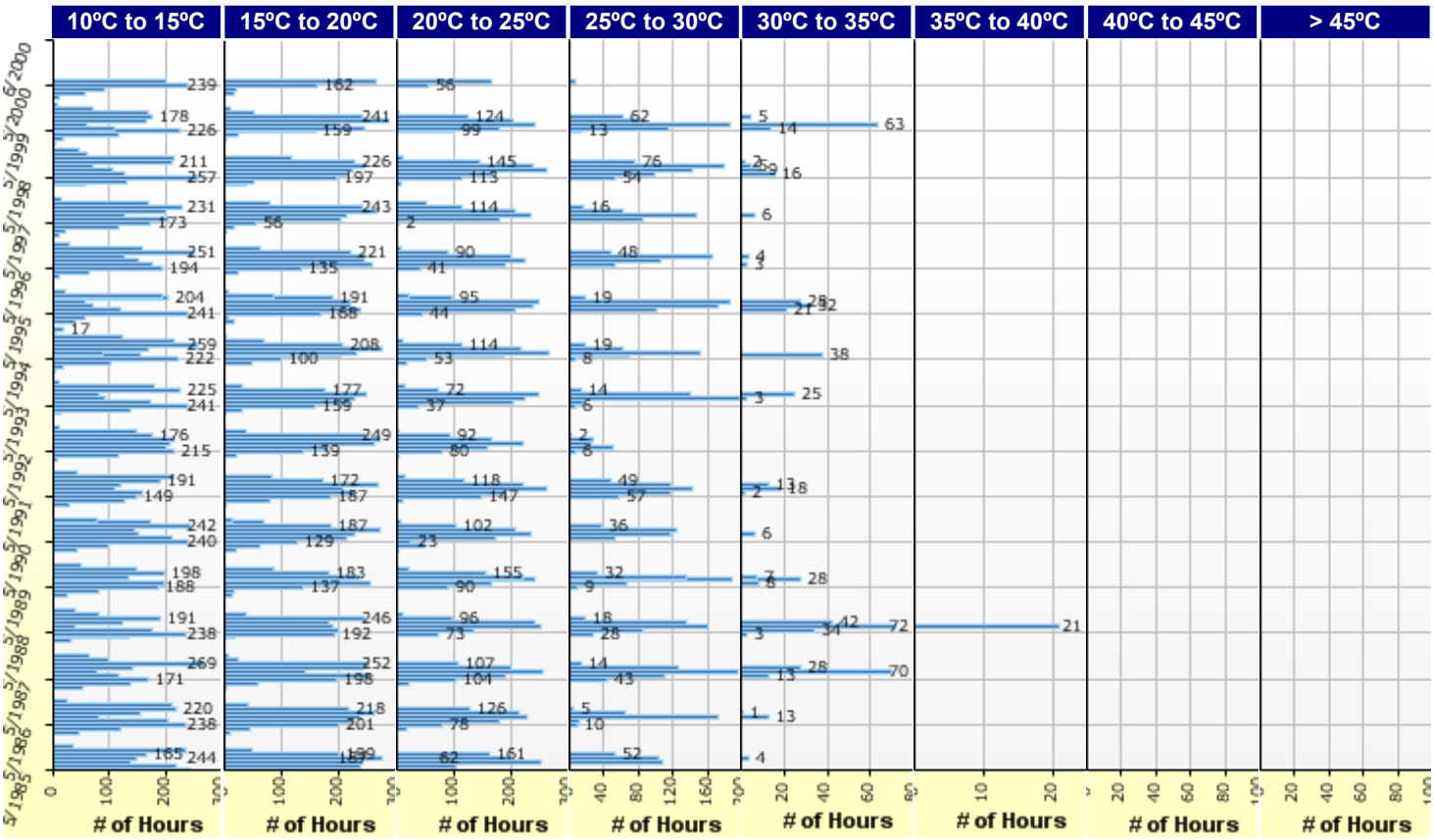

Design Properties

HMA Design Properties

Use Multilayer Rutting Model	False
Using G* based model (not nationally calibrated)	False
Is NCHRP 1-37A HMA Rutting Model Coefficients	True
Endurance Limit	-
Use Reflective Cracking	True

Structure - ICM Properties	
AC surface shortwave absorptivity	0.85

Layer Name	Layer Type	Interface Friction
Layer 1 Flexible : Default asphalt concrete	Flexible (1)	1.00
Layer 2 Chemically Stabilized : Soil cement	Chemically Stabilized (2)	1.00
Layer 3 Non-stabilized Base : Crushed stone	Non-stabilized Base (4)	1.00
Layer 4 Non-stabilized Base : Crushed gravel	Non-stabilized Base (4)	1.00
Layer 5 Subgrade : A-6	Subgrade (5)	-

Thermal Cracking

Thermal Contraction	
Is thermal contraction calculated?	True
Mix coefficient of thermal contraction (mm/mm/ºC)	-
Aggregate coefficient of thermal contraction (mm/mm/ºC)	9.0e-006
Voids in Mineral Aggregate (%)	18.8

Indirect Tensile Strength (Input Level: 3)	
Test Temperature (ºC)	**Indirect Tensilte Strength (Mpa)**
-10.0	2.79

Creep Compliance (1/GPa) (Input Level: 3)			
Loading time (sec)	**-20 ºC**	**-10 ºC**	**0 ºC**
1	5.57e-002	8.57e-002	1.16e-001
2	6.17e-002	1.01e-001	1.51e-001
5	7.07e-002	1.25e-001	2.15e-001
10	7.83e-002	1.48e-001	2.80e-001
20	8.68e-002	1.74e-001	3.65e-001
50	9.94e-002	2.16e-001	5.19e-001
100	1.10e-001	2.55e-001	6.77e-001

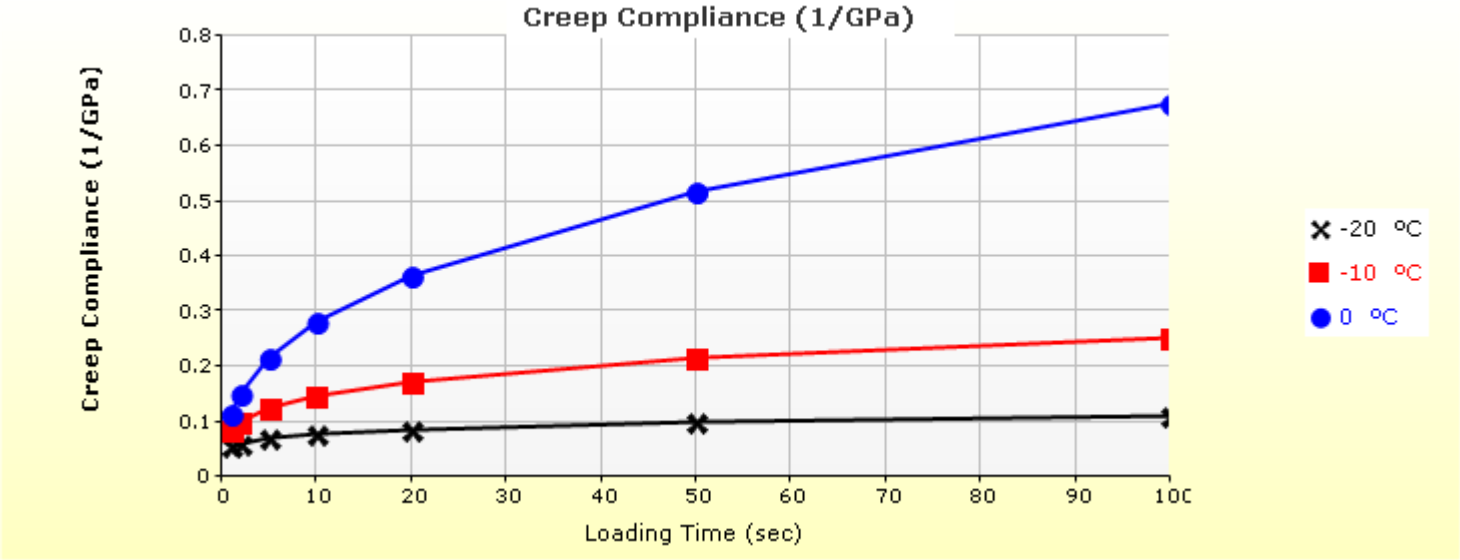

HMA Layer 1: Layer 1 Flexible : Default asphalt concrete

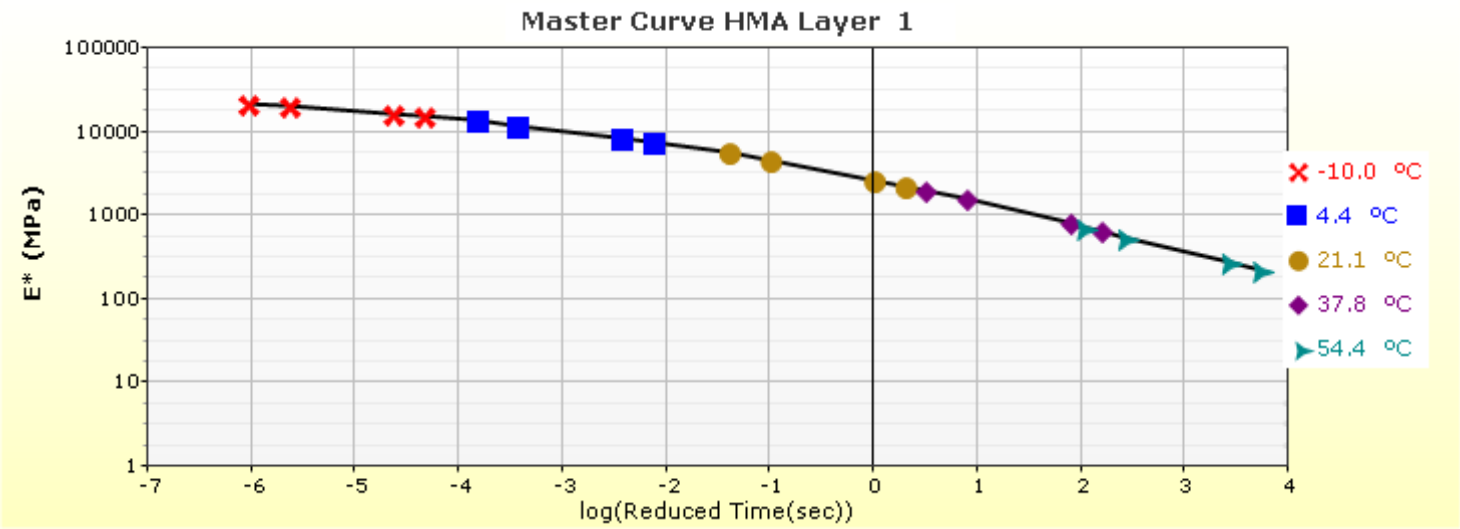

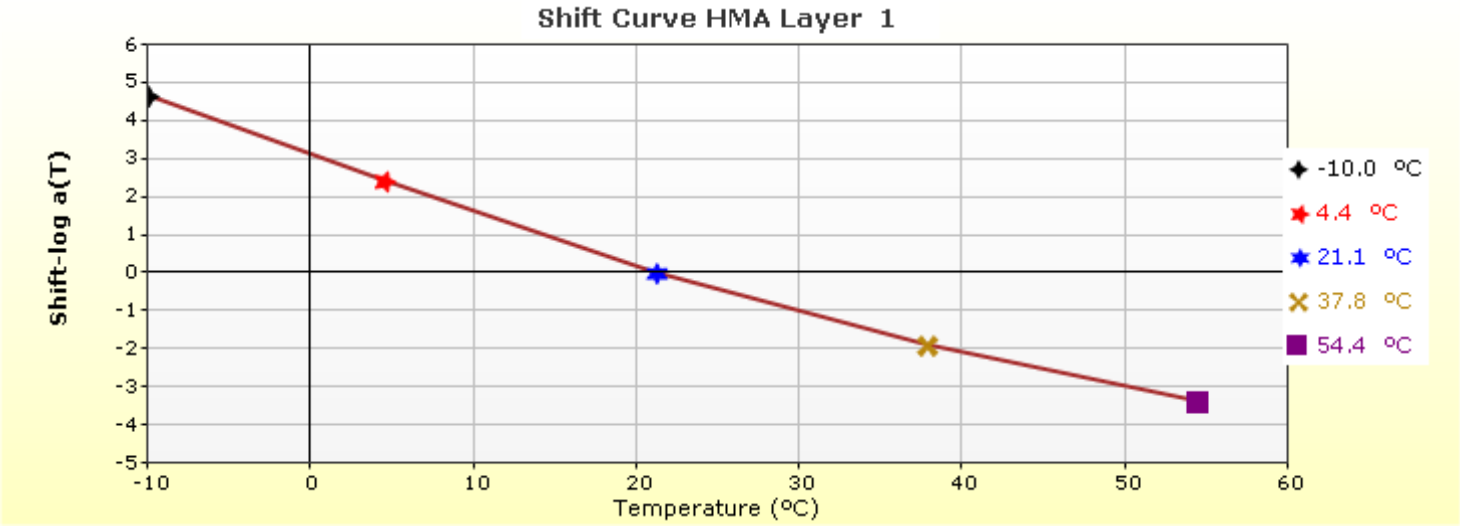

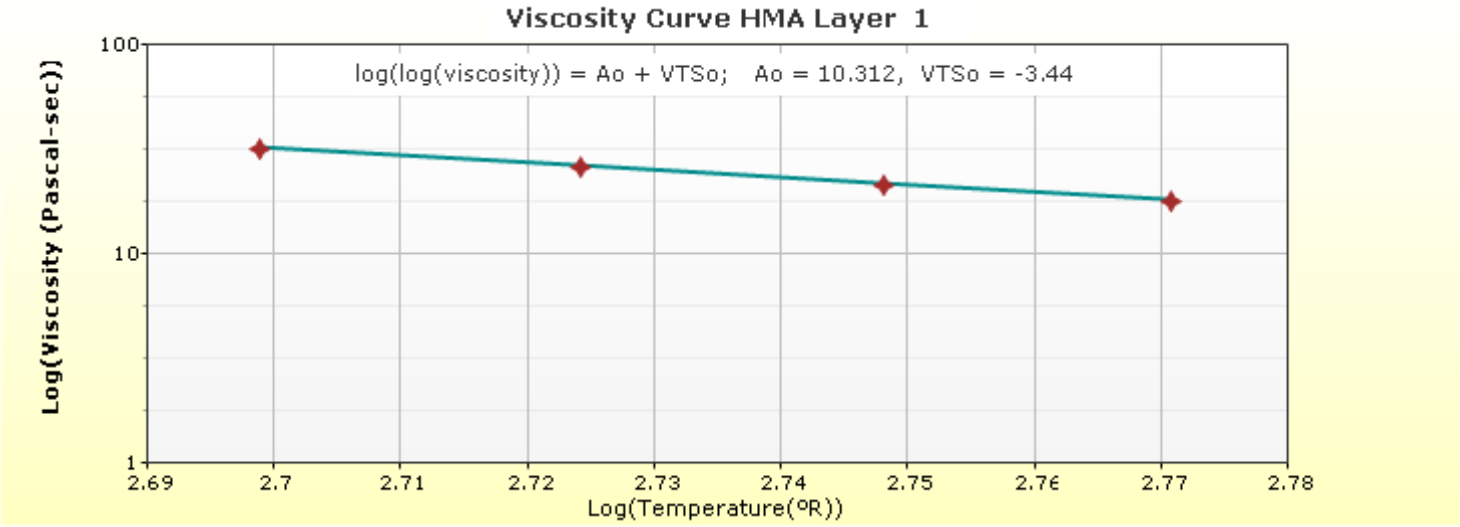

Analysis Output Charts

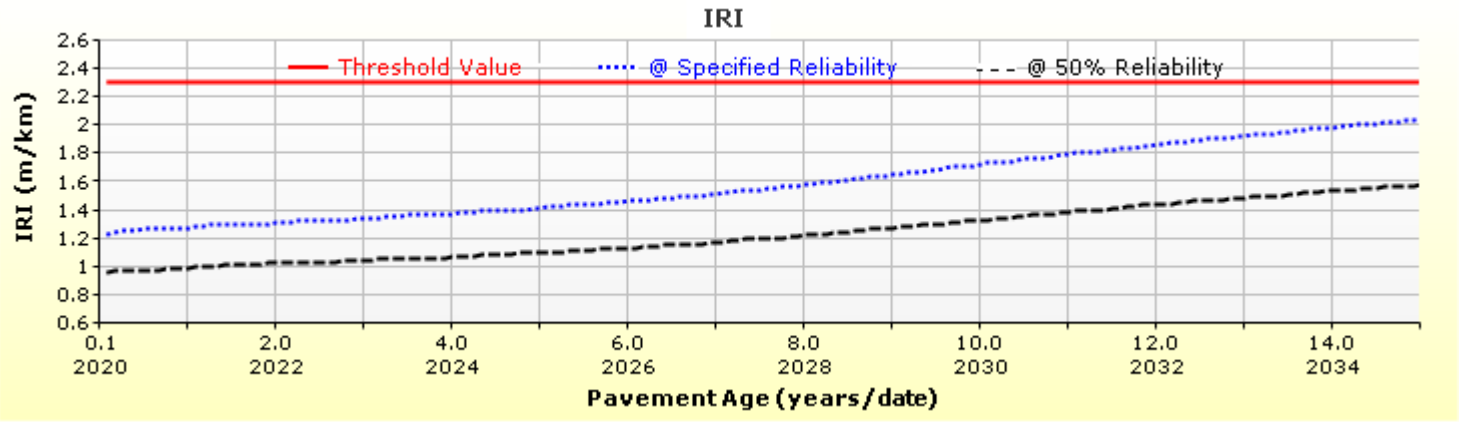

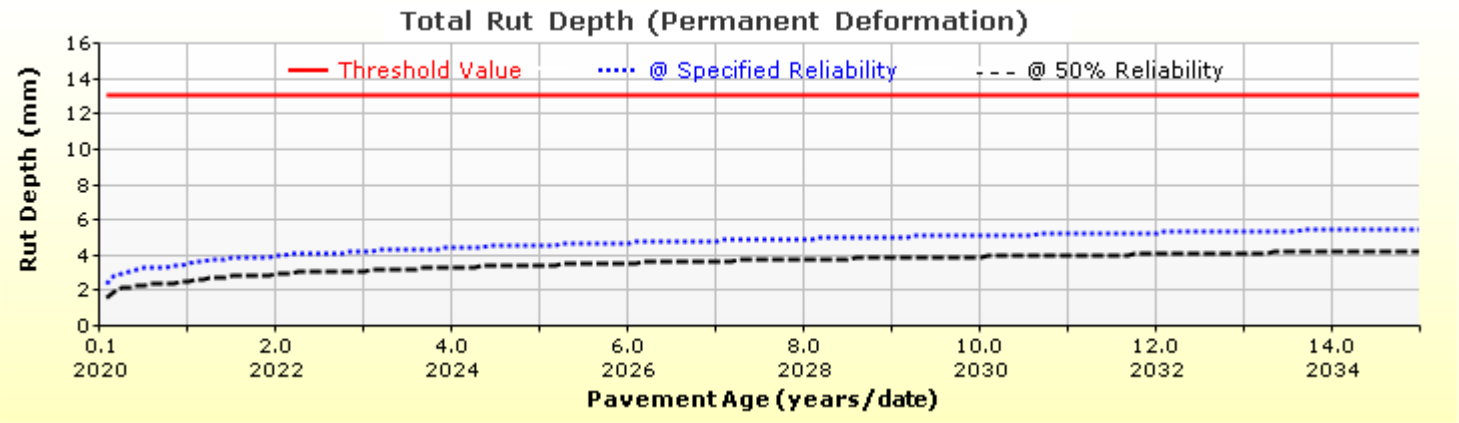

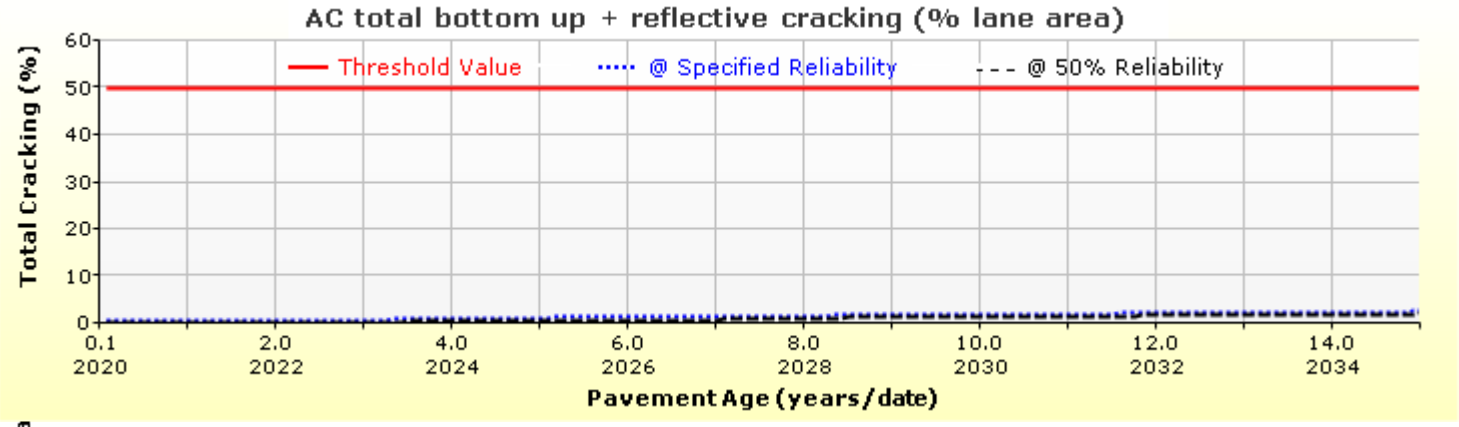

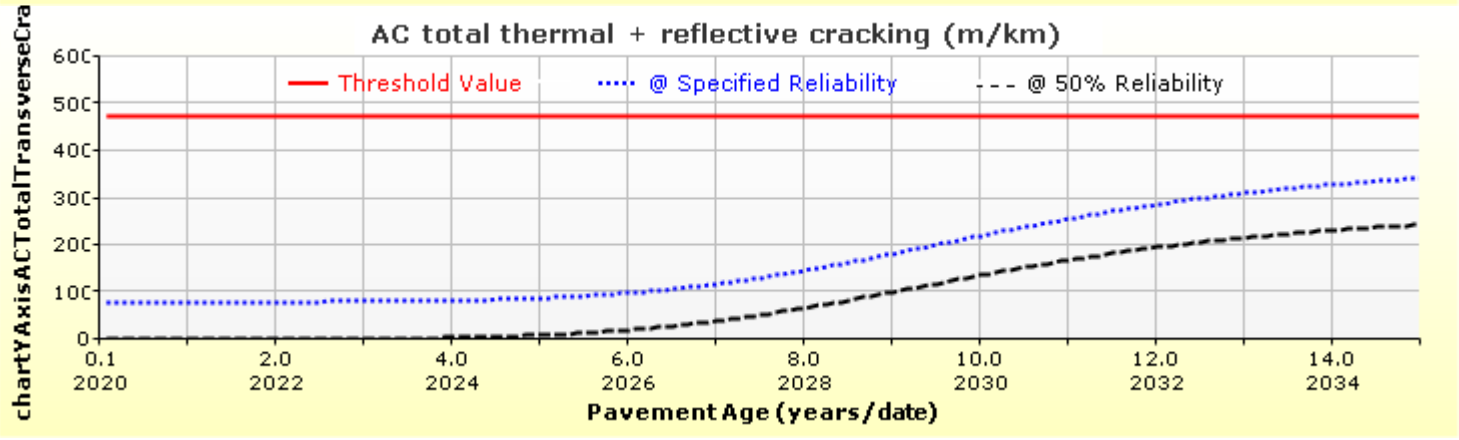

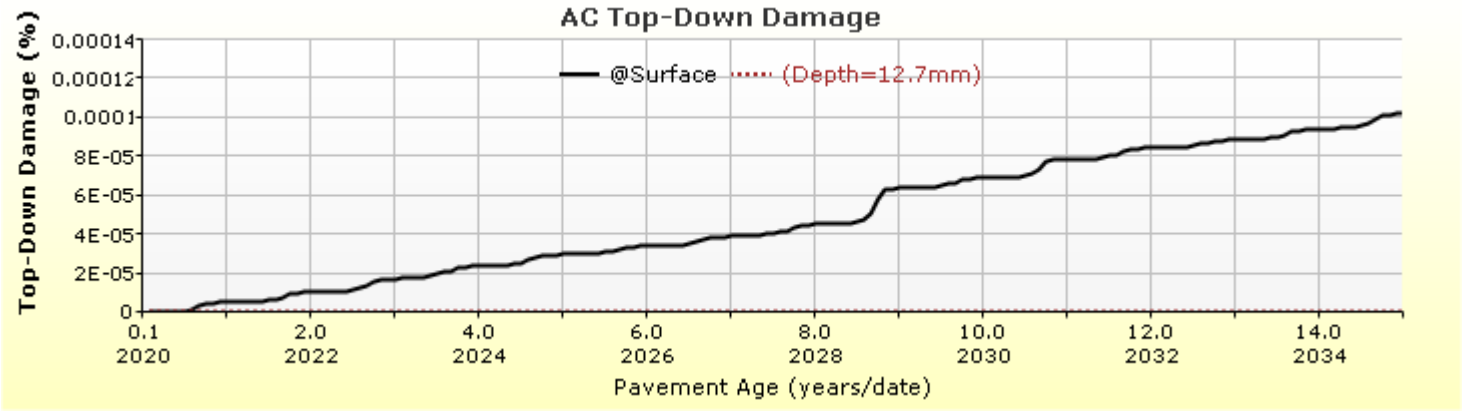
AC Top-Down Damage
Top-Down Damage (%)
0.00014
0.00012
0.0001
8E-05
6E-05
4E-05
2E-05
0
@Surface
(Depth=12.7mm)
0.1
2020
2.0
2022
4.0
2024
6.0
2026
8.0
2028
10.0
2030
12.0
2032
14.0
2034
Pavement Age (years/date)

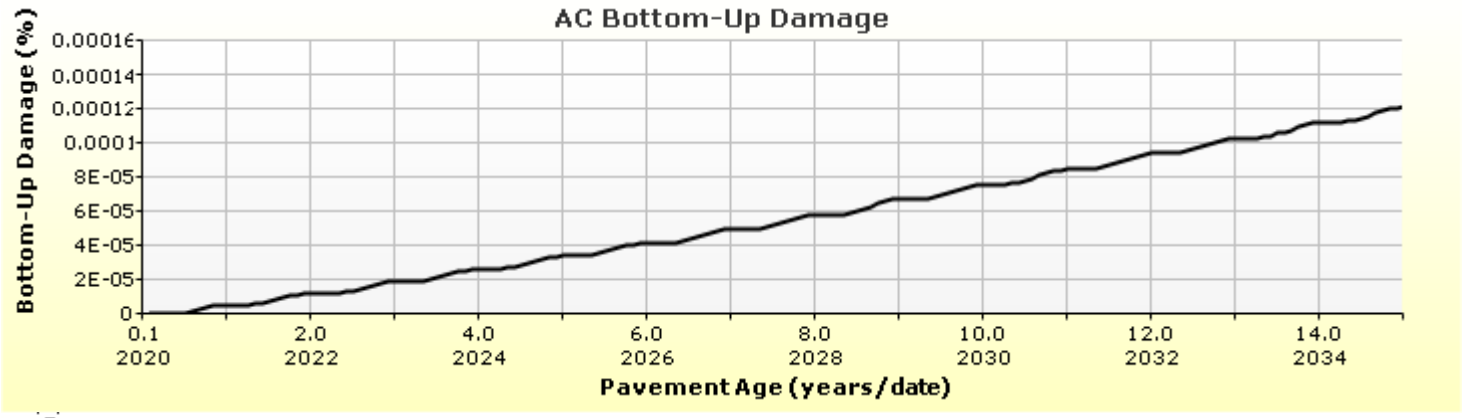
AC Bottom-Up Damage
Bottom-Up Damage (%)
0.00016
0.00014
0.00012
0.0001
8E-05
6E-05
4E-05
2E-05
0
0.1
2020
2.0
2022
4.0
2024
6.0
2026
8.0
2028
10.0
2030
12.0
2032
14.0
2034
Pavement Age (years/date)

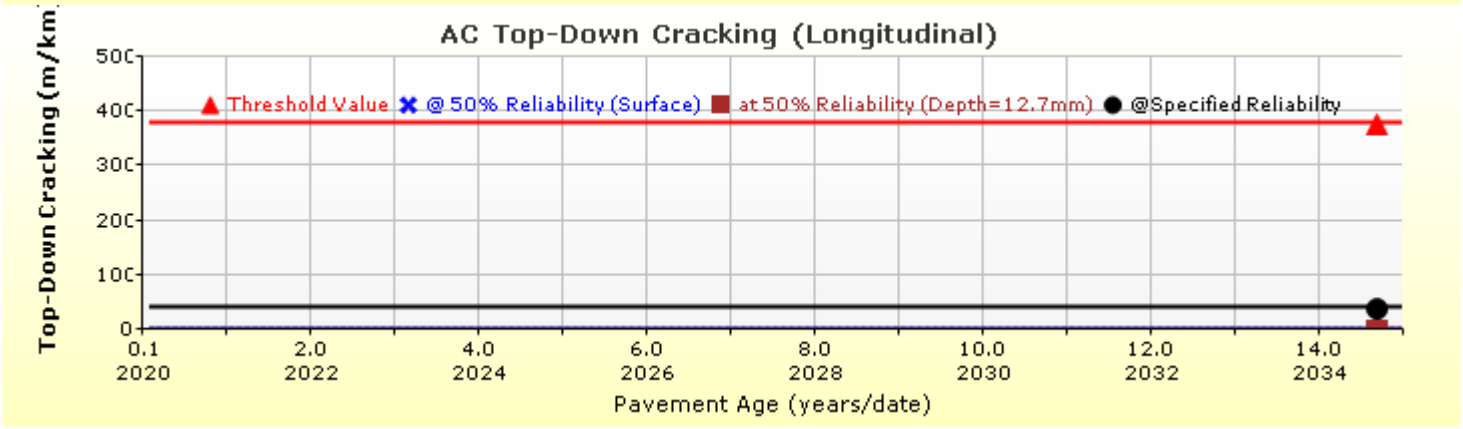
AC Top-Down Cracking (Longitudinal)
Top-Down Cracking (m/km)
500
400
300
200
100
0
Threshold Value
@ 50% Reliability (Surface)
at 50% Reliability (Depth=12.7mm)
@Specified Reliability
0.1
2020
2.0
2022
4.0
2024
6.0
2026
8.0
2028
10.0
2030
12.0
2032
14.0
2034
Pavement Age (years/date)

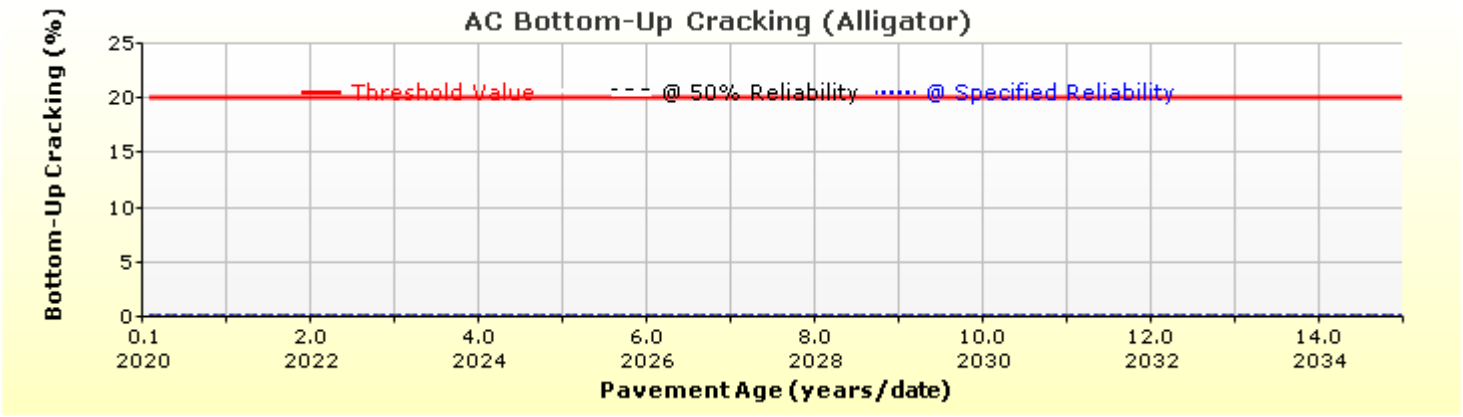
AC Bottom-Up Cracking (Alligator)
Bottom-Up Cracking (%)
25
20
15
10
5
0
Threshold Value
@ 50% Reliability
@ Specified Reliability
0.1
2020
2.0
2022
4.0
2024
6.0
2026
8.0
2028
10.0
2030
12.0
2032
14.0
2034
Pavement Age (years/date)

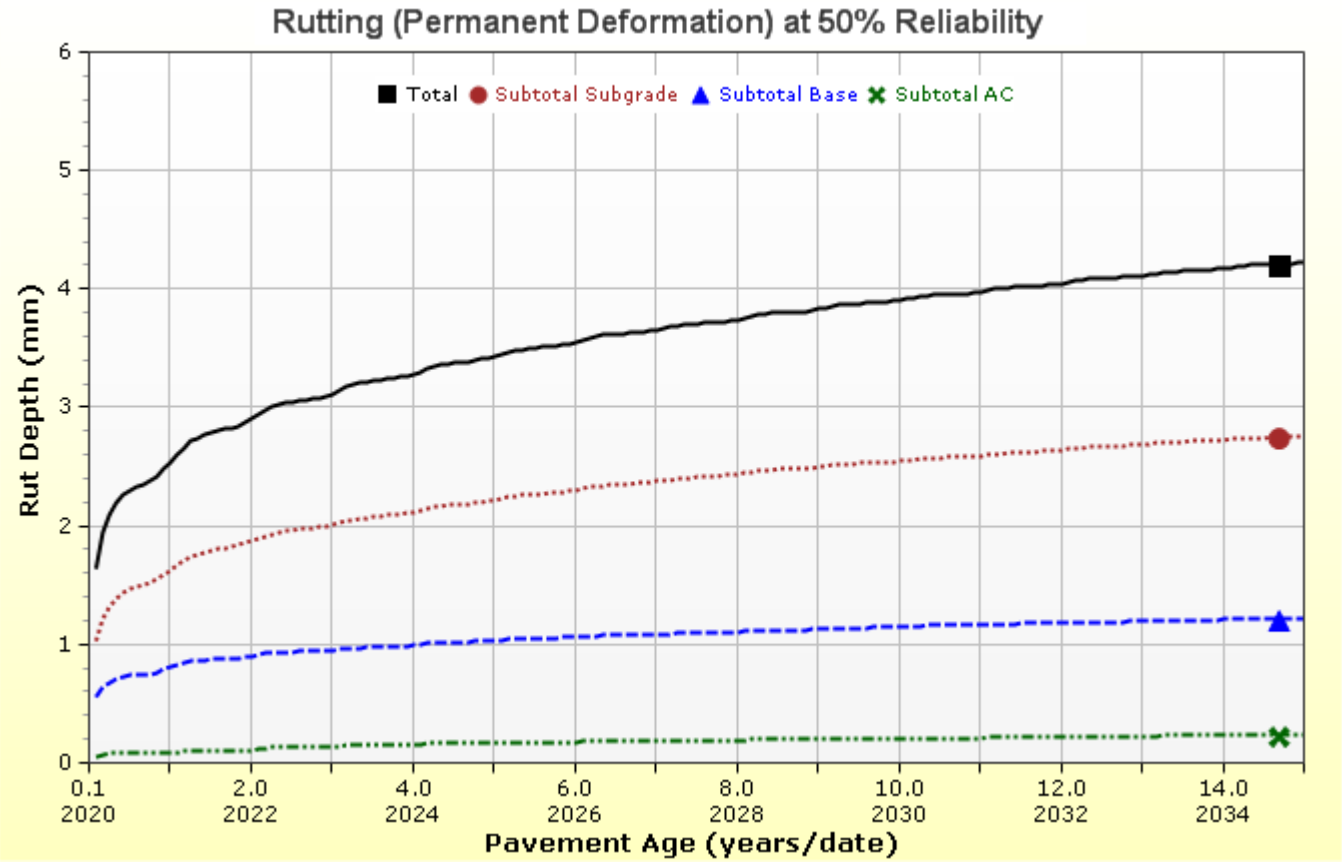
Rutting (Permanent Deformation) at 50% Reliability
Total
Subtotal Subgrade
Subtotal Base
Subtotal AC
Rut Depth (mm)
0
1
2
3
4
5
6
0.1
2020
2.0
2022
4.0
2024
6.0
2026
8.0
2028
10.0
2030
12.0
2032
14.0
2034
Pavement Age (years/date)

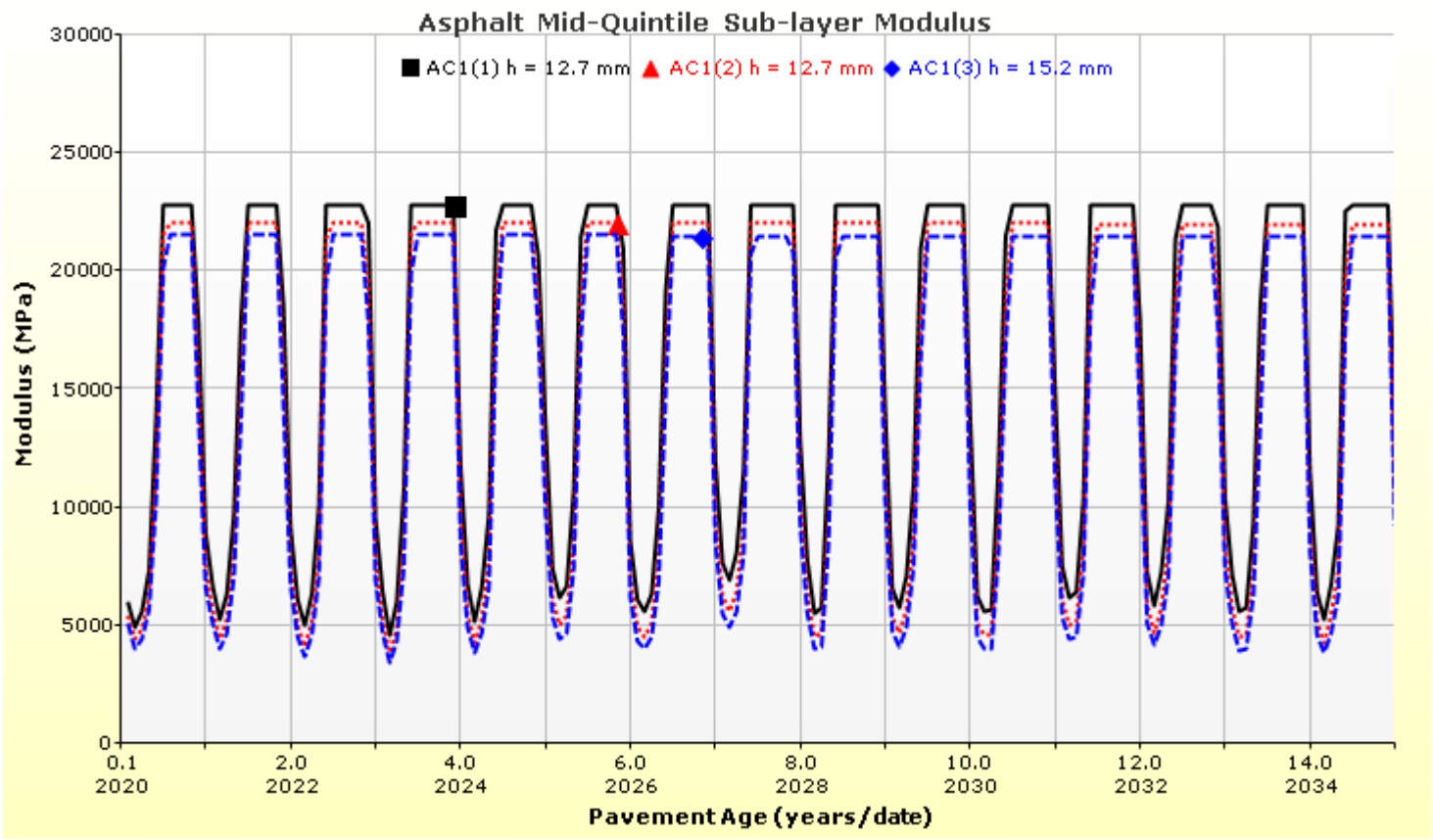
Asphalt Mid-Quintile Sub-layer Modulus
AC1(1) h = 12.7 mm
AC1(2) h = 12.7 mm
AC1(3) h = 15.2 mm
Modulus (MPa)
30000
25000
20000
15000
10000
5000
0
0.1
2020
2.0
2022
4.0
2024
6.0
2026
8.0
2028
10.0
2030
12.0
2032
14.0
2034
Pavement Age (years/date)

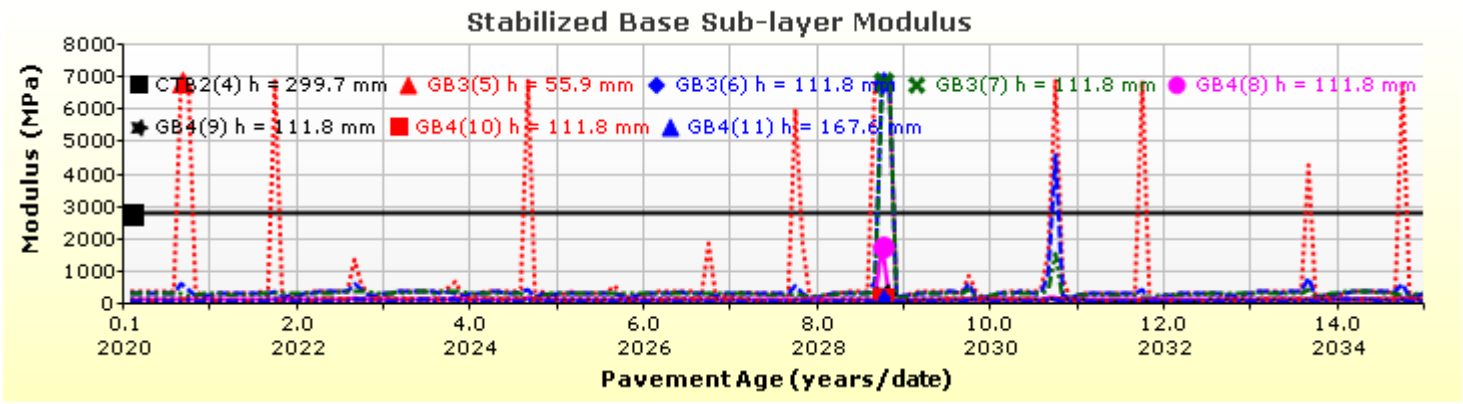
Stabilized Base Sub-layer Modulus
CTB2(4) h = 299.7 mm
GB3(5) h = 55.9 mm
GB3(6) h = 111.8 mm
GB3(7) h = 111.8 mm
GB4(8) h = 111.8 mm
GB4(9) h = 111.8 mm
GB4(10) h = 111.8 mm
GB4(11) h = 167.6 mm
Modulus (MPa)
8000
7000
6000
5000
4000
3000
2000
1000
0
0.1
2020
2.0
2022
4.0
2024
6.0
2026
8.0
2028
10.0
2030
12.0
2032
14.0
2034
Pavement Age (years/date)

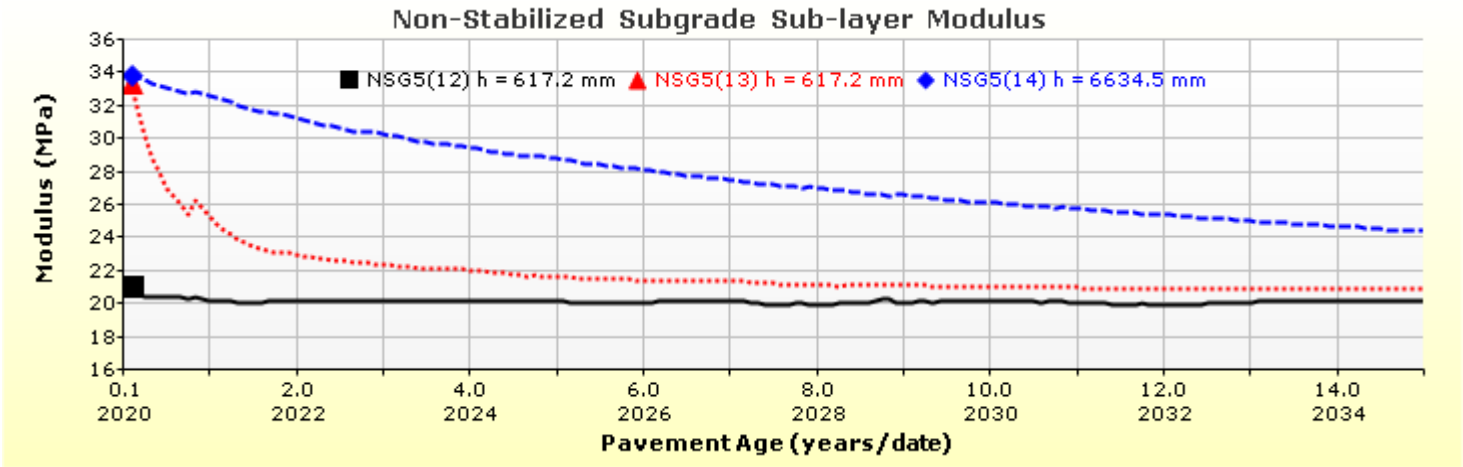
Non-Stabilized Subgrade Sub-layer Modulus
NSG5(12) h = 617.2 mm
NSG5(13) h = 617.2 mm
NSG5(14) h = 6634.5 mm
Modulus (MPa)
36
34
32
30
28
26
24
22
20
18
16
0.1
2020
2.0
2022
4.0
2024
6.0
2026
8.0
2028
10.0
2030
12.0
2032
14.0
2034
Pavement Age (years/date)

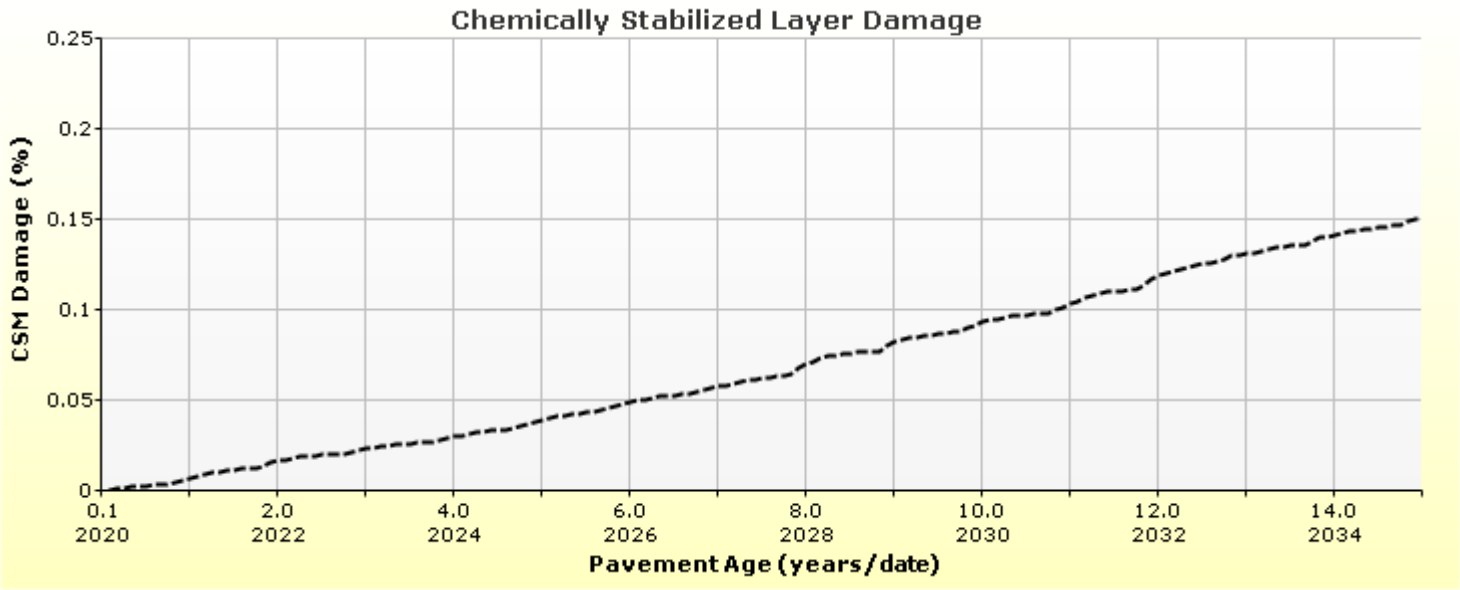
Chemically Stabilized Layer Damage
CSM Damage (%)
0.25
0.2
0.15
0.1
0.05
0
0.1
2020
2.0
2022
4.0
2024
6.0
2026
8.0
2028
10.0
2030
12.0
2032
14.0
2034
Pavement Age (years/date)

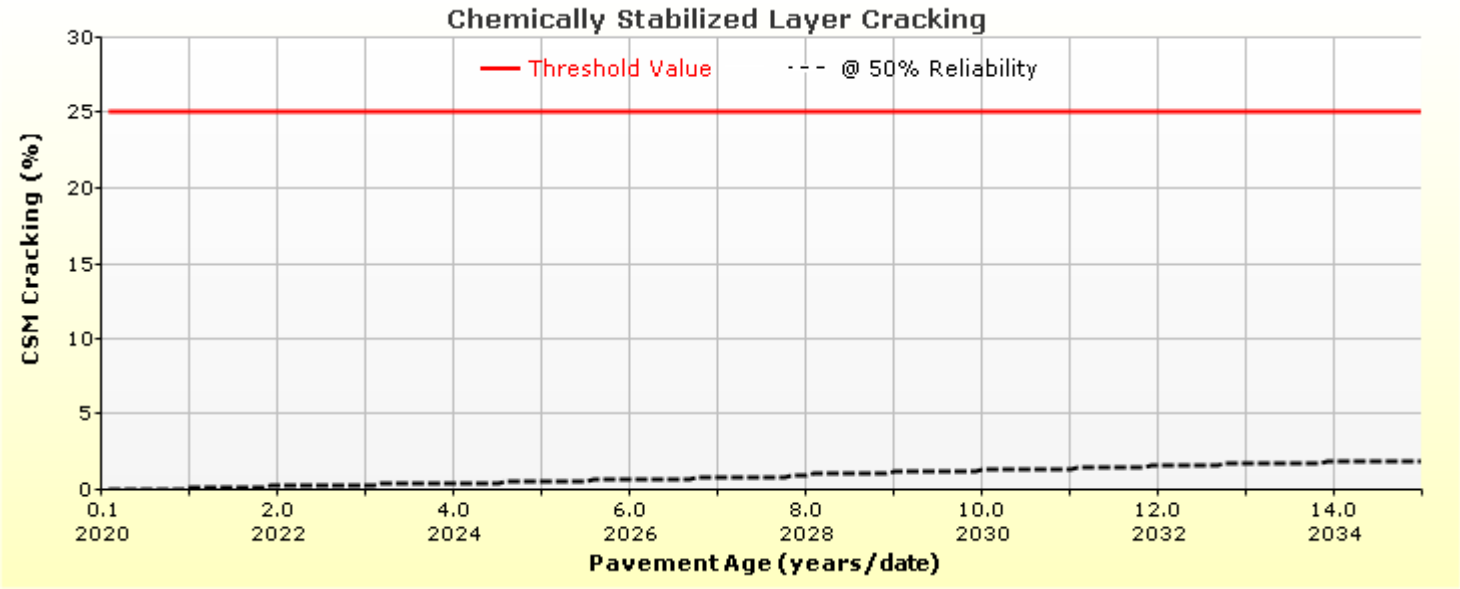
Chemically Stabilized Layer Cracking
Threshold Value
@ 50% Reliability
CSM Cracking (%)
30
25
20
15
10
5
0
0.1
2020
2.0
2022
4.0
2024
6.0
2026
8.0
2028
10.0
2030
12.0
2032
14.0
2034
Pavement Age (years/date)

Layer Information

Layer 1 Flexible : Default asphalt concrete

Asphalt		
Thickness (mm)	40.0	
Unit weight (kgf/m^3)	2460.0	
Poisson's ratio	Is Calculated?	False
	Ratio	0.35
	Parameter A	-
	Parameter B	-

Asphalt Dynamic Modulus (Input Level: 3)

Gradation	Percent Passing
19 mm sieve	100
9.5 mm sieve	77
4.75 mm sieve	60
0.075mm sieve	6

Asphalt Binder

Parameter	Value
Grade	Superpave Performance Grade
Binder Type	64-28
A	10.312
VTS	-3.44

General Info

Name	Value
Reference temperature (°C)	21.1
Effective binder content (%)	11.8
Air voids (%)	7
Thermal conductivity (watt/meter-kelvin)	1.16
Heat capacity (joule/kg-kelvin)	963

Identifiers

Field	Value
Display name/identifier	Default asphalt concrete
Description of object	
Author	
Date Created	9/16/2010 1:00:00 AM
Approver	
Date approved	9/16/2010 1:00:00 AM
State	
District	
County	
Highway	
Direction of Travel	
From station (km)	
To station (km)	
Province	
User defined field 1	
User defined field 2	
User defined field 3	
Revision Number	0

Layer 2 Chemically Stabilized : Soil cement

Semi-Rigid	
Chemically stabilized base crack spacing (m)	8
Chemically stabilized base transverse crack LTE (%)	50
Fatigue LTE (%)	50

Chemically Stabilized	
Layer thickness (mm)	300
Poisson's ratio	0.2
Unit weight (kgf/m^3)	2100

Strength	
Elastic/resilient modulus (MPa)	2834

Thermal	
Heat capacity (joule/kg-kelvin)	1172.3
Thermal conductivity (watt/meter-kelvin)	2.16

Identifiers

Field	Value
Display name/identifier	Soil cement
Description of object	Default material
Author	AASHTO
Date Created	1/1/2011 12:00:00 AM
Approver	
Date approved	1/1/2011 12:00:00 AM
State	
District	
County	
Highway	
Direction of Travel	
From station (km)	
To station (km)	
Province	
User defined field 1	
User defined field 2	
User defined field 3	
Revision Number	0

Layer 3 Non-stabilized Base : Crushed stone

Unbound	
Layer thickness (mm)	280.0
Poisson's ratio	0.35
Coefficient of lateral earth pressure (k0)	0.5

Modulus (Input Level: 3)

Analysis Type:	Modify input values by temperature/moisture
Method:	Resilient Modulus (MPa)

Resilient Modulus (MPa)
250.0

Use Correction factor for NDT modulus?	-
NDT Correction Factor:	-

Identifiers

Field	Value
Display name/identifier	Crushed stone
Description of object	Default material
Author	AASHTO
Date Created	1/1/2011 12:00:00 AM
Approver	
Date approved	1/1/2011 12:00:00 AM
State	
District	
County	
Highway	
Direction of Travel	
From station (km)	
To station (km)	
Province	
User defined field 1	
User defined field 2	
User defined field 3	
Revision Number	0

Sieve

Liquid Limit	6.0
Plasticity Index	1.0
Is layer compacted?	False

	Is User Defined?	Value
Maximum dry unit weight (kgf/m^3)	False	2048.3
Saturated hydraulic conductivity (m/hr)	False	2.257e-02
Specific gravity of solids	False	2.7
Water Content (%)	False	7

User-defined Soil Water Characteristic Curve (SWCC)	
Is User Defined?	False
af	3.0919
bf	2.6074
cf	0.7701
hr	110.0000

Sieve Size	% Passing
0.001mm	
0.002mm	
0.020mm	
0.075mm	5.0
0.150mm	
0.180mm	
0.250mm	
0.300mm	13.5
0.425mm	
0.600mm	
0.850mm	
1.18mm	27.5
2.0mm	
2.36mm	
4.75mm	45.0
9.5mm	61.5
12.5mm	
19.0mm	92.5
25.0mm	100.0
37.5mm	
50.0mm	
63.0mm	
75.0mm	
90.0mm	

Layer 4 Non-stabilized Base : Crushed gravel

Unbound	
Layer thickness (mm)	500.0
Poisson's ratio	0.35
Coefficient of lateral earth pressure (k0)	0.5

Modulus (Input Level: 3)

Analysis Type:	Modify input values by temperature/moisture
Method:	Resilient Modulus (MPa)

Resilient Modulus (MPa)
150.0

Use Correction factor for NDT modulus?	-
NDT Correction Factor:	-

Identifiers

Field	Value
Display name/identifier	Crushed gravel
Description of object	Default material
Author	AASHTO
Date Created	1/1/2011 12:00:00 AM
Approver	
Date approved	1/1/2011 12:00:00 AM
State	
District	
County	
Highway	
Direction of Travel	
From station (km)	
To station (km)	
Province	
User defined field 1	
User defined field 2	
User defined field 3	
Revision Number	0

Sieve

Liquid Limit	11.0
Plasticity Index	1.0
Is layer compacted?	False

	Is User Defined?	Value
Maximum dry unit weight (kgf/m^3)	False	2012.4
Saturated hydraulic conductivity (m/hr)	False	6.883e-03
Specific gravity of solids	False	2.7
Water Content (%)	False	8.2

User-defined Soil Water Characteristic Curve (SWCC)	
Is User Defined?	False
af	5.0935
bf	2.5668
cf	0.8576
hr	108.0000

Sieve Size	% Passing
0.001mm	
0.002mm	
0.020mm	
0.075mm	4.0
0.150mm	
0.180mm	
0.250mm	
0.300mm	33.5
0.425mm	
0.600mm	
0.850mm	
1.18mm	55.0
2.0mm	
2.36mm	
4.75mm	60.0
9.5mm	
12.5mm	
19.0mm	
25.0mm	75.0
37.5mm	
50.0mm	
63.0mm	
75.0mm	
90.0mm	

Layer 5 Subgrade : A-6

Unbound	
Layer thickness (mm)	Semi-infinite
Poisson's ratio	0.35
Coefficient of lateral earth pressure (k0)	0.5

Modulus (Input Level: 3)

Analysis Type:	Modify input values by temperature/moisture
Method:	Resilient Modulus (MPa)

Resilient Modulus (MPa)
35.0

Use Correction factor for NDT modulus?	-
NDT Correction Factor:	-

Identifiers

Field	Value
Display name/identifier	A-6
Description of object	Default material
Author	AASHTO
Date Created	1/1/2011 12:00:00 AM
Approver	
Date approved	1/1/2011 12:00:00 AM
State	
District	
County	
Highway	
Direction of Travel	
From station (km)	
To station (km)	
Province	
User defined field 1	
User defined field 2	
User defined field 3	
Revision Number	0

Sieve

Liquid Limit	42.0
Plasticity Index	15.0
Is layer compacted?	False

	Is User Defined?	Value
Maximum dry unit weight (kgf/m^3)	False	1693.8
Saturated hydraulic conductivity (m/hr)	False	3.012e-06
Specific gravity of solids	False	2.7
Water Content (%)	False	18.2

User-defined Soil Water Characteristic Curve (SWCC)	
Is User Defined?	False
af	114.8407
bf	0.6389
cf	0.1739
hr	500.0000

Sieve Size	% Passing
0.001mm	
0.002mm	25.0
0.020mm	
0.075mm	82.0
0.150mm	
0.180mm	91.0
0.250mm	
0.300mm	
0.425mm	95.0
0.600mm	
0.850mm	
1.18mm	
2.0mm	98.0
2.36mm	
4.75mm	100.0
9.5mm	100.0
12.5mm	100.0
19.0mm	100.0
25.0mm	100.0
37.5mm	
50.0mm	
63.0mm	
75.0mm	
90.0mm	100.0

Calibration Coefficients

AC Fatigue

$$N_f = 0.00432 * C * \beta_{f1} k_1 \left(\frac{1}{\varepsilon_1}\right)^{k_2 \beta_{f2}} \left(\frac{1}{E}\right)^{k_3 \beta_{f3}}$$

$$C = 10^M$$

$$M = 4.84\left(\frac{V_b}{V_a + V_b} - 0.69\right)$$

k1: 3.75	
k2: 2.87	
k3: 1.46	
Bf1: 0.02054	
Bf2: 1.38	
Bf3: 0.88	

AC Rutting

$$\frac{\varepsilon_p}{\varepsilon_r} = k_z \beta_{r1} 10^{k_1 T^{k_2 \beta_{r2}} N^{k_3 \beta_{r3}}}$$

$$k_z = (C_1 + C_2 * depth) * 0.328196^{depth}$$

$$C_1 = -0.1039 * H_{ac}^2 + 2.4868 * H_{ac} - 17.342$$

$$C_2 = 0.0172 * H_{ac}^2 - 1.7331 * H_{ac} + 27.428$$

Where:

$H_{ac} = total\ AC\ thickness(in)$

$\varepsilon_p = plastic\ strain\left({}^{in}/_{in}\right)$

$\varepsilon_r = resilient\ strain\left({}^{in}/_{in}\right)$

$T = layer\ temperature(^{\circ}F)$

$N = number\ of\ load\ repetitions$

AC Rutting Standard Deviation	0.24 * Pow(RUT,0.8026) + 0.001	
AC Layer 1	K1:-2.45 K2:3.01 K3:0.22	Br1:0.128 Br2:0.52 Br3:1.36

Thermal Fracture

$$C_f = 400 * N\left(\frac{\log C / h_{ac}}{\sigma}\right)$$

$$\Delta C = (k * \beta t)^{n+1} * A * \Delta K^n$$

$$A = 10^{(4.389 - 2.52 * \log(E * \sigma_m * n))}$$

$C_f = observed\ amount\ of\ thermal\ cracking(ft/500ft)$
$k = refression\ coefficient\ determined\ through\ field\ calibration$
$N(\,) = standard\ normal\ distribution\ evaluated\ at(\,)$
$\sigma = standard\ deviation\ of\ the \log\ of\ the\ depth\ of\ cracks\ in\ the\ pavments$
$C = crack\ depth(in)$
$h_{ac} = thickness\ of\ asphalt\ layer(in)$
$\Delta C = Change\ in\ the\ crack\ depth\ due\ to\ a\ cooling\ cycle$
$\Delta K = Change\ in\ the\ stress\ intensity\ factor\ due\ to\ a\ cooling\ cycle$
$A, n = Fracture\ parameters\ for\ the\ asphalt\ mixture$
$E = mixture\ stiffness$
$\sigma_M = Undamaged\ mixture\ tensile\ strength$
$\beta_t = Calibration\ parameter$

Level 1 K: ((3 * Pow(10,-7)) * Pow(MAAT,4.0319)) * 1 + 0	
Level 2 K: ((3 * Pow(10,-7)) * Pow(MAAT,4.0319)) * 1 + 0	
Level 3 K: ((3 * Pow(10,-7)) * Pow(MAAT,4.0319)) * 1 + 0	

CSM Fatigue

$$N_f = 10^{\left(\frac{k_1 \beta_{c1} \left(\frac{\sigma_s}{M_r}\right)}{k_2 \beta_{c2}}\right)}$$

$N_f = number\ of\ repetitions\ to\ fatigue\ cracking$
$\sigma_s = Tensile\ stress(psi)$
$M_r = modulus\ of\ rupture(psi)$

k1: 0.972	k2: 0.0825	Bc1: 1	Bc2:1

Unbound Layer Rutting

$$\delta_a(N) = \beta_{s_1} k_1 \varepsilon_v h \left(\frac{\varepsilon_0}{\varepsilon_r}\right) \left| e^{-\left(\frac{\rho}{N}\right)^{\beta}} \right|$$

$\delta_a = permanent\ deformation\ for\ the\ layer$
$N = number\ of\ repetitions$
$\varepsilon_v = average\ veritcal\ strain(in/in)$
$\varepsilon_0, \beta, \rho = material\ properties$
$\varepsilon_r = resilient\ strain(in/in)$

Base Rutting		Subgrade Rutting	
k1: 0.965	Bs1: 1	k1: 0.675	Bs1: 1
Standard Deviation (BASERUT) 0.1477 * Pow(BASERUT,0.6711) + 0.001		Standard Deviation (BASERUT) 0.1235 * Pow(SUBRUT,0.5012) + 0.001	

AC Cracking

AC Top Down Cracking

$$FC_{top} = \left(\frac{C_4}{1 + e^{(C_1 - C_2 * log_{10}(Damage))}}\right) * 10.56$$

c1: 7	c2: 3.5	c3: 0	c4: 1000

Top down AC Cracking Standard Deviation

200 + 2300/(1+exp(1.072-2.1654*LOG10(TOP+0.0001)))

AC Bottom Up Cracking

$$FC = \left(\frac{6000}{1 + e^{(C_1 * C_1' + C_2 * C_2' log_{10}(D * 100))}}\right) * \left(\frac{1}{60}\right)$$

$$C_2' = -2.40874 - 39.748 * (1 + h_{ac})^{-2.856}$$

$$C_1' = -2 * C_2'$$

c1: 1.31	c2: 2.1585	c3: 6000

Bottom up AC Cracking Standard Deviation

1.13 + 13/(1+exp(7.57-15.5*LOG10(BOTTOM+0.0001)))

CSM Cracking

$$FC_{ctb} = C_1 + \frac{C_2}{1 + e^{C_3 - C_4 * log_{10}(Damage)}}$$

C1: 0	C2: 75	C3: 2	C4: 2

CSM Standard Deviation

CTB*1

IRI Flexible Pavements

C1 - Rutting
C2 - Fatigue Crack
C3 - Transverse Crack
C4 - Site Factors

C1: 55	C2: 0.4	C3: 0.008	C4: 0.015

Reflective Cracking

$$\Delta C = k_1 \Delta_{bending} + k_2 \Delta_{shaering} + k_3 \Delta_{thermal}$$

$$\Delta D = \frac{C_1 k_1 \Delta_{bending} + C_2 k_2 \Delta_{shearing} + C_3 k_3 \Delta_{thermal}}{h_{OL}}$$

$$\Delta_{Bending} = A(SIF)_B^n$$

$$\Delta_{Shearing} = A(SIF)_S^n$$

$$\Delta_{Thermal} = A(SIF)_T^n$$

$$D = \sum_{i=1}^{N} \Delta D$$

$$RCR = \left(\frac{100}{C4 + e^{C5 \log D}}\right) * EX\_CRK$$

Where

ΔC	=	Crack length increment, in
ΔD	=	Incremental damage ratio
$k_1, k_2, k_3, C_1, C_2, C_3, C_4, C_5$	=	Calibration factors (local and global)
$\Delta_{bending}, \Delta_{shearing}, \Delta_{thermal}$	=	Crack length increments caused by bending, shearing, and thermal loading
A, n	=	HMA material fracture properties
N	=	Total number of days
$(SIF)_B, (SIF)_S, (SIF)_T$	=	Stress intensity factors caused by bending, shearing, and thermal loading
D	=	Damage ratio
h_{OL}	=	Overlay thickness, in
RCR	=	Cracks in the underlying layers reflected, %
EX_CRK	=	Transverse cracking in underlying pavement layers, ft/mile (transverse cracking) Alligator cracking in underlying pavement layers, % lane area (alligator cracking)

Pavement Type	Distress Type	k1	k2	k3	C1	C2	C3	C4	C5	Standard Deviation
Semi-Rigid	Transverse	0.45	0.05	1	0.1	0.9809	0.19	165.3	-5.1048	0.000027 * Pow (TRANSVERSE,2.1187) + 399.9
Semi-Rigid	Fatigue	0.45	0.05	1	1.64	1.1	0.19	62.1	-404.6	1.3897 * Pow (FATIGUE,0.2960) + 0.4212

Semi-Rigid Pavement_FDR+HRB2__ONTARIO

File Name: C:\Users\admin\Desktop\Eskedil_ME\Kossuth\Semi-Rigid Pavement_FDR+HRB2__ONTARIO.dgpx

Design Inputs

Design Life: 15 years
Design Type: SEMI_RIGID

Base construction: May, 2020
Pavement construction: June, 2020
Traffic opening: June, 2020

Climate Data Sources (Lat/Lon): 43.5, -80.625; 43, -80

Design Structure

Layer type	Material Type	Thickness(mm)
Flexible	Default asphalt concrete	40.0
Cement_Base	Soil cement	300.0
NonStabilized	Crushed stone	280.0
NonStabilized	Crushed gravel	500.0
Subgrade	A-6	Semi-infinite

Volumetric at Construction:	
Effective binder content (%)	11.8
Air voids (%)	7.0

Traffic

Age (year)	Heavy Trucks (cumulative)
2020 (initial)	1,272
2027 (7 years)	1,721,680
2035 (15 years)	3,794,600

Design Outputs

Distress Prediction Summary

Distress Type	Distress @ Specified Reliability		Reliability (%)		Criterion Satisfied?
	Target	Predicted	Target	Achieved	
Terminal IRI (m/km)	2.30	2.04	85.00	94.80	Pass
Permanent deformation - total pavement (mm)	13.00	5.50	85.00	100.00	Pass
AC total fatigue cracking: bottom up + reflective (% lane area)	50.00	1.98	85.00	100.00	Pass
AC total transverse cracking: thermal + reflective (m/km)	473.40	340.46	85.00	99.25	Pass
AC bottom-up fatigue cracking (percent)	20.00	0.00	50.00	100.00	Pass
AC thermal cracking (m/km)	190.00	0.19	50.00	100.00	Pass
AC top-down fatigue cracking (m/km)	380.00	39.32	85.00	100.00	Pass
Permanent deformation - AC only (mm)	6.00	0.42	85.00	100.00	Pass
Chemically stabilized layer - fatigue fracture (percent)	25.00	1.54	-	-	-

Distress Charts

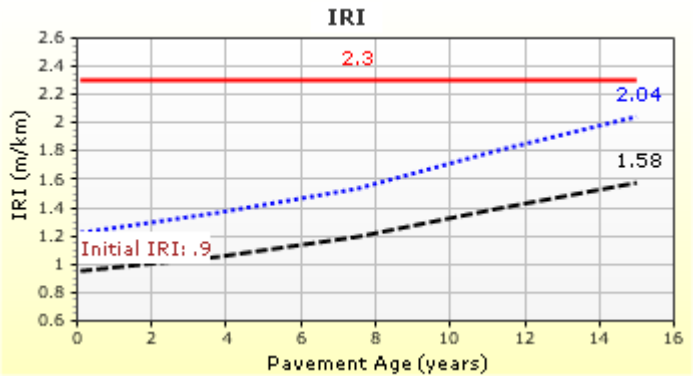

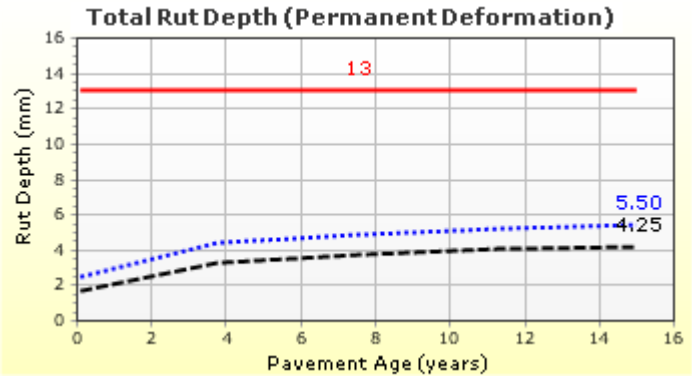

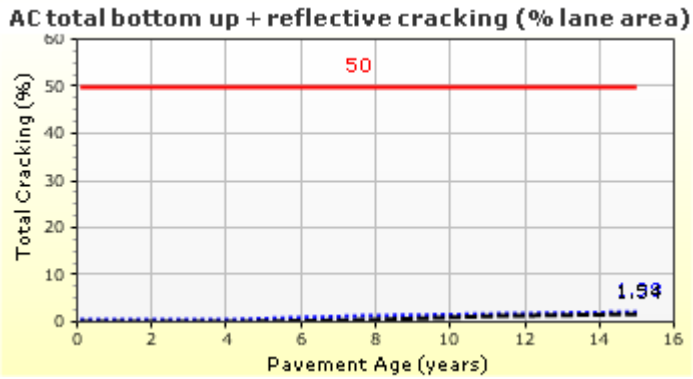

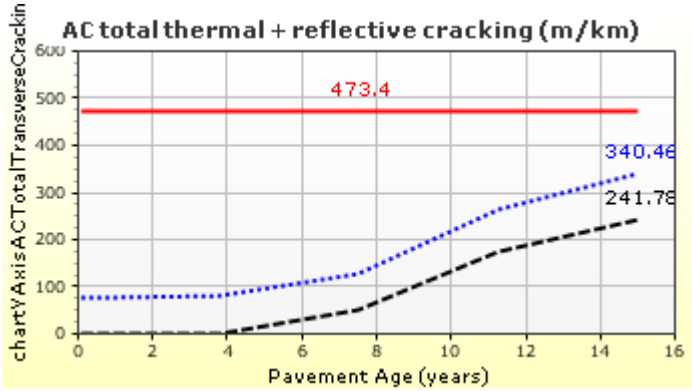

Traffic Inputs

Graphical Representation of Traffic Inputs

Initial two-way AADTT:	1,272	Percent of trucks in design direction (%):	50.0
Number of lanes in design direction:	2	Percent of trucks in design lane (%):	90.0
		Operational speed (kph)	100.0

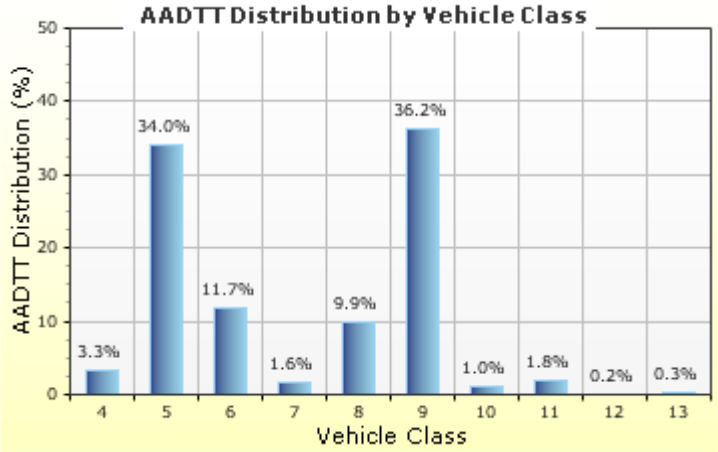

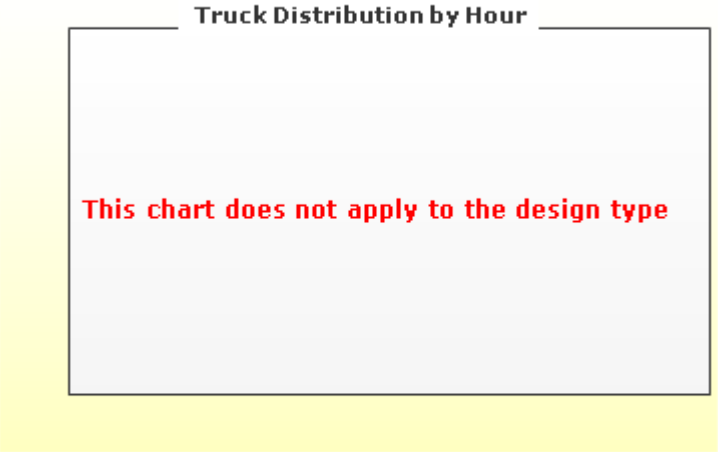

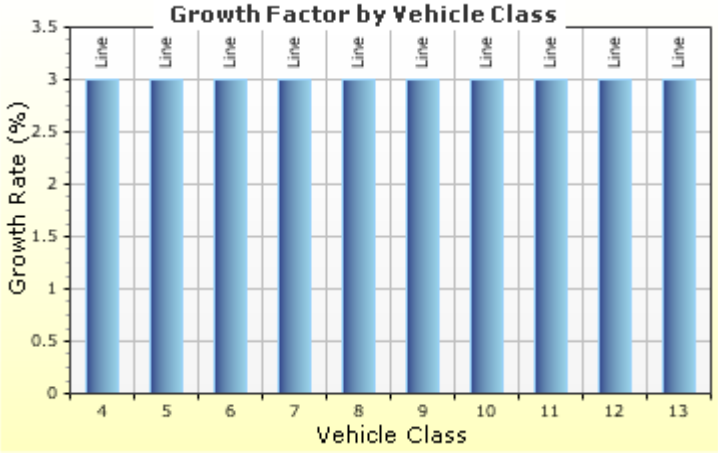

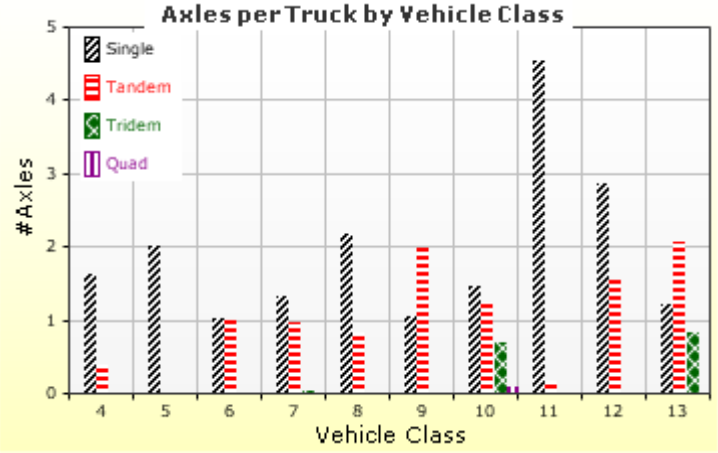

Traffic Volume Monthly Adjustment Factors

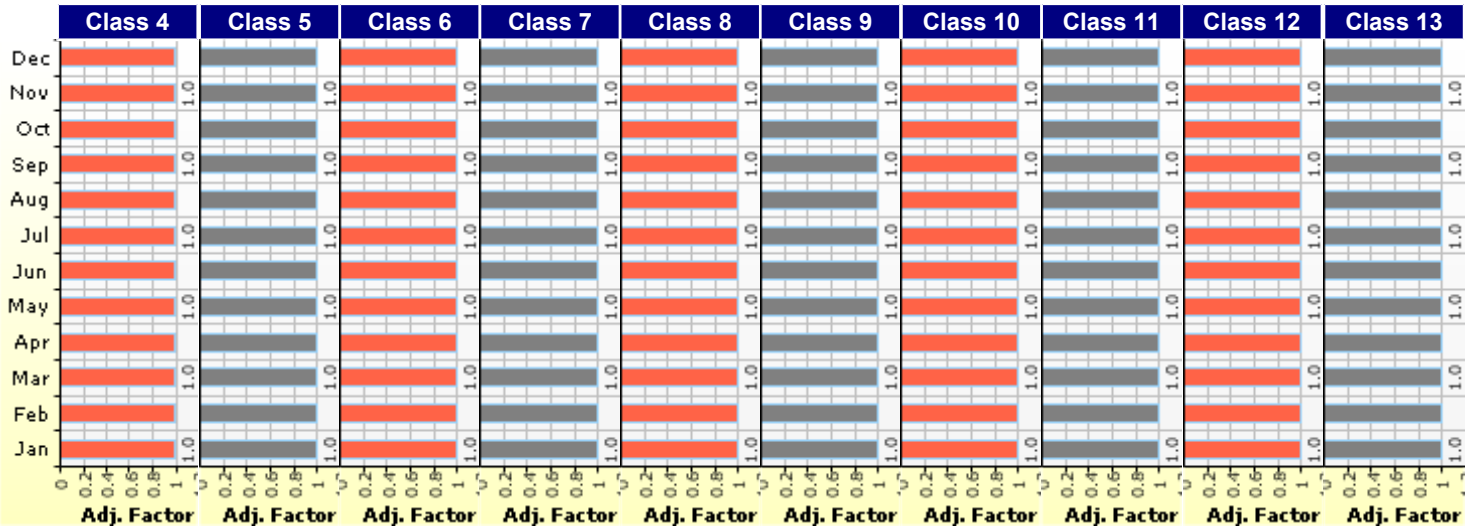

Tabular Representation of Traffic Inputs

Volume Monthly Adjustment Factors

Level 3: Default MAF

Month	Vehicle Class									
	4	5	6	7	8	9	10	11	12	13
January	1.0	1.0	1.0	1.0	1.0	1.0	1.0	1.0	1.0	1.0
February	1.0	1.0	1.0	1.0	1.0	1.0	1.0	1.0	1.0	1.0
March	1.0	1.0	1.0	1.0	1.0	1.0	1.0	1.0	1.0	1.0
April	1.0	1.0	1.0	1.0	1.0	1.0	1.0	1.0	1.0	1.0
May	1.0	1.0	1.0	1.0	1.0	1.0	1.0	1.0	1.0	1.0
June	1.0	1.0	1.0	1.0	1.0	1.0	1.0	1.0	1.0	1.0
July	1.0	1.0	1.0	1.0	1.0	1.0	1.0	1.0	1.0	1.0
August	1.0	1.0	1.0	1.0	1.0	1.0	1.0	1.0	1.0	1.0
September	1.0	1.0	1.0	1.0	1.0	1.0	1.0	1.0	1.0	1.0
October	1.0	1.0	1.0	1.0	1.0	1.0	1.0	1.0	1.0	1.0
November	1.0	1.0	1.0	1.0	1.0	1.0	1.0	1.0	1.0	1.0
December	1.0	1.0	1.0	1.0	1.0	1.0	1.0	1.0	1.0	1.0

Distributions by Vehicle Class

Truck Distribution by Hour does not apply

Vehicle Class	AADTT Distribution (%) (Level 3)	Growth Factor	
		Rate (%)	Function
Class 4	3.3%	3%	Linear
Class 5	34%	3%	Linear
Class 6	11.7%	3%	Linear
Class 7	1.6%	3%	Linear
Class 8	9.9%	3%	Linear
Class 9	36.2%	3%	Linear
Class 10	1%	3%	Linear
Class 11	1.8%	3%	Linear
Class 12	0.2%	3%	Linear
Class 13	0.3%	3%	Linear

Axle Configuration

Traffic Wander	
Mean wheel location (mm)	460.0
Traffic wander standard deviation (mm)	254.0
Design lane width (m)	3.7

Axle Configuration	
Average axle width (m)	2.6
Dual tire spacing (mm)	305.0
Tire pressure (kPa)	827.4

Average Axle Spacing	
Tandem axle spacing (m)	1.5
Tridem axle spacing (m)	1.7
Quad axle spacing (m)	1.3

Wheelbase does not apply

Number of Axles per Truck

Vehicle Class	Single Axle	Tandem Axle	Tridem Axle	Quad Axle
Class 4	1.62	0.39	0	0
Class 5	2	0	0	0
Class 6	1.01	0.993	0	0
Class 7	1.314	0.989	0.03	0
Class 8	2.163	0.845	0	0
Class 9	1.055	1.968	0.003	0
Class 10	1.446	1.234	0.7	0.088
Class 11	4.546	0.168	0	0
Class 12	2.857	1.526	0	0
Class 13	1.201	2.058	0.848	0.024

AADTT (Average Annual Daily Truck Traffic) Growth

*** Traffic cap is not enforced**

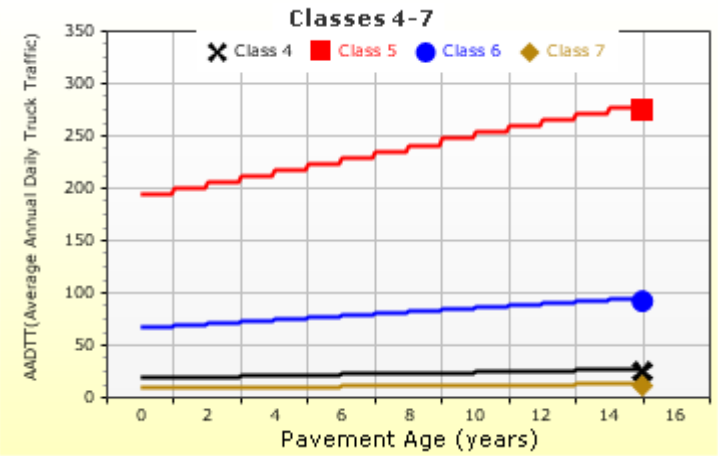

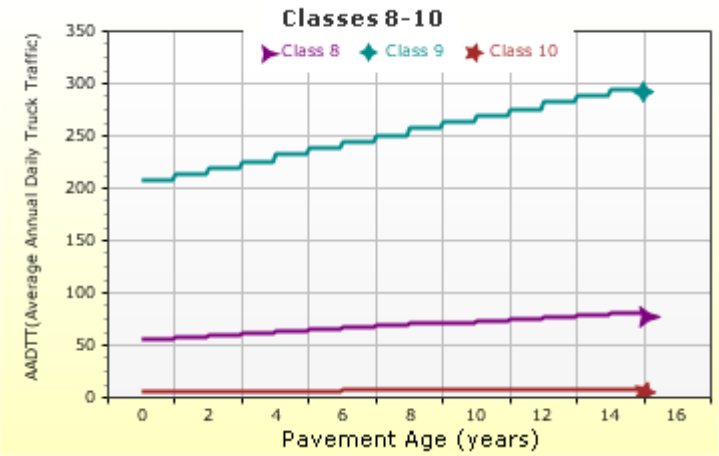

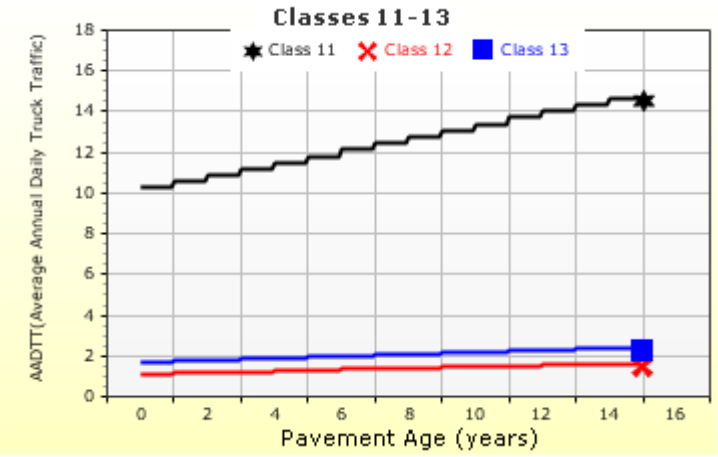

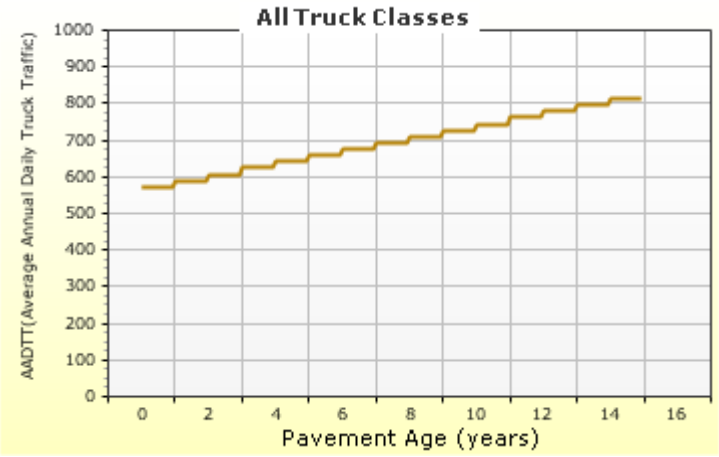

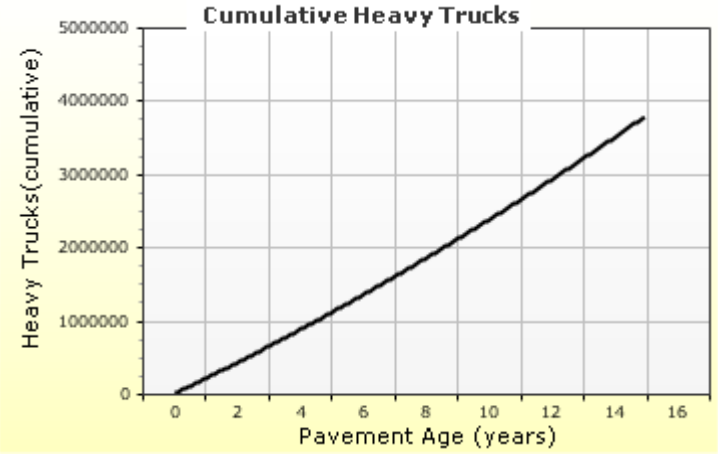

Climate Inputs

Climate Data Sources:

Climate Station Cities:	Location (lat lon elevation(m))
CA, ON	43.50000 -80.62500 369
CA, ON	43.00000 -80.00000 210

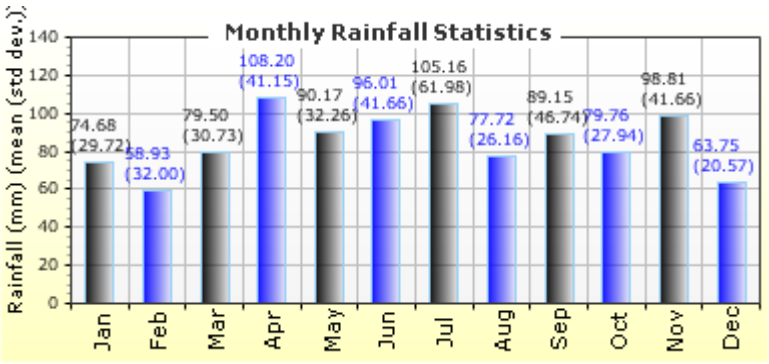

Annual Statistics:

Mean annual air temperature (°C)	7.96
Mean annual precipitation (mm)	1022.60
Freezing index (°C - days)	521.04
Average annual number of freeze/thaw cycles:	80.61

Water table depth (m)	10.00

Monthly Climate Summary:

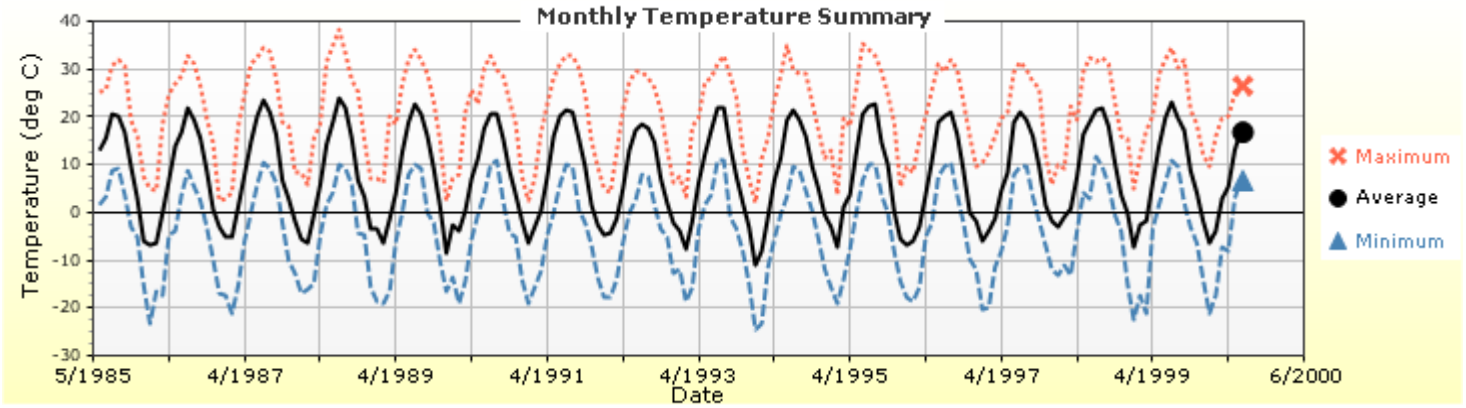

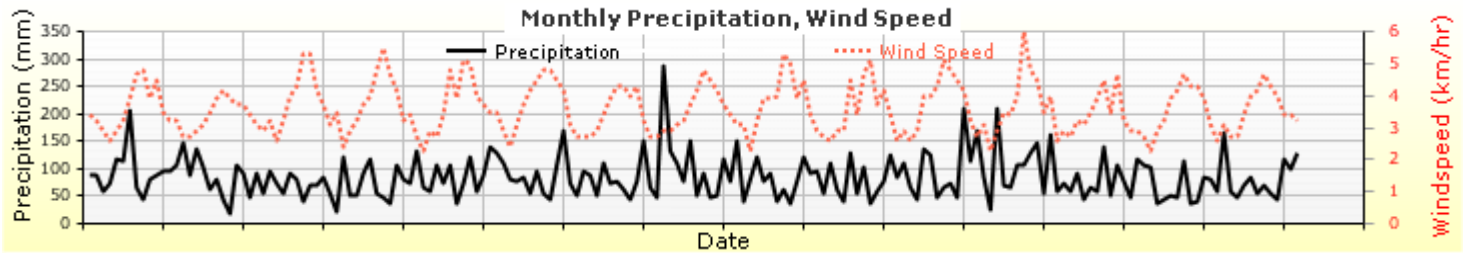

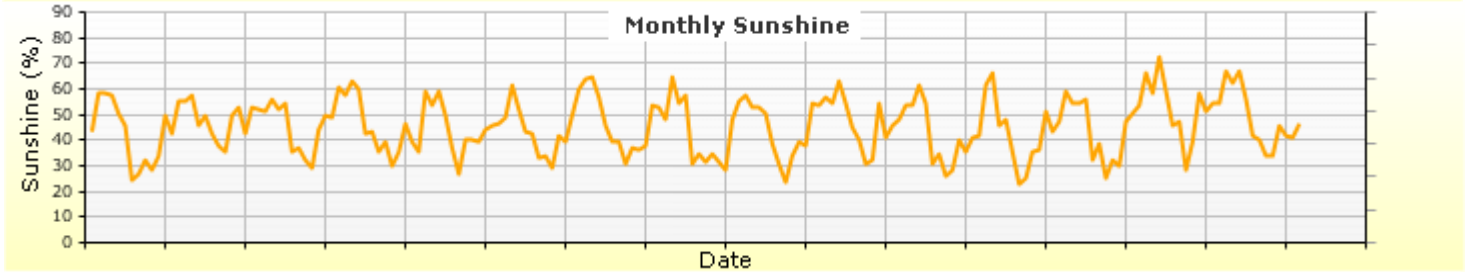

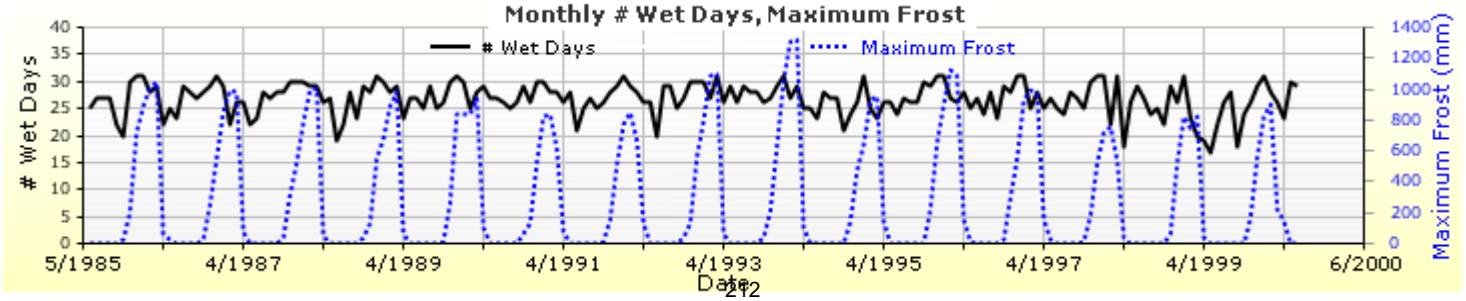

Hourly Air Temperature Distribution by Month:

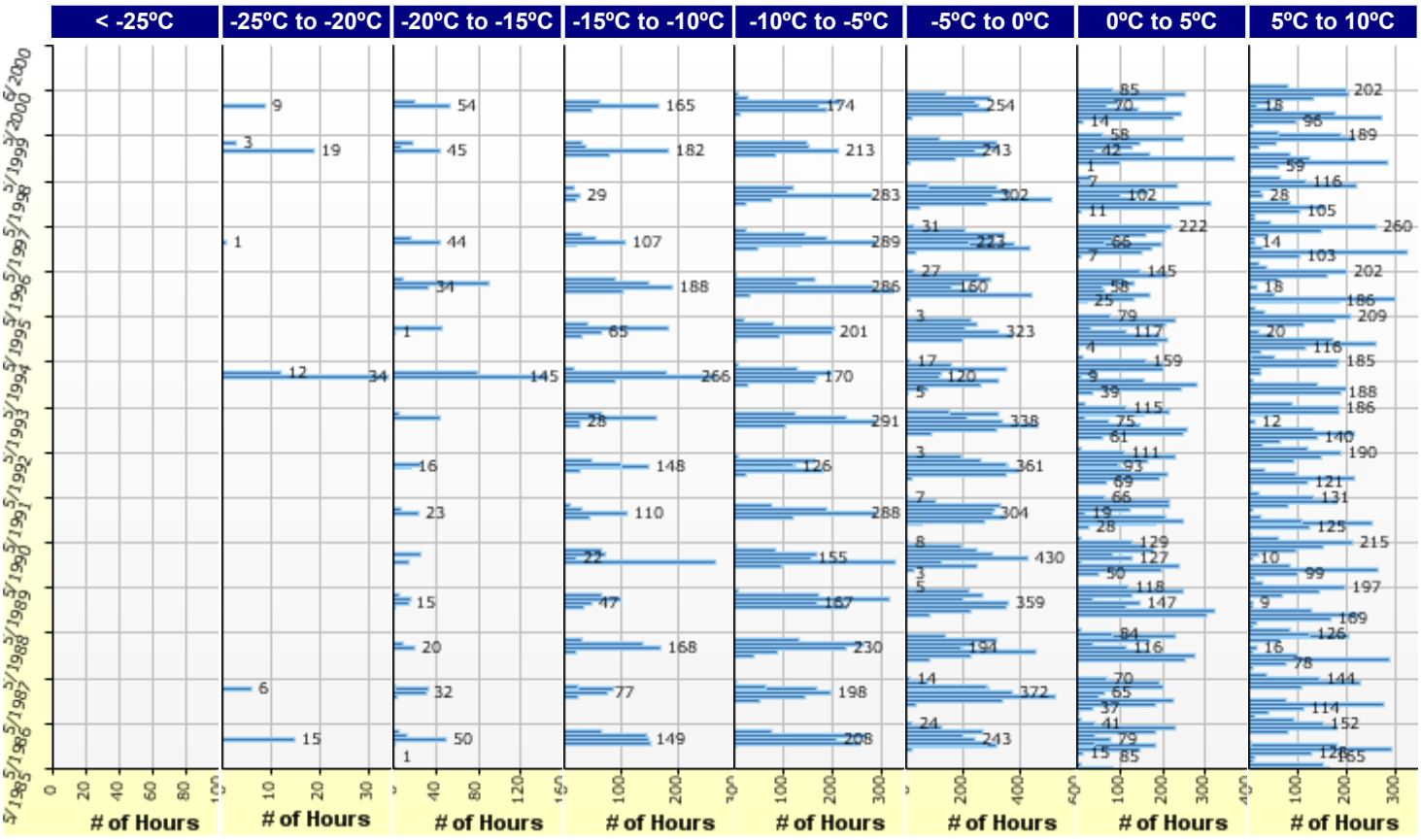

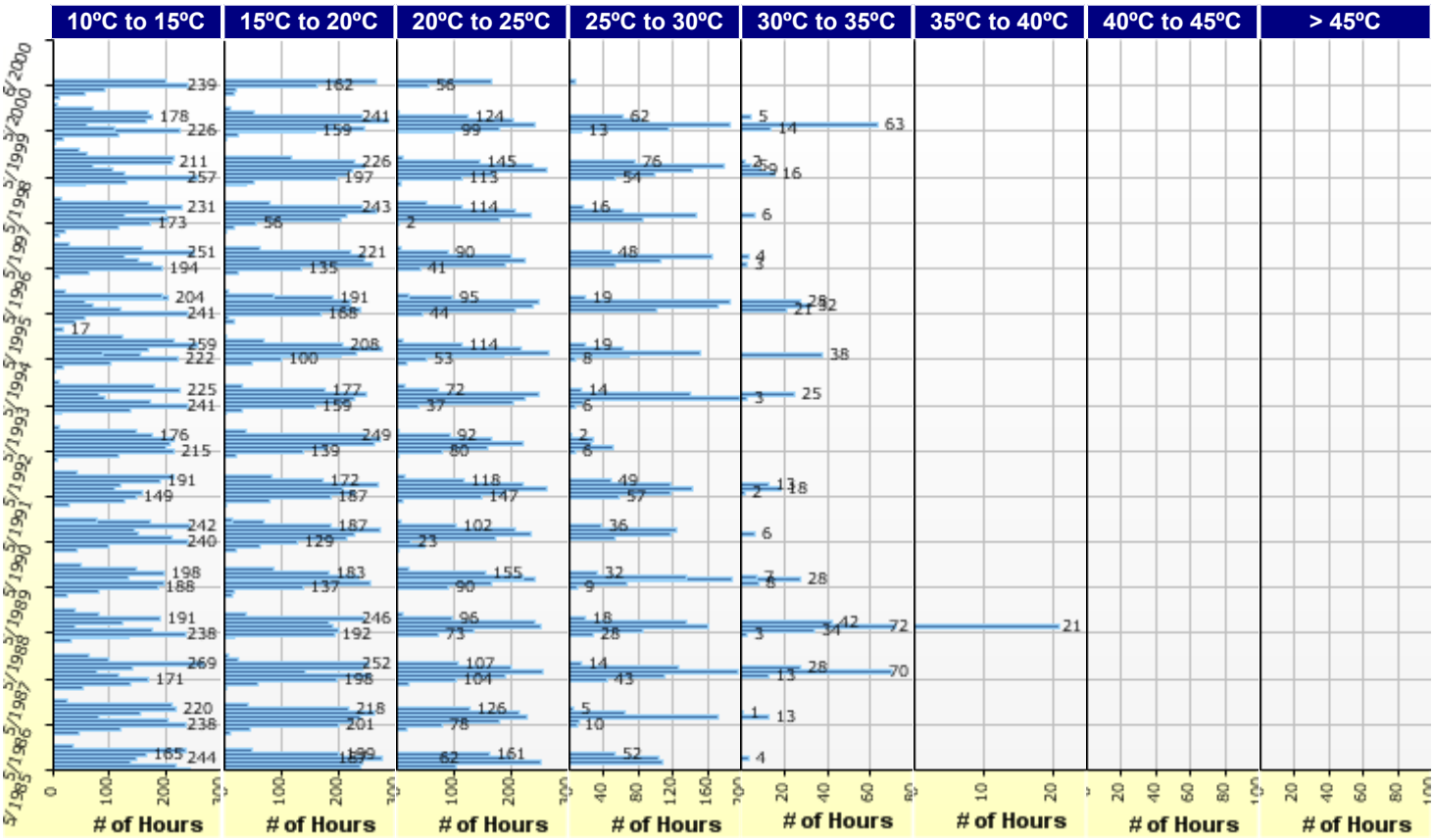

Design Properties

HMA Design Properties

Use Multilayer Rutting Model	False
Using G* based model (not nationally calibrated)	False
Is NCHRP 1-37A HMA Rutting Model Coefficients	True
Endurance Limit	-
Use Reflective Cracking	True

Structure - ICM Properties	
AC surface shortwave absorptivity	0.85

Layer Name	Layer Type	Interface Friction
Layer 1 Flexible : Default asphalt concrete	Flexible (1)	1.00
Layer 2 Chemically Stabilized : Soil cement	Chemically Stabilized (2)	1.00
Layer 3 Non-stabilized Base : Crushed stone	Non-stabilized Base (4)	1.00
Layer 4 Non-stabilized Base : Crushed gravel	Non-stabilized Base (4)	1.00
Layer 5 Subgrade : A-6	Subgrade (5)	-

Thermal Cracking

Thermal Contraction	
Is thermal contraction calculated?	True
Mix coefficient of thermal contraction (mm/mm/ºC)	-
Aggregate coefficient of thermal contraction (mm/mm/ºC)	9.0e-006
Voids in Mineral Aggregate (%)	18.8

Indirect Tensile Strength (Input Level: 3)	
Test Temperature (ºC)	**Indirect Tensilte Strength (Mpa)**
-10.0	2.79

Creep Compliance (1/GPa) (Input Level: 3)			
Loading time (sec)	**-20 ºC**	**-10 ºC**	**0 ºC**
1	5.57e-002	8.57e-002	1.16e-001
2	6.17e-002	1.01e-001	1.51e-001
5	7.07e-002	1.25e-001	2.15e-001
10	7.83e-002	1.48e-001	2.80e-001
20	8.68e-002	1.74e-001	3.65e-001
50	9.94e-002	2.16e-001	5.19e-001
100	1.10e-001	2.55e-001	6.77e-001

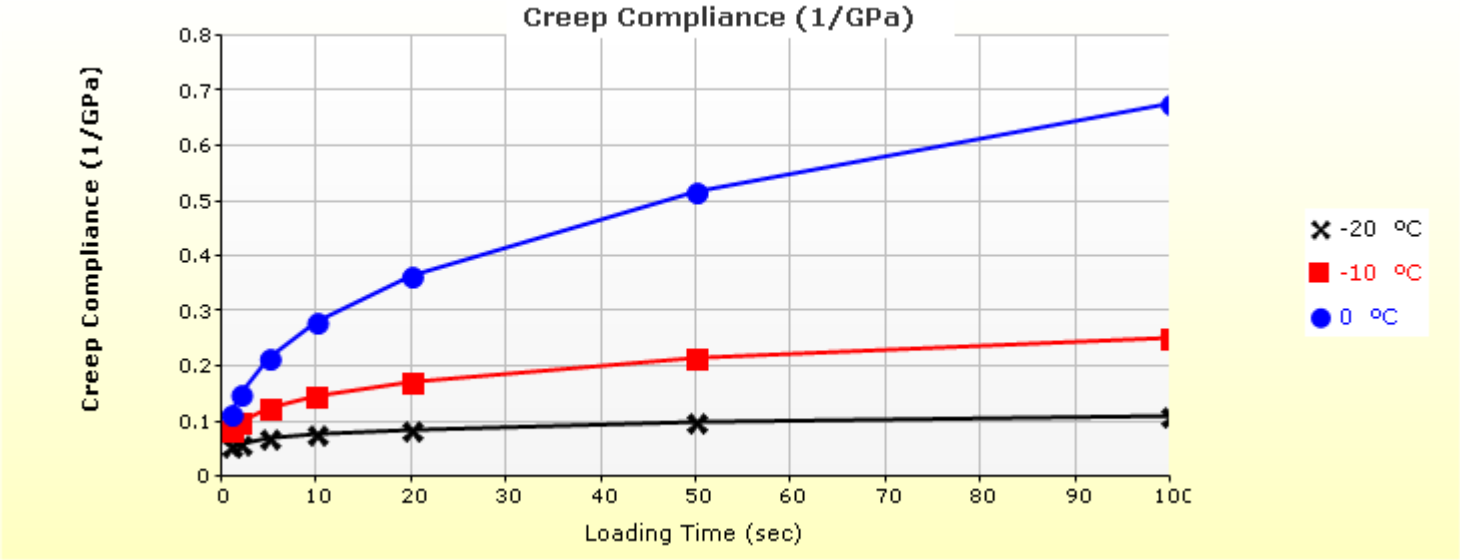

HMA Layer 1: Layer 1 Flexible : Default asphalt concrete

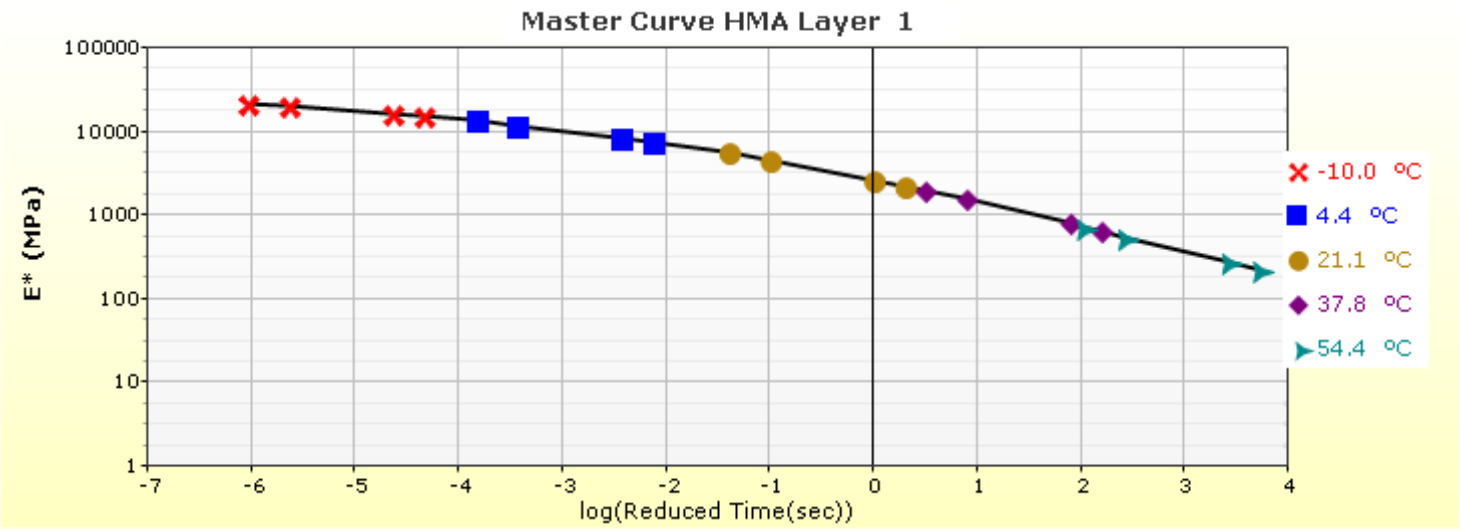

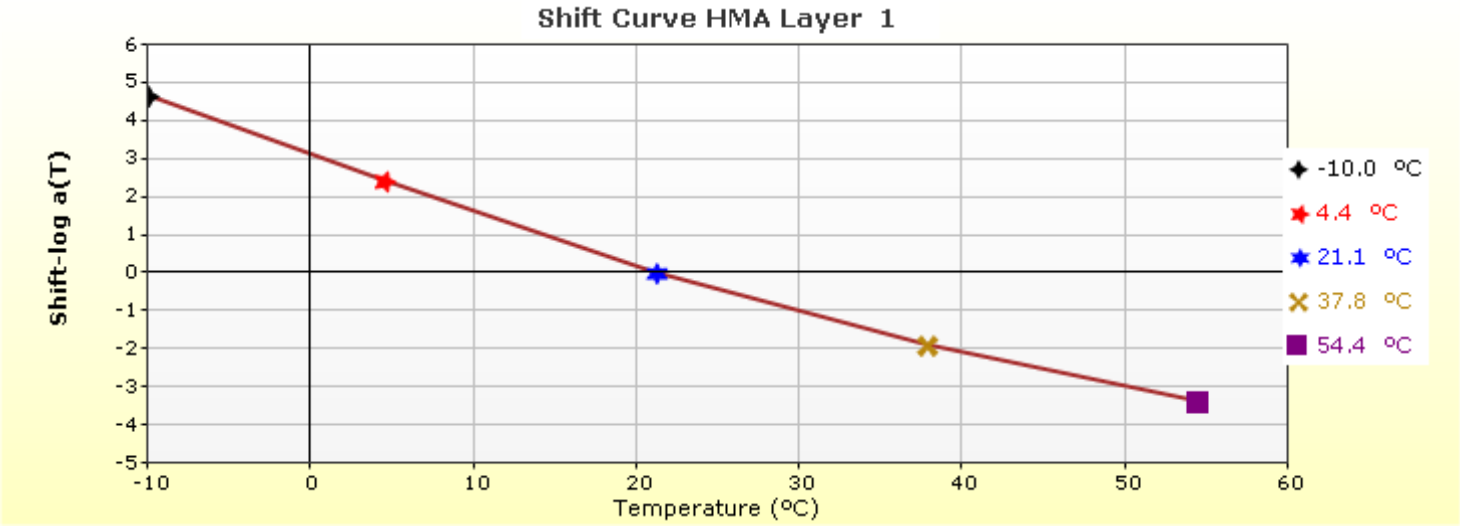

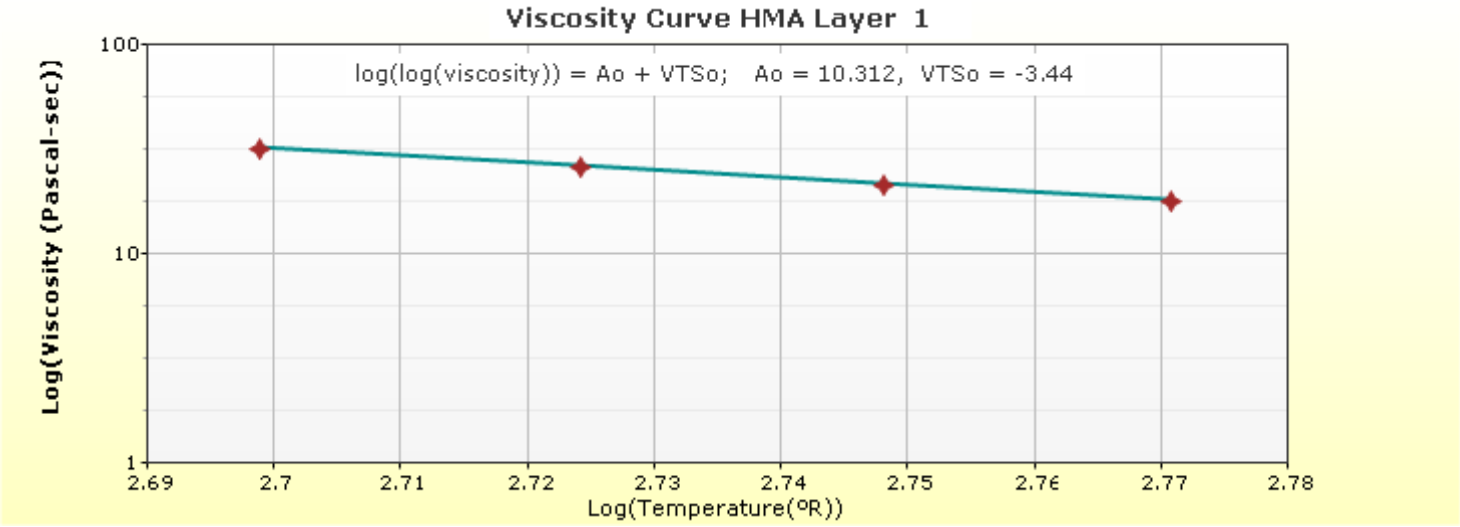

Analysis Output Charts

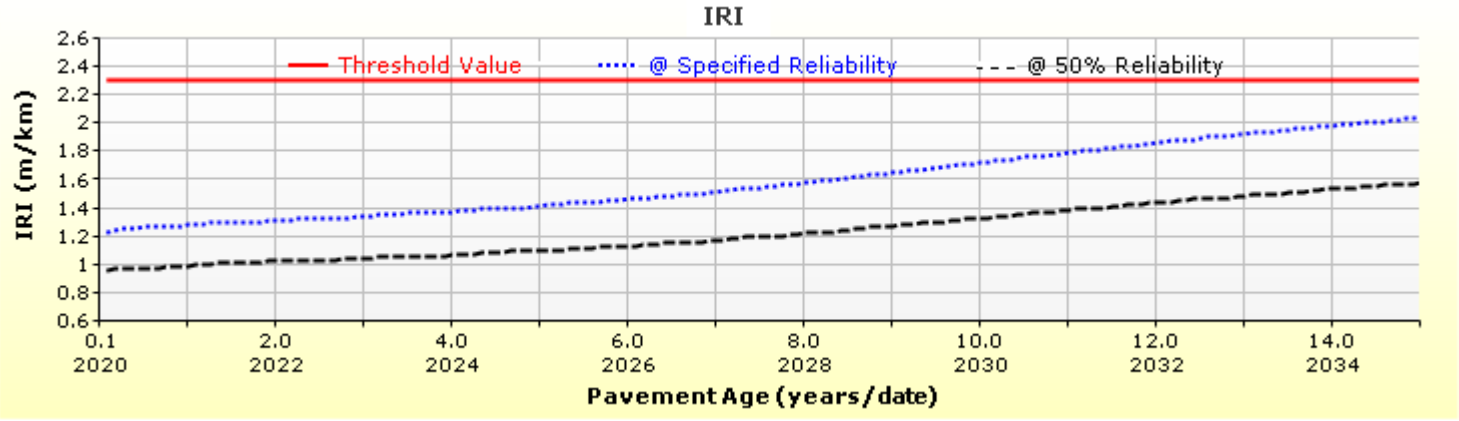

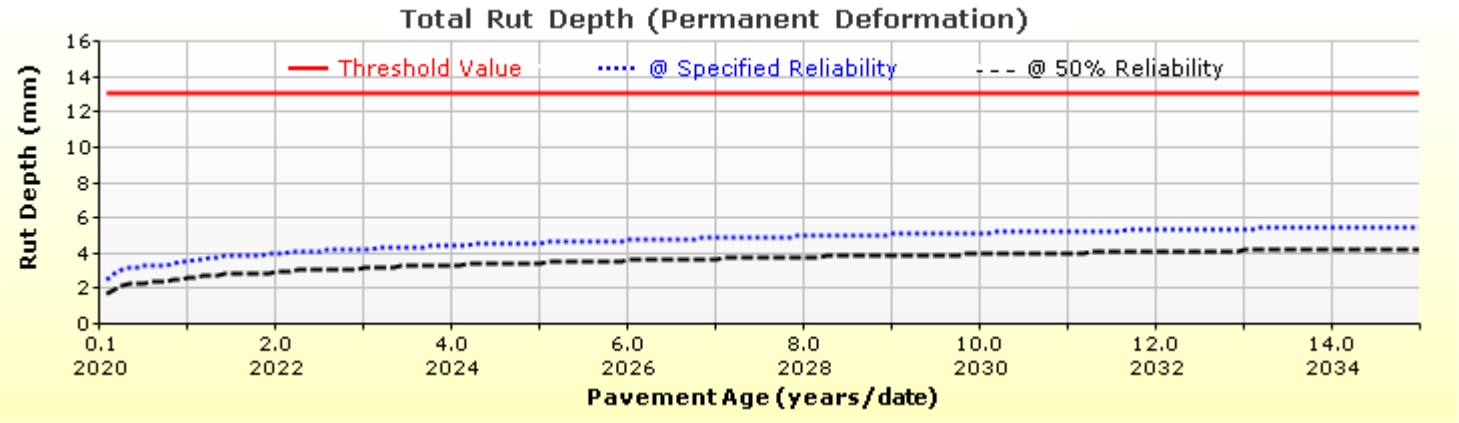

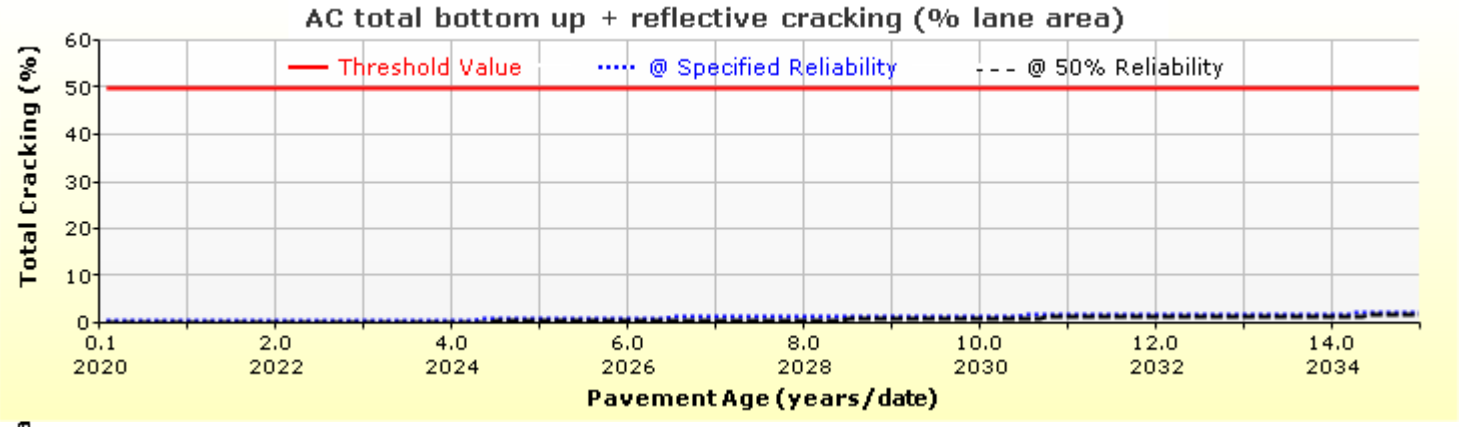

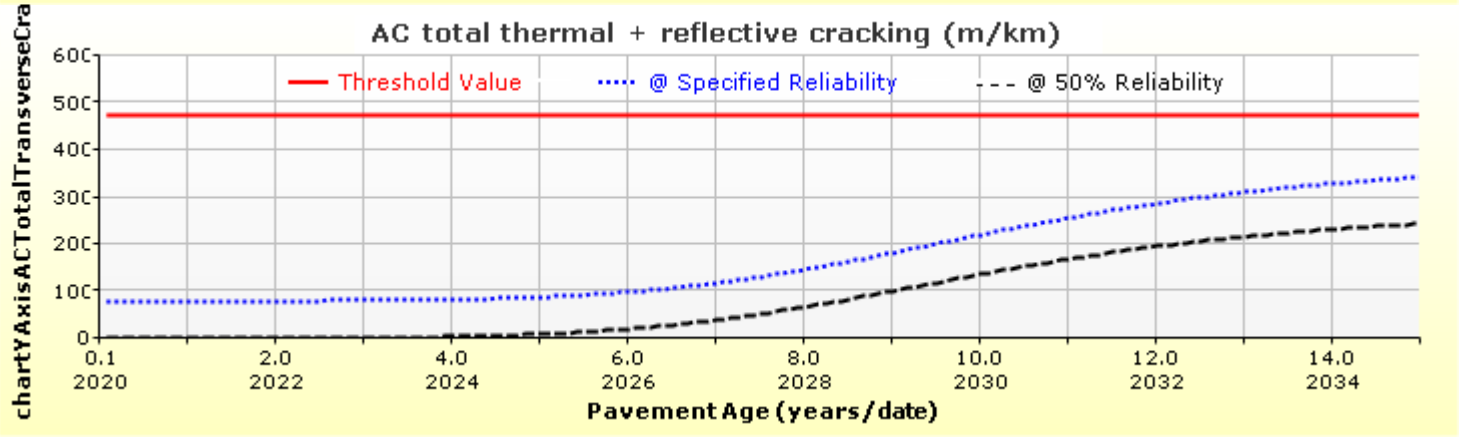

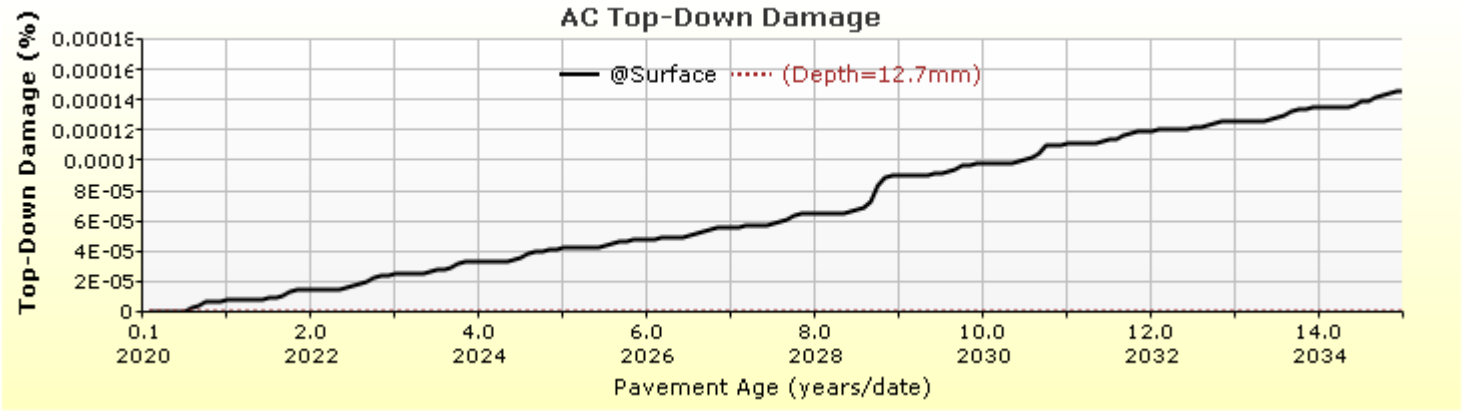
AC Top-Down Damage
@Surface
(Depth=12.7mm)
Top-Down Damage (%)
0.00018
0.00016
0.00014
0.00012
0.0001
8E-05
6E-05
4E-05
2E-05
0
0.1
2020
2.0
2022
4.0
2024
6.0
2026
8.0
2028
10.0
2030
12.0
2032
14.0
2034
Pavement Age (years/date)

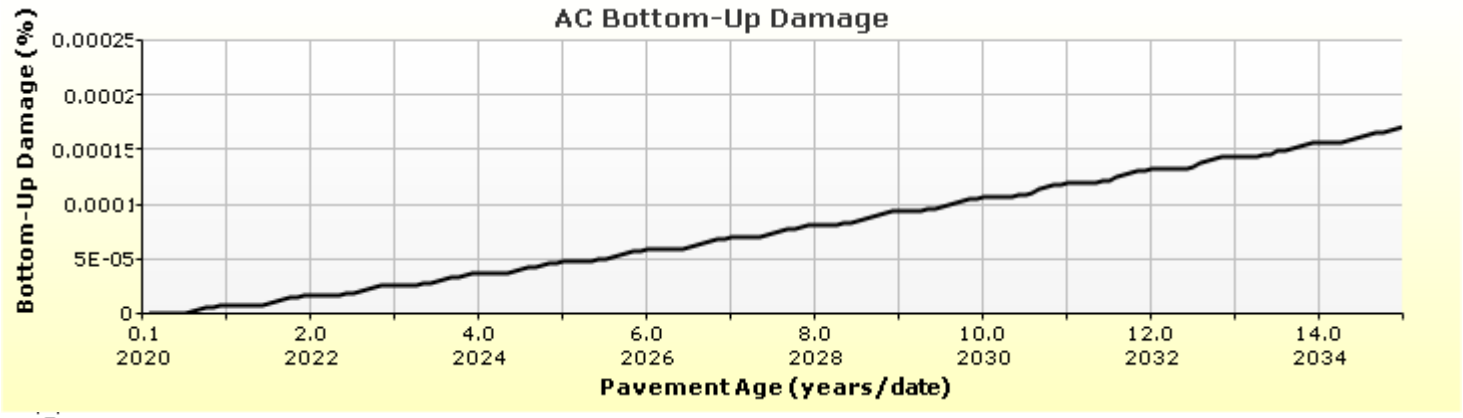
AC Bottom-Up Damage
Bottom-Up Damage (%)
0.00025
0.0002
0.00015
0.0001
5E-05
0
0.1
2020
2.0
2022
4.0
2024
6.0
2026
8.0
2028
10.0
2030
12.0
2032
14.0
2034
Pavement Age (years/date)

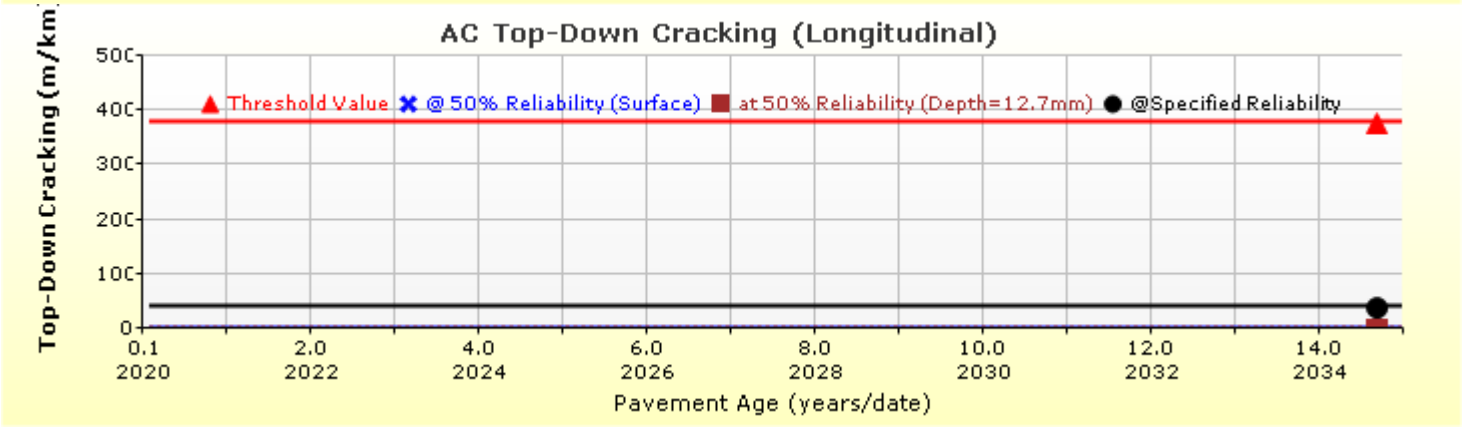
AC Top-Down Cracking (Longitudinal)
Threshold Value
@ 50% Reliability (Surface)
at 50% Reliability (Depth=12.7mm)
@Specified Reliability
Top-Down Cracking (m/km)
500
400
300
200
100
0
0.1
2020
2.0
2022
4.0
2024
6.0
2026
8.0
2028
10.0
2030
12.0
2032
14.0
2034
Pavement Age (years/date)

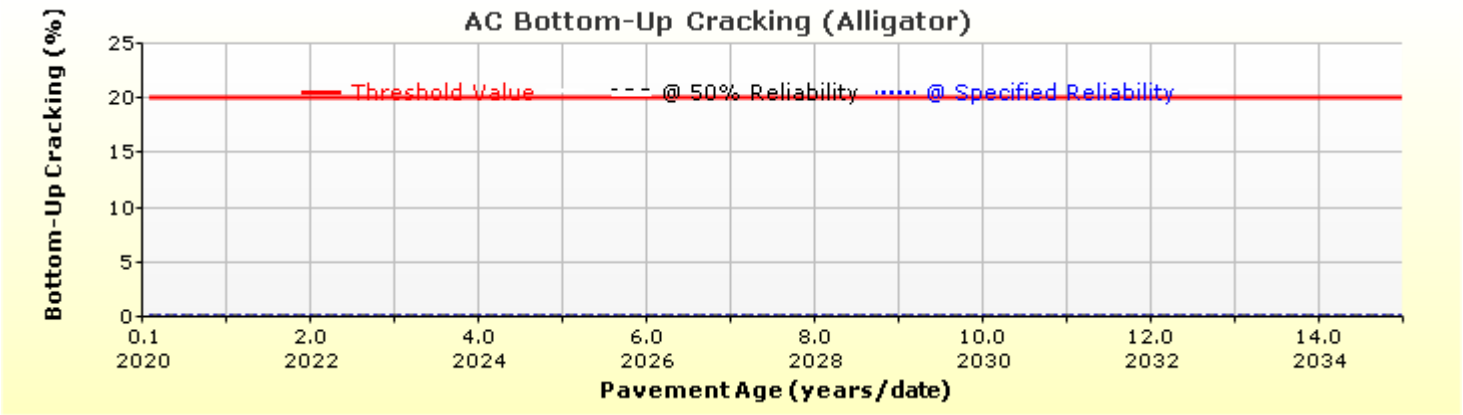
AC Bottom-Up Cracking (Alligator)
Threshold Value
@ 50% Reliability
@ Specified Reliability
Bottom-Up Cracking (%)
25
20
15
10
5
0
0.1
2020
2.0
2022
4.0
2024
6.0
2026
8.0
2028
10.0
2030
12.0
2032
14.0
2034
Pavement Age (years/date)

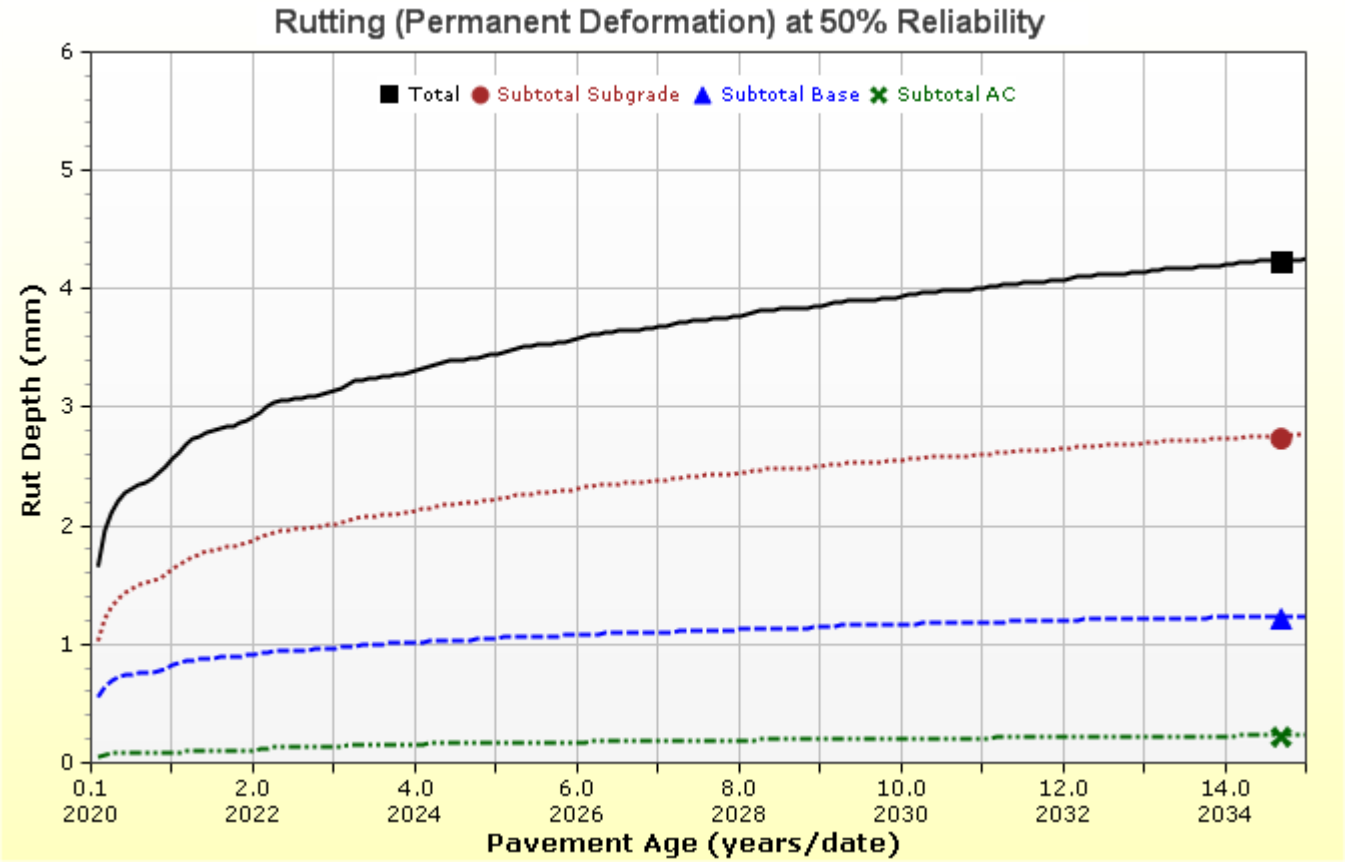
Rutting (Permanent Deformation) at 50% Reliability
Total
Subtotal Subgrade
Subtotal Base
Subtotal AC
Rut Depth (mm)
0
1
2
3
4
5
6
0.1
2020
2.0
2022
4.0
2024
6.0
2026
8.0
2028
10.0
2030
12.0
2032
14.0
2034
Pavement Age (years/date)

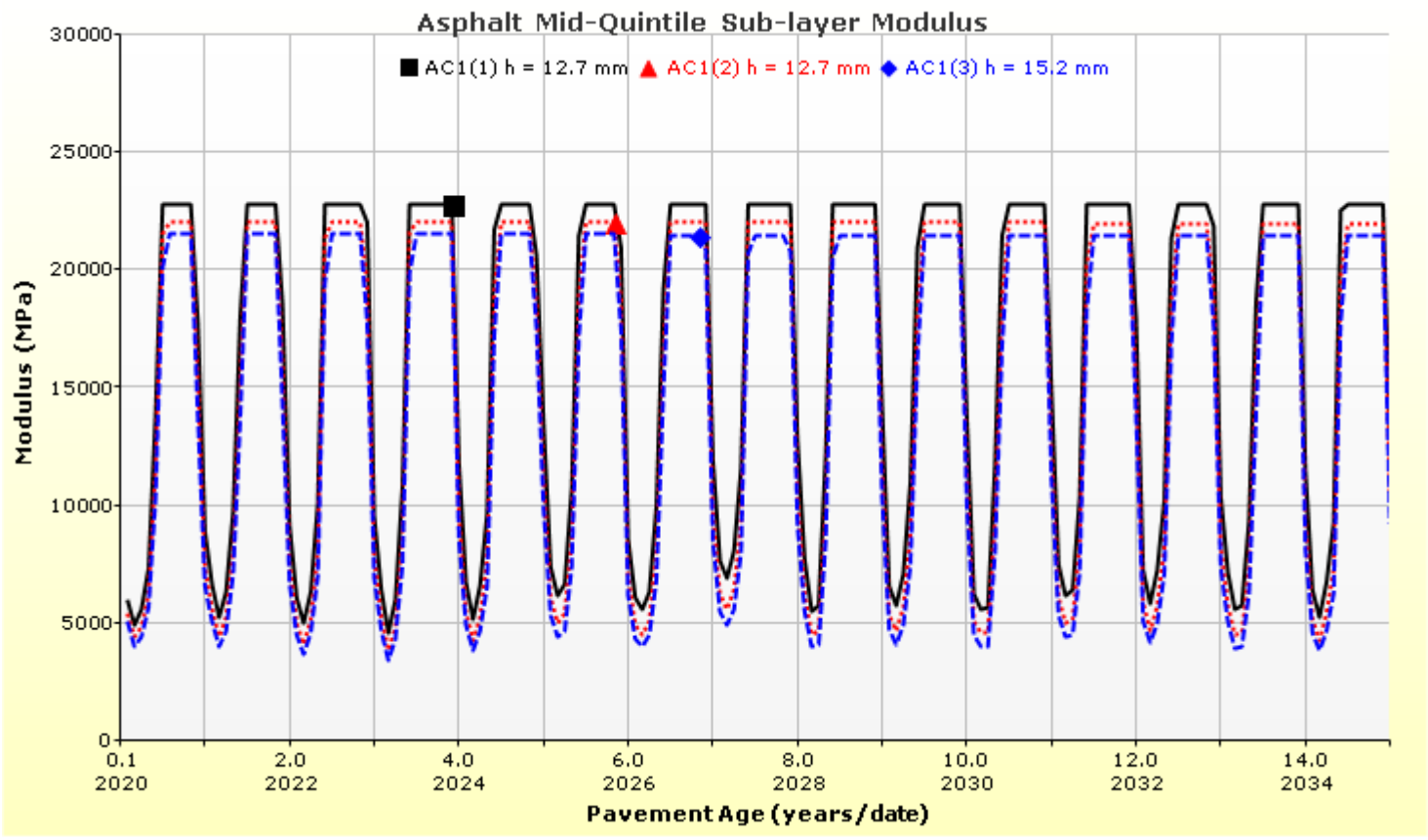
Asphalt Mid-Quintile Sub-layer Modulus
AC1(1) h = 12.7 mm
AC1(2) h = 12.7 mm
AC1(3) h = 15.2 mm
Modulus (MPa)
Pavement Age (years/date)

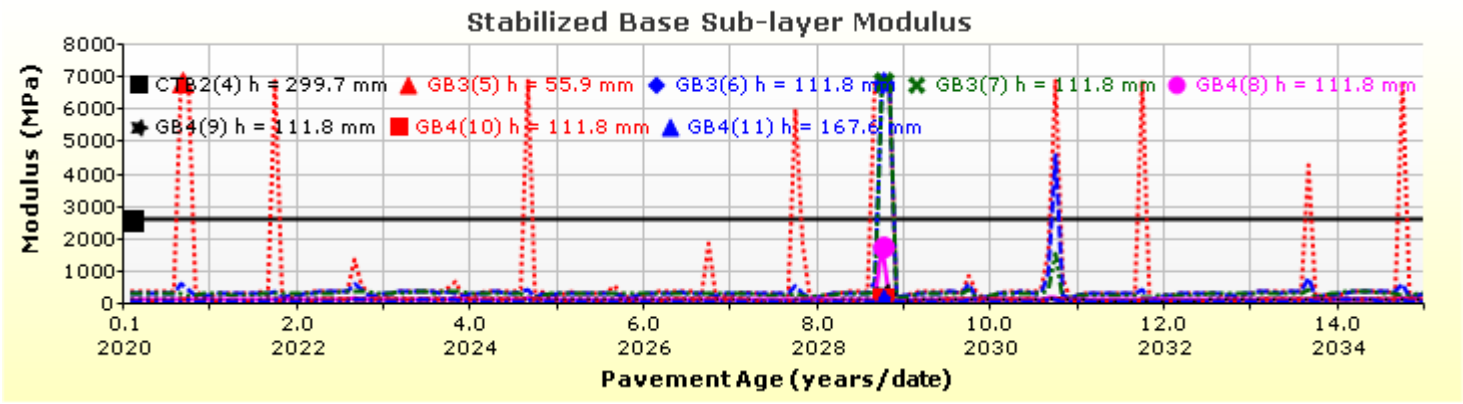
Stabilized Base Sub-layer Modulus
CTB2(4) h = 299.7 mm
GB3(5) h = 55.9 mm
GB3(6) h = 111.8 mm
GB3(7) h = 111.8 mm
GB4(8) h = 111.8 mm
GB4(9) h = 111.8 mm
GB4(10) h = 111.8 mm
GB4(11) h = 167.6 mm
Modulus (MPa)
Pavement Age (years/date)

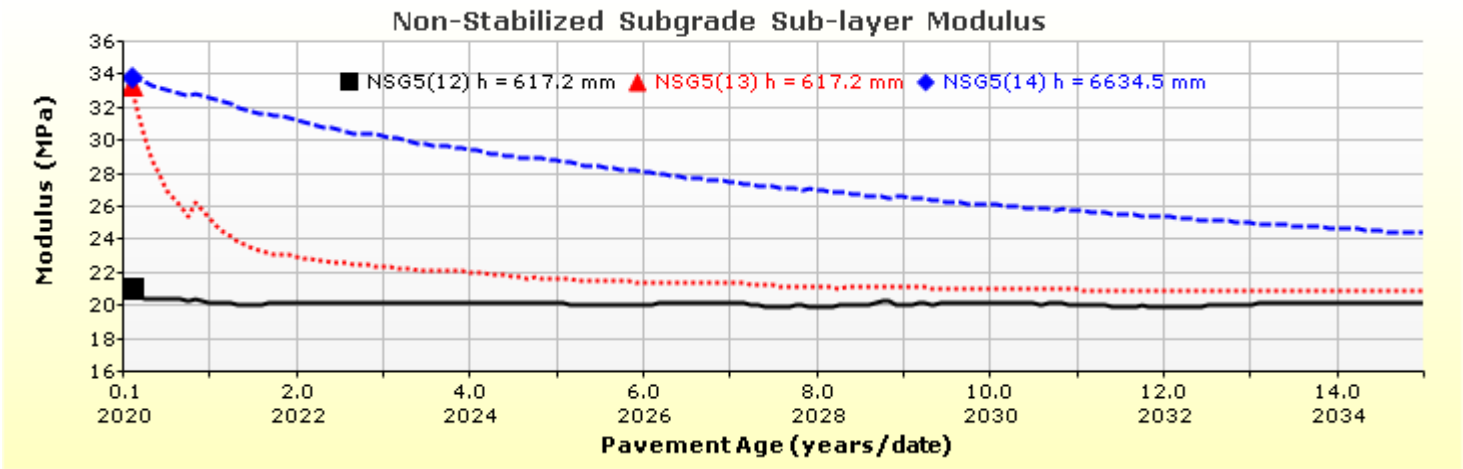
Non-Stabilized Subgrade Sub-layer Modulus
NSG5(12) h = 617.2 mm
NSG5(13) h = 617.2 mm
NSG5(14) h = 6634.5 mm
Modulus (MPa)
Pavement Age (years/date)

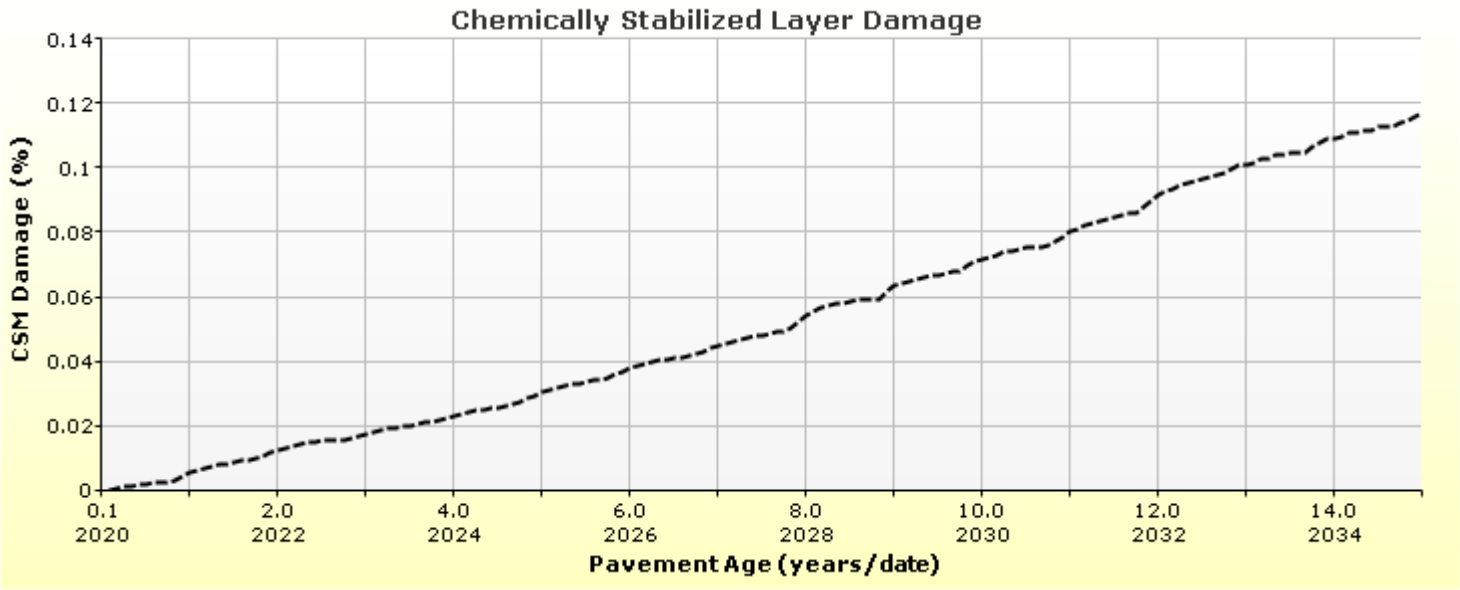
Chemically Stabilized Layer Damage
CSM Damage (%)
0.14
0.12
0.1
0.08
0.06
0.04
0.02
0
0.1
2020
2.0
2022
4.0
2024
6.0
2026
8.0
2028
10.0
2030
12.0
2032
14.0
2034
Pavement Age (years/date)

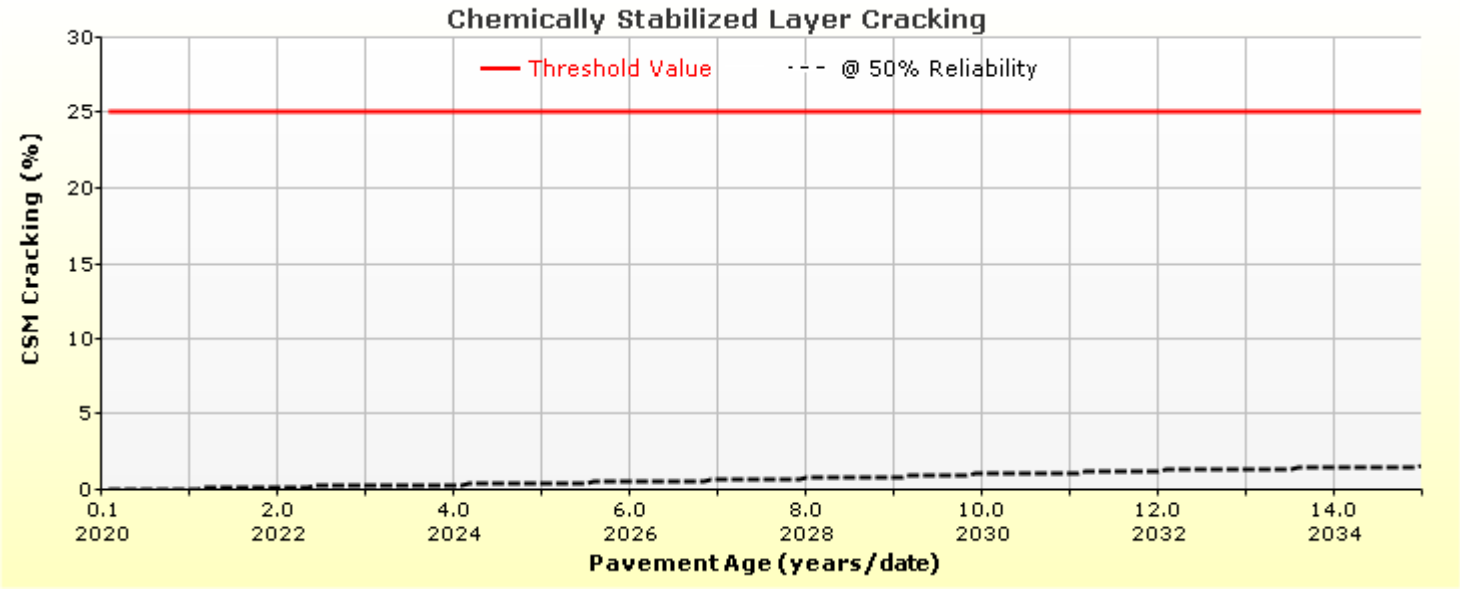
Chemically Stabilized Layer Cracking
Threshold Value
@ 50% Reliability
CSM Cracking (%)
30
25
20
15
10
5
0
0.1
2020
2.0
2022
4.0
2024
6.0
2026
8.0
2028
10.0
2030
12.0
2032
14.0
2034
Pavement Age (years/date)

Layer Information

Layer 1 Flexible : Default asphalt concrete

Asphalt		
Thickness (mm)	40.0	
Unit weight (kgf/m^3)	2460.0	
Poisson's ratio	Is Calculated?	False
	Ratio	0.35
	Parameter A	-
	Parameter B	-

Asphalt Dynamic Modulus (Input Level: 3)

Gradation	Percent Passing
19 mm sieve	100
9.5 mm sieve	77
4.75 mm sieve	60
0.075mm sieve	6

Asphalt Binder

Parameter	Value
Grade	Superpave Performance Grade
Binder Type	64-28
A	10.312
VTS	-3.44

General Info

Name	Value
Reference temperature (°C)	21.1
Effective binder content (%)	11.8
Air voids (%)	7
Thermal conductivity (watt/meter-kelvin)	1.16
Heat capacity (joule/kg-kelvin)	963

Identifiers

Field	Value
Display name/identifier	Default asphalt concrete
Description of object	
Author	
Date Created	9/16/2010 1:00:00 AM
Approver	
Date approved	9/16/2010 1:00:00 AM
State	
District	
County	
Highway	
Direction of Travel	
From station (km)	
To station (km)	
Province	
User defined field 1	
User defined field 2	
User defined field 3	
Revision Number	0

Layer 2 Chemically Stabilized : Soil cement

Semi-Rigid	
Chemically stabilized base crack spacing (m)	8
Chemically stabilized base transverse crack LTE (%)	50
Fatigue LTE (%)	50

Chemically Stabilized	
Layer thickness (mm)	300
Poisson's ratio	0.2
Unit weight (kgf/m^3)	2100

Strength	
Elastic/resilient modulus (MPa)	2664

Thermal	
Heat capacity (joule/kg-kelvin)	1172.3
Thermal conductivity (watt/meter-kelvin)	2.16

Identifiers

Field	Value
Display name/identifier	Soil cement
Description of object	Default material
Author	AASHTO
Date Created	1/1/2011 12:00:00 AM
Approver	
Date approved	1/1/2011 12:00:00 AM
State	
District	
County	
Highway	
Direction of Travel	
From station (km)	
To station (km)	
Province	
User defined field 1	
User defined field 2	
User defined field 3	
Revision Number	0

Layer 3 Non-stabilized Base : Crushed stone

Unbound	
Layer thickness (mm)	280.0
Poisson's ratio	0.35
Coefficient of lateral earth pressure (k0)	0.5

Modulus (Input Level: 3)

Analysis Type:	Modify input values by temperature/moisture
Method:	Resilient Modulus (MPa)

Resilient Modulus (MPa)
250.0

Use Correction factor for NDT modulus?	-
NDT Correction Factor:	-

Identifiers

Field	Value
Display name/identifier	Crushed stone
Description of object	Default material
Author	AASHTO
Date Created	1/1/2011 12:00:00 AM
Approver	
Date approved	1/1/2011 12:00:00 AM
State	
District	
County	
Highway	
Direction of Travel	
From station (km)	
To station (km)	
Province	
User defined field 1	
User defined field 2	
User defined field 3	
Revision Number	0

Sieve

Liquid Limit	6.0
Plasticity Index	1.0
Is layer compacted?	False

	Is User Defined?	Value
Maximum dry unit weight (kgf/m^3)	False	2048.3
Saturated hydraulic conductivity (m/hr)	False	2.257e-02
Specific gravity of solids	False	2.7
Water Content (%)	False	7

User-defined Soil Water Characteristic Curve (SWCC)	
Is User Defined?	False
af	3.0919
bf	2.6074
cf	0.7701
hr	110.0000

Sieve Size	% Passing
0.001mm	
0.002mm	
0.020mm	
0.075mm	5.0
0.150mm	
0.180mm	
0.250mm	
0.300mm	13.5
0.425mm	
0.600mm	
0.850mm	
1.18mm	27.5
2.0mm	
2.36mm	
4.75mm	45.0
9.5mm	61.5
12.5mm	
19.0mm	92.5
25.0mm	100.0
37.5mm	
50.0mm	
63.0mm	
75.0mm	
90.0mm	

Layer 4 Non-stabilized Base : Crushed gravel

Unbound	
Layer thickness (mm)	500.0
Poisson's ratio	0.35
Coefficient of lateral earth pressure (k0)	0.5

Modulus (Input Level: 3)

Analysis Type:	Modify input values by temperature/moisture
Method:	Resilient Modulus (MPa)

Resilient Modulus (MPa)
150.0

Use Correction factor for NDT modulus?	-
NDT Correction Factor:	-

Identifiers

Field	Value
Display name/identifier	Crushed gravel
Description of object	Default material
Author	AASHTO
Date Created	1/1/2011 12:00:00 AM
Approver	
Date approved	1/1/2011 12:00:00 AM
State	
District	
County	
Highway	
Direction of Travel	
From station (km)	
To station (km)	
Province	
User defined field 1	
User defined field 2	
User defined field 3	
Revision Number	0

Sieve

Liquid Limit	11.0
Plasticity Index	1.0
Is layer compacted?	False

	Is User Defined?	Value
Maximum dry unit weight (kgf/m^3)	False	2012.4
Saturated hydraulic conductivity (m/hr)	False	6.883e-03
Specific gravity of solids	False	2.7
Water Content (%)	False	8.2

User-defined Soil Water Characteristic Curve (SWCC)	
Is User Defined?	False
af	5.0935
bf	2.5668
cf	0.8576
hr	108.0000

Sieve Size	% Passing
0.001mm	
0.002mm	
0.020mm	
0.075mm	4.0
0.150mm	
0.180mm	
0.250mm	
0.300mm	33.5
0.425mm	
0.600mm	
0.850mm	
1.18mm	55.0
2.0mm	
2.36mm	
4.75mm	60.0
9.5mm	
12.5mm	
19.0mm	
25.0mm	75.0
37.5mm	
50.0mm	
63.0mm	
75.0mm	
90.0mm	

Layer 5 Subgrade : A-6

Unbound	
Layer thickness (mm)	Semi-infinite
Poisson's ratio	0.35
Coefficient of lateral earth pressure (k0)	0.5

Modulus (Input Level: 3)

Analysis Type:	Modify input values by temperature/moisture
Method:	Resilient Modulus (MPa)

Resilient Modulus (MPa)
35.0

Use Correction factor for NDT modulus?	-
NDT Correction Factor:	-

Identifiers

Field	Value
Display name/identifier	A-6
Description of object	Default material
Author	AASHTO
Date Created	1/1/2011 12:00:00 AM
Approver	
Date approved	1/1/2011 12:00:00 AM
State	
District	
County	
Highway	
Direction of Travel	
From station (km)	
To station (km)	
Province	
User defined field 1	
User defined field 2	
User defined field 3	
Revision Number	0

Sieve

Liquid Limit	42.0
Plasticity Index	15.0
Is layer compacted?	False

	Is User Defined?	Value
Maximum dry unit weight (kgf/m^3)	False	1693.8
Saturated hydraulic conductivity (m/hr)	False	3.012e-06
Specific gravity of solids	False	2.7
Water Content (%)	False	18.2

User-defined Soil Water Characteristic Curve (SWCC)	
Is User Defined?	False
af	114.8407
bf	0.6389
cf	0.1739
hr	500.0000

Sieve Size	% Passing
0.001mm	
0.002mm	25.0
0.020mm	
0.075mm	82.0
0.150mm	
0.180mm	91.0
0.250mm	
0.300mm	
0.425mm	95.0
0.600mm	
0.850mm	
1.18mm	
2.0mm	98.0
2.36mm	
4.75mm	100.0
9.5mm	100.0
12.5mm	100.0
19.0mm	100.0
25.0mm	100.0
37.5mm	
50.0mm	
63.0mm	
75.0mm	
90.0mm	100.0

Calibration Coefficients

AC Fatigue

$$N_f = 0.00432 * C * \beta_{f1} k_1 \left(\frac{1}{\varepsilon_1}\right)^{k_2\beta_{f2}} \left(\frac{1}{E}\right)^{k_3\beta_{f3}}$$

$$C = 10^M$$

$$M = 4.84\left(\frac{V_b}{V_a + V_b} - 0.69\right)$$

k1: 3.75	
k2: 2.87	
k3: 1.46	
Bf1: 0.02054	
Bf2: 1.38	
Bf3: 0.88	

AC Rutting

$$\frac{\varepsilon_p}{\varepsilon_r} = k_z \beta_{r1} 10^{k_1 T^{k_2 \beta_{r2}}} N^{k_3 \beta_{r3}}$$

$$k_z = (C_1 + C_2 * depth) * 0.328196^{depth}$$

$$C_1 = -0.1039 * H_\alpha^2 + 2.4868 * H_\alpha - 17.342$$

$$C_2 = 0.0172 * H_\alpha^2 - 1.7331 * H_\alpha + 27.428$$

Where:

$$H_{ac} = total\ AC\ thickness(in)$$

$\varepsilon_p = plastic\ strain\left({}^{in}/_{in}\right)$
$\varepsilon_r = resilient\ strain\left({}^{in}/_{in}\right)$
$T = layer\ temperature(^{\circ}F)$
$N = number\ of\ load\ repetitions$

AC Rutting Standard Deviation	0.24 * Pow(RUT,0.8026) + 0.001	
AC Layer 1	K1:-2.45 K2:3.01 K3:0.22	Br1:0.128 Br2:0.52 Br3:1.36

Thermal Fracture

$$C_f = 400 * N\left(\frac{\log C / h_{ac}}{\sigma}\right)$$

$$\Delta C = (k * \beta t)^{n+1} * A * \Delta K^n$$

$$A = 10^{(4.389 - 2.52 * \log(E * \sigma_m * n))}$$

$C_f = observed\ amount\ of\ thermal\ cracking(ft/500ft)$
$k = refression\ coefficient\ determined\ through\ field\ calibration$
$N(\,) = standard\ normal\ distribution\ evaluated\ at(\,)$
$\sigma = standard\ deviation\ of\ the\ \log\ of\ the\ depth\ of\ cracks\ in\ the\ pavments$
$C = crack\ depth(in)$
$h_{ac} = thickness\ of\ asphalt\ layer(in)$
$\Delta C = Change\ in\ the\ crack\ depth\ due\ to\ a\ cooling\ cycle$
$\Delta K = Change\ in\ the\ stress\ intensity\ factor\ due\ to\ a\ cooling\ cycle$
$A, n = Fracture\ parameters\ for\ the\ asphalt\ mixture$
$E = mixture\ stiffness$
$\sigma_M = Undamaged\ mixture\ tensile\ strength$
$\beta_t = Calibration\ parameter$

Level 1 K: ((3 * Pow(10,-7)) * Pow(MAAT,4.0319)) * 1 + 0	
Level 2 K: ((3 * Pow(10,-7)) * Pow(MAAT,4.0319)) * 1 + 0	
Level 3 K: ((3 * Pow(10,-7)) * Pow(MAAT,4.0319)) * 1 + 0	

CSM Fatigue

$$N_f = 10^{\left(\frac{k_1 \beta_{c1} \left(\frac{\sigma_s}{M_r}\right)}{k_2 \beta_{c2}}\right)}$$

$N_f = number\ of\ repetitions\ to\ fatigue\ cracking$
$\sigma_s = Tensile\ stress(psi)$
$M_r = modulus\ of\ rupture(psi)$

k1: 0.972	k2: 0.0825	Bc1: 1	Bc2:1

Unbound Layer Rutting

$$\delta_a(N) = \beta_{s_1} k_1 \varepsilon_v h \left(\frac{\varepsilon_0}{\varepsilon_r}\right) \left| e^{-\left(\frac{\rho}{N}\right)^{\beta}} \right|$$

$\delta_a = permanent\ deformation\ for\ the\ layer$
$N = number\ of\ repetitions$
$\varepsilon_v = average\ veritcal\ strain(in/in)$
$\varepsilon_0, \beta, \rho = material\ properties$
$\varepsilon_r = resilient\ strain(in/in)$

Base Rutting		Subgrade Rutting	
k1: 0.965	Bs1: 1	k1: 0.675	Bs1: 1
Standard Deviation (BASERUT) 0.1477 * Pow(BASERUT,0.6711) + 0.001		Standard Deviation (BASERUT) 0.1235 * Pow(SUBRUT,0.5012) + 0.001	

AC Cracking

AC Top Down Cracking

$$FC_{top} = \left(\frac{C_4}{1 + e^{(C_1 - C_2 * log_{10}(Damage))}}\right) * 10.56$$

c1: 7	c2: 3.5	c3: 0	c4: 1000

Top down AC Cracking Standard Deviation

200 + 2300/(1+exp(1.072-2.1654*LOG10(TOP+0.0001)))

AC Bottom Up Cracking

$$FC = \left(\frac{6000}{1 + e^{(C_1 * C_1' + C_2 * C_2' log_{10}(D * 100))}}\right) * \left(\frac{1}{60}\right)$$

$$C_2' = -2.40874 - 39.748 * (1 + h_{ac})^{-2.856}$$

$$C_1' = -2 * C_2'$$

c1: 1.31	c2: 2.1585	c3: 6000

Bottom up AC Cracking Standard Deviation

1.13 + 13/(1+exp(7.57-15.5*LOG10(BOTTOM+0.0001)))

CSM Cracking

$$FC_{ctb} = C_1 + \frac{C_2}{1 + e^{C_3 - C_4 * log_{10}(Damage)}}$$

C1: 0	C2: 75	C3: 2	C4: 2

CSM Standard Deviation

CTB*1

IRI Flexible Pavements

C1 - Rutting
C2 - Fatigue Crack
C3 - Transverse Crack
C4 - Site Factors

C1: 55	C2: 0.4	C3: 0.008	C4: 0.015

Reflective Cracking

$$\Delta C = k_1 \Delta_{bending} + k_2 \Delta_{shaering} + k_3 \Delta_{thermal}$$

$$\Delta D = \frac{C_1 k_1 \Delta_{bending} + C_2 k_2 \Delta_{shearing} + C_3 k_3 \Delta_{thermal}}{h_{OL}}$$

$$\Delta_{Bending} = A(SIF)_B^n$$

$$\Delta_{Shearing} = A(SIF)_S^n$$

$$\Delta_{Thermal} = A(SIF)_T^n$$

$$D = \sum_{i=1}^{N} \Delta D$$

$$RCR = \left(\frac{100}{C4 + e^{C5 \log D}}\right) * EX\_CRK$$

Where

ΔC	=	Crack length increment, in
ΔD	=	Incremental damage ratio
$k_1, k_2, k_3, C_1, C_2, C_3, C_4, C_5$	=	Calibration factors (local and global)
$\Delta_{bending}, \Delta_{shearing}, \Delta_{thermal}$	=	Crack length increments caused by bending, shearing, and thermal loading
A, n	=	HMA material fracture properties
N	=	Total number of days
$(SIF)_B, (SIF)_S, (SIF)_T$	=	Stress intensity factors caused by bending, shearing, and thermal loading
D	=	Damage ratio
h_{OL}	=	Overlay thickness, in
RCR	=	Cracks in the underlying layers reflected, %
EX_CRK	=	Transverse cracking in underlying pavement layers, ft/mile (transverse cracking) Alligator cracking in underlying pavement layers, % lane area (alligator cracking)

Pavement Type	Distress Type	k1	k2	k3	C1	C2	C3	C4	C5	Standard Deviation
Semi-Rigid	Transverse	0.45	0.05	1	0.1	0.9809	0.19	165.3	-5.1048	0.000027 * Pow (TRANSVERSE,2.1187) + 399.9
Semi-Rigid	Fatigue	0.45	0.05	1	1.64	1.1	0.19	62.1	-404.6	1.3897 * Pow (FATIGUE,0.2960) + 0.4212

Semi-Rigid Pavement_FDR+HRB3_ONTARIO

File Name: C:\Users\admin\Desktop\Eskedil_ME\Kossuth\Semi-Rigid Pavement_FDR+HRB3_ONTARIO.dgpx

Design Inputs

Design Life: 15 years
Design Type: SEMI_RIGID

Base construction: May, 2020
Pavement construction: June, 2020
Traffic opening: June, 2020

Climate Data Sources (Lat/Lon): 43.5, -80.625 ; 43, -80

Design Structure

Layer type	Material Type	Thickness(mm)
Flexible	Default asphalt concrete	40.0
Cement_Base	Soil cement	300.0
NonStabilized	Crushed stone	280.0
NonStabilized	Crushed gravel	500.0
Subgrade	A-6	Semi-infinite

Volumetric at Construction:	
Effective binder content (%)	11.8
Air voids (%)	7.0

Traffic

Age (year)	Heavy Trucks (cumulative)
2020 (initial)	1,272
2027 (7 years)	1,721,680
2035 (15 years)	3,794,600

Design Outputs

Distress Prediction Summary

Distress Type	Distress @ Specified Reliability		Reliability (%)		Criterion Satisfied?
	Target	Predicted	Target	Achieved	
Terminal IRI (m/km)	2.30	2.04	85.00	94.80	Pass
Permanent deformation - total pavement (mm)	13.00	5.50	85.00	100.00	Pass
AC total fatigue cracking: bottom up + reflective (% lane area)	50.00	1.98	85.00	100.00	Pass
AC total transverse cracking: thermal + reflective (m/km)	473.40	340.46	85.00	99.25	Pass
AC bottom-up fatigue cracking (percent)	20.00	0.00	50.00	100.00	Pass
AC thermal cracking (m/km)	190.00	0.19	50.00	100.00	Pass
AC top-down fatigue cracking (m/km)	380.00	39.32	85.00	100.00	Pass
Permanent deformation - AC only (mm)	6.00	0.42	85.00	100.00	Pass
Chemically stabilized layer - fatigue fracture (percent)	25.00	1.54	-	-	-

Distress Charts

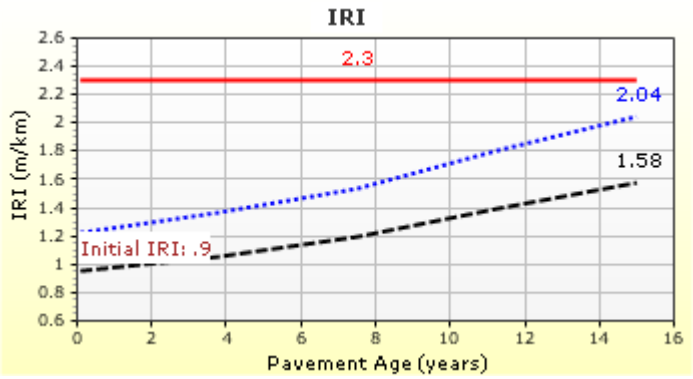

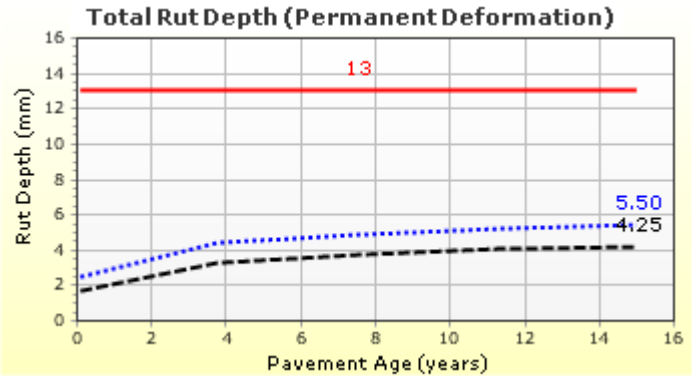

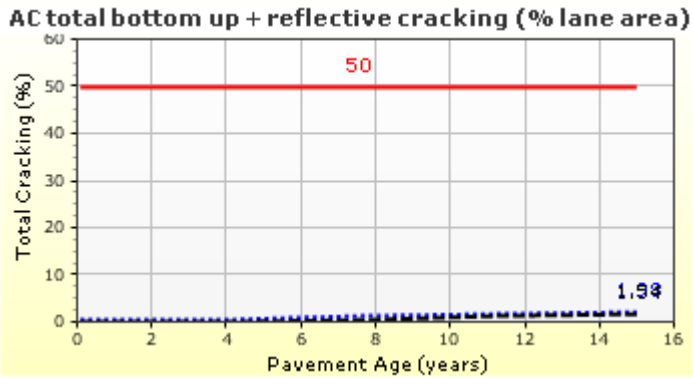

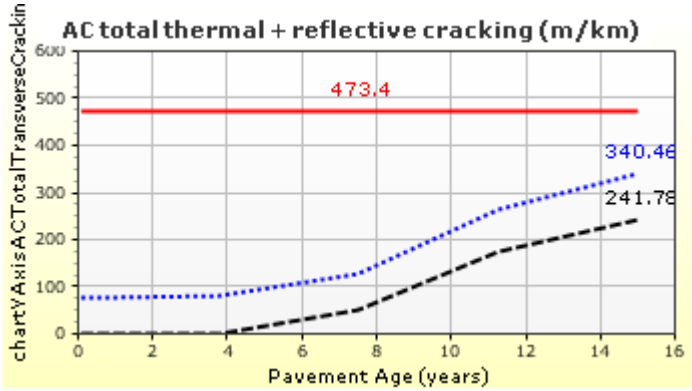

Traffic Inputs

Graphical Representation of Traffic Inputs

Initial two-way AADTT:	1,272	Percent of trucks in design direction (%):	50.0
Number of lanes in design direction:	2	Percent of trucks in design lane (%):	90.0
		Operational speed (kph)	100.0

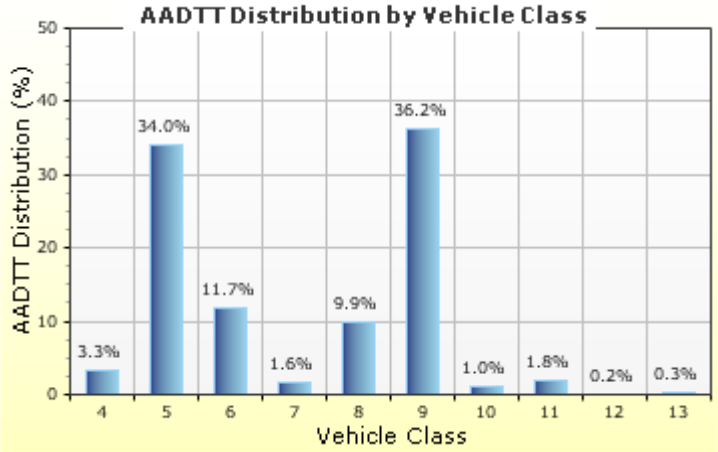

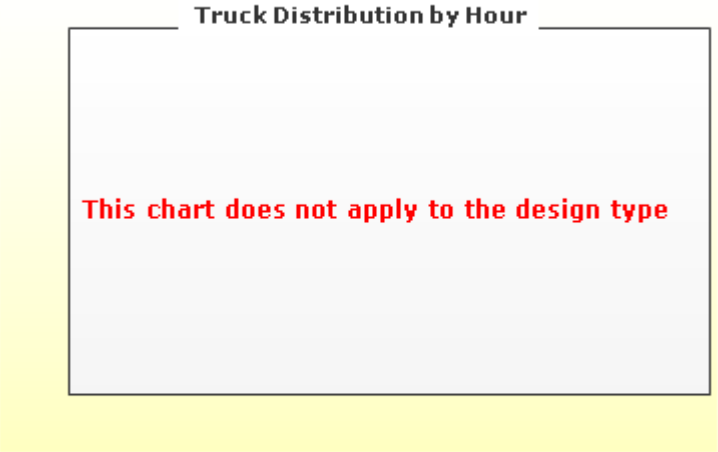

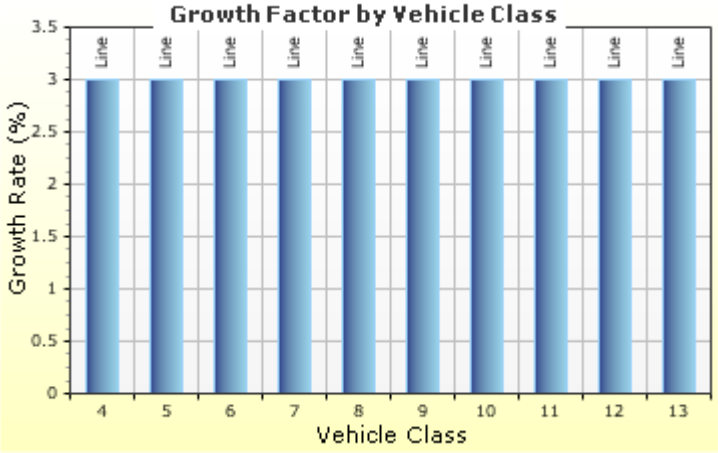

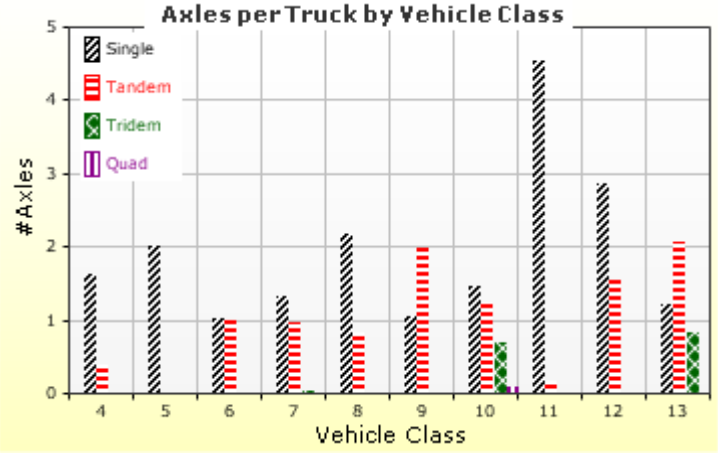

Traffic Volume Monthly Adjustment Factors

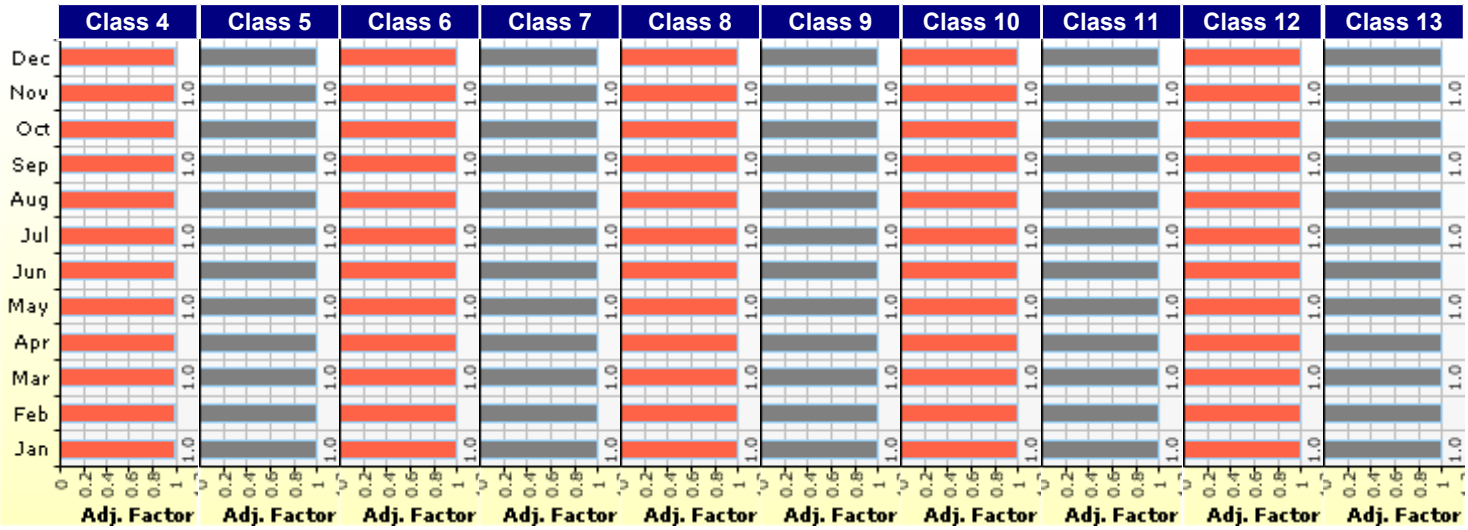

Tabular Representation of Traffic Inputs

Volume Monthly Adjustment Factors

Level 3: Default MAF

Month	Vehicle Class									
	4	5	6	7	8	9	10	11	12	13
January	1.0	1.0	1.0	1.0	1.0	1.0	1.0	1.0	1.0	1.0
February	1.0	1.0	1.0	1.0	1.0	1.0	1.0	1.0	1.0	1.0
March	1.0	1.0	1.0	1.0	1.0	1.0	1.0	1.0	1.0	1.0
April	1.0	1.0	1.0	1.0	1.0	1.0	1.0	1.0	1.0	1.0
May	1.0	1.0	1.0	1.0	1.0	1.0	1.0	1.0	1.0	1.0
June	1.0	1.0	1.0	1.0	1.0	1.0	1.0	1.0	1.0	1.0
July	1.0	1.0	1.0	1.0	1.0	1.0	1.0	1.0	1.0	1.0
August	1.0	1.0	1.0	1.0	1.0	1.0	1.0	1.0	1.0	1.0
September	1.0	1.0	1.0	1.0	1.0	1.0	1.0	1.0	1.0	1.0
October	1.0	1.0	1.0	1.0	1.0	1.0	1.0	1.0	1.0	1.0
November	1.0	1.0	1.0	1.0	1.0	1.0	1.0	1.0	1.0	1.0
December	1.0	1.0	1.0	1.0	1.0	1.0	1.0	1.0	1.0	1.0

Distributions by Vehicle Class

Truck Distribution by Hour does not apply

Vehicle Class	AADTT Distribution (%) (Level 3)	Growth Factor	
		Rate (%)	Function
Class 4	3.3%	3%	Linear
Class 5	34%	3%	Linear
Class 6	11.7%	3%	Linear
Class 7	1.6%	3%	Linear
Class 8	9.9%	3%	Linear
Class 9	36.2%	3%	Linear
Class 10	1%	3%	Linear
Class 11	1.8%	3%	Linear
Class 12	0.2%	3%	Linear
Class 13	0.3%	3%	Linear

Axle Configuration

Traffic Wander	
Mean wheel location (mm)	460.0
Traffic wander standard deviation (mm)	254.0
Design lane width (m)	3.7

Axle Configuration	
Average axle width (m)	2.6
Dual tire spacing (mm)	305.0
Tire pressure (kPa)	827.4

Average Axle Spacing	
Tandem axle spacing (m)	1.5
Tridem axle spacing (m)	1.7
Quad axle spacing (m)	1.3

Wheelbase does not apply

Number of Axles per Truck

Vehicle Class	Single Axle	Tandem Axle	Tridem Axle	Quad Axle
Class 4	1.62	0.39	0	0
Class 5	2	0	0	0
Class 6	1.01	0.993	0	0
Class 7	1.314	0.989	0.03	0
Class 8	2.163	0.845	0	0
Class 9	1.055	1.968	0.003	0
Class 10	1.446	1.234	0.7	0.088
Class 11	4.546	0.168	0	0
Class 12	2.857	1.526	0	0
Class 13	1.201	2.058	0.848	0.024

AADTT (Average Annual Daily Truck Traffic) Growth

*** Traffic cap is not enforced**

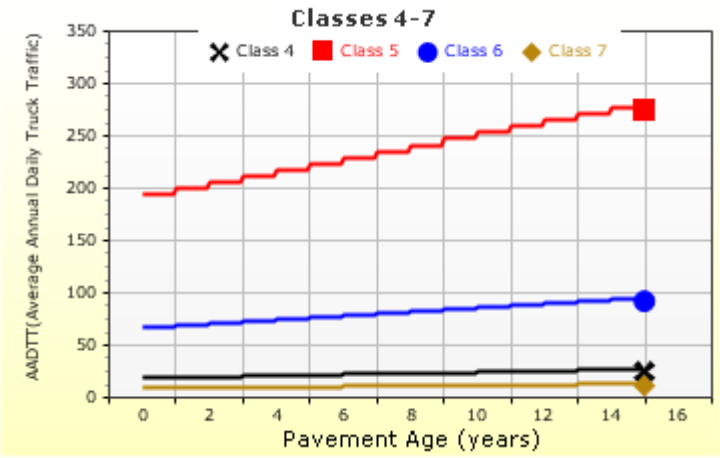

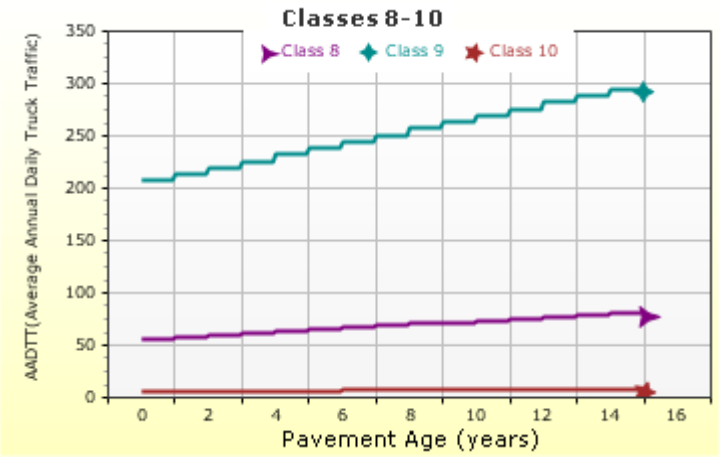

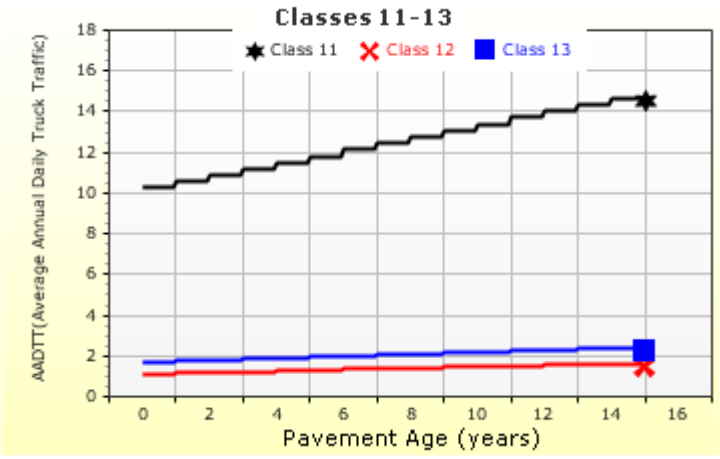

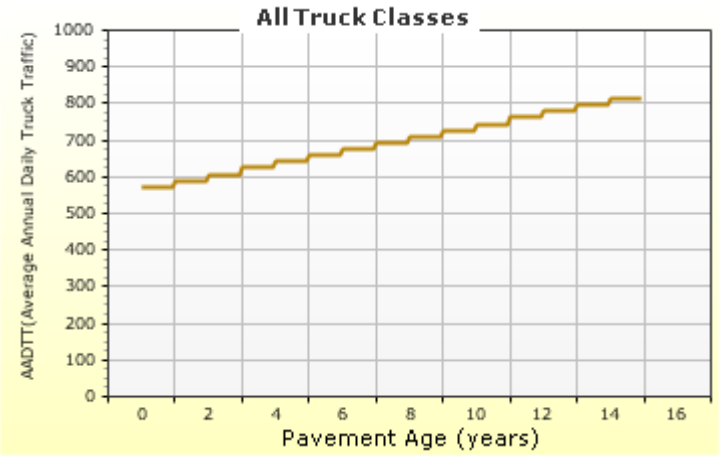

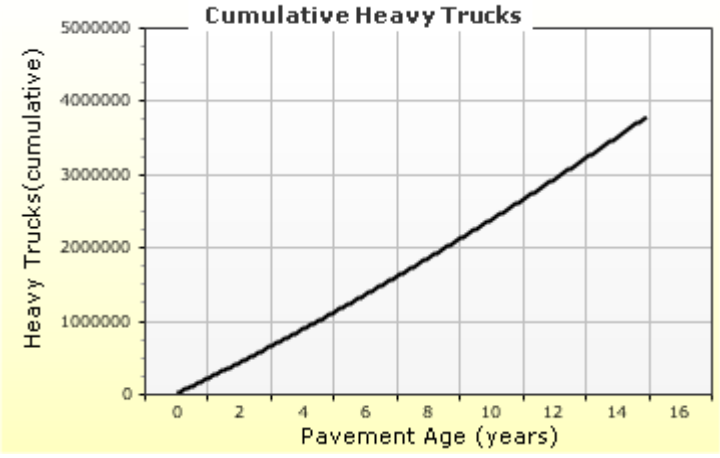

Climate Inputs

Climate Data Sources:

Climate Station Cities:	Location (lat lon elevation(m))
CA, ON	43.50000 -80.62500 369
CA, ON	43.00000 -80.00000 210

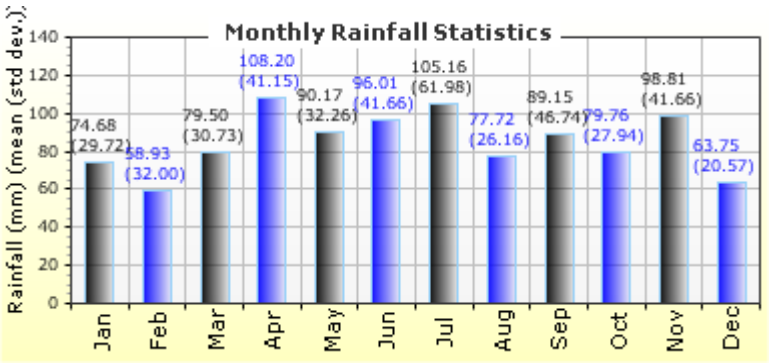

Annual Statistics:

Mean annual air temperature (°C)	7.96
Mean annual precipitation (mm)	1022.60
Freezing index (°C - days)	521.04
Average annual number of freeze/thaw cycles:	80.61

Water table depth (m)	10.00

Monthly Climate Summary:

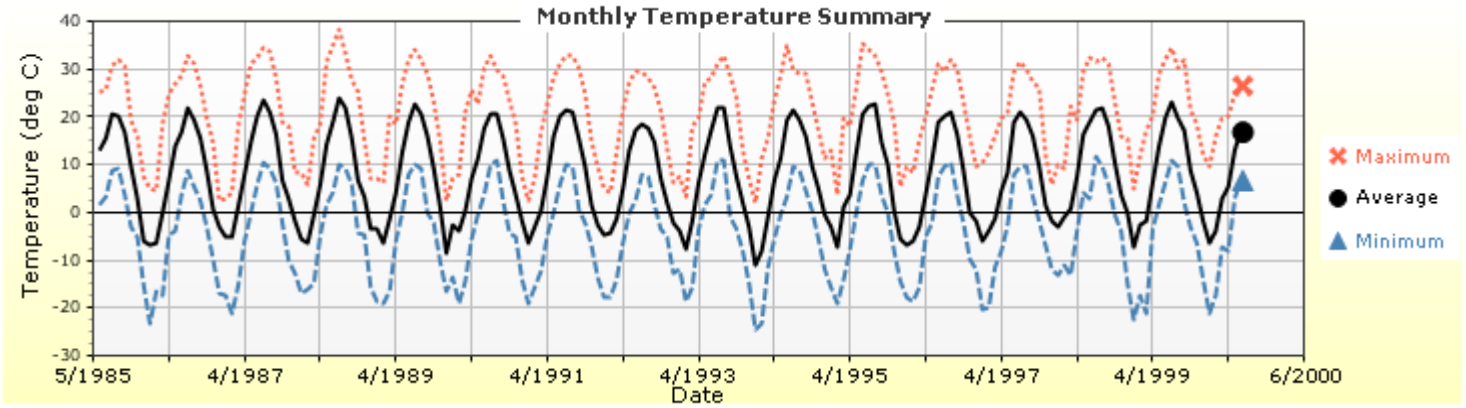

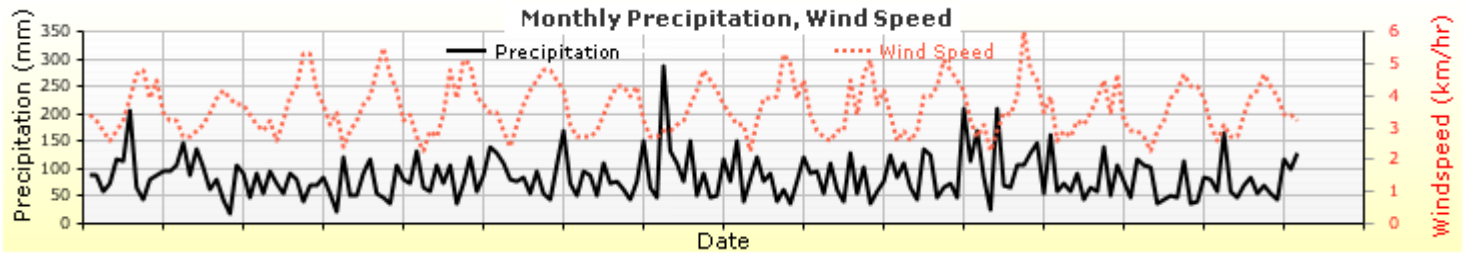

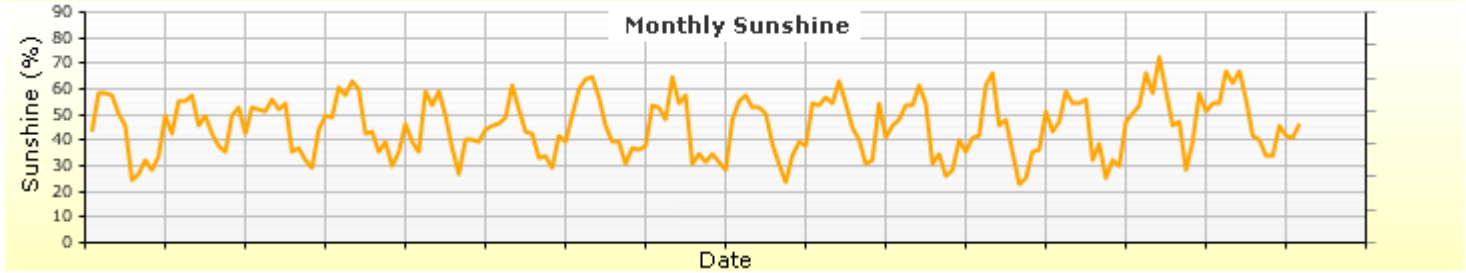

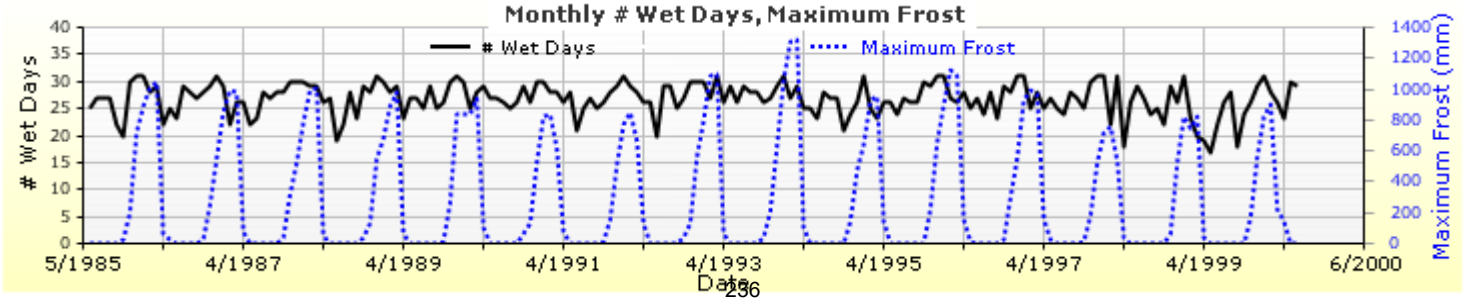

Hourly Air Temperature Distribution by Month:

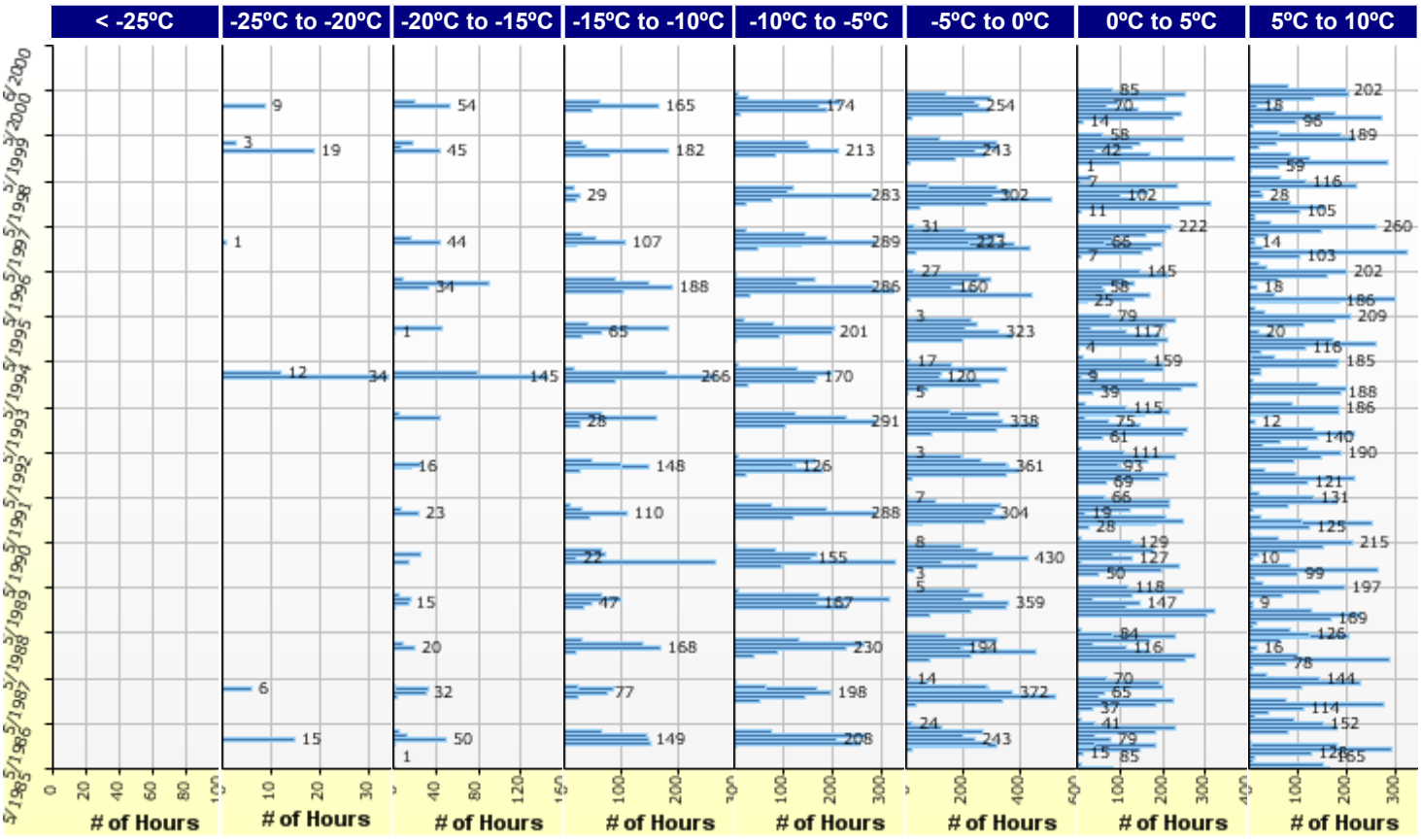

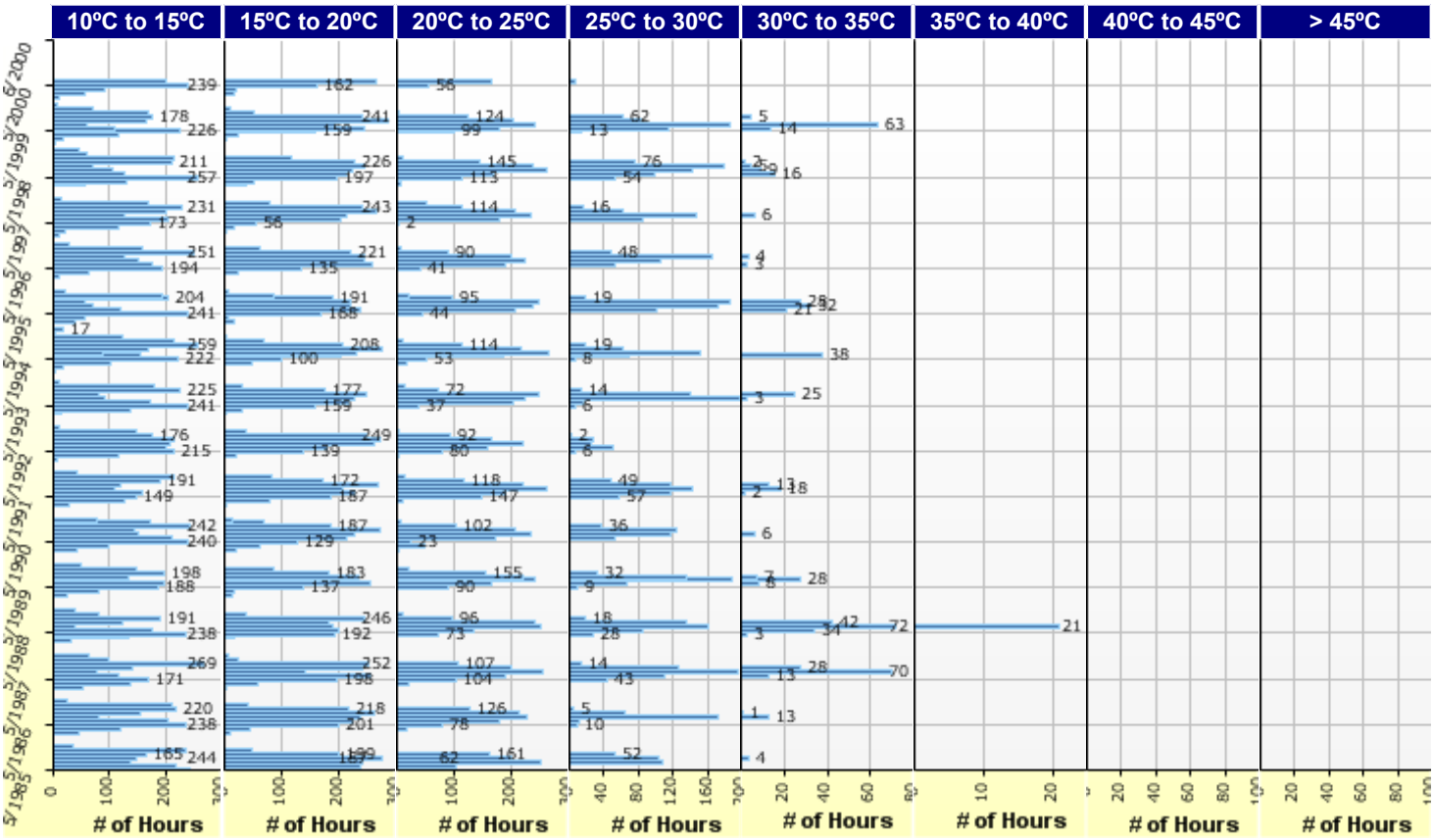

Design Properties

HMA Design Properties

Use Multilayer Rutting Model	False
Using G* based model (not nationally calibrated)	False
Is NCHRP 1-37A HMA Rutting Model Coefficients	True
Endurance Limit	-
Use Reflective Cracking	True

Structure - ICM Properties	
AC surface shortwave absorptivity	0.85

Layer Name	Layer Type	Interface Friction
Layer 1 Flexible : Default asphalt concrete	Flexible (1)	1.00
Layer 2 Chemically Stabilized : Soil cement	Chemically Stabilized (2)	1.00
Layer 3 Non-stabilized Base : Crushed stone	Non-stabilized Base (4)	1.00
Layer 4 Non-stabilized Base : Crushed gravel	Non-stabilized Base (4)	1.00
Layer 5 Subgrade : A-6	Subgrade (5)	-

Thermal Cracking

Thermal Contraction	
Is thermal contraction calculated?	True
Mix coefficient of thermal contraction (mm/mm/ºC)	-
Aggregate coefficient of thermal contraction (mm/mm/ºC)	9.0e-006
Voids in Mineral Aggregate (%)	18.8

Indirect Tensile Strength (Input Level: 3)	
Test Temperature (ºC)	**Indirect Tensilte Strength (Mpa)**
-10.0	2.79

Creep Compliance (1/GPa) (Input Level: 3)			
Loading time (sec)	**-20 ºC**	**-10 ºC**	**0 ºC**
1	5.57e-002	8.57e-002	1.16e-001
2	6.17e-002	1.01e-001	1.51e-001
5	7.07e-002	1.25e-001	2.15e-001
10	7.83e-002	1.48e-001	2.80e-001
20	8.68e-002	1.74e-001	3.65e-001
50	9.94e-002	2.16e-001	5.19e-001
100	1.10e-001	2.55e-001	6.77e-001

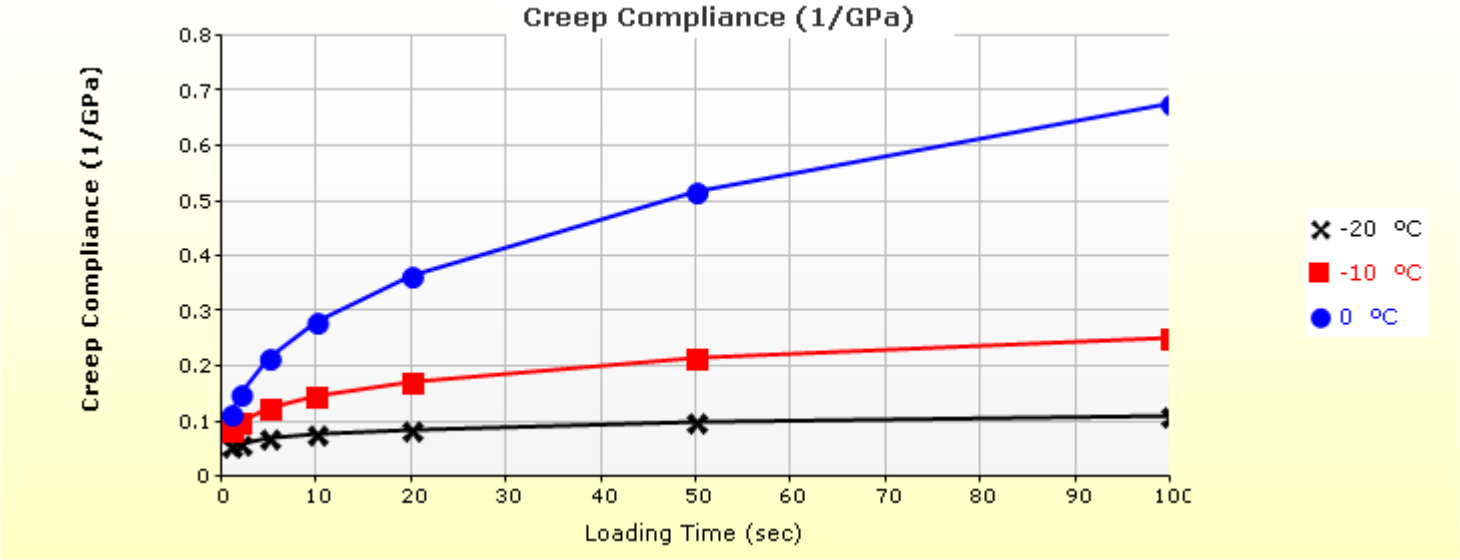

HMA Layer 1: Layer 1 Flexible : Default asphalt concrete

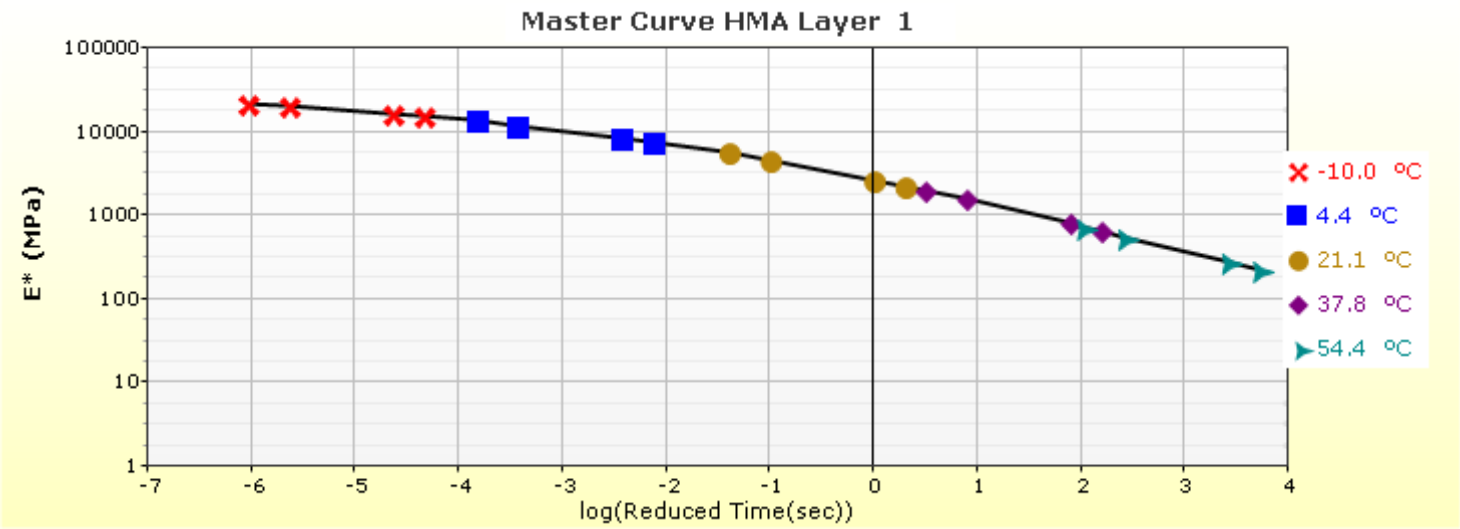

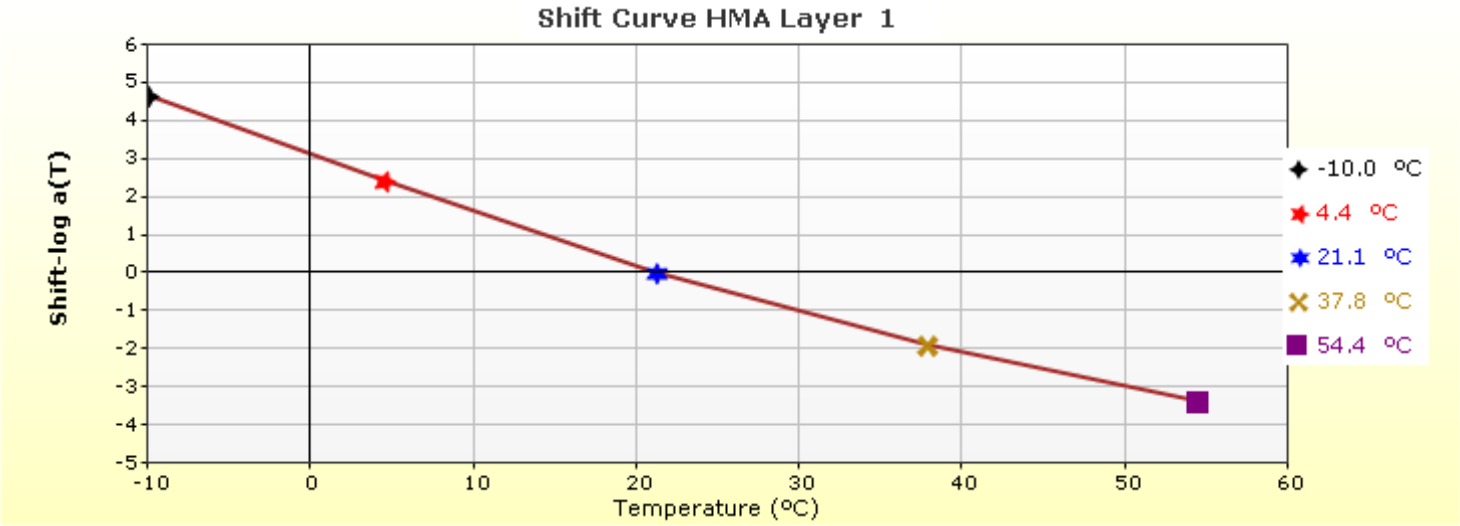

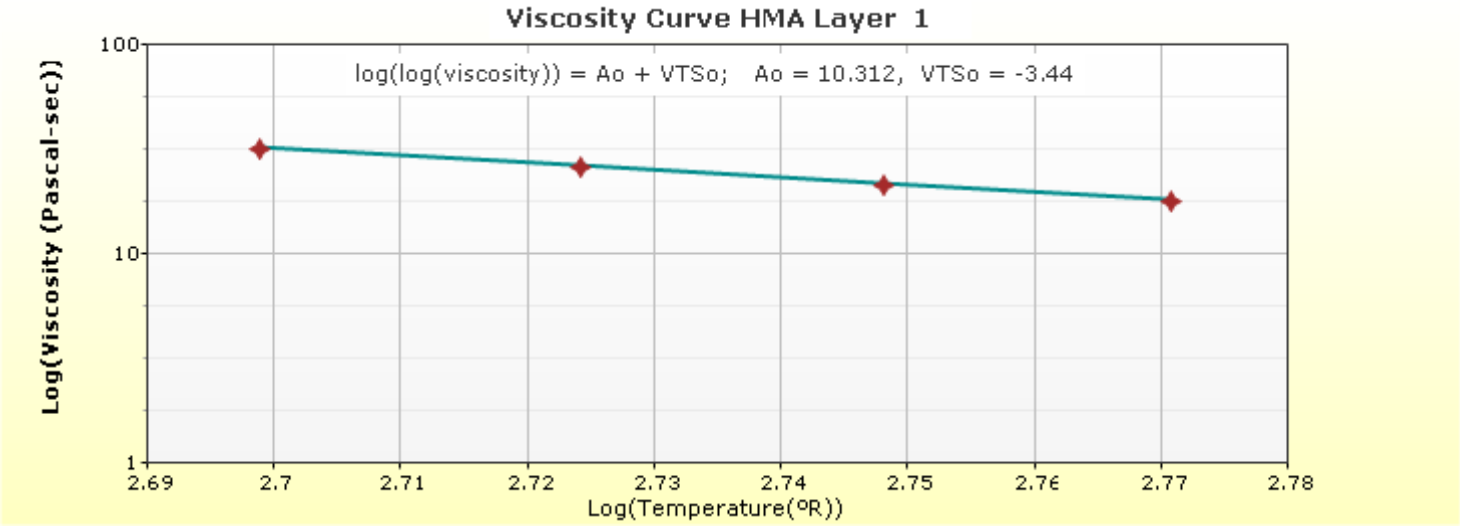

Analysis Output Charts

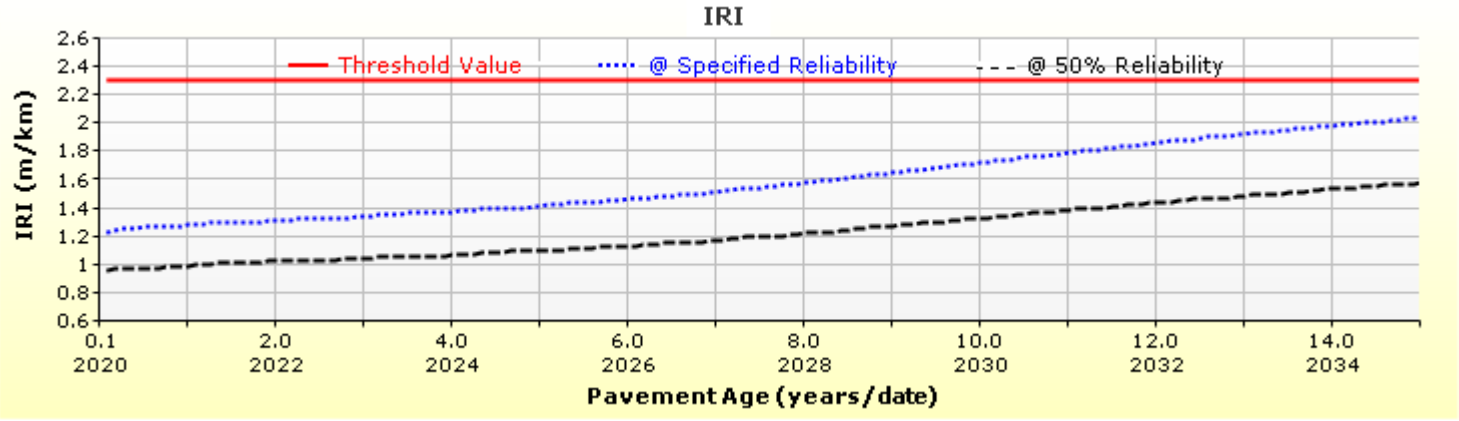

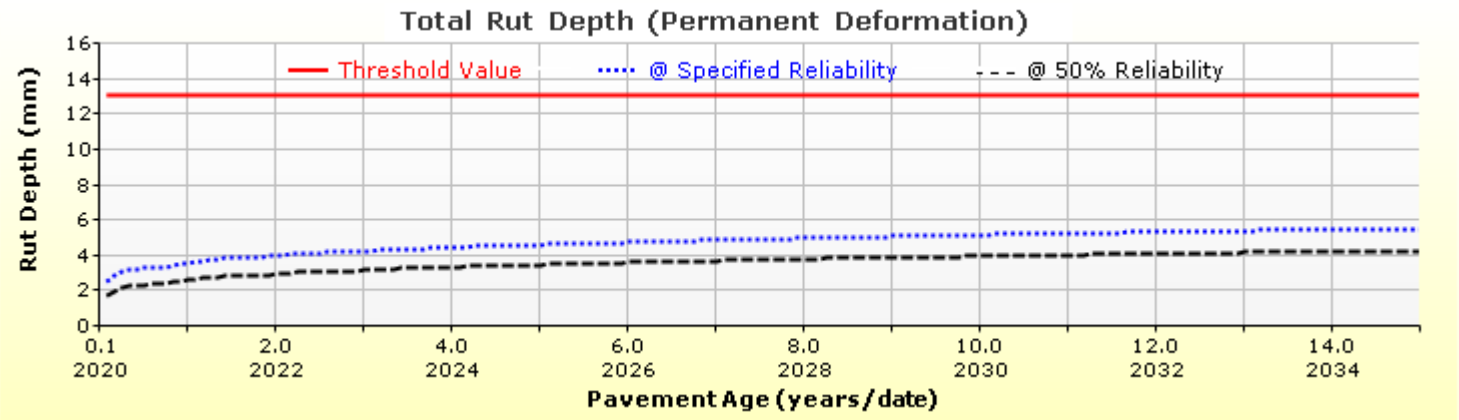

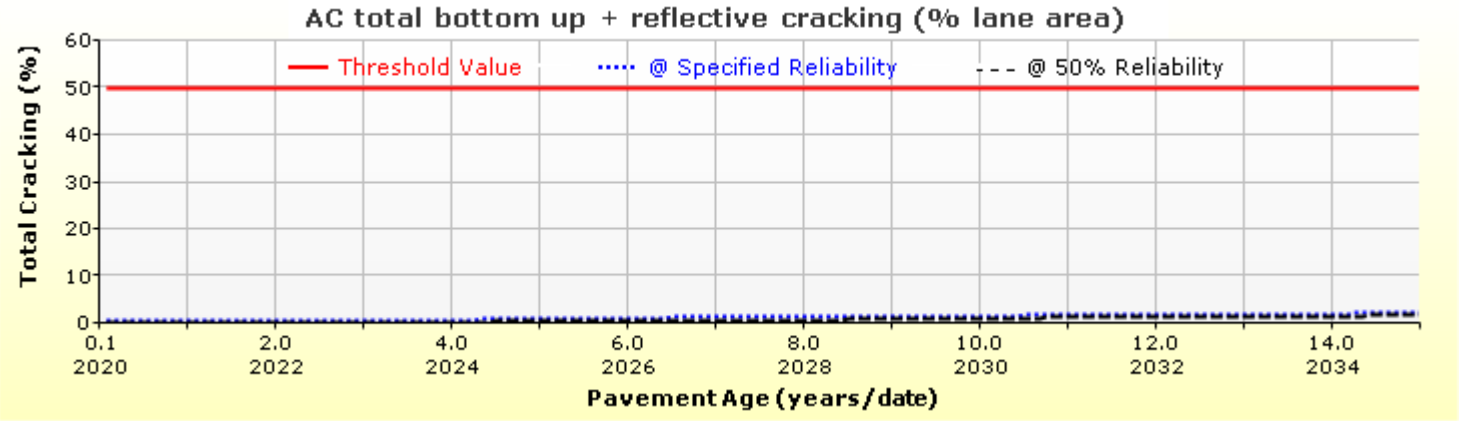

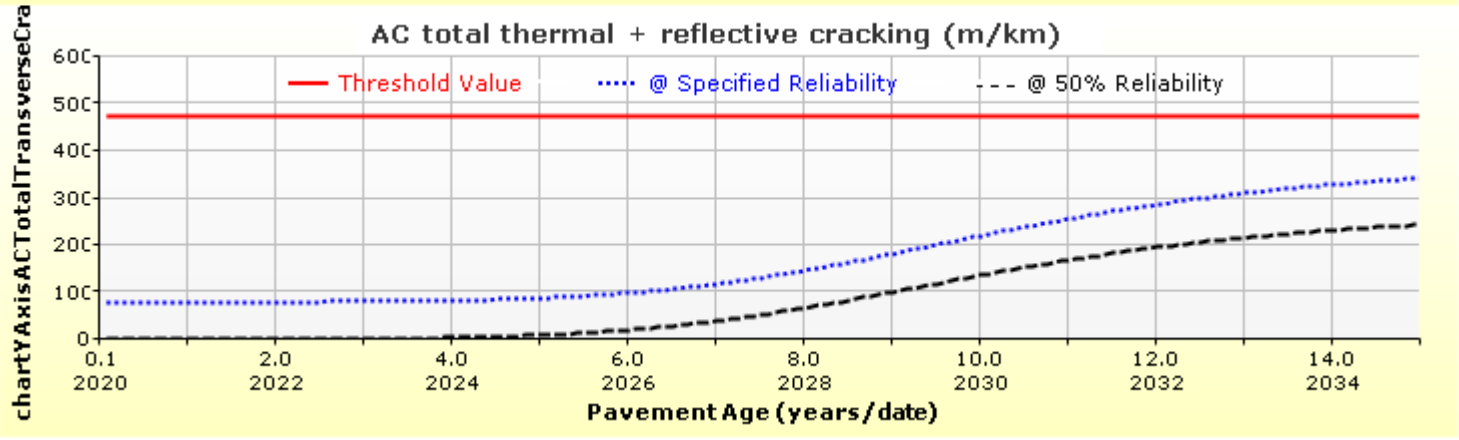

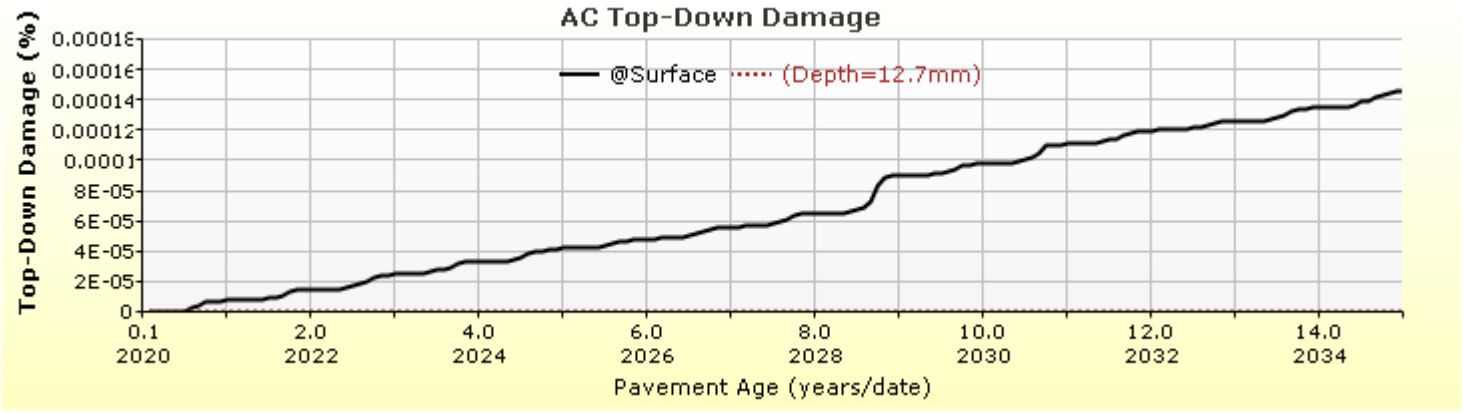
AC Top-Down Damage
Top-Down Damage (%)
@Surface
(Depth=12.7mm)
0.00018
0.00016
0.00014
0.00012
0.0001
8E-05
6E-05
4E-05
2E-05
0
0.1
2020
2.0
2022
4.0
2024
6.0
2026
8.0
2028
10.0
2030
12.0
2032
14.0
2034
Pavement Age (years/date)

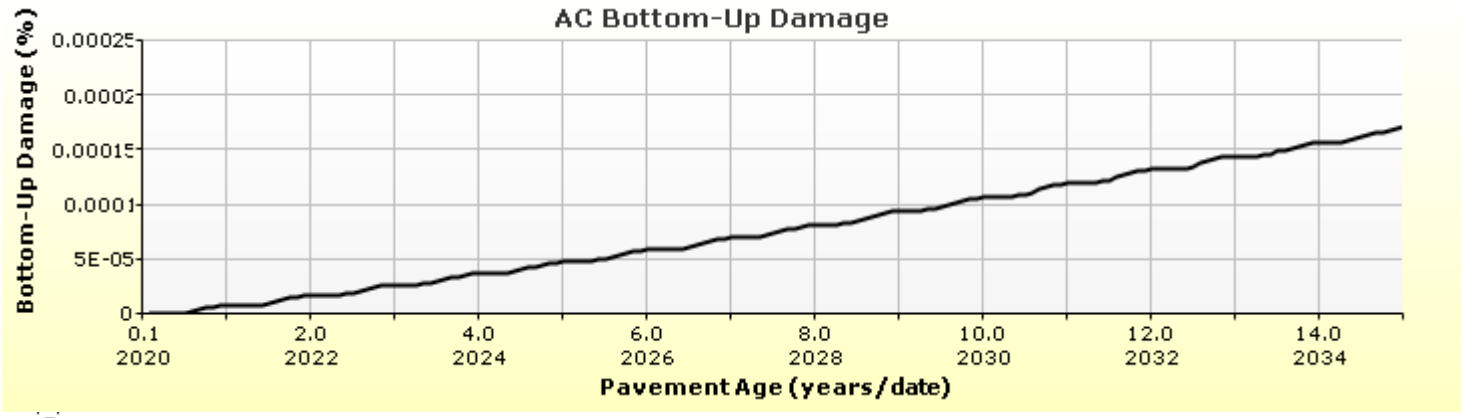
AC Bottom-Up Damage
Bottom-Up Damage (%)
0.00025
0.0002
0.00015
0.0001
5E-05
0
0.1
2020
2.0
2022
4.0
2024
6.0
2026
8.0
2028
10.0
2030
12.0
2032
14.0
2034
Pavement Age (years/date)

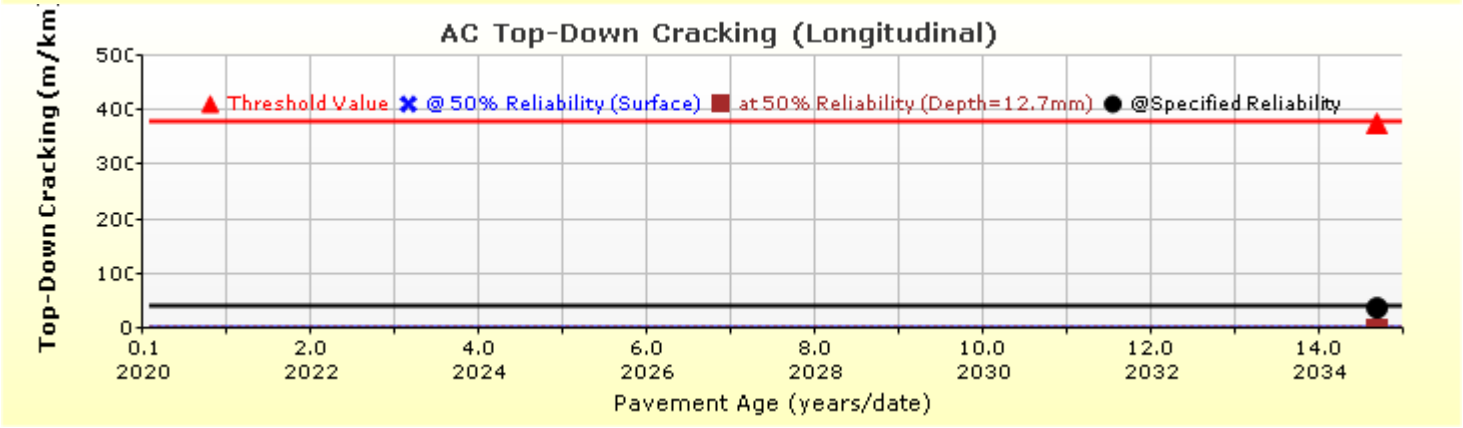
AC Top-Down Cracking (Longitudinal)
Top-Down Cracking (m/km)
Threshold Value
@ 50% Reliability (Surface)
at 50% Reliability (Depth=12.7mm)
@Specified Reliability
500
400
300
200
100
0
0.1
2020
2.0
2022
4.0
2024
6.0
2026
8.0
2028
10.0
2030
12.0
2032
14.0
2034
Pavement Age (years/date)

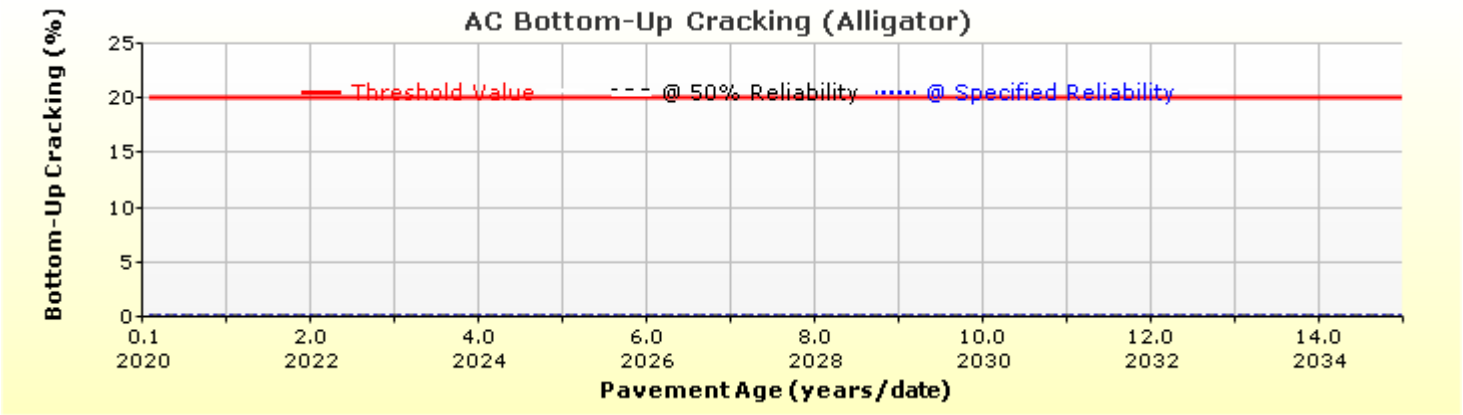
AC Bottom-Up Cracking (Alligator)
Bottom-Up Cracking (%)
Threshold Value
@ 50% Reliability
@ Specified Reliability
25
20
15
10
5
0
0.1
2020
2.0
2022
4.0
2024
6.0
2026
8.0
2028
10.0
2030
12.0
2032
14.0
2034
Pavement Age (years/date)

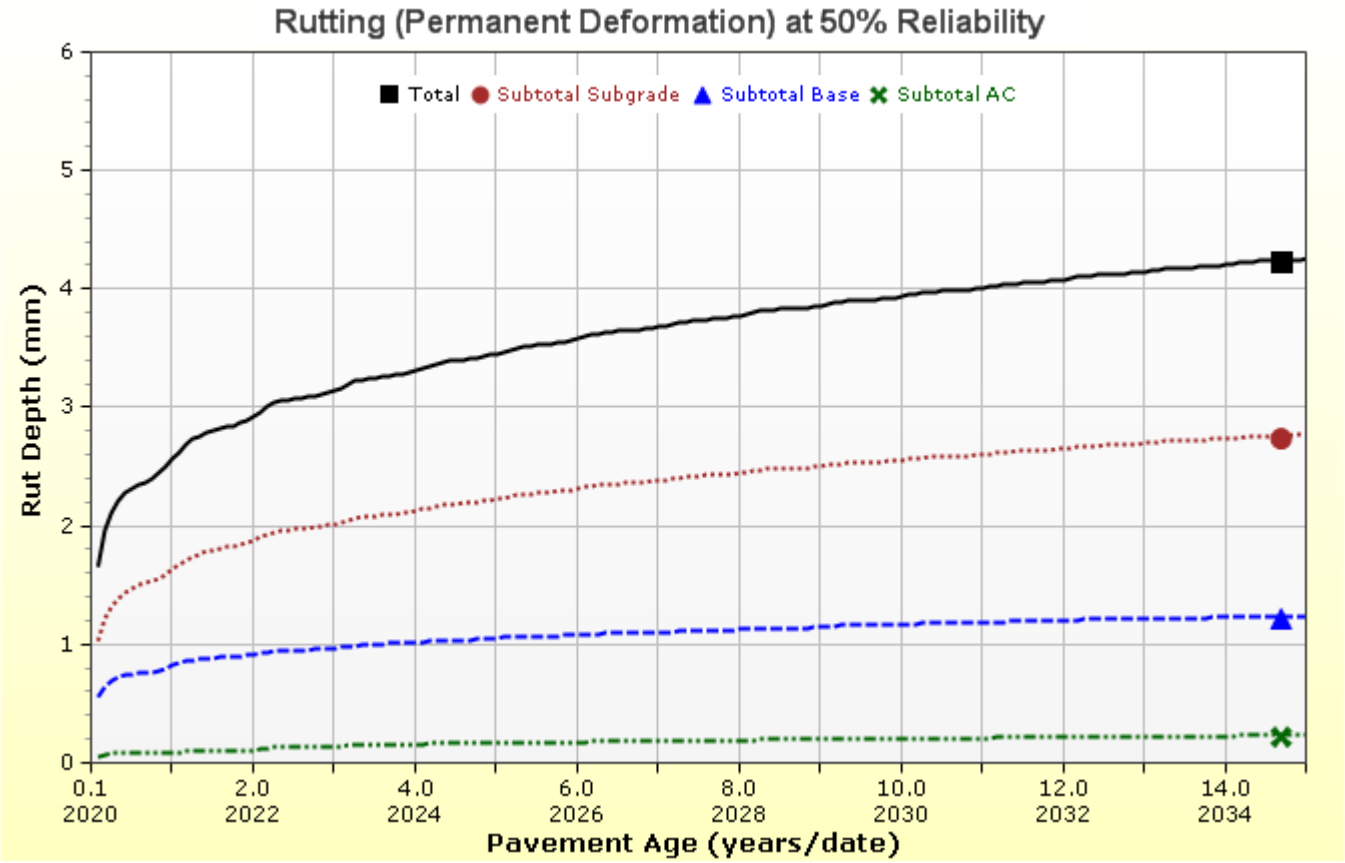
Rutting (Permanent Deformation) at 50% Reliability
Total
Subtotal Subgrade
Subtotal Base
Subtotal AC
Rut Depth (mm)
0
1
2
3
4
5
6
0.1
2020
2.0
2022
4.0
2024
6.0
2026
8.0
2028
10.0
2030
12.0
2032
14.0
2034
Pavement Age (years/date)

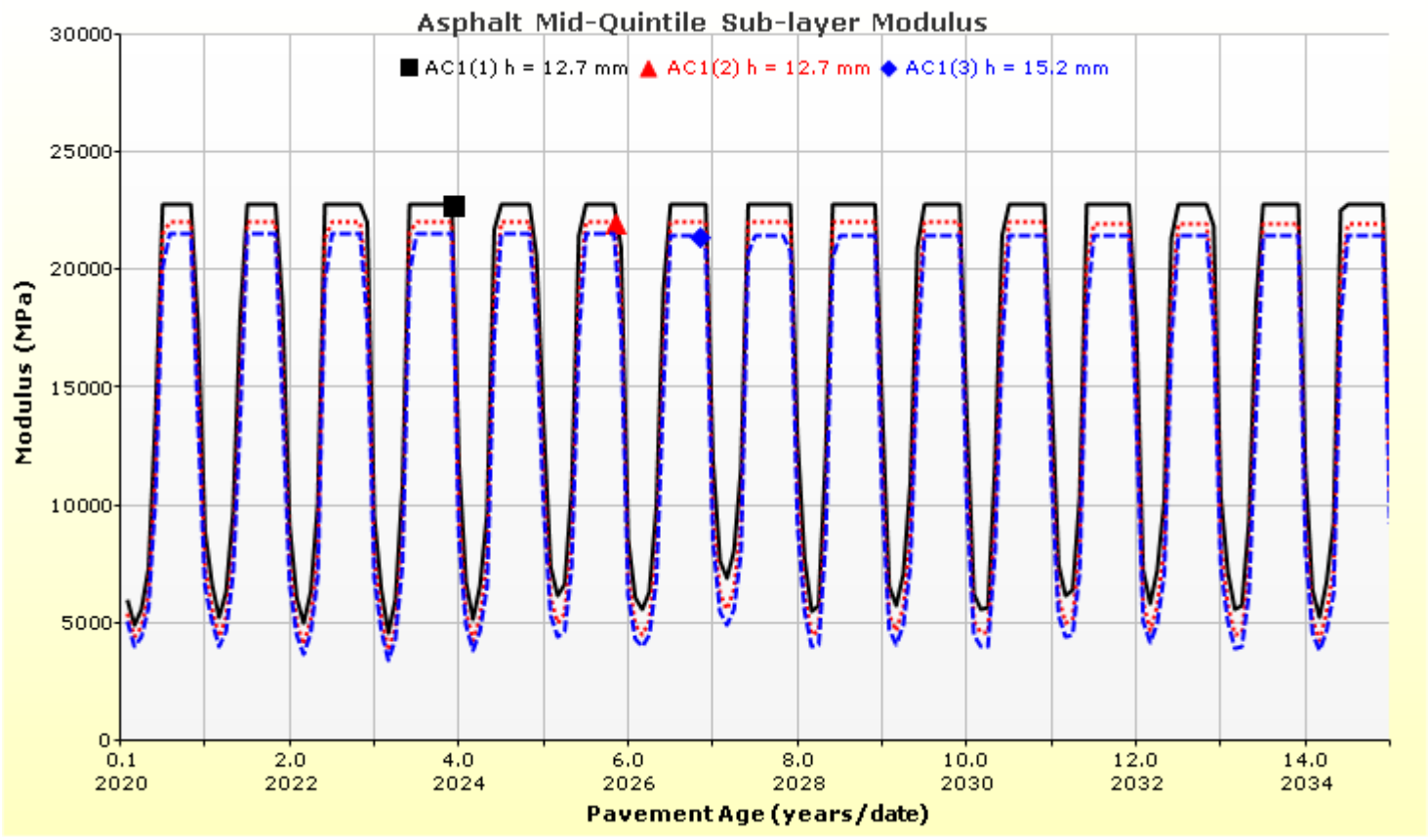
Asphalt Mid-Quintile Sub-layer Modulus
AC1(1) h = 12.7 mm
AC1(2) h = 12.7 mm
AC1(3) h = 15.2 mm
Modulus (MPa)
30000
25000
20000
15000
10000
5000
0
0.1
2020
2.0
2022
4.0
2024
6.0
2026
8.0
2028
10.0
2030
12.0
2032
14.0
2034
Pavement Age (years/date)

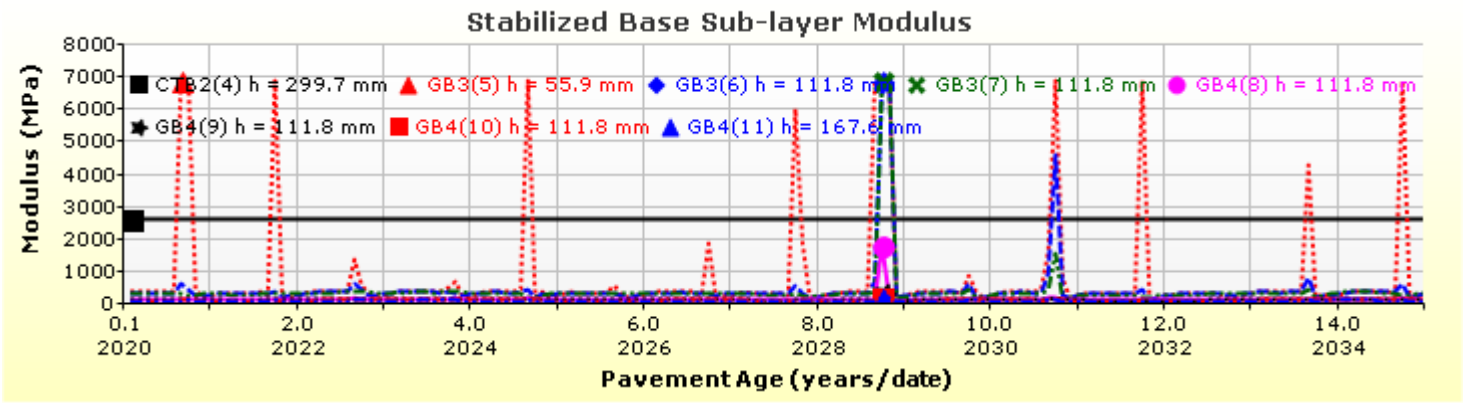
Stabilized Base Sub-layer Modulus
CTB2(4) h = 299.7 mm
GB3(5) h = 55.9 mm
GB3(6) h = 111.8 mm
GB3(7) h = 111.8 mm
GB4(8) h = 111.8 mm
GB4(9) h = 111.8 mm
GB4(10) h = 111.8 mm
GB4(11) h = 167.6 mm
Modulus (MPa)
8000
7000
6000
5000
4000
3000
2000
1000
0
0.1
2020
2.0
2022
4.0
2024
6.0
2026
8.0
2028
10.0
2030
12.0
2032
14.0
2034
Pavement Age (years/date)

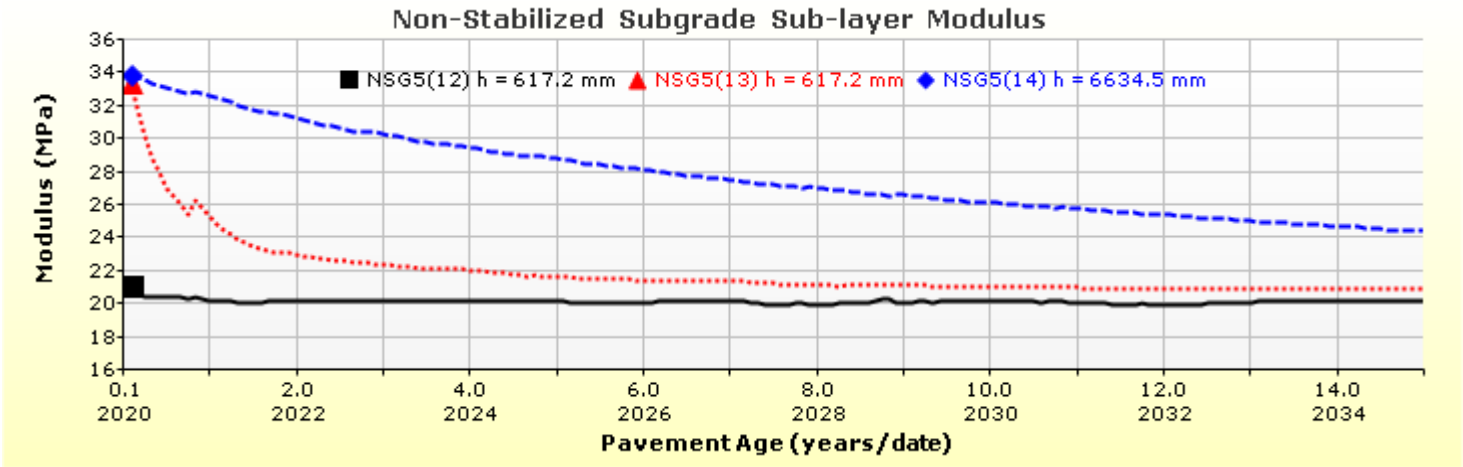
Non-Stabilized Subgrade Sub-layer Modulus
NSG5(12) h = 617.2 mm
NSG5(13) h = 617.2 mm
NSG5(14) h = 6634.5 mm
Modulus (MPa)
36
34
32
30
28
26
24
22
20
18
16
0.1
2020
2.0
2022
4.0
2024
6.0
2026
8.0
2028
10.0
2030
12.0
2032
14.0
2034
Pavement Age (years/date)

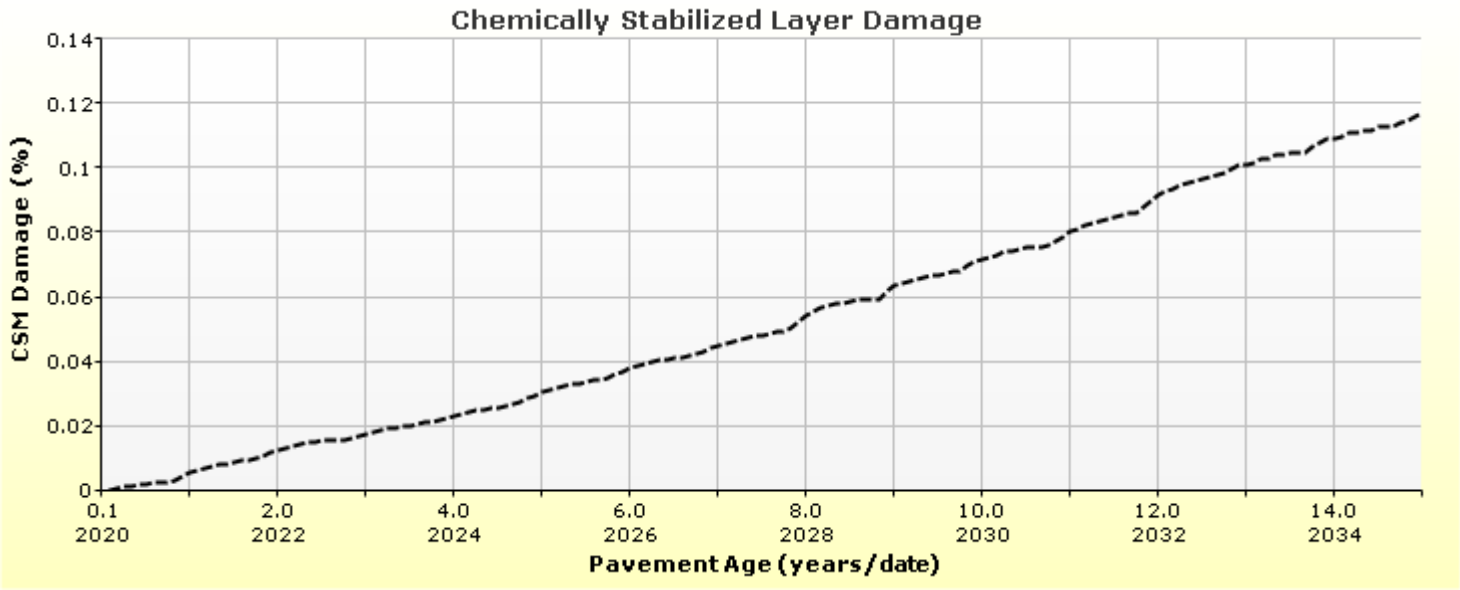
Chemically Stabilized Layer Damage
CSM Damage (%)
0.14
0.12
0.1
0.08
0.06
0.04
0.02
0
0.1
2020
2.0
2022
4.0
2024
6.0
2026
8.0
2028
10.0
2030
12.0
2032
14.0
2034
Pavement Age (years/date)

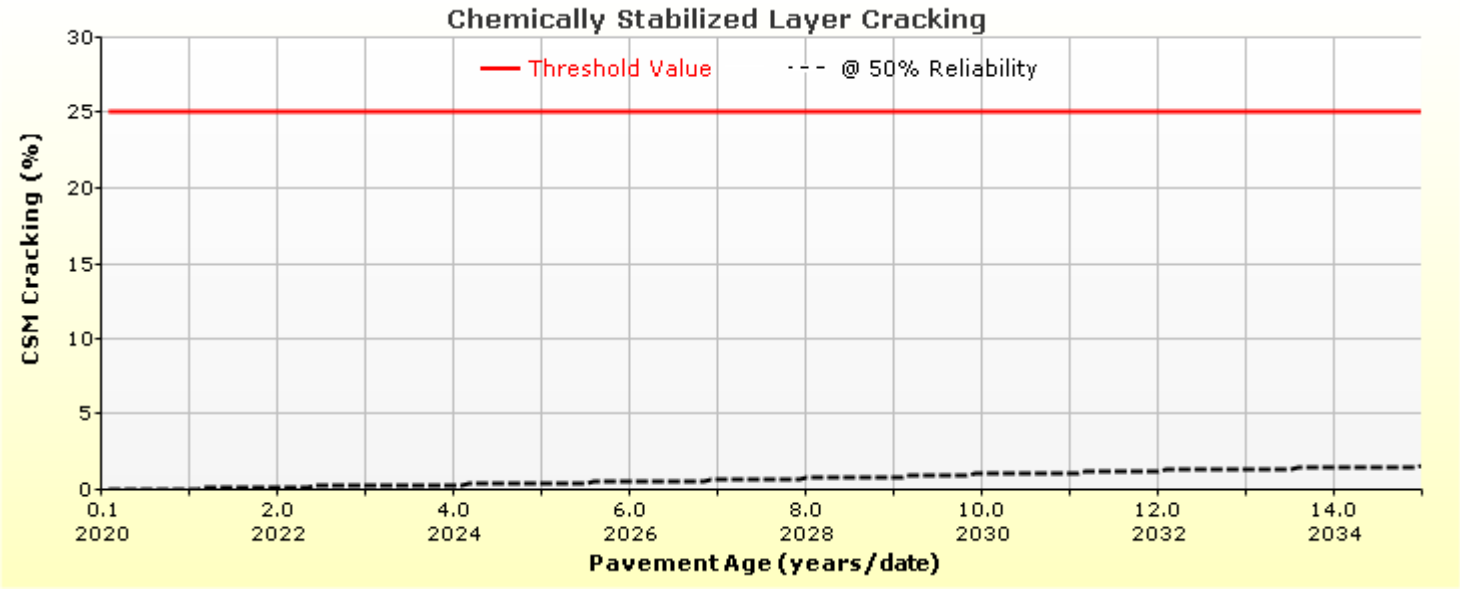
Chemically Stabilized Layer Cracking
Threshold Value
@ 50% Reliability
CSM Cracking (%)
30
25
20
15
10
5
0
0.1
2020
2.0
2022
4.0
2024
6.0
2026
8.0
2028
10.0
2030
12.0
2032
14.0
2034
Pavement Age (years/date)

Layer Information

Layer 1 Flexible : Default asphalt concrete

Asphalt		
Thickness (mm)	40.0	
Unit weight (kgf/m^3)	2460.0	
Poisson's ratio	Is Calculated?	False
	Ratio	0.35
	Parameter A	-
	Parameter B	-

Asphalt Dynamic Modulus (Input Level: 3)

Gradation	Percent Passing
19 mm sieve	100
9.5 mm sieve	77
4.75 mm sieve	60
0.075mm sieve	6

Asphalt Binder

Parameter	Value
Grade	Superpave Performance Grade
Binder Type	64-28
A	10.312
VTS	-3.44

General Info

Name	Value
Reference temperature (°C)	21.1
Effective binder content (%)	11.8
Air voids (%)	7
Thermal conductivity (watt/meter-kelvin)	1.16
Heat capacity (joule/kg-kelvin)	963

Identifiers

Field	Value
Display name/identifier	Default asphalt concrete
Description of object	
Author	
Date Created	9/16/2010 1:00:00 AM
Approver	
Date approved	9/16/2010 1:00:00 AM
State	
District	
County	
Highway	
Direction of Travel	
From station (km)	
To station (km)	
Province	
User defined field 1	
User defined field 2	
User defined field 3	
Revision Number	0

Layer 2 Chemically Stabilized : Soil cement

Semi-Rigid	
Chemically stabilized base crack spacing (m)	8
Chemically stabilized base transverse crack LTE (%)	50
Fatigue LTE (%)	50

Chemically Stabilized	
Layer thickness (mm)	300
Poisson's ratio	0.2
Unit weight (kgf/m^3)	2100

Strength	
Elastic/resilient modulus (MPa)	2664

Thermal	
Heat capacity (joule/kg-kelvin)	1172.3
Thermal conductivity (watt/meter-kelvin)	2.16

Identifiers

Field	Value
Display name/identifier	Soil cement
Description of object	Default material
Author	AASHTO
Date Created	1/1/2011 12:00:00 AM
Approver	
Date approved	1/1/2011 12:00:00 AM
State	
District	
County	
Highway	
Direction of Travel	
From station (km)	
To station (km)	
Province	
User defined field 1	
User defined field 2	
User defined field 3	
Revision Number	0

Layer 3 Non-stabilized Base : Crushed stone

Unbound	
Layer thickness (mm)	280.0
Poisson's ratio	0.35
Coefficient of lateral earth pressure (k0)	0.5

Modulus (Input Level: 3)

Analysis Type:	Modify input values by temperature/moisture
Method:	Resilient Modulus (MPa)

Resilient Modulus (MPa)
250.0

Use Correction factor for NDT modulus?	-
NDT Correction Factor:	-

Identifiers

Field	Value
Display name/identifier	Crushed stone
Description of object	Default material
Author	AASHTO
Date Created	1/1/2011 12:00:00 AM
Approver	
Date approved	1/1/2011 12:00:00 AM
State	
District	
County	
Highway	
Direction of Travel	
From station (km)	
To station (km)	
Province	
User defined field 1	
User defined field 2	
User defined field 3	
Revision Number	0

Sieve

Liquid Limit	6.0
Plasticity Index	1.0
Is layer compacted?	False

	Is User Defined?	Value
Maximum dry unit weight (kgf/m^3)	False	2048.3
Saturated hydraulic conductivity (m/hr)	False	2.257e-02
Specific gravity of solids	False	2.7
Water Content (%)	False	7

User-defined Soil Water Characteristic Curve (SWCC)	
Is User Defined?	False
af	3.0919
bf	2.6074
cf	0.7701
hr	110.0000

Sieve Size	% Passing
0.001mm	
0.002mm	
0.020mm	
0.075mm	5.0
0.150mm	
0.180mm	
0.250mm	
0.300mm	13.5
0.425mm	
0.600mm	
0.850mm	
1.18mm	27.5
2.0mm	
2.36mm	
4.75mm	45.0
9.5mm	61.5
12.5mm	
19.0mm	92.5
25.0mm	100.0
37.5mm	
50.0mm	
63.0mm	
75.0mm	
90.0mm	

Layer 4 Non-stabilized Base : Crushed gravel

Unbound	
Layer thickness (mm)	500.0
Poisson's ratio	0.35
Coefficient of lateral earth pressure (k0)	0.5

Modulus (Input Level: 3)

Analysis Type:	Modify input values by temperature/moisture
Method:	Resilient Modulus (MPa)

Resilient Modulus (MPa)
150.0

Use Correction factor for NDT modulus?	-
NDT Correction Factor:	-

Identifiers

Field	Value
Display name/identifier	Crushed gravel
Description of object	Default material
Author	AASHTO
Date Created	1/1/2011 12:00:00 AM
Approver	
Date approved	1/1/2011 12:00:00 AM
State	
District	
County	
Highway	
Direction of Travel	
From station (km)	
To station (km)	
Province	
User defined field 1	
User defined field 2	
User defined field 3	
Revision Number	0

Sieve

Liquid Limit	11.0
Plasticity Index	1.0
Is layer compacted?	False

	Is User Defined?	Value
Maximum dry unit weight (kgf/m^3)	False	2012.4
Saturated hydraulic conductivity (m/hr)	False	6.883e-03
Specific gravity of solids	False	2.7
Water Content (%)	False	8.2

User-defined Soil Water Characteristic Curve (SWCC)	
Is User Defined?	False
af	5.0935
bf	2.5668
cf	0.8576
hr	108.0000

Sieve Size	% Passing
0.001mm	
0.002mm	
0.020mm	
0.075mm	4.0
0.150mm	
0.180mm	
0.250mm	
0.300mm	33.5
0.425mm	
0.600mm	
0.850mm	
1.18mm	55.0
2.0mm	
2.36mm	
4.75mm	60.0
9.5mm	
12.5mm	
19.0mm	
25.0mm	75.0
37.5mm	
50.0mm	
63.0mm	
75.0mm	
90.0mm	

Layer 5 Subgrade : A-6

Unbound	
Layer thickness (mm)	Semi-infinite
Poisson's ratio	0.35
Coefficient of lateral earth pressure (k0)	0.5

Modulus (Input Level: 3)

Analysis Type:	Modify input values by temperature/moisture
Method:	Resilient Modulus (MPa)

Resilient Modulus (MPa)
35.0

Use Correction factor for NDT modulus?	-
NDT Correction Factor:	-

Identifiers

Field	Value
Display name/identifier	A-6
Description of object	Default material
Author	AASHTO
Date Created	1/1/2011 12:00:00 AM
Approver	
Date approved	1/1/2011 12:00:00 AM
State	
District	
County	
Highway	
Direction of Travel	
From station (km)	
To station (km)	
Province	
User defined field 1	
User defined field 2	
User defined field 3	
Revision Number	0

Sieve

Liquid Limit	42.0
Plasticity Index	15.0
Is layer compacted?	False

	Is User Defined?	Value
Maximum dry unit weight (kgf/m^3)	False	1693.8
Saturated hydraulic conductivity (m/hr)	False	3.012e-06
Specific gravity of solids	False	2.7
Water Content (%)	False	18.2

User-defined Soil Water Characteristic Curve (SWCC)	
Is User Defined?	False
af	114.8407
bf	0.6389
cf	0.1739
hr	500.0000

Sieve Size	% Passing
0.001mm	
0.002mm	25.0
0.020mm	
0.075mm	82.0
0.150mm	
0.180mm	91.0
0.250mm	
0.300mm	
0.425mm	95.0
0.600mm	
0.850mm	
1.18mm	
2.0mm	98.0
2.36mm	
4.75mm	100.0
9.5mm	100.0
12.5mm	100.0
19.0mm	100.0
25.0mm	100.0
37.5mm	
50.0mm	
63.0mm	
75.0mm	
90.0mm	100.0

Calibration Coefficients

AC Fatigue

$$N_f = 0.00432 * C * \beta_{f1} k_1 \left(\frac{1}{\varepsilon_1}\right)^{k_2\beta_{f2}} \left(\frac{1}{E}\right)^{k_3\beta_{f3}}$$

$$C = 10^M$$

$$M = 4.84\left(\frac{V_b}{V_a + V_b} - 0.69\right)$$

k1: 3.75	
k2: 2.87	
k3: 1.46	
Bf1: 0.02054	
Bf2: 1.38	
Bf3: 0.88	

AC Rutting

$$\frac{\varepsilon_p}{\varepsilon_r} = k_z \beta_{r1} 10^{k_1 T^{k_2\beta_{r2}} N^{k_3\beta_{r3}}}$$

$$k_z = (C_1 + C_2 * depth) * 0.328196^{depth}$$

$$C_1 = -0.1039 * H_\alpha^2 + 2.4868 * H_\alpha - 17.342$$

$$C_2 = 0.0172 * H_\alpha^2 - 1.7331 * H_\alpha + 27.428$$

Where:

$H_{ac} = total\ AC\ thickness(in)$

$\varepsilon_p = plastic\ strain\left({}^{in}/_{in}\right)$
$\varepsilon_r = resilient\ strain\left({}^{in}/_{in}\right)$
$T = layer\ temperature(^{\circ}F)$
$N = number\ of\ load\ repetitions$

AC Rutting Standard Deviation	0.24 * Pow(RUT,0.8026) + 0.001	
AC Layer 1	K1:-2.45 K2:3.01 K3:0.22	Br1:0.128 Br2:0.52 Br3:1.36

Thermal Fracture

$$C_f = 400 * N\left(\frac{\log C / h_{ac}}{\sigma}\right)$$

$$\Delta C = (k * \beta t)^{n+1} * A * \Delta K^n$$

$$A = 10^{(4.389 - 2.52 * \log(E * \sigma_m * n))}$$

$C_f = observed\ amount\ of\ thermal\ cracking(ft/500ft)$
$k = refression\ coefficient\ determined\ through\ field\ calibration$
$N(\,) = standard\ normal\ distribution\ evaluated\ at(\,)$
$\sigma = standard\ deviation\ of\ the \log\ of\ the\ depth\ of\ cracks\ in\ the\ pavments$
$C = crack\ depth(in)$
$h_{ac} = thickness\ of\ asphalt\ layer(in)$
$\Delta C = Change\ in\ the\ crack\ depth\ due\ to\ a\ cooling\ cycle$
$\Delta K = Change\ in\ the\ stress\ intensity\ factor\ due\ to\ a\ cooling\ cycle$
$A, n = Fracture\ parameters\ for\ the\ asphalt\ mixture$
$E = mixture\ stiffness$
$\sigma_M = Undamaged\ mixture\ tensile\ strength$
$\beta_t = Calibration\ parameter$

Level 1 K: ((3 * Pow(10,-7)) * Pow(MAAT,4.0319)) * 1 + 0	
Level 2 K: ((3 * Pow(10,-7)) * Pow(MAAT,4.0319)) * 1 + 0	
Level 3 K: ((3 * Pow(10,-7)) * Pow(MAAT,4.0319)) * 1 + 0	

CSM Fatigue

$$N_f = 10^{\left(\frac{k_1 \beta_{c1} \left(\frac{\sigma_s}{M_r}\right)}{k_2 \beta_{c2}}\right)}$$

$N_f = number\ of\ repetitions\ to\ fatigue\ cracking$
$\sigma_s = Tensile\ stress(psi)$
$M_r = modulus\ of\ rupture(psi)$

k1: 0.972	k2: 0.0825	Bc1: 1	Bc2:1

Unbound Layer Rutting

$$\delta_a(N) = \beta_{s_1} k_1 \varepsilon_v h \left(\frac{\varepsilon_0}{\varepsilon_r}\right) \left| e^{-\left(\frac{\rho}{N}\right)^{\beta}} \right|$$

$\delta_a = permanent\ deformation\ for\ the\ layer$
$N = number\ of\ repetitions$
$\varepsilon_v = average\ veritcal\ strain(in/in)$
$\varepsilon_0, \beta, \rho = material\ properties$
$\varepsilon_r = resilient\ strain(in/in)$

Base Rutting		Subgrade Rutting	
k1: 0.965	Bs1: 1	k1: 0.675	Bs1: 1
Standard Deviation (BASERUT) 0.1477 * Pow(BASERUT,0.6711) + 0.001		Standard Deviation (BASERUT) 0.1235 * Pow(SUBRUT,0.5012) + 0.001	

AC Cracking

AC Top Down Cracking

$$FC_{top} = \left(\frac{C_4}{1 + e^{(C_1 - C_2 * log_{10}(Damage))}}\right) * 10.56$$

c1: 7	c2: 3.5	c3: 0	c4: 1000

Top down AC Cracking Standard Deviation

200 + 2300/(1+exp(1.072-2.1654*LOG10(TOP+0.0001)))

AC Bottom Up Cracking

$$FC = \left(\frac{6000}{1 + e^{(C_1 * C_1' + C_2 * C_2' log_{10}(D * 100))}}\right) * \left(\frac{1}{60}\right)$$

$$C_2' = -2.40874 - 39.748 * (1 + h_{ac})^{-2.856}$$

$$C_1' = -2 * C_2'$$

c1: 1.31	c2: 2.1585	c3: 6000

Bottom up AC Cracking Standard Deviation

1.13 + 13/(1+exp(7.57-15.5*LOG10(BOTTOM+0.0001)))

CSM Cracking

$$FC_{ctb} = C_1 + \frac{C_2}{1 + e^{C_3 - C_4 * log_{10}(Damage)}}$$

C1: 0	C2: 75	C3: 2	C4: 2

CSM Standard Deviation

CTB*1

IRI Flexible Pavements

C1 - Rutting
C2 - Fatigue Crack
C3 - Transverse Crack
C4 - Site Factors

C1: 55	C2: 0.4	C3: 0.008	C4: 0.015

Reflective Cracking

$$\Delta C = k_1 \Delta_{bending} + k_2 \Delta_{shaering} + k_3 \Delta_{thermal}$$

$$\Delta D = \frac{C_1 k_1 \Delta_{bending} + C_2 k_2 \Delta_{shearing} + C_3 k_3 \Delta_{thermal}}{h_{OL}}$$

$$\Delta_{Bending} = A(SIF)_B^n$$

$$\Delta_{Shearing} = A(SIF)_S^n$$

$$\Delta_{Thermal} = A(SIF)_T^n$$

$$D = \sum_{i=1}^{N} \Delta D$$

$$RCR = \left(\frac{100}{C4 + e^{C5 \log D}}\right) * EX\_CRK$$

Where

ΔC	=	Crack length increment, in
ΔD	=	Incremental damage ratio
$k_1, k_2, k_3, C_1, C_2, C_3, C_4, C_5$	=	Calibration factors (local and global)
$\Delta_{bending}, \Delta_{shearing}, \Delta_{thermal}$	=	Crack length increments caused by bending, shearing, and thermal loading
A, n	=	HMA material fracture properties
N	=	Total number of days
$(SIF)_B, (SIF)_S, (SIF)_T$	=	Stress intensity factors caused by bending, shearing, and thermal loading
D	=	Damage ratio
h_{OL}	=	Overlay thickness, in
RCR	=	Cracks in the underlying layers reflected, %
EX_CRK	=	Transverse cracking in underlying pavement layers, ft/mile (transverse cracking) Alligator cracking in underlying pavement layers, % lane area (alligator cracking)

Pavement Type	Distress Type	k1	k2	k3	C1	C2	C3	C4	C5	Standard Deviation
Semi-Rigid	Transverse	0.45	0.05	1	0.1	0.9809	0.19	165.3	-5.1048	0.000027 * Pow (TRANSVERSE,2.1187) + 399.9
Semi-Rigid	Fatigue	0.45	0.05	1	1.64	1.1	0.19	62.1	-404.6	1.3897 * Pow (FATIGUE,0.2960) + 0.4212

APPENDICES-II:

Calculation of Energy Input and Emissions Output for Blending Process

Machine Information (source: Lafarge Canada):

Capacity of Blower package = 250 hp = 186.425 kW

1kWh = 3.6 MJ

Energy consumption if the machine operate at full-capacity for 1-hr = 186.425 kWh = 671 MJ

Machine type: CB-Series

Machine specification (Source: Machine manufacturer webpage):

Capacity = 80 metric tons per hour

Material-to-air ratio = 50 – 20 (50 was chosen for analysis)

➔ *production rate = 80*0.5 = 40 metric tons per hour (assuming full-production capacity)*

➔ *Energy consumed per ton of HRB = 671 MJ / 40 = 16.8 MJ*

Emissions (Source: A Life Cycle Perspective of Concrete and Asphalt Roadways_Embodied and Global Warming Potential, page 67, Table 6)

$$\mathbf{GWP = CO2 + 23\ CH_4 + 296\ N_2O}$$

Emissions (kg) per GJ of electricity (Ontario)

$CO_2 = 86.7$

$CH_4 = 0.19622$

$N_2O = 0.000645$

Ontario			
	HRB1	**HRB2**	**HRB3**
FDR-Binder mix unit wt. (mt/m^3)	2.130	2.106	2.064
Vol. of mix/km-lane (m^3)	3.75*1000*0.3 = 1,125		
Wt. of mix/km-lane (mt)	2,396.25	2,369.25	2,322.00
Quantity of binder (mt) = 6% of the mix	143.78	142.16	139.32
Electric energy (GJ)	2.4	2.4	2.3
Emissions			
CO_2 (kg)	209	207	203
CH_4 (kg)	0.47	0.47	0.46
N_2O (kg)	0.00	0.00	0.00
GWP (kgCO2eq)	221	218	214

Emissions (kg) per GJ of electricity (Manitoba = Canada)

CO_2 = 71.83

CH_4 = 0.15158

N_2O = 0.000525

Manitoba			
	HRB1	**HRB2**	**HRB3**
Quantity (metric tons)	143.8	142.2	139.3
Electric energy (GJ)	2.4	2.4	2.3
Emissions			
CO_2 (kg)	174	172	168
CH_4 (kg)	0.37	0.36	0.35
N_2O (kg)	0.00	0.00	0.00
GWP (kgCO2eq)	182	180	177

Emissions (kg) per GJ of electricity (Quebec = Canada)

CO_2 = 2.02

CH_4 = 0.00157

N_2O = 0.000006

Quebec			
	HRB1	**HRB2**	**HRB3**
Quantity (metric tons)	143.8	142.2	139.3
Electric energy (GJ)	2.4	2.4	2.3
Emissions			
CO_2 (kg)	4.8	4.8	4.7
CH_4 (kg)	0.0038	0.0038	0.0037
N_2O (kg)	0.00	0.00	0.00
GWP (kgCO2eq)	4.9	4.9	4.7